Chapter 19

Inhibition of the HIF-1 Survival Pathway as a Strategy to Augment Photodynamic Therapy Efficacy

Mark J. de Keijzer, Daniel J. de Klerk, Lianne R. de Haan, Robert T. van Kooten, Leonardo P. Franchi, Lionel M. Dias, Tony G. Kleijn, Diederick J. van Doorn, and Michal Heger and on behalf of the Photodynamic Therapy Study Group

Abstract

Photodynamic therapy (PDT) is a non-to-minimally invasive treatment modality that utilizes photoactivatable drugs called photosensitizers to disrupt tumors with locally photoproduced reactive oxygen species (ROS). Photosensitizer activation by light results in hyperoxidative stress and subsequent tumor cell death, vascular shutdown and hypoxia, and an antitumor immune response. However, sublethally afflicted tumor cells initiate several survival mechanisms that account for decreased PDT efficacy. The hypoxia inducible factor 1 (HIF-1) pathway is one of the most effective cell survival pathways that contributes to cell recovery from PDT-induced damage. Several hundred target genes of the HIF-1 heterodimeric complex collectively mediate processes that are involved in tumor cell survival directly and indirectly (e.g., vascularization, glucose metabolism, proliferation, and metastasis). The broad spectrum of biological ramifications culminating from the activation of HIF-1 target genes reflects the importance of HIF-1 in the context of therapeutic recalcitrance. This chapter elaborates on the involvement of HIF-1 in cancer biology, the hypoxic response mechanisms, and the role of HIF-1 in PDT. An overview of inhibitors that either directly or indirectly impede HIF-1-mediated survival signaling is provided. The inhibitors may be used as pharmacological adjuvants in combination with PDT to augment therapeutic efficacy.

Key words Photobiology and photochemistry, Survival signaling, Hypoxia-inducible factor 1, Pharmacology, Inhibitor, Tumor biology and biochemistry

Abbreviations

$^1O_2$	Singlet oxygen
2ME2	2-Methoxyestradiol
2OG	2-Oxoglutarate (α-ketoglutarate)
5-ALA	5-Aminolevulinic acid
ADP	Adenosine diphosphate

Mark J. de Keijzer and Daniel J. de Klerk contributed equally.

Mans Broekgaarden et al. (eds.), *Photodynamic Therapy: Methods and Protocols*, Methods in Molecular Biology, vol. 2451, https://doi.org/10.1007/978-1-0716-2099-1_19,

Akt	Protein kinase B
ANGPT1/2	Angiopoietin 1 and 2
ANGPTL4	Angiopoietin-like 4
AP-1	Activator protein 1
APAF1	Apoptotic protease activating factor 1
ARF	Alternate reading frame
ATF4/6	Activating transcription factor 4 and 6
ATP	Adenosine triphosphate
BAK	BCL-2 homologous antagonist killer
BAX	BCL-2-associated X protein
bFGF	Basic fibroblast growth factor
BH3-only	BCL-2 homology domain 3-only
BNIP3	BCL-2 19 kD interacting protein 3
CAF	Cancer-associated fibroblasts
CAM	Chorioallantoic membrane
CCO	Cytochrome c oxidase
CDAMP	Cell death-associated molecular pattern
CDC	Cell division cycle
CDK	Cyclin-dependent kinase
CDT1	Chromatin licensing and DNA replicator factor 1
CEP192	Centrosomal protein of 192 kDa
CIP	CDK interacting protein
c-MET	Mesenchymal-epithelial transition factor
COX	Cyclooxygenase
CSF	Colony-stimulating factor 1
C-TAD	C-terminal transactivation domain
CXCL16	C-X-C motif ligand 16
CXCR4	C-X-C chemokine receptor type 4
CXCR6	C-X-C chemokine receptor type 6
DAMP	Damage-associated molecular pattern
DEC1	Deleted in esophageal cancer 1
DR	Death receptor
ECM	Extracellular matrix
EGF	Endothelial growth factor
Em	Emission
EMT	Epithelial-to-mesenchymal transition
EPC	Endothelial progenitor cells
EPO	Erythropoietin
ER	Endoplasmic reticulum
ERK1/2	Extracellular signal-regulated kinase 1 and 2
ES cells	Embryonic stem cells
Ex	Excitation
FAD	Flavin adenine dinucleotide
FasR	First apoptosis signal receptor
FH	Fumarate hydratase
FIH	Factor inhibiting HIF-1
$G_{1/2}$ phase	Gap 1 and 2 phase (cell division cycle)
GAPDH	Glyceraldehyde-3-phosphate dehydrogenase
GFP	Green fluorescent protein
GI_{50}	Half maximum growth inhibitory concentration
GINS	Go-ichi-ni-san

GLUT1/3	Glucose transporter 1 and 3
HDAC3	Histone deacetylase 3
HES1	Hairy and enhancer of split-1
HEY1	Hairy/enhancer of split related with YRPW motif protein 1
HIF-1	Hypoxia-inducible factor 1
HK2	Hexokinase 2
HMME	Hematoporphyrin monomethyl ether (photosensitizer)
HMOX1	Heme oxygenase 1
HRE	Hypoxia response element
HSF1	Heat shock factor 1
i.p.	Intraperitoneal (administration)
i.v.	Intravenous (administration)
IC_{50}	Half maximum inhibitory concentration
ICAM-1	Intercellular adhesion molecule-1
IGF	Insulin-like growth factor
INK4	Inhibitor of CDK4
KIP	Kinase inhibitory protein
LC_{50}	Half maximum lethal concentration
LD_{50}	Half maximum lethal dose
LDHA	Lactate dehydrogenase A
LDIO	Lowest dose causing death
LDL	Low-density lipoprotein
LogP	Octanol:water partition coefficient
LOX	Lysyl oxidase
M phase	Mitotic phase (cell division cycle)
MAD	MAX dimerization protein 1
MAX	MYC-associated factor X
Max. TLD	Maximum tolerated dose
MC540	Merocyanine 540 (photosensitizer)
MCL1	Myeloid cell leukemia-1
MCM2-7	Minichromosome maintenance complex component 2 to 7
MCP-1	Monocyte chemoattractant protein 1
MCT4	Monocarboxylate transporter 4
MDM2	Mouse double minute 2
MET	Mesenchymal-to-epithelial transition
MHC1	Major histocompatibility complex 1
MMP	Matrix metalloproteinase
MOMP	Mitochondrial outer membrane permeabilization
MSC	Mesenchymal stem cell
MT-MMP	Membrane-type MMP
mTOR	Mammalian target of rapamycin
MW	Molecular weight
MXI1	MAX interactor 1
NA	Information not available
NAD	Nicotinamide adenine dinucleotide
NADPH	Nicotinamide adenine dinucleotide phosphate
NF-kB	Nuclear factor kappa-light-chain-enhancer of activated B cells
NICD	Intracellular domain of NOTCH
NOTCH1	Notch homolog 1, translocation associated (Drosophila)
NOX1	NADPH oxidase 1

NRF2	Nuclear factor erythroid 2-related factor 2
ODD domain	Oxygen-dependent degradation domain
ORC	Origin recognition complex
PDC	Pyruvate dehydrogenase complex
PDGFB	Platelet-derived growth factor B
PDK1	Pyruvate dehydrogenase kinase 1
PDT	Photodynamic therapy
PFK1	6-Phosphofructo-1-kinase
PFKFK1-4	6-Phospho-2-kinase/fructose 2,6-bisphosphatase
PGC-1β	Peroxisome proliferator-activated receptor-γ coactivator 1β
PGF	Placental growth factor
PGI	Phosphoglucose isomerase
PGK1	Phosphoglycerate kinase
PGM-1	Phosphoglycerate mutase 1
PHD 1/2/3	Prolyl hydroxylase domain 1, 2, and 3
PI3K	Phosphatidylinositol 3-kinase
PK-M	Pyruvate kinase M
PPIX	Protoporphyrin IX (photosensitizer)
PS	Photosensitizer
PTEN	Phosphate and tensin homolog
PTGS2	Prostaglandin-endoperoxide synthase 2
Rac1	Ras-related C3 botulinum toxin substrate 1
Rb	Retinoblastoma
RBX1	Ring box protein 1
RHEB	Ras homolog enriched in brain
ROS	Reactive oxygen species
RPA	Replication protein A
S phase	Synthesis phase
s.c.	Subcutaneous (administration)
SCF	Stem cell factor
SCF^{SKP2}	Skp, cullin, F-box-containing complex and S-phase kinase-associated protein 2
SDF1	Stromal derived factor 1
SDH B/C/D	Succinate dehydrogenase B, C, and D
SLC2A1/3	Gene encoding for glucose transporter 1 and 3
SRC	Rous sarcoma
ssDNA	Single-stranded DNA
$t_{1/2}$	Circulation half-life
TAM	Tumor-associated macrophages
TDLO	Lowest dose causing a toxic effect
TFAM	Mitochondrial transcription factor A
TGFβ	Transforming growth factor β
TNF-α	Tissue necrosis factor alpha
TNFR	Tumor necrosis factor receptor
TPI	Triosephosphate isomerase
TSC2	Tuberous sclerosis complex 2
uPA	Urokinase plasminogen activator
uPAR	uPA receptor
UPP	Ubiquitin proteasome pathway
UTR	Untranslated region
VEGF	Vascular endothelial growth factor

VHL	Von Hippel-Lindau
XBP1	X-box-binding protein 1
ZnPC	Zinc phthalocyanine
ZO-1	Zona occludens-1

1 Introduction

Photodynamic therapy (PDT) is a last-line alternative to conventional cancer therapies such as chemotherapy, radiotherapy, and surgery, especially in cases of inoperable tumors. PDT is a non-to-minimally invasive treatment modality that comprises the topical or systemic administration of a photosensitizer (PS) and its subsequent accumulation in solid tumor tissue, followed by local illumination of the PS-loaded tumor. Photoactivation of the PS is performed with light at a wavelength that aligns with an absorption band of the PS, which typically resides in the therapeutic window (600–800 nm).

Activated PSs can induce chemical changes via two competing pathways, from which either an electron is transferred (type I photochemical reaction) or energy is donated (type II photochemical reaction) to molecular oxygen. Molecular oxygen is thereby converted to the reactive oxygen species (ROS) superoxide anion ($O_2^{\bullet -}$) and singlet oxygen ($^1O_2$), respectively [1]. Type I reactions can also entail electron transfer to biomolecules. The photogenerated ROS and radical transients and their chemical and metabolic derivatives induce a state of hyperoxidative stress, ultimately culminating in cancer cell death, thrombosis-mediated vascular shutdown and consequent hypoxia, and an antitumor immune response. The immune system is mobilized through receptor-mediated signal relay by tumor-associated antigens, damage-associated molecular patterns (DAMPs), and/or cell death-associated molecular patterns (CDAMPs) that leak from PDT-afflicted cells [2–4].

Cancer cells that are exposed to sublethal levels of ROS/radicals or those that are less stricken by the ramifications of tumor vascular shutdown may activate survival pathways, culminating in an increase in therapeutic recalcitrance and tumor regrowth. Survival signaling generally correlates with the three-dimensional tumor architecture. Bulky, rapidly growing tumors in particular may harness tissue regions that are less amenable to PDT due to insufficient PS buildup in sparsely vascularized sections, poor optical penetration, and low fluence rates in distally located tumor regions (relative to the light source), or inadequate local oxygenation that impedes ROS production.

PDT-induced survival signaling can be stratified into five main pathways that include (1) an antioxidant response mediated by nuclear factor erythroid 2-related factor 2 (NRF2); (2) a hypoxia-induced stress response mediated by hypoxia-inducible factor 1 (HIF-1); (3) an inflammatory response mediated by nuclear factor kappa-light-chain-enhancer of activated B cells (NF-κB); (4) an immediate early stress response in reaction to endoplasmic reticulum (ER) stress and ASK-1 activation, mediated by AP-1; and (5) a proteotoxic stress response mediated by transcription factors ATF4, ATF6, HSF1, and XBP1. The survival pathways are summarized in Fig. 1 [5–7]. The PDT-induced survival pathways regulate angiogenesis, apoptosis, glucose metabolism, inflammation, and protein refolding, among others, and enable sublethally afflicted cancer cells to cope with hyperoxidative stress and damage. Survival signaling may be countered by using pharmacological inhibitors that can be administered before PDT together with the PS [5].

Through its regulation of more than 500 genes, HIF-1 is one of the most influential tumor survival pathways that can contribute to the recovery and progression of PDT-subjected cancer cells. HIF-1 is induced not only by ROS but also by PDT-mediated vascular shutdown (*see* Fig. 1). Vascular shutdown can be considered a double-edged sword, on the one hand inducing apoptosis through metabolic catastrophe and on the other hand activating survival signaling in cancer cells. Correspondingly, pharmacological blockade of HIF-1 (survival) signaling is expected to increase the therapeutic efficacy of PDT [6]. Proof of concept was recently provided in vitro, where human epidermoid carcinoma (A431) cells photosensitized with liposomal zinc phthalocyanine were killed more effectively under hypoxic conditions when the selective HIF-1α inhibitor acriflavine was co-administered with the PS delivery system [8, 9]. However, acriflavine is not the only eligible inhibitor of the HIF-1 signaling pathway. This review therefore first addresses the involvement of HIF-1 in cancer biology and the hypoxic response mechanisms. Next, a detailed overview of inhibitors that directly or indirectly interfere with HIF-1 pro-tumorigenic signaling is provided to pave the way for novel fourth-generation PSs, pharmacological intervention strategies, and PDT modalities.

2 HIF-1 in Cancer Biology

HIF-1 is a transcription factor that responds to changes in intracellular oxygen levels. Rapid cancer cell proliferation often outpaces the development of tumor vasculature required for the provision of nutrients and oxygen to sustain cell metabolism. In response, cancer cells activate an inflammatory response and augment

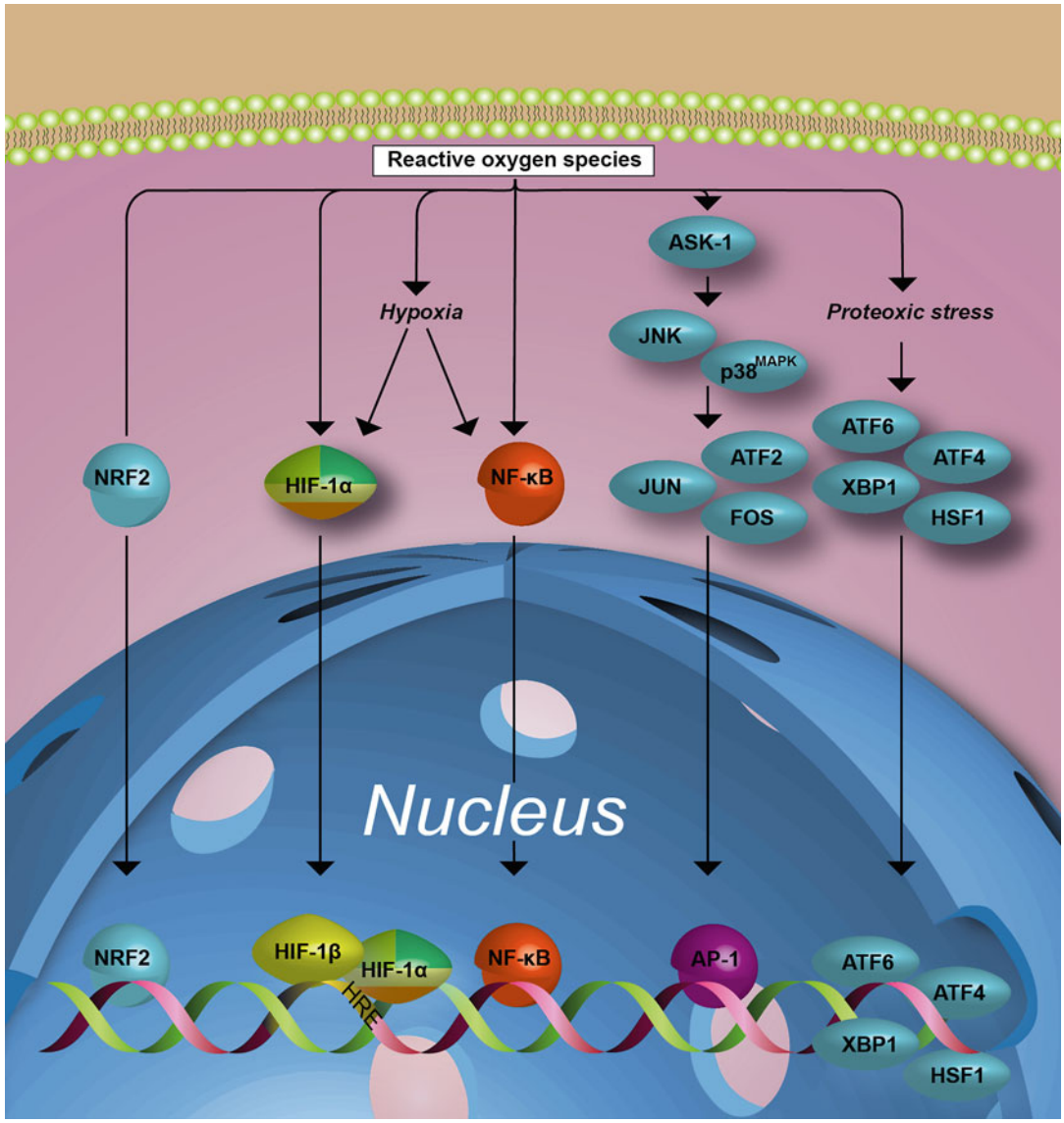

Fig. 1 PDT-activated survival mechanisms. Photoproduced ROS are capable of inducing (1) an antioxidant response through NRF2, (2) a hypoxic stress response through HIF-1α, (3) an inflammatory response through NF-κB, (4) an immediate early stress response through AP-1, and (5) a proteotoxic stress and unfolded protein response (also known as the heat-shock response) through ATF4, ATF6, HSF1, and XBP1

intracellular levels of HIF-1, resulting in increased transcriptional activity of HIF-1 target genes [10]. Direct target genes of HIF-1 have been associated with multiple key biological processes that govern tumor survival such as vascularization, anti-apoptotic signaling, switch to glucose metabolism, proliferation, and metastasis [11–13].

2.1 Activation of HIF-1

2.1.1 HIF-1 Activation by Hypoxia

Functional HIF-1 is a nuclear heterodimeric protein consisting of HIF-1α and HIF-1β subunits. HIF-1β is constitutively expressed irrespective of intracellular oxygen levels and permanently located in the nucleus. HIF-1α is the oxygen-responsive transcriptional activator that resides in the cytoplasm under normoxic conditions [14].

HIF-1α is actively catabolized through the ubiquitin proteasome pathway (UPP) under normoxic conditions. After de novo synthesis, HIF-1α is rapidly hydroxylated by prolyl hydroxylase domain (PHD) 1, 2, and 3 enzymes at two prolyl residues (Pro402 and Pro564) in the oxygen-dependent degradation domain, after which HIF-1α interacts with the von Hippel-Lindau (VHL) protein, the substrate recognition domain of the VHL E3 ubiquitin ligase complex [15]. Subsequently, HIF-1α is polyubiquitinated by the VHL E3 ubiquitin ligase complex. This complex consists of cullin 2, RBX1 (RING-box protein 1), elongin B and C, and VHL. Polyubiquitination further requires the assistance of the E1 ubiquitin-activating enzyme and the E2 ubiquitin-conjugating enzyme. Polyubiquitinated HIF-1α is delivered to the 26S proteasome in the cytoplasm by the VHL complex, where it is degraded, resulting in abrogation of HIF-1 signaling [15–19]. Additionally, factor-inhibiting HIF-1 (FIH-1) hydroxylates an asparagine residue (Asn803) in the C-terminal transactivation domain (C-TAD) of HIF-1α, preventing HIF-1α C-TAD interaction with the CH-1 domain of the transcriptional co-activator p300, thereby inhibiting HIF-1 transcriptional activity [20].

PHD and FIH enzymes are inhibited as the intracellular oxygen levels decrease, leading to less HIF-1α hydroxylation and a lower rate of proteasomal degradation. This effectuates stabilization and nuclear translocation of HIF-1α, where HIF-1α dimerizes with HIF-1β and recruits the p300/CBP family of coactivators. Binding of the HIF-1/p300/CBP complex to the hypoxia response elements (HRE) at the HIF-1 5′-(A/G)CGTG-3′ consensus sequences on DNA initiates transcription of genes. The transcription of HIF-1 genes is conducive to cell survival under hypoxic conditions and elaborated in Subheadings 2.2 through 2.6. The HIF-1α signaling pathways are depicted in Fig. 2 [21–23].

2.1.2 HIF-1 Activation by ROS

As explained in the previous section, cytosolic HIF-1α levels are increased through inactivation of dioxygenases such as PHDs and FIH-1 and corollary preclusion of HIF-1α ubiquitination. The activity of PHDs and FIH-1 is dependent on Fe^{2+} and 2-oxoglutarate (2OG; also known as α-ketoglutarate). Inactivation of dioxygenases can thus be achieved through the depletion of Fe^{2+} ions, as these are an essential cofactor in the hydroxylation of HIF-1α [24–26].

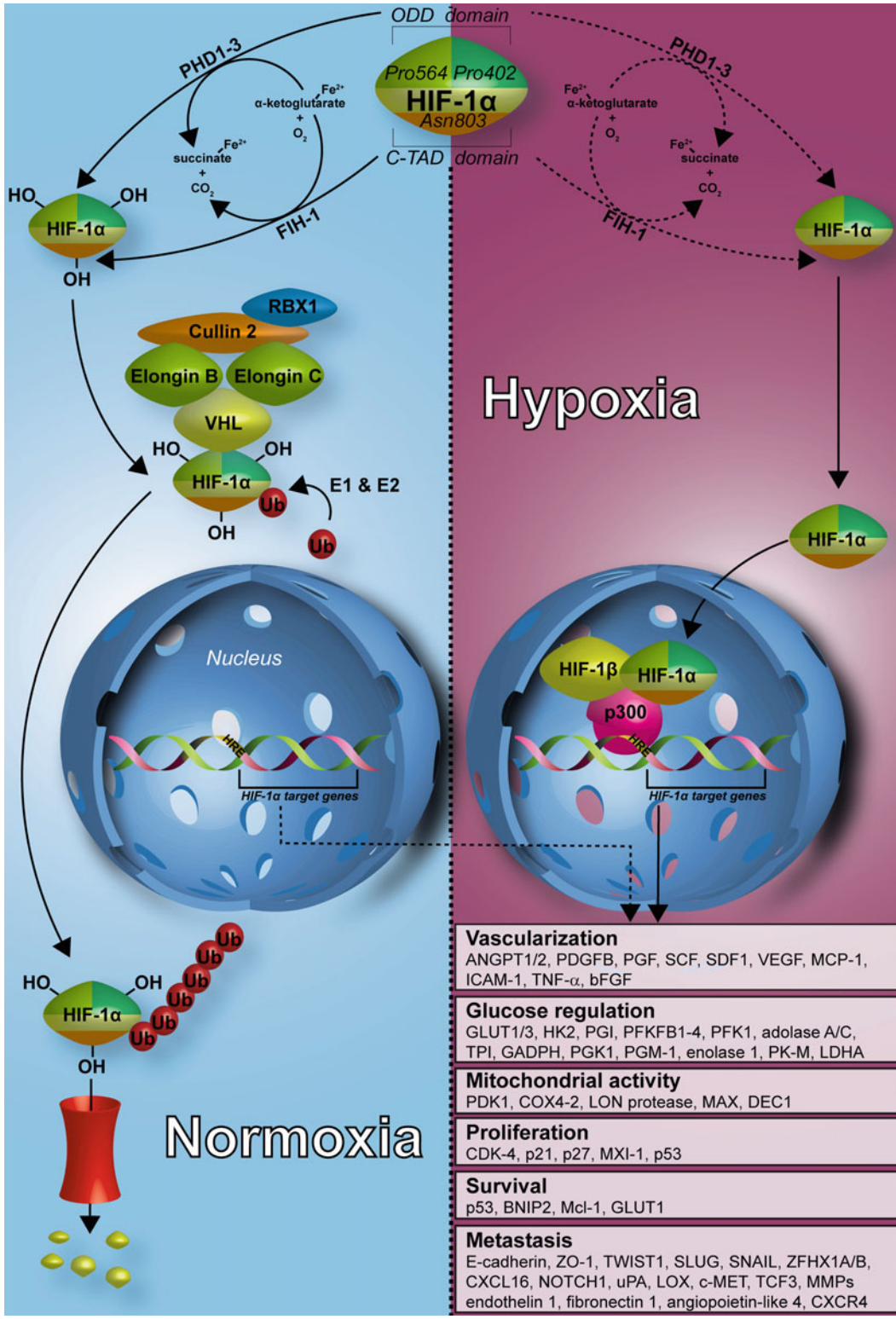

Fig. 2 Hypoxia-induced activation of HIF-1 signaling. Under normoxic conditions (left panel), HIF-1α is actively hydroxylated by PHD1-3 at Pro402 and Pro564 and by FIH-1 at Asn803 in the cytoplasm. The hydroxylation requires molecular O_2, Fe^{2+}, and α-ketoglutarate. The VHL E3 ubiquitin ligase complex (consisting of Rbx1,

Under normoxia and in the absence of redox stress, an Fe^{2+} ion is chelated by the 1-carboxylate and 2-oxoacid functional groups of the co-substrate 2OG of the PHD and FIH-1 enzymes. The 5-carboxylate of 2OG forms hydrogen bonds with a distinct sub-site of PHDs and FIH-1, as well as with HIF-1α. Subsequently, PHD and FIH-1 split O_2 and incorporate one oxygen atom into a Pro402, Pro564, or Asn803 residue of HIF-1α and the other at the 2-carbon of 2OG (oxidative decarboxylation), forming hydroxylated HIF-1α, succinate, and CO_2 [24–26]. The hydroxylated HIF-1α is then polyubiquitinated and proteasomally degraded.

It has been demonstrated that ROS and nitric oxide (NO) are capable of oxidizing Fe^{2+} to Fe^{3+} and thereby inhibit the catalytic activity of PHD and FIH-1, effectuating HIF-1α stabilization and accumulation [25]. ROS-mediated inactivation of HIF-1α hydroxylation and degradation can be actualized in multiple ways. First, ROS produced in mitochondria are capable of inactivating HIF-1α hydroxylation, even under normoxic conditions [27]. Second, hypoxia increases mitochondrial ROS production at mitochondrial complex III, although the exact mechanism is elusive [28]. Lastly, nicotinamide adenine dinucleotide phosphate (NADPH) oxidases (NOXs) contribute to ROS production in both hypoxic and normoxic environments [27, 29]. NOX1 is a membrane-bound $O_2^{\bullet -}$-producing flavin dehydrogenase. NOX1 knockdown with short hairpin RNAs inactivated HIF-1α in cultured colon cancer (HT-29) cells and mouse xenografts. Moreover, NOX1 knockdown was associated with a two- to threefold increase in tumor cell doubling time, reduced vascular endothelial growth factor (VEGF) levels, and decreased blood vessel density [30]. Mitochondrial and NOX1-mediated production of ROS during hypoxia therefore promotes HIF-1 signaling and transcriptional regulation of downstream target genes, ultimately leading to increased cancer cell proliferation and vascularization.

2.1.3 HIF-1 Activation by NF-κB

NF-κB is a family of proteins that modulate the inflammatory response and function as transcription factors that act on genes involved in immunity, inflammation, apoptosis, and HIF-1α signaling [31]. The NF-κB family consists of at least five proteins

Fig. 2 (continued) cullin 2, elongin B and C, and VHL) subsequently mediates the polyubiquitination of hydroxylated HIF-1α, marking it for proteasomal degradation (red cylinder) and ensuring a low level of active HIF-1α. Under hypoxic conditions (right side) the absence of molecular oxygen prevents PHD1-3- and FIH-mediated hydroxylation. Consequently, polyubiquitination and proteasomal degradation are stalled, leading to the cytoplasmatic accumulation of HIF-1α. HIF-1α subsequently translocates to the nucleus, where it heterodimerizes with HIF-1β and complexes with p300/CBP coactivators (depicted as p300). The HIF-1/p300/CBP complex binds to hypoxia response elements (HREs) on DNA to initiate gene transcription. An overview of HIF-1-activated processes and responsible regulators is provided in the bottom right corner. The dashed arrows in the Hypoxia panel indicate the process as it would be under normoxic conditions

(NF-κB1, NF-κB2, RelA, RelB, and RelC) that perform their activity as homodimeric and heterodimeric complexes [31, 32]. NF-κB proteins recognize and are activated by inflammatory stimuli and/or hypoxia. The mature NF-κB transcription factors p50 (NF-κB1) and p65 (RelA) bind to the HIF-1α promotor, resulting in transcriptional upregulation of HIF-1α. RelC regulates transcription of miR-93 and miR-199a-5p, two microRNAs that promote Dicer1-mediated HIF-1α downregulation through 3'UTR (untranslated region) binding. However, miR-93 and miR-199a-5p transcription and Dicer1 levels are reduced under acute hypoxic conditions but rescued under prolonged hypoxic conditions. This leads to a sliding scale where HIF-1 is upregulated under acute hypoxia and subsequently downregulated when hypoxia persists [33]. Moreover, selective inhibition of NF-κB by pyrrolidine dithiocarbamate results in reduced HIF-1 transactivation and concomitant reduction in erythropoietin (EPO), [34] a cytokine secreted mainly by renal fibroblasts in response to cellular hypoxia that stimulates erythropoiesis to resolve the low oxygen levels by augmenting oxygen transport.

2.1.4 HIF-1 Activation Through Loss/Gain-of-Function Mutations

Cancer cells thrive on genetic mutations that boost their growth, invasion, and survival capacity. Mutations that lead to upregulation of HIF-1α may potentiate tumor vascularization. For example, loss-of-function mutations in succinate dehydrogenase (SDH) subunits B/C/D, fumarate hydratase (FH), VHL, and p53 yield blockade of HIF-1α ubiquitination and subsequent decrease in proteasomal degradation, leading to HIF-1α accumulation [35].

Loss-of-function mutations in TSC2 (tuberous sclerosis complex 2), a protein responsible for inhibiting RHEB (Ras homolog enriched in brain) and thereby the mTOR (mammalian target of rapamycin) pathway with HIF-1α as downstream target, might lead to upregulated HIF-1α synthesis [35, 36]. Phosphatase and tensin homolog (PTEN) is a protein that blocks phosphatidylinositol 3-kinase (PI3K) signaling through inhibition of PIP3-dependent membrane recruitment and subsequent activation of protein kinase B (Akt), the upstream activator of mTOR. Therefore, loss-of-function mutations in PTEN may also result in the upregulation of HIF-1α synthesis [35, 37].

Alternate reading frame product ($p14^{ARF}$) on the INK4a/ARF locus codes for a tumor-suppressor protein that is responsible for blocking mouse double minute 2 (MDM2) E3 ubiquitin ligase activity and nucleolar sequestration. This prevents p53 ubiquitination and proteasomal degradation and RB (retinoblastoma) protein inactivation, resulting in cell cycle arrest in the G_1 and G_2 (Gap 1 and Gap 2) phases (more information on the influence of HIF-1 on the cell cycle is presented in Subheading 2.4) [35, 38–40]. Similarly, $p14^{ARF}$ represses HIF-1α transcriptional activity through nucleolar sequestration. Loss-of-function mutations in $p14^{ARF}$ may therefore lead to increased transcriptional activity of HIF-1α [41].

SRC (Rous sarcoma) is a proto-oncogene that stimulates cancer cell proliferation, angiogenesis, and survival upon overactivation due to gain-of-function mutations, transgressing it to an oncogene. SRC is involved in many pathways that may activate HIF-1 depending on cell type and activating signals. One route is PHD2 inhibition through ROS production via NOX that involves Rac1 (Ras-related C3 botulinum toxin substrate 1). Another route is through SCR-induced upregulation of the cap-dependent translation apparatus. Gain-of-function mutations in SRC may translate to stabilization or upregulation of HIF-1α [35, 42, 43].

2.2 HIF-1-Mediated Angiogenesis

Prolonged hypoxia, as often found in solid tumors, stresses cellular metabolic demand for oxygen and usually concurs with rapid tumor growth in conjunction with lagging angiogenesis. Tumors resolve a hypoxic state by biochemically engineering vascular plexuses for the supply of oxygenated blood. Increased vascularization of hypoxic tumors is achieved by angiogenesis, vasculogenesis, and possibly arteriogenesis.

Angiogenesis is the foremost mechanism for tumor neovascularization and involves the formation and branching of new capillaries from preexisting blood vessels. HIF-1 upregulates the vast majority of angiogenic growth factors that steer neovascularization through transcriptional modulation. This includes but is not limited to angiopoietin 1 and 2 (ANGPT1 and 2), platelet-derived growth factor B (PDGFB), placental growth factor (PGF), stem cell factor (SCF), stromal derived factor 1 (SDF1), and VEGF. How angiogenesis is regulated by HIF-1 differs per cell type [44, 45]. The upregulated growth factors are excreted by cancer cells and bind to cognate membrane receptors on the cell surface of proximal vascular endothelial cells and vascular pericytes, activating signaling cascades that lead to capillary formation.

Vasculogenesis entails the formation of blood vessels from circulating vascular progenitor cells, endothelial progenitor cells (EPCs), and pericyte progenitor cells [22, 44]. Whereas angiogenesis is the predominant mechanism at the onset of tumor vascularization, vasculogenesis takes over the formation of blood vessels when angiogenesis is abrogated after, e.g., tumor irradiation [44].

Arteriogenesis encompasses remodeling of preexisting arterioles by increasing the luminal diameter, thereby increasing blood flow. Although there is no direct evidence for intratumoral arteriogenesis owing to hypoxia, HIF-1α has been shown to upregulate genes that play key roles in this mechanism. One of the genes encodes for monocyte chemoattractant protein 1 (MCP-1), a protein that plays a role in the initiation of arteriogenesis through attraction of monocytes and upregulation of Mac-1, a monocyte receptor for intercellular adhesion molecule-1 (ICAM-1). ICAM-1 enables adherence and subsequent migration of monocytes into the arteriolar wall, allowing monocytes to locally secrete cytokines such

as tumor necrosis factor alpha (TNF-α) and basic fibroblast growth factor (bFGF) to promote arterial growth. Other HIF-1-α-upregulated genes that are important in arteriogenesis include VEGF and PGF [22, 46–48].

2.3 Regulation of Cancer Cell Metabolism by HIF-1

2.3.1 Glucose Metabolism

To understand how HIF-1 affects energy metabolism in cancer cells it is important to provide a backdrop on aerobic respiration (normoxic conditions) and lactic acid fermentation (hypoxic conditions) (*see* Fig. 3). The most efficient means of adenosine triphosphate (ATP) production is aerobic respiration, where glucose is catabolized in the cytoplasm to pyruvate via glycolysis. Glycolysis requires an investment of one glucose and two ATP molecules and yields 2 pyruvate +2 NADH +4 ATP + $2H^+$, resulting in a net gain of 2 ATP molecules. Besides ATP, additional energy is stored in NADH that in turn is used in ATP production through oxidative phosphorylation in the presence of oxygen.

Pyruvate is shuttled into mitochondria where it is converted to acetyl CoA by the pyruvate dehydrogenase complex (PDC), netting 2 NADH +2 H^+ + 2 CO_2 per glucose molecule, before entering the Krebs cycle (citric acid cycle). Acetyl CoA is used to generate CoA + 6 NADH +2 $FADH_2$ + 4 H^+ + 4 CO_2 + 2 ATP per glucose molecule. Subsequently, NADH and $FADH_2$ are subjected to oxidative phosphorylation, which entails two steps. First, as part of the electron transport chain, electron carriers (mitochondrial complex I, II, III, ubiquinone, and cytochrome c) located in the inner mitochondrial membrane facilitate the formation of a proton gradient in the mitochondrial intermembrane space through the oxidation of NADH (at complex I) and $FADH_2$ (at complex II) to NAD^+ and FAD, respectively. The electrons from the redox reactions are passed along the electron transport chain to complex IV that reduces an oxygen molecule (terminal substrate) to water. Concurrently, protons in the mitochondrial matrix are transported to the intermembrane space by mitochondrial complexes I, III, and IV. Second, the protons in the intermembrane space reenter the mitochondrial matrix by chemiosmosis that is mediated by ATP synthase (mitochondrial complex V), where ADP is phosphorylated to ATP, resulting in a net gain of 26 or 28 ATP molecules. The net yield depends on which shuttle transports electrons from the two cytosolic NADH molecules to either mitochondrial NAD^+ (final yield 2.5 ATP) or FAD (final yield 1.5 ATP). In sum, the two ATP molecules from glycolysis, the two ATP molecules from the Krebs cycle, and the 26 to 28 ATP molecules from oxidative phosphorylation result in a net maximum gain of 30 or 32 ATP per glucose molecule [49].

During hypoxia, O_2 molecules are no longer available as terminal substrate for oxidative phosphorylation, halting the proton motive force that accounts for the majority of ATP production. Hypoxia therefore forces cells to switch to lactic acid fermentation

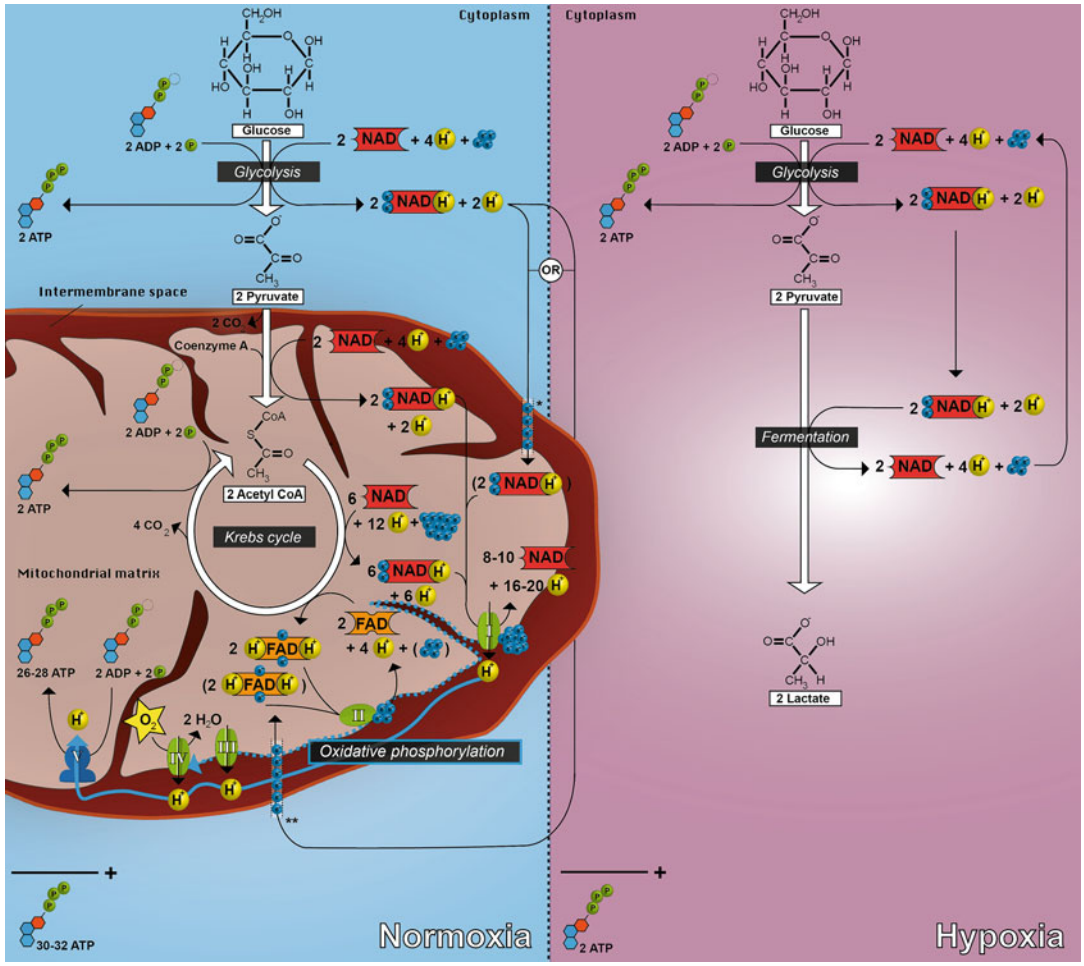

Fig. 3 Glucose metabolism in cells under normoxic and hypoxic conditions. Under normoxia (left panel) glucose is metabolized into 2 pyruvate molecules through glycolysis, yielding 2 ATP, 2 NADH, and 2 H^+. Pyruvate is subsequently transported into mitochondria, where it is converted to 2 acetyl CoA, producing 2 NADH, 2 H^+, and 2 CO_2, after which acetyl CoA enters the Krebs cycle (citric acid cycle). Here, acetyl CoA is used to generate 6 NADH, 2 $FADH_2$, $4H^+$, 4 CO_2, and 2 ATP per glucose molecule. The NADH and $FADH_2$ are then subjected to oxidative phosphorylation, where both molecules undergo oxidation by mitochondrial complexes I and II, respectively. This establishes a proton gradient in the mitochondrial intermembrane space. The protons reenter the mitochondrial matrix via ATP synthase (mitochondrial complex V), producing 2.5 ATP per NADH and 1.5 ATP per $FADH_2$, netting 23 ATP molecules. The 2 NADH molecules from the glycolysis step can enter oxidative phosphorylation by donating a proton through an electron shuttle to either NAD^+ or FADH, which nets another 5 or 3 ATP molecules, respectively. Cumulatively, 30 to 32 ATP molecules are produced per glucose molecule by glycolysis, the Krebs cycle, and oxidative phosphorylation. Under hypoxic conditions (right panel), glucose is catabolized to 2 pyruvate, 2 NADH, 4 ATP, and $2H^+$ by glycolysis (this costs 2 ATP). Subsequently, pyruvate molecules undergo lactic acid fermentation, where pyruvate is converted to lactate and NADH molecules that in turn are oxidized to NAD^+, which is needed for additional glycolysis reactions. This results in a net ATP yield of 2 per glucose molecule

as a source of ATP. Lactic acid fermentation involves the same initial steps of glycolysis, where glucose is catabolized to phosphoenolpyruvate before it is finally catabolized by lactate dehydrogenase A (LDHA) into 2 pyruvate + 2 NADH + 4 ATP + 2 H^+, yielding a net gain of 2 ATP molecules per glucose molecule. Where NADH would be oxidized to NAD^+ by complex I during oxidative phosphorylation under aerobic conditions, the NADH/NAD^+ redox reactions are carried out by LDHA under anaerobic conditions. LDHA mediates the donation of an electron to pyruvate, forming lactate, the ionized form of lactic acid. Two pyruvate molecules are converted to two lactate molecules per glucose molecule [49].

Cancer cells tend to favor lactic acid fermentation as the main source of energy even when oxygen is available (Warburg effect). This is a less efficient means of ATP production than via oxidative phosphorylation, albeit much faster, resulting in an increased glucose demand and turnover. The main difference between hypoxia- and Warburg-driven lactic acid fermentation is that the mitochondria remain active during Warburg metabolism and partially engage oxidative phosphorylation for ATP repletion, which is absent during hypoxia and anoxia [50].

2.3.2 HIF-1-Mediated Glucose Regulation

HIF-1 is an important transcription factor that modulates Warburg metabolism mainly by increasing glycolysis and decreasing mitochondrial function. HIF-1 increases extracellular glucose import through transcriptional upregulation of glucose transporter 1 and 3 (GLUT1/3 or *SLC2A1/3*) [51, 52]. Many genes coding for enzymes that are involved in glycolytic catabolism of intracellular glucose are upregulated by HIF-1, including hexokinase 2 (HK2) [51, 53], phosphoglucose isomerase (PGI), 6-phospho-2-kinase/fructose 2,6 bisphosphatase (PFKFB1–4) [54], 6-phosphofructo-1-kinase (PFK1), aldolase A and C [51, 55, 56], triosephosphate isomerase (TPI) [51], glyceraldehyde-3-phosphate dehydrogenase (GAPDH) [51], phosphoglycerate kinase (PGK1) [51, 55, 56], phosphoglycerate mutase 1 (PGM-1) [57], enolase 1 [56], pyruvate kinase M (PK-M) [57], and LDHA [56–58]. Upregulation of these enzymes facilitates higher catabolic rates in the glucose→lactate conversion steps [56–58]. To counter excessive intracellular lactate accumulation and intracellular lactic acidosis, HIF-1 upregulates the expression of the monocarboxylate transporter 4 (MCT4) protein which subsequently mediates lactic acid efflux into the extracellular environment [59]. The increased level of extracellular lactate results in a more acidic tumor microenvironment [60].

2.3.3 HIF-1 Modulation of Mitochondrial Activity

HIF-1-mediated upregulation of pyruvate dehydrogenase kinase 1 (PDK1) leads to increased PDC phosphorylation, consequently limiting the pyruvate→acetyl CoA conversion and thereby the Krebs cycle. This directs more pyruvate into anaerobic metabolism

(*see* Fig. 3). Moreover, mitochondrial cytochrome c oxidase (CCO), also referred to as mitochondrial complex IV, is a large mitochondrial transmembrane protein complex that catalyzes the reduction of O_2 to H_2O under both normoxic and hypoxic conditions. CCO can contain either the subunit cytochrome oxidase isoform 1 or 2 (CCO–1 or 2). CCO–1 is more efficient under aerobic conditions whereas CCO–2 is more efficient under hypoxic conditions. HIF-1 upregulates CCO–2 and LON protease, a protease that degrades CCO–1, resulting in optimized mitochondrial O_2 consumption and continued Warburg metabolism under hypoxic circumstances [61].

C-MYC is a proto-oncogenic transcription factor that forms heterodimers with MAX (MYC-associated factor X) and binds to E-box sites on DNA to regulate genes involved in proliferation, metabolism, and cell growth. The genetic regulation also exacerbates mitochondrial biogenesis to increase mitochondrial respiration [62]. Increased mitochondrial biogenesis is effectuated by, e.g., c-MYC-upregulated PGC-1β (peroxisome proliferator-activated receptor-γ coactivator 1β) and TFAM (mitochondrial transcription factor A). To skew energy metabolism toward the anaerobic end, HIF-1 upregulates MAX interactor 1 (MXI1) that forms heterodimers with MAD (MAX dimerization protein 1), which in turn binds to E-boxes and recruits mSin3 transcriptional repressor protein and histone deacetylases, thereby antagonizing c-MYC-regulated transcription and curtailing mitochondrial metabolism [63–65].

Finally, HIF-1 upregulates DEC1 (deleted in esophageal cancer 1, also called STR13 or BHLHE40), which functions as a transcriptional repressor for PGC-1α, a central regulator of energy metabolism, leading to decreased expression of TFAM and impaired mitochondrial biogenesis [66].

2.4 Cell Cycle and Proliferation Control by HIF-1

2.4.1 Proliferation and Its Regulation Through the Cell Cycle

Cells are either quiescent (G_0) or actively progressing through the cell cycle to proliferate, grow, and divide. The eukaryotic cell cycle is divided into four main stages: mRNA and proteins are synthesized during the G_1 (first gap) phase, DNA is replicated during the S (synthesis) phase, more mRNA and proteins are produced during the G_2 (second gap) phase, and cell division takes place during the M (mitosis) phase. Progression through the cell cycle is accommodated by specific regulation of cyclins and their complementary cyclin-dependent kinases (CDKs). During the early G_1 phase, cyclin D1, D2, or D3 forms a complex with either CDK4 or CDK6. During the late G_1 phase, cyclin E1 or E2 is complexed with CDK2, which is necessary for the $G_1 \rightarrow S$ phase transition. Together, cyclin D and cyclin E complexes phosphorylate RB, leading to dissociation of RB from E2F transcription factors and freeing of the E2F proteins for DNA replication in the S phase. This

leads to upregulation of various proteins, RNA, and assembly of pre-replication proteins. During the S phase, cyclin A1 and chiefly A2 [67] replace the E-cyclins and complex with CDK2 to initiate DNA replication. From the late S phase till late G_2 phase, cyclin A complexes with CDK1 where cyclin A is eventually replaced by cyclin B1 and B2 [68] to allow cell division during the M phase. An overview is provided in Fig. 4 [69–72]. The cell cycle may be arrested during stress or damage to allow the cell to remediate any potentially deleterious conditions before division. If the situation is not resolved, the cell may revert to G_0 (e.g., as a salvage operation) or enter apoptosis, which is context-dependent [73].

Another layer of regulation occurs at the level of the pre-replication process, which involves the binding of the hexameric origin recognition complex (ORC 1 to 6) to the origins of replication. This subsequently leads to the recruitment of MCM2–7 (minichromosome maintenance complex component 2 to 7)—a hexameric DNA helicase responsible for unwinding DNA as well as CDT1 (chromatin licensing and DNA replication factor 1) and CDC6 (cell division cycle 6), two proteins that are responsible for MCM2–7 inhibition until the onset of the S phase. During the S phase CDKs phosphorylate CDC6 and CDT1, after which they dissociate from the pre-replication complex. Next, CDC7 kinase phosphorylates MCM4, stimulating the association of CDC45 and the GINS complex (go-ichi-ni-san or SLD5, PSF1, PSF2, and PSF3) [72, 74]. Once activated, MCM2–7 unwinds the DNA at the origin to expose the single-stranded DNA (ssDNA) template that is required for the recruitment of replication protein A (RPA) and DNA polymerases, ultimately leading to the initiation of DNA replication. RPA prevents ssDNA from rewinding during DNA replication [72].

The cell cycle is further controlled by CDK inhibitors. CDK activity is regulated by the INK4 (inhibitor of CDK4), CIP (CDK interacting protein), and KIP (kinase inhibitory protein) family of CDK inhibitors ($p15^{INK4B}$, $p16^{INK4A}$, $p18^{INK4C}$, $p19^{INK4D}$, $p21^{CIP1}$, $p27^{KIP1}$, and $p57^{KIP2}$). Inhibition of CDK1 and CDK2 is actuated by $p21^{CIP1}$, $p27^{KIP1}$, and $p57^{KIP2}$. CDK4 and CDK6 inhibition is mediated by $p15^{INK4B}$, $p16^{INK4A}$, $p18^{INK4C}$, $p19^{INK4D}$, $p21^{CIP1}$, and $p27^{KIP1}$ [75, 76].

2.4.2 Cell Cycle Modulation by HIF-1

When the need for energy becomes dire as a result of hypoxia and glucose shortage, energy has to be conserved to prevent metabolic catastrophe and cell death. Inasmuch as proliferative processes require large amounts of energy, ATP utilization is curtailed by HIF-1 upregulation and interference in the c-MYC signaling axis. As addressed in Subheading 2.3.3, c-MYC is a proto-oncogenic transcription factor that positively regulates genes required for proliferation, metabolism, and cell growth. With respect to proliferation, c-MYC regulates the expression of cell cycle proteins [69]

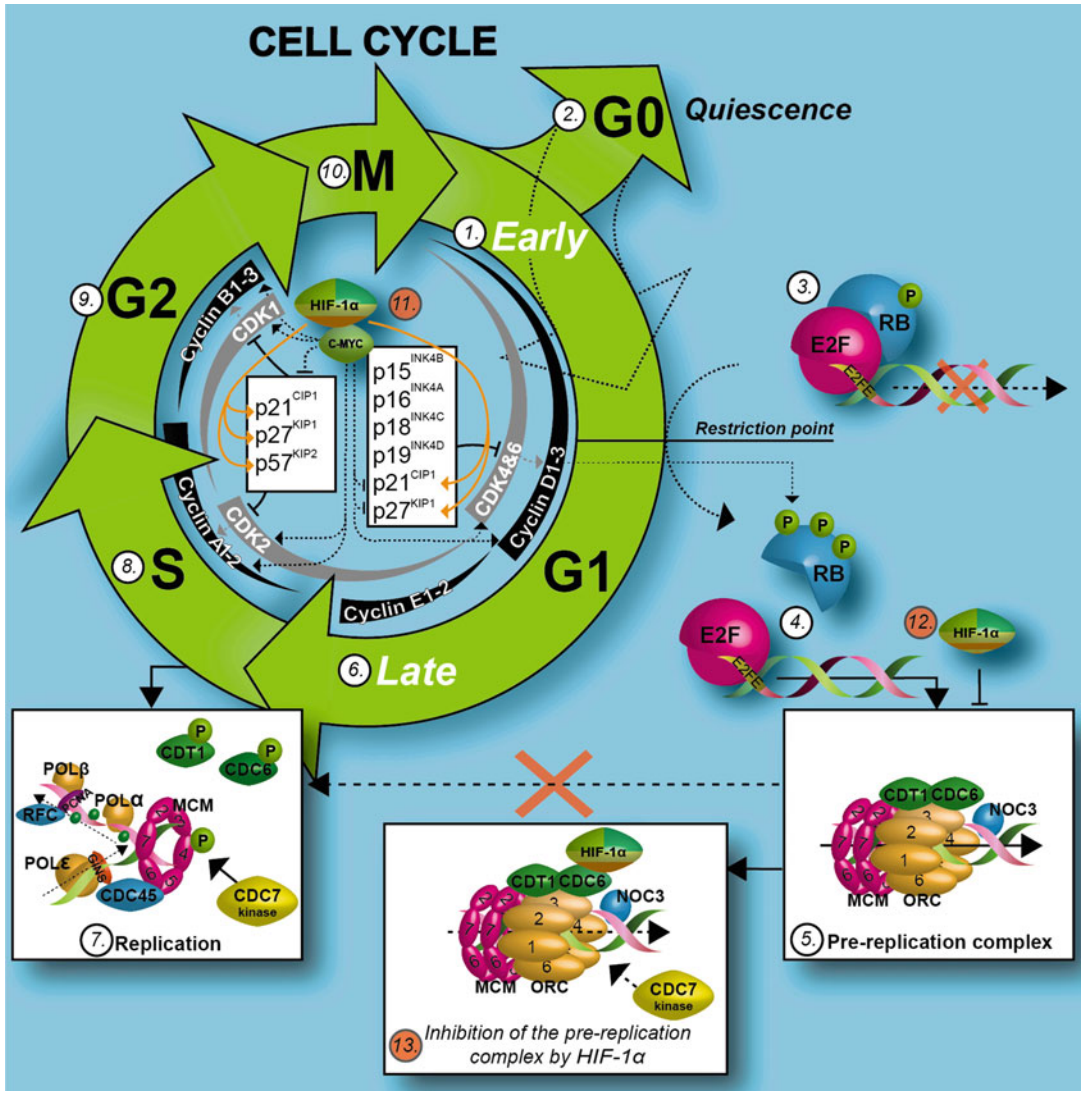

Fig. 4 The cell cycle and points of modulation by HIF-1α (orange points 11, 12, and 13). During the early G_1 phase (1), cyclin D1–3 complexes with CDK4/6. During the late G_1 phase (6), cyclins D and E complex with CDK 2 to facilitate the $G_1 \rightarrow S$ phase transition. Together, cyclins D and E migrate to unphosphorylated RB (3) to hyperphosphorylate RB (4), causing the dissociation of RB from E2F and enabling the upregulation and assembly of the pre-replication protein complex (5). If for any reason not enough of the aforementioned CDKs and cyclins are produced, the cell cycle does not progress past the G_1 restriction points and cells revert to the G_0 phase (2), also known as quiescence or nondividing state. During the S phase (8) cyclins A1 and A2 replace the E cyclins and complex with CDK2, initiating DNA replication (7). From late S phase till late G_2 phase (9), cyclin A complexes with CDK1. During the M phase (10), cyclin A is replaced by cyclins B1, B2, and B3 to initiate cell division. HIF-1α is capable of suppressing c-MYC; preventing c-MYC-mediated induction of CDK 1, 2, 4, 6, and 7 and cyclins D1–3, E1/2, A, and B1; and preventing c-MYC-mediated suppression of the cyclin-dependent kinase inhibitors p15, p21, p27, and p57 (11). This results in the upregulation of said CDKs through the transcriptional function of HIF-1α (orange arrows) and subsequent downregulation of CDK4 and 6 with consequent G_1/S-phase cell cycle arrest. Additionally, HIF-1α can directly inhibit transcription (12) by binding to CDC6 and the MCM complex, leading to the association of MCM proteins with chromatin that in turn decreases DNA replication by preventing CDC7-mediated phosphorylation of MCM4, ultimately resulting in cell cycle arrest (13)

in that c-MYC induces cyclins (D1–3, E1/2, A, and B1) and CDKs (CDK1, 2, 4, 6, and 7) but also represses CDK inhibitors ($p15^{INK4B}$, $p21^{CIP1}$, and $p27^{KIP1}$), thereby preventing their inhibitory effects on the cell cycle. Upregulation of HIF-1 results in reduced CDK4 activity, upregulation of p21 and p27 ("derepression"), hypophosphorylation of RB, and cell cycle arrest in G_0/G_1 [77, 78] supposedly through direct binding of HIF-1 to c-MYC and to c-MYC target consensus sites. HIF-1-mediated upregulation of MXI-1, a c-MYC antagonist, might also result in cell cycle arrest [71]. It is worth noting that HIF-1α-deficient embryonic stem cells (ES) exhibit upregulation of p27 under hypoxic conditions, suggesting that a HIF-1-independent hypoxia-driven derepression mechanism exists [79].

Regulation of proliferation is also instituted through cross talk between HIF-1 and p53. HIF-1 can up- or downregulate p53 [80] depending on the cell type and oxygen level. P53 plays a pivotal role in many similar processes as HIF-1 but is capable of instigating opposite effects. For example, HIF-1 promotes metabolic reprogramming, autophagy, and survival pathways that are inhibited by p53, although both propagation and inhibitory functions are executed by p53 in case of autophagy [80]. HIF-1 could potentially induce cell cycle arrest through the p53-p21 pathway to conserve energy for survival purposes [81]. The HIF-1-p53 signaling axis is important in tumor biology inasmuch as gain- and loss-of-function mutations in the p53 gene are highly prevalent and comprise roughly 50% of all mutations in tumors [82]. Mutations in p53 differentially affect HIF-1 signaling cascades, as exemplified below (e.g., *see* Subheading 2.5.2).

Moreover, a non-transcriptional role for HIF-1α leading to cell cycle arrest in hypoxic colorectal carcinoma (HCT116) cells has been reported [83]. Stabilized HIF-1α subunits are capable of binding to CDC6 and promote nuclear accumulation of CDC6, thereby enabling the interaction between CDC6 and the MCM complex. The binding of HIF-1α to CDC6 increases the association of the MCM proteins with chromatin and decreases CDC7-dependent phosphorylation of the MCM complex, which in turn hampers DNA replication and induces cell cycle arrest. This mechanism [83], illustrated in Fig. 4, is another example of how HIF-1 can revert energy-consuming proliferation under hypoxic conditions for the benefit of metabolic sustenance and survival.

It should be noted that deterrence of proliferation for purposes of energy conservation during hypoxia can proceed independently from HIF-1. One such pathway is mediated by PHD1, which is responsible for hydroxylation of HIF-1α, leading to its ubiquitination and proteasomal degradation (*see* Subheading 2.1.2). PHD1 can be phosphorylated at serine residue 130 in a CDK-dependent manner, reducing its interaction with HIF-1α, but increasing its

association and subsequent hydroxylation of CEP192 (centrosomal protein of 192 kDa) on proline residue 1717—an essential component for centrosome duplication and maturation—leading to ubiquitination of CEP192 by SCF^{SKP2} (Skp, cullin, F-box-containing complex, and S-phase kinase-associated protein 2), proteasomal degradation of CEP192, and G_1 or S (reversible) phase cell cycle arrest due to centrosomal defects [84, 85].

2.5 Regulation of Cell Death and Survival by HIF-1

2.5.1 Modes of Cell Death

To understand how HIF-1 modulates cell death mechanistically, it is key to outline the different modes of cell death. Classically, there are three main cell death pathways, namely apoptosis, necrosis, and autophagy. Apoptosis encompasses programmed (energy-dependent) cell death in response to excessive intracellular damage or binding of signaling molecules to cell membrane receptors, and is executed to maintain healthy tissue populations. Autophagy is an auto-catabolic recycling process involving lysosomes that can steer a cell toward survival or death, depending on the prevailing circumstances. Necrosis is an energy depletion-dependent cell death mechanism mainly caused by external factors such as trauma or toxins. HIF-1 mainly plays a role in the regulation of apoptosis and is capable of inducing and preventing cell death [86]. The following sections are therefore centered on apoptosis in the context of HIF-1 signaling.

Apoptosis entails chromatin condensation, membrane blebbing, phosphatidylserine exposure on the cell surface, cytoplasmic shrinkage, formation of apoptotic bodies, and DNA fragmentation [86, 87]. Apoptosis is triggered through the extrinsic, intrinsic, and immune-mediated pathways. The extrinsic pathway (*see* Fig. 5) requires the activation of transmembrane death receptors (DRs) such as FasR (first apoptosis signal receptor) and TNFR (tumor necrosis factor receptor) via ligand binding and protein cross-linking. DR ligation leads to activation of procaspase-8 and -10, which in turn activate caspase-3 and -7, thereby initiating the execution pathway that ultimately results in apoptosis [88–90].

The intrinsic pathway (*see* Fig. 5) can be activated by lethal stimuli, including but not limited to DNA damage, ER stress, hypoxia, and metabolic stress. These stimuli activate BCL-2 homology domain 3 (BH3)-only proteins, also referred to as BCL-2 family members [91], which in turn activate BAX (BCL-2-associated X protein) and BAK (BCL-2 homologous antagonist killer), leading to BAX- and BAK-mediated mitochondrial outer membrane permeabilization (MOMP). Cytochrome c is then released into the cytosol where it binds to APAF1 (apoptotic protease activating factor 1) proteins, forming the multimeric apoptosome complex. The apoptosome converts procaspase-9 to caspase-9 that subsequently activates caspase-3 and -7. The downstream signaling of caspase-3 and -7 is the same as that for the extrinsic pathway and results in apoptosis [88–90].

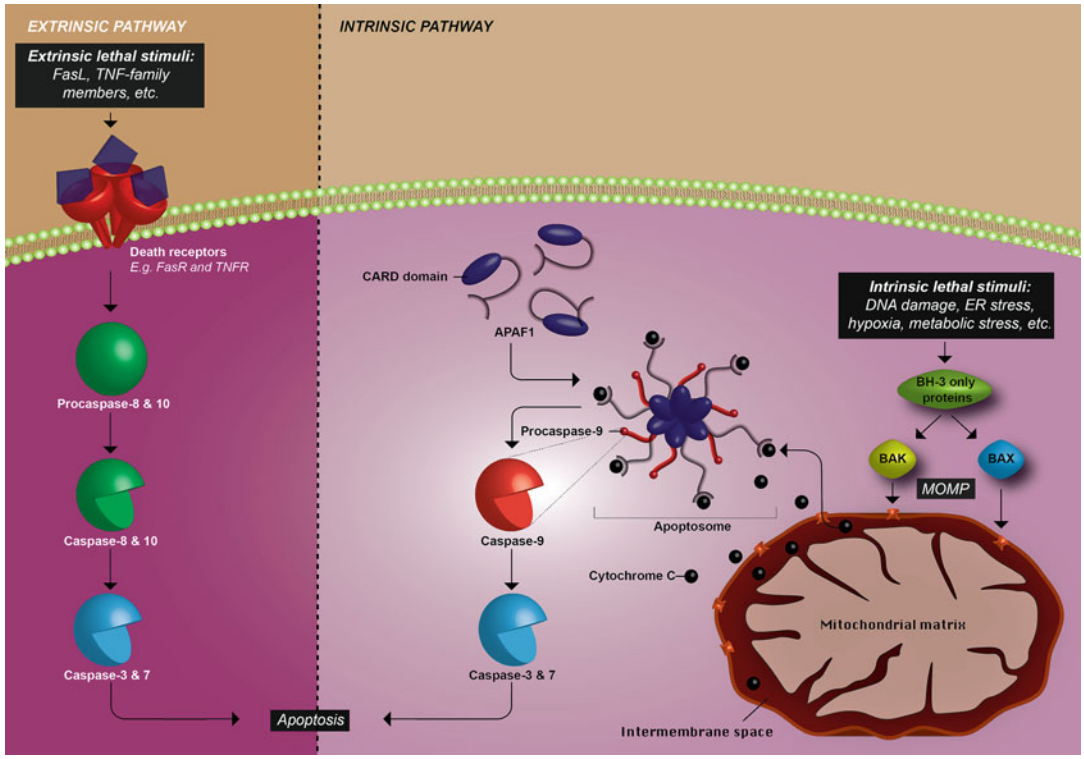

Fig. 5 Intrinsic and extrinsic apoptosis pathways. Extrinsic apoptosis (left panel) features the activation of cell membrane death receptors (DRs) such as FasR and TNFR through extracellular ligand binding and protein cross-linking by, e.g., FasL and TNF family members. Ligated DRs (dark blue squares in red funnel-shaped structures) activate procaspase-8 and -10 that in turn activate caspase-3 and -7. Caspase-3 and -7 initiate the execution pathway that results in apoptosis. Intrinsic apoptosis (right panel) can be triggered by a wide array of stimuli shown in the black box. These stimuli activate BH-3-only proteins, which in turn activate BAK and BAX, leading to mitochondrial outer membrane permeabilization (MOMP). MOMP facilitates cytochrome c release into the cytosol, where it binds to APAF-1 to form apoptosomes together with procaspase-9. The apoptosomes convert procaspase-9 into caspase-9, which activates caspase-3 and -7 and eventually apoptosis

Immunological cell death involves $CD8^+$ cytotoxic T cells that become cross-primed following exposure to tumor-associated antigens (TAAs) conferred by antigen-presenting cells (e.g., dendritic cells, B cells, macrophages). Cancer cells present TAAs via MHC1 (major histocompatibility complex 1) proteins on their outer membrane, which are processed by antigen-presenting cells for cross-presentation to $CD8^+$ cells. Primed $CD8^+$ cells recognize cancer cells and secrete granzymes and perforin (a pore-forming protein), enabling entrance of the granzymes into the target cell. Granzyme B triggers apoptosis via caspase-3 and -8, while granzyme A induces apoptosis by increasing NM23-H1 DNase activity by inactivation of its inhibitor protein, SET. DNA cleavage by DNase leads to p53-mediated BAX and BAK induction and apoptotic signaling as described above and in Fig. 5 [86, 88].

2.5.2 Cell Death and Survival Modulation by HIF-1α

HIF-1α is involved in hypoxia-induced apoptosis, which is modulated via different routes that result in apoptotic or anti-apoptotic signaling depending on prevailing conditions and cell type. Generally, persistent hypoxia, especially when it concurs with other stressors, leads to HIF-1α-induced pro-apoptotic signaling as evidenced by the fact that hypoxia in combination with hypoglycemia reduced proliferation and increased apoptosis in wild-type embryonic stem (ES) cells, but not when HIF-1α was knocked out in ES cells [79].

In the first pro-apoptotic route, hypoxia-stabilized HIF-1α directly binds to MDM2, the E3 ubiquitin ligase that is responsible for p53 degradation, resulting in p53 stabilization. Stabilized p53 in turn activates PUMA (p53 upregulated modulator of apoptosis) that is ensued by BCL-2 downregulation, BAX upregulation, and apoptosis [92–94]. It should be noted that forced overexpression of HIF-1α through transfection of HIF-1α cDNA containing pcDNA3.1/V5-His TOPO-expressing vectors increased BCL-2 and BCL-xL levels in oral squamous cell carcinoma (OSC-4) cells that was accompanied by a reduction in cytosolic cytochrome c accumulation, lower levels of BAX and BAK, reduced activity of caspase-9 and -3, and a lower extent of apoptosis under hypoxia [95].

Second, HIF-1α can interact both directly with the oxygen-dependent degradation (ODD) domain in the basic DNA-binding core of p53 and indirectly following complexation with p300, both leading to stabilization of wild-type p53. HIF-1α does not bind to mutant p53 [96, 97], so this mechanism does not work for a sizeable proportion of cancers given the relatively high prevalence of p53 mutations [82]. HIF-1α-(p300)-p53 interactions can lead to either HIF-1α-mediated inhibition or activation of p53 transcriptional activity. Masking of the p53 DNA-binding core leads to reduced apoptotic signaling, while HIF-1α binding to MDM2 offsets this effect by increasing p53 levels and pro-apoptotic signaling [98].

A third mechanism of pro-apoptotic signaling under hypoxic conditions is based on HIF-1α-mediated upregulation of BNIP3 (BCL-2 nineteen kilodalton interacting protein 3), a BH-3-only and mitochondria-localized transmembrane protein that is overexpressed in the perinecrotic regions of solid tumors. BNIP3 inhibits BCL-2 and BCL-xL, which translates to activation of BAX, BAK, and various caspases to culminate in apoptosis [99–101]. There is evidence that BNIP3 is also capable of mediating autophagic and necrotic cell death pathways [99, 102], all of which can be reduced by growth factors such as insulin-like growth factor (IGF) and endothelial growth factor (EGF) [103].

In terms of anti-apoptotic effects, HIF-1α may deter apoptosis by upregulating myeloid cell leukemia-1 (MCL1), a BH3-only protein, as was demonstrated in immortalized human bronchial epithelial (HBE1) [104, 105] and human hepatocellular carcinoma

(HepG2) cells [106]. MCL1 contains a HIF-1α-specific HRE site through which MCL1 expression is regulated. Forced overexpression of MCL1 in HepG2 cells through transfection of pCMV-HA-Mcl-1 vectors leads to a reduced rate of apoptosis following an oxidative stress stimulus with tert-butyl hydroperoxide (a HIF-1α stabilization event; Fig. 1 and Subheading 2.1.2) compared to cells with normal MCL1 levels [105, 106]. Additionally, HIF-1-α-mediated upregulation of GLUT1 prevented apoptosis in HIF-1α knockdown experiments with A204 rhabdomyosarcoma and A673 Ewing sarcoma cells [105, 107], altogether attesting to the pleiotropic and conditional modulation of cell death signaling by HIF-1α.

2.6 Regulation of Cancer Metastasis by HIF-1

2.6.1 Metastasis

Metastasis involves a series of steps where cancer cells detach and disperse from the primary tumor to distal tissues where they form secondary tumors. Tumors must achieve significant growth to prepare for metastasis. To that end, tumors engage angiogenesis for the supply of oxygen and nutrients to the hypermetabolic, rapidly dividing cells. Following sizable expansion, cancer cells undergo epithelial-to-mesenchymal transition (EMT), a process of biochemical changes where polarized cancer cells with epithelial phenotype, which normally interact with the basement membrane via its basolateral surface, transition into a more mesenchymal-like phenotype. Due to this transition, cancer cells lose their cell-to-cell contact (disassembly of cell-cell junctions) by downregulating E-cadherin and zona occludens-1 (ZO-1) to gain motility [108], enhance invasiveness, increase production of extracellular matrix (ECM) and ECM-altering proteins, and impart resistance to anoikis. Anoikis constitutes a form of programmed cell death in anchorage-dependent cells that occurs when these cells detach from the surrounding ECM [109–111].

EMT is accompanied by enzymatic degradation of the basement membrane, local invasion, and migration toward proximal blood vessels. Metastatic cells cross the pericyte and endothelial cell barriers of blood vessels through a process called intravasation. Upon arrival in the circulation, cancer cells augment their survivability by expressing tissue factors and/or L- and P-selectins, thereby recruiting and activating platelets and forming a thrombus coating that shields the cancer cells from shear forces and immune detection [111, 112]. Depending on the type of carcinoma and the location of the primary tumor, circulating cancer cells migrate to specific distant organ sites by mechanically lodging into capillary beds. Stationary metastatic cells initiate intraluminal growth and form microcolonies, which eventually ruptures the capillary wall and enables the cancer cells to come in contact with the tissue parenchyma. Alternatively, immobilized cancer cells extravasate into the tissue parenchyma. It is hypothesized that primary tumor-derived secreted factors mediate the development of

pre-metastatic niches in distal tissues to eventually provide a hospitable environment to future malignant guests [113]. At the colonized secondary locations, the cancer cells proliferate and form solid tumors. The proliferation of metastasized cells is facilitated by mesenchymal-to-epithelial transition (MET), a process where EMT is reversed and cancer cells gradually reacquire epithelial traits such as interaction potential with the basement membrane, cancer cell cross talk, and rapid proliferation. Currently the MET is mechanistically not fully understood [114]. Lastly, the expanding tumor mass of the new metastasized colonies accounts for the manifestation of hypoxia, resulting in the production and stabilization of HIF-1α (*see* Subheading 2.1.1) and consequent angiogenesis [114, 115].

2.6.2 Metastasis Modulation by HIF-1

HIF-1 regulates transcription of a wide array of genes that differentially contribute to cancer progression. First, as has been demonstrated in renal cell carcinoma (RCC4) cells, HIF-1 promotes metastasis by upregulating the EMT transcription factors TWIST1, SLUG, SNAIL, TCF3, ZFHX1A, and XFHX1B, which bind to the proximal promoter of the cell-cell adhesion molecule E-cadherin and repress its transcription. A reduction in E-cadherin is essential for EMT [108, 116, 117]. In addition, TWIST1 promotes EMT by facilitating invadopodia formation through the induction of the PDGFRα pathway, leading to downstream activation of SRC that in turn activates cortactin, Tks4, and Tks5, which are instrumental in the development of invadopodia [118, 119]. Invadopodia degrade the ECM by secreting various matrix metalloproteinases (MMPs) or by expressing membrane-type MMPs (MT-MMP) [120]. Vasculogenic mimicry formation, the mimicry of embryonic vasculogenic networks by aggressive tumors, has also been attributed to TWIST1 [121].

In a second metastasis-promoting mechanism, elucidated in triple-negative breast cancer (MDA-MB-231) cells, a positive feedback loop is created in which C-X-C motif ligand 16 (CXCL16) secretion into the extracellular environment is stimulated by HIF-1. CXCL16 binds to C-X-C chemokine receptor type 6 (CXCR6) on the surface of mesenchymal stem cells (MSCs), prompting MSCs to secrete CXCL10. CXCL10 in turn binds to CXCR3 receptors on the breast cancer cells, leading to additional MSC recruitment. MSCs then initiate a second loop where C-C motif ligand 5 is produced and secreted, activating C-C chemokine receptor 5 on the breast cancer cells. Subsequently, the breast cancer cells secrete cytokine CSF1 (colony-stimulating factor 1) that binds to CSF1 receptor on MSCs and induces the recruitment of tumor-associated macrophages (TAMs) and myeloid-derived suppressor cells [122]. MSCs further secrete survival factors and transforming growth factor beta (TGFβ) that steer cancer cell EMT [123]. TAMs are stimulated to produce EGF by tumor cell-derived

CSF1, which creates a loop where CSF1 activates TAMs to secrete EGF while tumor cells secrete CSF1. TAM-derived EGF subsequently guides cell migration along collagen fibers toward blood vessels [124].

In a third pro-metastasis signaling axis, HIF-1α potentiates the activation of NOTCH1 (Notch homolog 1, translocation associated (Drosophila)) downstream gene transcription and maintenance in human glioblastoma (U251) cells by stabilizing NOTCH1 through interactions with NICD, the intracellular domain of NOTCH [125]. In human breast cancer (MCF-7 and MDA-MB-231) cells it was demonstrated that the downstream targets of NOTCH1, namely HEY1 (hairy enhancer of split related with YRPW motif protein 1), HES1 (hairy and enhancer of split-1), and NF-κB p65 are important in the EMT process. Knockdown of NOTCH1 with siRNAs abrogated EMT, migration, and invasion [126].

The fourth mechanism hinges on HIF-1 upregulating the transcription of urokinase plasminogen activator (uPA) in cancer cells and cancer-associated fibroblasts (CAFs). uPA is subsequently secreted and binds to uPA receptors (uPAR) on the cell surface of cancer cells. Autocrine and paracrine activation of uPAR leads to activation of ERK1/2 (extracellular signal-regulated kinase 1 and 2) and PI3K, which in turn activates Rac1 and promotes cell migration [127, 128].

HIF-1 also upregulates the transcription of lysyl oxidase (LOX), an enzyme that cross-links the extracellular matrix proteins collagen and elastin, thereby modulating the connective tissue matrices in the extracellular space. LOX upregulation has been associated with both tumor suppression and progression, depending on cellular location, cell type, and transformation status [129, 130]. Angiogenic properties have also been attributed to LOX in colorectal cancers [131].

Additionally, HIF-1 directly or indirectly regulates proteins and/or enzymes that mediate cell-matrix interactions, as well as proteins and/or enzymes that facilitate motility and invasion. Cell-matrix modulation is achieved through the regulation of LOX/-LOX2, HEY1, HES1, and uPA expression. Epigenetic regulators such as histone deacetylase 3 (HDAC3) are required for hypoxia-induced EMT [108].

Finally, the protein products of other HIF-1 target genes can exacerbate the invasiveness of cancer cells. A few examples are mesenchymal-epithelial transition factor (c-MET), endothelin-1, fibronectin-1, MMPs, angiopoietin-like 4 (ANGPTL4), and CXCR4 [132].

3 PDT and HIF-1 Signaling

PDT generates ROS and causes hypoxia as a result of thrombosis-mediated vascular shutdown and conversion of molecular O_2 to ROS that are eventually incorporated into biomolecular structures [133]. Both ROS and hypoxia activate HIF-1(α) (*see* Subheadings 2.1.1 and 2.1.2). This section summarizes the studies that have investigated HIF-1 signaling following PDT, starting with the lowest level of evidence (in vitro studies) and advancing to the most relevant form of empirical proof (clinical trials).

PDT of human cholangiocarcinoma (Sk-ChA-1) cells with liposome-delivered zinc phthalocyanine (ZnPC) resulted in HIF-1α protein stabilization and increased transcription of HIF-1α downstream genes, including *VEGF*, *PTGS2* (prostaglandin-endoperoxide synthase 2), *SERPINE1* (plasminogen activator inhibitor-1), *HMOX1* (heme oxygenase 1), and *BIRC5* (survivin) [6, 8, 9, 134]. Cells were photosensitized with 1.5 μM ZnPC delivered via neutral DPPC:DSPE-PEG liposomes (30-min incubation) [6] or with 30 nM ZnPC delivered via cationic DPPC:cholesterol:DC-cholesterol:DSPE-PEG liposomes (60-min incubation) [9], illuminated with a 671 nm solid-state diode laser (500 mW, cumulative radiant exposure of 15 J/cm^2), and deprived of serum to emulate the hyponutritional status post-PDT. After PDT, cells were maintained in either a normoxic or a hypoxic atmosphere. The priming of cells with the selective HIF-1α inhibitor acriflavine exacerbated the extent of Sk-ChA-1 cell death at 24 h post-PDT in an acriflavine concentration- and hypoxia-dependent manner [9]. Acriflavine caused cell cycle arrest in the S phase and predominantly G_2/M phase. The cells died chiefly by apoptosis and to a mild extent by necrosis. Similar results were obtained in human epidermoid carcinoma (A431) cells, which are monoallelic for P53 [135] that additionally carries an R273H missense mutation, leading to gain of function with respect to evasion and migration but not increased cell cycle progression and cell survival [136]. PDT with liposomal ZnPC caused HIF-1α protein levels to increase under hypoxic conditions and dysregulated the following HIF-1-related genes: *HIF1A* (down), *BCL2* (down), *BIRC5* (down), *PTGS2* (up), *EDN1* (endothelin, down), *HMOX1* (up), and *VEGF* (up) [8]. Co-delivery of acriflavine also significantly augmented the degree of cell death under hypoxic conditions in A431 cells but not in Sk-ChA-1 cells. Finally, HIF-1 pathway activation was independently reproduced in Sk-ChA-1 and A431 cells and observed in human primary endothelial cells as well as mouse (RAW 264.7) macrophages subjected to PDT with liposomal ZnPC (DPPC:cholesterol:DC-cholesterol:DSPE-PEG), although the level of transcriptional dysregulation differed among cell lines [134]. Sk-ChA-1 cells exhibited profound perturbations

in nucleotide and carbohydrate metabolism, glycolysis, and the Krebs cycle, although it was not clear whether these were direct ramifications of the hyperoxidative stress or indirect consequences of HIF-1 transcriptional dysregulation, or both.

Lamberti et al. reported increased HIF-1α transcription levels in human colorectal adenocarcinoma (SW480) spheroids that were genetically engineered to express green fluorescent protein (GFP) under regulation of an HRE promoter. Spheroids were photosensitized with 0.3 mM 5-aminolevulinic acid methyl ester (5-ALA-ME), the prodrug of the PS protoporphyrin IX (PPIX), and illuminated after 4 or 24 h (monochromatic light source emitting at 636 ± 17 nm, irradiance of 0.89 mW/cm^2, cumulative radiant exposure of 0–1.5 J/cm^2). Inhibition of ROS with *N*-acetylcysteine resulted in decreased HIF-1 expression, while RNA interference against HIF-1α downregulated HIF-1α production and reduced resistance against PDT [137].

Ferrario et al. reported an increase in HIF-1α protein expression in cultured mouse mammary carcinoma (BA) cells 5 min after PDT with Photofrin. Cells had been incubated for 16 h with 25 μg/mL Photofrin in medium containing 5% FCS, followed by 30-min incubation in medium containing 10% FCS and illumination (Mylar-filtered fluorescent bulbs, 570–650 nm, irradiance of 0.35 mW/cm^2). An increase in HIF-1α protein levels was also observed in C3H mice bearing mammary carcinoma (BA) xenografts that had been subjected to PDT (5 mg/kg Photofrin i.v., 630 nm argon-pumped dye laser, irradiance of 75 mW/cm^2, cumulative radiant exposure of 200 J/cm^2). The increase in HIF-1α coincided with a strong increase in VEGF protein levels up to 24 h post-treatment [138].

Another study on 5- to 6-week-old male BALB/c nu/nu mice bearing glioma (U251) xenografts reported increased levels of HIF-1α and its downstream target VEGF-A after PDT. Animals received 5 mg/kg hematoporphyrin monomethyl ether (HMME) i.p. and tumors were illuminated with a 630-nm diode laser ~3 h after PS administration (120 J/cm^2 for 10 min). HIF-1α and VEGF-A levels were significantly reduced by combination therapy with the anti-angiogenic agent endostar, a recombinant human endostatin, and HMME-PDT. Kaplan-Meier survival analysis showed that HMME-PDT achieved longer survival than endostatin treatment alone, and that endostatin + HMME-PDT yielded the longest survival [139].

Top-tier evidence for the role of HIF-1 in PDT outcome was provided in a clinical study comprising 37 early esophageal cancer patients. Patients received hematoporphyrin derivative (5 mg/kg i.v.) and PDT was performed after a drug-light interval of 48–72 h (630 nm argon dye laser, 500 mW output power, cumulative radiant exposure of 300 J/cm^2). Illumination was applied through optical fibers with a 1–3 cm linear diffuser tip. A strong increase in

HIF-1α was confirmed by nuclear/cytoplasmic immunostaining of tumor biopsies in 19 tumors. Analysis of HIF-1α and BCL-2 protein levels revealed that only 1 of 16 patients that exhibited both high levels of HIF-1α and an absence of anti-apoptotic BCL-2 protein experienced a complete response compared to 12 out of the 21 remaining patients. Bivariate analysis showed that high HIF-1α expression was independently correlated with an incomplete PDT response, whereas the correlation with high BCL-2 was not significant. Neither HIF-1α nor BCL-2 were significantly associated with local relapse-free survival [140].

4 Inhibition of the HIF-1 Pathway and Its Implications in PDT

HIF-1 is a transcription factor that plays a key role in many pro-tumorigenic processes such as vascularization, glucose metabolism, mitochondrial activity, proliferation, cell survival, and metastasis. Pharmacological inhibition of HIF-1 in cancer cells therefore constitutes a viable strategy to increase the efficacy of therapies that activate HIF-1 signaling [5].

Numerous studies have reported successful inhibition of the HIF-1 pathway using in vitro and in vivo models. The biological end results are often characterized by anti-angiogenic effects, anti-proliferative effects, anti-invasive effects, anti-migratory effects, tumor growth inhibition, G_2/M cell cycle arrest, and apoptosis. Table 1 features a non-exhaustive list of HIF-1 inhibitors with information on the molecular mechanisms, pharmacological effects, biological effects, test models, and application in PDT. The molecular structures and chemical properties are provided in Fig. 6 and serve as a guide for drug selection and formulation development, including nanoparticulate drug delivery systems and fourth-generation PSs [5, 8, 9, 133]. The inhibitors were selected on the basis of their ability to directly or indirectly inhibit HIF-1 signaling. In this last section the focus was placed on studies that investigated HIF-1 inhibitors in the context of PDT. The compounds that have not been investigated in that context can still be considered equally eligible candidates for combinatorial modalities.

With respect to the combination therapies of HIF-1 inhibitors and PDT that are described below, the antitumor efficacy is commonly designated as additive, synergistic, or antagonistic. Additive effects exhibit an end result that is equal to the sum of the individual treatments (i.e., singular inhibitor and singular PDT treatment; $1 + 1 = 2$). Synergistic effects exhibit an end result that is greater than the sum of the individual treatments (i.e., a combination effect that is greater than the expected additive effect; $1 + 1 = 3$) and can therefore be of greater interest. Antagonistic effects exhibit the

Table 1
Non-exhaustive summary of HIF-1α inhibitors and mechanism of action, pharmacological and biological effects, test systems, and application in PDT

Name	Mechanism	Pharmacological effect	Biological effect	Test system	Notes	Tested in PDT
17-AAG (tanespimycin) [7, 142, 221–227]	Inhibition of HSP90 by binding to the amino terminal ATP-binding pocket of HSP90	Downregulation of HIF-1α protein levels and inhibition of HIF-1α transcriptional activity	Anti-angiogenic; anti-invasive; anti-migratory; antiproliferative [142, 225]	*In vitro*: A375, AML, AML-71, BA, Caki-1, UMRC2, UMRC6, 786-O, TGB lymphoma (c-Kit$^+$Sca1$^+$), TGB lymphoma (c-Kit$^-$Sca1$^-$), Mel-Juso, SK-Mel-28, SK-Mel-2, SK-Mel-30, HeLa, Hep3B, HUVEC, HDMEC, MEXF 276 L, MEXF 462 NL, and MEXF 514 L cells *In vivo*: chicken embryo chorioallantoic membrane; BA xenografts in female C3H/HeJ mice (8–12 weeks); HUVEC and HDMEC cell-containing Matrigel plug assay in female C57BL/6N mice (4 weeks); TCR transgenic B line mice with B10.BR background (spontaneous	Less potent than 17-DMAG [227]; combination with Photofrin-PDT reduced Akt, p-Akt, survivin, and p-survivin protein expression compared to the single treatments. Photofrin-PDT-induced HIF-1α was reduced to baseline values, expression and proteolytic activity of MMP-2 and MMP-9 were inhibited, and VEGF expression was reduced when 17-AAG was added [7]	Yes [7]

(continued)

Table 1
(continued)

Name	Mechanism	Pharmacological effect	Biological effect	Test system	Notes	Tested in PDT
				lymphoma development); AML xenografts in SCID mice; B16.F10 xenografts in C57BL/6 mice *Ex vivo*: panel of 64 patient-derived tumor explants, aortic ring from chicken embryos (13 days) overlaid with Matrigel [7, 142, 221, 223, 225–227] *Clinical*: Patients with metastatic or unresectable tumors.		
17-DMAG (alvespimycin) [143, 221, 226–228]	Inhibition of HSP90 by blocking nucleotide binding	Downregulation of HIF-1α protein levels and inhibition of HIF-1α transcriptional activity	Anti-angiogenic; antiproliferative; increased G_2-phase cell cycle arrest (in combination with hypericin-PDT) [143]	*In vitro*: HeLa, Hep3B, HUVEC, HDMEC, SKBR-3, MCF-7, MEXF 276 L, MEXF 462 NL, and MEXF 514 L cells *Ex vivo*: panel of 64 patient-derived tumor explants *In vivo*: HUVEC and HDMEC cell-containing Matrigel	More potent than 17-AAG [227]; combination with hypericin-PDT depleted Akt and p-ERK1/2 and decreased survivin protein levels [143]	Yes [143]

				plug assay in female C57BL/6N mice (4 weeks) *Clinical*: patients with advanced solid tumors [143, 221, 227, 228]		
2-Methoxyestradiol (2ME2) [179–182, 229–231]	Disruption of interphase microtubules by binding to the colchicine-binding site of tubulin	Downregulation of HIF-1α protein levels and inhibition of HIF-1α transcriptional activity	Inhibition of tumor growth; anti-angiogenic; G_2/M-phase cell cycle arrest; apoptosis [181, 182]	*In vitro*: A549, CT-26, LLC, MDC, T47-D, PANC-1, HPAF-II, HPAC, T24, MDA-MB-231, MDR1/231, OE33, HUVEC, U87-MG, HT-29, PC-3, 1A9, 1A9/A8, and 1A9/PTX10 cells *In vivo*: LLC xenografts in male C57BL/6J mice (6 weeks), MDA-MB-231 xenografts in female CB.17 SCID mice (10 weeks), MDA-MB-231 xenografts in female BALB/c nu/nu mice (8–10 weeks); LCC xenografts in $B6D2F_1$ mice; C26 xenograft in BALB/c mice (8-12 weeks); OE33 xenografts in male athymic nude BALB/c nu/nu mice (8 weeks) *Clinical*: patients with	–	Yes 180, 181]

(continued)

Table 1
(continued)

Name	Mechanism	Pharmacological effect	Biological effect	Test system	Notes	Tested in PDT
				refractory solid tumors [179–182, 229–231]		
AC1–004 [232]	Inhibition of HSP90-mediated phosphorylation of Akt and GSK3β	Inhibition of the HSP90-Akt pathway; downregulation of HIF-1α target genes *VEGF* and *EPO*	Inhibition of tumor growth; anti-angiogenic	*In vitro*: HCT-166, Caki-1, SK-HEP1, HUVEC, and MDA-MB-435 cells *In vivo*: MDA-MB-435 xenografts in female athymic Crj:BALB/c nu/nu mice (4–6 weeks)	–	No
Acetyldigoxin [233, 234]	Unclear mechanism	Inhibition of HIF-1α protein expression	Inhibition of tumor growth	*In vitro*: Hep3B-c1 cells	Cardiac glycoside	No
Acriflavine [9, 235, 236]	Inhibition of HIF-1α and HIF-2α dimerization with HIF-1β	Inhibition of HIF-1α dimerization and transcriptional activity	Inhibition of tumor growth; anti-angiogenic; anti-migratory	*In vitro*: HEK293, P493, PC-3, and SK-ChA-1 cells *In vivo*: PC-3 and Hep3B-c1 xenografts in SCID mice	–	Yes [9]
AJM290 [237]	Inhibition of thioredoxin	Upregulation of HIF-1α expression but decrease in transcriptional activity and DNA binding; inhibition of HIF-1α degradation	Anti-angiogenic; antiproliferative; decreased resistance to apoptosis	*In vitro*: MDA-MB-468, MDA-MD-231, MDA-MB-435, RCC4, and 786–0 cells	–	No

Aminoflavone [238, 239]	Inhibition of HIF-1α mRNA expression	Inhibition of HIF-1α transcriptional activity and HIF-1α and HIF-2α protein accumulation [238]	Antiproliferative; inhibition of tumor growth [238, 239]	*In vitro*: MCF-7, MDA-MB-231, MDA-MB-435, PC-3, Ah^{R100}, and MDA/SULT1A1 cells *In vivo*: MCF-7 xenografts in female athymic nude NCr mice [239, 238]	Active component of anticancer agent AFP464	No
Amphotericin B [23, 144, 145]	Inhibition of p300 recruitment by the CAD domain of HIF-1α	Downregulation of HIF-1α transcriptional activity of genes (*EPO*, *VEGF*, *PGK1*, and *ENOL1*) [23]	Combination treatment increases photokilling of MC540-sensitized leukemia cells, wild-type small cell lung cancer cells, and cisplatin-resistant small cell lung cancer cells [145]	*In vitro*: Hep3B, HEK293, CCL 219, H69, hCFU-GM, mCFU-GM, and H69/CDDP cells *In vivo*: Pathogen-free adult male Sprague-Dawley rats [23, 145]	–	Yes [145]
Apicidin [203]	Inhibition of histone deacetylases	Downregulation of HIF-1α protein levels and transcriptional activity of HIF-1α	Pro-apoptotic and anti-angiogenic	*In vitro*: HeLa, B16F10, and 293T (transfected with pSV40pro-EpoHRE-Luc, pBOS-hHIF-1α, and pBOS-hHIF-1β) cells	–	No
Apigenin [240–243]	Inhibition of HSP90 pathway	Increased degradation of HIF-1α and concomitant inhibition of *VEGF* and *EPO* expression [240]	Anti-angiogenic and antiproliferative	*In vitro*: Hep3B, NCI-H157, and HUA-EC cells [243, 240]	–	No
Ascofuranone [244–246]	Inhibition of Akt/mTOR/p70S6 kinase	Suppression of phosphorylation of mTOR, Akt, and p70S6K but not ERK/JNK/p38 kinase	Anti-angiogenic [244]	*In vitro*: MDA-MB-231 and MCF-7 cells *In vivo*: MDA-MB-231 Matrigel plug assay in	–	No

(continued)

Table 1
(continued)

Name	Mechanism	Pharmacological effect	Biological effect	Test system	Notes	Tested in PDT
		through suppression of EGF, leading to decreased HIF-1α and VEGF protein levels [244]		female C57BL/6N mice (6 weeks) [244]		
Ascorbic acid (vitamin C) [146, 147]	Cofactor for proline and asparagine hydroxylases	Downregulation of HIF-1α protein levels and inhibition of HIF-1α transcriptional activity affecting CA-IX, GLUT1, and VEGF protein levels	Inhibition of tumor growth [147]	*In vitro*: HL-60 and U937 cells *In vivo*: B16-F10 and LL/2 xenografts in C57BL/6 Gulo$^{-/-}$ mice [146, 147]	Combination treatment with PDT might be either advantageous, ineffectual, or disadvantageous [147]	Yes [147]
AW464 [237]	Inhibition of thioredoxin	Upregulation of HIF-1α expression but decrease in transcriptional activity and DNA binding; inhibition of HIF-1α degradation	Anti-angiogenic; antiproliferative; decreased resistance to apoptosis	*In vitro*: MDA-MB-468, MDA-MB-231, MDA-MB-435, RCC4, and 786–0 cells	–	No
Baicalein [148, 149, 151–154, 247]	Inhibition of HIF-1α by impairing its nuclear accumulation and activity; inhibition of the LOX pathway	Impairment of MAPK-dependent phosphorylation of HIF-1α; decreased HIF-1α nuclear accumulation	Inhibition of tumor growth; antiproliferative; pro-apoptotic [149, 151, 152]	*In vitro*: AsPC-1, HeLa, MiaPaCa2, Capan2, PANC-1, HT-29, LNCap, CWR22Rv1, C4–2, HPAF, CD18, PC-3, and DU145 cells *In vivo*: HPAC and AsPC-1 xenografts in female BALB/c nu/nu	–	Yes [154]

				mice (5 weeks) [148, 149, 151–154, 247]		
BAY 87–2243 [248]	Inhibition of mitochondrial complex I	Inhibition of HIF-1α and HIF-2α accumulation under hypoxic conditions; downregulation of HIF-1α protein levels and HIF-1α target gene expression	Antitumor activity; antiproliferative under glucose depletion	*In vitro*: H460, RCC4, SH-SY5Y, and H1299luc cells *In vivo*: H460 xenografts in female athymic nude NMRI mice (7–9 weeks)	–	No
Berberine [155, 156, 249, 250]	Inhibition of HIF-1α protein stabilization	Downregulation of HIF-1α transcriptional activity; inhibition of VEGF, COX-2, TNF-α, and NF-κB protein levels [155, 249]	Anti-angiogenic; antiproliferative; anti-migratory [155, 249]	*In vitro*: HUVEC, CL1–5, U87-MG, and SC-M1 cells *In vivo*: B16F-10 xenografts in male C57BL/6 mice (4–6 weeks) [155, 156, 249]	–	Yes [156]
Bortezomib [159, 160, 252]	Inhibition of PI3K/Akt/mTOR pathway through inhibition of the 26S proteasome	Downregulation of HIF-1α protein levels and inhibition of HIF-1α transcriptional activity (*VEGF, CA9, EPO*) and VEGF release; dephosphorylation of p-Akt, p-p70S6K, p-S6RP; inhibition of p44/42 MAPK phosphorylation [160]	Inhibition of tumor growth; anti-angiogenic; pro-apoptotic; combination treatment with verteporfin-PDT exacerbated tumor volume reduction compared to verteporfin-PDT singular treatment [161]	*In vitro*: Hep3B, ARH77, U266, HEK293 (co-transfected with HIF-1α and FIH or p300 plasmids), LNCaP, SVEC4–10, and PC-3 cells *In vivo*: PC-3 xenografts in male athymic nude NRC mice (6–8 weeks) [160, 161]	Combination treatment with verteporfin-PDT resulted in greater accumulation of ubiquitinated proteins post-PDT compared to the PDT-only group	Yes [161]
Caldoramide [253]	Unclear mechanism but known inhibitor of histone deacetylases	–	Inhibition of tumor growth; stronger antiproliferative activity	*In vitro*: HCT116, HCT116$^{HIF\text{-}1\alpha-/-HIF\text{-}}$	IC_{50} values of caldoramide were much higher than	No

(continued)

Table 1
(continued)

Name	Mechanism	Pharmacological effect	Biological effect	Test system	Notes	Tested in PDT
			in cells that contain oncogenic KRAS or HIF transcription factors (compared to knocked-out HIF-1 or oncogenic KRAS)	$^{2\alpha-/-}$, and HCT116$^{WT}_{KRAS}$ cells	dolastatin 10 and largazole for the tested cell lines	
Chaetocin [254, 255]	Inhibition of HIF-1α and p300/CBP complex formation; disruption of the CH1 domain of p300	Downregulation of *VEGFA*, *LDHA*, *ENO1*; lower levels of VEGF	Inhibition of tumor growth; anti-angiogenic	*In vitro*: PC-3, HCT116, and SUV39H1 cells *In vivo*: PC-3 and DU-145 xenografts in male Fox Chase SCID beige mice (5 weeks) *Ex-vivo:* Rat aortic ring assay	–	No
Chetomin [254, 256–258]	Inhibition of HIF-1α and p300/CBP complex formation; disruption of the CH1 domain of p300	Downregulation of *VEGFA*, *LDHA*, *ENO1*, *GLUT1*, and *EPO*; lower levels of VEGF	Inhibition of tumor growth; anti-angiogenic	*In vitro*: Hep3B, HeLa, PC-3 and HCT116 cells; human myeloma cell line panel; bone marrow-derived multiple myeloma cells (patients) *Ex-vivo:* Rat aortic ring assay *In vivo*: PC-3 and DU-145 xenografts in male Fox Chase SCID beige mice (5 weeks); PC-3 and HCT116 xenografts in NCr/nude mice	–	No

Cinnamic aldehyde [259–261]	Inhibition of mTOR activation	Inhibition of HIF-1α and VEGF protein expression	Inhibition of tumor growth; anti-angiogenic; antiproliferative; pro-apoptotic; cell cycle arrest (G_2/M)	*In vitro*: HepG2, Renca, SVEC, and HEK293 (co-transfected with an HIF-1α expression vector) cells; many other systems *In vivo*: Renca xenografts in male BALB/c mice	–	No
Colchicine [179]	Inhibition of HIF-1α pathway through disruption of the microtubule cytoskeleton	Downregulation of HIF-1α protein but not mRNA levels; inhibition of HIF-1α transcriptional activity; inhibition of VEGF	Inhibition of tumor growth; anti-angiogenic	*In vitro*: 1A9, MDA-MB-231, A459, MCF-7, LN229, and PC-3 cells [179]	–	No
Compound 7 [262, 263]	Inhibition of malate dehydrogenase 2	Suppression of HIF-1α accumulation and expression of its target genes (*VEGF* and *GLUT1*); reduction in mitochondrial ATP production; activation of AMPK; inactivation of ACC and mTOR pathways	Inhibition of tumor growth	*In vitro*: HCT116, HeLa, HepG2, and H1073 cells *In vivo*: HCT116 xenografts in female nude mice (6 weeks)	–	No
Compound DJ12 [264]	Inhibition of HIF-1α DNA binding activity	Inhibition of HIF-1α transcriptional activity and downregulation of target genes	Decreased cell viability	*In vitro*: MDA-MB-468, ZR-75, MDA-MB-435, RCC4, and 786–0 cells	–	No
Convallatoxin [234, 265, 266]	Unclear mechanism	Inhibition of HIF-1α protein expression and decrease in *VEGF* mRNA [234, 265]	Antiproliferative; apoptosis [265, 266]	*In vitro*: Hep3B-c1, MCF-7, MDA-MB-231, MDA-MB-468, and U251 cells [234, 265, 266]	Cardiac glycoside	No

(continued)

Table 1
(continued)

Name	Mechanism	Pharmacological effect	Biological effect	Test system	Notes	Tested in PDT
Cucurbitacin B [267–272]	Dephosphorylation of mTOR, p70S6K, 4EBP1, and ERK1/2; activation of Akt [267]	Downregulation of HIF-1α target genes; inhibition of HIF-1α protein synthesis (but not HIF-1α mRNA or HIF-1α degradation); reduction of VEGF secretion [267]	Anti-angiogenic; anti-invasive; inhibition of tumor growth [267, 272]	*In vitro*: SKBR-3, MCF-7, U87, HeLa, SK-Hep1, Hep3B, HEK293 (co-transfected with His-Ub, HA-VHL, and Flag-HIF-1α vectors), and AGS cells *In vivo*: HeLa xenografts in female athymic nude Crj:BALB/c mice (6 weeks) [267, 271, 272]	–	No
Cymarin [234, 270, 273]	Unclear mechanism	Inhibition of HIF-1α transcriptional activity	Decreased cell viability; apoptosis [273]	*In vitro*: A2780, Caov3, and Hep3B-c1 [234, 273]	Cardiac glycoside	No
Daunorubicin [162–165, 274, 275]	Inhibition of HIF-1α DNA binding activity	Downregulation of HIF-1α expression; downregulation of HIF-1α target genes (*VEGF*, *GLUT1*)	Anti-angiogenic; decreased cell viability	*In vitro*: Hep3B-c1, HEK293, A375, SMCC-7721, HeLa, H9c2, PC-3, OVCAR-4, PANC-1, MCF-7, HCT-15, NCI-H460, A-498, and L3.6 cells *In vivo*: Hep3B-c1 and PC-3 xenografts in male SCID mice [162, 164, 165, 274, 275]	Anthracycline	Yes [165, 166]

Deoxysappanone B 7,3′-dimethyl ether acetate [216, 234, 276]	Unclear mechanism	Downregulation of HIF-1α mRNA expression, but no effect on protein levels; downregulation of HIF-1α target genes (*VEGFA, HK2, DPP4, GAPDH, PDK1, ACSL5*, and *ANGPTL4*) [216]	Antiproliferative; decreased cell viability; exacerbated cytotoxicity in cells that express functional HIF-1, HIF-2, and KRAS compared to cells where proteins were knocked out	*In vitro*: HCT116, $HCT116^{HIF\text{-}1\alpha-/-HIF\text{-}2\alpha-/-}$, $HCT116^{WT\ KRAS}$, SN143, SN175, SN179, SN185, and G144 cells	–	No
Digitoxin [277, 278]	Unclear mechanism	Inhibition of HIF-1α protein expression	Antiproliferative	*In vitro*: UACC-62, TK-10, Hep3B-c1, and MCF-7 cells	Cardiac glycoside	No
Digoxin [234, 277, 279–282]	Binding to PKM2 and inhibition of PKM2-triggered transactivation of the HIF-1α gene	Downregulation of HIF-1α protein levels and transcriptional activity of HIF-1α; downregulation of *VEGF*, *G6PC*, *GLUT1*, *HK1*, *HK2*, *SRebf1*, *NDRG1*, and *IL1B* expression	Antiproliferative; inhibition of tumor growth	*In vitro*: Hep3B, Hep3B-c1, RAW 264.7, THP-1, HeLa, HT29, HCT116, CC20, TK-10, MCF-7, UACC-62, and A549 cells *In vivo*: P493-Myc, P493-Myc-Luc, PC-3, PC-3-EV, and PC-3-CA5 xenografts in athymic SCID mice [234, 277, 279–281]	Cardiac glycoside	No
Dihydrotanshinone I (DHTS) [283–285]	Inhibition of HIF-1α protein synthesis through downregulation of mTOR/p70S6K/4E-BP1, and MEK/ERK pathways	Dephosphorylation of mTOR, ERK1/2, p70S6K, 4E-BP1, and elF4E; reduced HIF-1α and VEGF protein expression; increased cleaved caspase-3, cleaved caspase-9,	Inhibition of tumor growth; antiproliferative; apoptosis	*In vitro*: HeLa, Hep3B, AGS, SGC7901, MGC803, and SNU638 cells *In vivo*: HeLa xenografts in female athymic nude Crj:BALB/c mice	–	No

(continued)

Table 1
(continued)

Name	Mechanism	Pharmacological effect	Biological effect	Test system	Notes	Tested in PDT
		cleaved PARP, p-JNK, and p-P38 protein expression				
Diphenylene iodonium (DPI) [167–170, 286]	Inhibition of NADPH oxidases	Downregulation of HIF-1α and VEGF protein levels and HIF-1α transcriptional activity; downregulation of HIF-1α target genes (*VEGF*); downregulation of *Nox1, HDAC4, FEN1*; upregulation of p21, DUSP4 protein levels and PDK4, PPAR-α, PPAR-γ transcript levels; downregulation of cyclin A, D1, and E protein expression [168, 169]	Antiproliferative; inhibition of tumor growth; cell cycle arrest (G_1/S) [168, 169]	*In vitro*: OVCAR-3, A2780, IOSE-386, IOSE-397, HT-29, HeLa, LS-174T, LS-180, Caco2, COH-BR6, MDA-MB-468, BT474, A2058, SK-MEL5, MCF-7, MCF-12A, HEK293, PMN, HL-60, UACC-257, and DU145 cells *In vivo*: HT-29 and LS-174T xenografts in male athymic nude mice (6–8 weeks) [167–170, 286]	Inhibits endogenous ROS production [169]	Yes [170]
Discodermolide [179, 287]	Inhibition of HIF-1α pathway by disruption of the microtubule cytoskeleton	Downregulation of HIF-1α protein but not mRNA levels; inhibition of HIF-1α transcriptional activity; downstream inhibition of VEGF [179]	Inhibition of tumor growth; anti-angiogenic; cell cycle arrest (G_2/M) [179, 287]	*In vitro*: 1A9, A549, and MDA-MB-231 cells [179, 287]	–	No

Docetaxel (Taxotere) [179, 183, 184]	Inhibition of HIF-1α through microtubule stabilization	Downregulation of HIF-1α protein but not mRNA levels; inhibition of HIF-1α transcriptional activity; downstream inhibition of VEGF [179]	Inhibition of tumor growth; anti-angiogenic; apoptosis; cell cycle arrest (G_2/M) [183, 184]	*In vitro*: 1A9, 4T1, and MDA-MB-231 cells *In vivo*: 4T1 xenografts in BALB/c mice [179, 184]	Combination with IR820 co-loaded in micelles + PDT resulted in additive cytotoxic effect	Yes [184]
Dolastatin 10 [216, 253, 288–290]	Unclear mechanism but known to target microtubules	Complete inhibition of HIF-1α protein expression and downregulation of HIF-1α target genes such as *VEGFA* [216]	Antiproliferative; apoptosis [288]	*In vitro*: HeLa, MCF-7, MDA-MB-231, $HCT116^{HIF\text{-}1\alpha-/-HIF\text{-}2\alpha-/-}$, and $HCT116^{WT\ KRAS}$ cells [216, 253, 288]	Dolastatin analog; effects not known on HIF-1α	No
Doxorubicin [163, 173, 274, 275]	Inhibition of HIF-1α DNA-binding activity	Downregulation of HIF-1α expression and HIF-1α target genes such as *VEGF* and *GLUT1*	Anti-angiogenic; decreased cell viability	*In vitro*: HepG2, Hep3B-c1, H9c2, PC-3, OVCAR-4, PANC-1, MCF-7, HCT-15, NCI-H460, A498, and L3.6 cells *In vivo*: Hep3B-c1 and PC-3 xenografts in male SCID mice; HepG2 xenografts in male BALB/c nude mice (6–7 weeks)	Anthracycline	Yes [173]
Echinomycin (NSC-13502) [292, 293]	Inhibition of HIF-1α binding to DNA (specifically the HRE sequence of VEGF)	Inhibition of *VEGF*, *GLUT1*, *BCL2*, *NOTCH1*, *MYC* mRNA expression; suppression of proteins in mTOR/Akt signaling (PTEN, Akt, p-Akt, mTOR, p-mTOR); increased	Antiproliferative; apoptosis	*In vitro*: U251, U251-HRE, U251-pGL3, Jurkat, KOPT-K1, DND-41, THP-1, NB4, and TMD7 cells	–	No

(continued)

Table 1
(continued)

Name	Mechanism	Pharmacological effect	Biological effect	Test system	Notes	Tested in PDT
		cleaved caspase-3 protein levels				
ENMD-1198 [182]	Disruption of interphase microtubules by binding to the colchicine-binding site of tubulin	Downregulation of HIF-1α protein levels; inhibition of HIF-1α transcriptional activity	Increased antiproliferative effect compared to 2-methoxy-estradiol; anti-angiogenic; G_2/M-phase cell cycle arrest; apoptosis	*In vitro*: MDA-MB-231, MDR1/231, U87-MG, PC-3, LCC, HUVEC, and HT-29 cells *In vivo*: LCC xenografts in male C57BL/6J mice (6 weeks), MDA-MB-231 xenografts in female CB.17 SCID mice (10 weeks)	Synthetic analog of 2ME2	No
ENMD-1200 [182]	Disruption of interphase microtubules by binding to the colchicine-binding site of tubulin	Downregulation of HIF-1α protein levels; inhibition of HIF-1α transcriptional activity	Increased antiproliferative effect compared to 2-methoxyestradiol; anti-angiogenic; G_2/M-phase cell cycle arrest; apoptosis	*In vitro*: MDA-MB-231, MDR1/231, U87-MG, PC-3, LCC, HUVEC, and HT-29 cells *In vivo*: LCC xenografts in male C57BL/6J mice (6 weeks), MDA-MB-231 xenografts in female CB.17 SCID mice (10 weeks)	Synthetic analog of 2ME2	No

ENMD-1237 [182]	Disruption of interphase microtubules by binding to the colchicine-binding site of tubulin	Downregulation of HIF-1α protein levels; inhibition of HIF-1α transcriptional activity	Inhibition of tumor growth; anti-angiogenic; cell cycle arrest (G_2/M); apoptosis	*In vitro*: MDA-MB-231, MDR1/231, U87-MG, PC-3, LCC, HUVEC, and HT-29 cells *In vivo*: LCC xenografts in male C57BL/6J mice (6 weeks), MDA-MB-231 xenografts in female CB.17 SCID mice (10 weeks)	Synthetic analog of 2ME2	No
Epirubicin [163, 174, 294]	Inhibition of HIF-1α DNA-binding activity	Downregulation of HIF-1α expression; downregulation of HIF-1α target genes such as *VEGF* and *GLUT1*	Anti-angiogenic	*In vitro*: Hep3B-c1 cells; panel of squamous cell carcinoma cell lines	Anthracycline	Yes [174]
Epothilone B [179, 295–298]	Impaired nuclear accumulation of HIF-1α through extensive microtubule stabilization	Downregulation of HIF-1α protein but not mRNA levels; inhibition of HIF-1α transcriptional activity; downstream inhibition of VEGF	Inhibition of tumor growth; anti-angiogenic; cell cycle arrest (G_2/M); antiproliferative; decreased cell viability	*In vitro*: 1A9, 1A9/A8 (Thrβ^{274}Ile), Hs578T, HeLa, KB3–1, KBV-1, RPMI 8226, U266, MM.1S, MM.1R, and MDA-MB-231 cells; bone marrow-derived multiple myeloma cells (patients) *Clinical:* patients with advanced colon cancer [179, 295–298]	–	No
Ethacrynic acid [257, 299]	Blockade of protein-protein interaction between the CTAD domain of HIF-1α and the CH1 region of p300/CBP	Inhibition of HIF-1α/p300/CBP complex formation; downregulation of HIF-1α target genes, specifically *VEGF*	Decreased cell viability	*In vitro*: HeLa cells	–	No

(continued)

Table 1
(continued)

Name	Mechanism	Pharmacological effect	Biological effect	Test system	Notes	Tested in PDT
ETPs (gliotoxin) [254, 300]	Inhibition of HIF-1α and p300/CBP complex formation; disruption of the CH1 domain of p300	Downregulation of *VEGFA*, *LDHA*, *ENO1*; lower levels of VEGF	Inhibition of tumor growth; anti-angiogenic; antiproliferative	*In vitro*: MCF-7, T47D, BT474, ZR75-1, MDA-MB-231, MDA-MB-435, PC-3, and HCT116 cells *Ex-vivo:* Rat aortic ring assay *In vivo*: PC-3 and DU-145 xenografts in male Fox Chase SCID beige mice (5 weeks); NMU-induced mammary tumors in female (Ludwig/Wistar/Olac) rats	–	No
Everolimus [301, 302]	Inhibition of mTOR by binding to FKBP12	Inhibition of P70S6K, 4E-BP1, and mTOR phosphorylation; downstream suppression of HIF-1α and VEGF protein expression	Inhibition of tumor growth; antiproliferative; cell cycle arrest (G_0/G_1)	*In vitro*: BT474, HER2-overexpressing primary breast cancer, RMG-1, and W3uF cells *In vivo*: RMG-1 xenografts in nude mice (6 weeks); BT474 xenografts in female BALB/c nude mice (4–6 weeks)	–	No
EZN-2208 [303, 304]	Inhibition of topoisomerase I	Downregulation of HIF-1α protein and mRNA expression;	Anti-angiogenic; antiproliferative	*In vivo*: U251-HRE xenografts in female nude mice (6 weeks)	PEGylated conjugate of SN38	No

		downregulation of HIF-1α target genes VEGF, GLUT1, and MMP2 at mRNA and protein levels		*Clinical*: patients with advanced solid tumors (including those who had failed prior irinotecan therapy)		
EZN-2968 [305]	Inhibition of HIF-1α protein synthesis through antagonistic binding of HIF-1α mRNA	Downregulation of HIF-1α protein synthesis and mRNA levels; downregulation of HIF-1α transcriptional targets (*VEGFA*, *MMP-2*)	Inhibition of tumor growth; anti-angiogenic	*In vitro*: 15PC3, PC-3, U373, A549, and DU145 cells *In vivo*: DU145 xenografts in female athymic nu/nu mice (6 weeks)	–	No
Fisetin [153, 243, 306, 307]	Inhibition of HIF-1α	Impairment of MAPK-dependent phosphorylation of HIF-1α; decreased HIF-1α nuclear accumulation; downregulation of HIF-1α, VEGF, eNOS, and survivin protein levels; possibly inhibition of STAT3 [153, 243]	Anti-angiogenic; antiproliferative; G_1 (strong) and G_2/M (moderate) cell cycle arrest; apoptosis [307]	*In vitro*: HeLa, HEK 293, HUVEC, A549, H157, and DU145 cells *In vivo*: HUVEC cell-containing Matrigel plug in male Swiss albino mice (8 weeks) [153, 243, 307]	–	No
FK228 (romidepsin) [308, 309]	Inhibition of histone deacetylase	Downregulation of HIF-1α protein but not mRNA levels; inhibition of VEGF protein expression [308]	Inhibition of tumor growth; anti-angiogenic [308]	*In vitro*: LLC and HT1080 cells *In vivo*: LLC xenografts in male C57BL/6J mice (7 weeks) [308]	–	No
G0811 [310]	Inhibition of HIF-1α protein synthesis	Inhibition of HIF-1α signal transduction; decreased VEGF protein expression	Anti-angiogenic	*In vitro*: HUVEC, HeLa, and HepG2 cells *In vivo*: chicken embryo chorioallantoic membrane	–	No

(continued)

Table 1
(continued)

Name	Mechanism	Pharmacological effect	Biological effect	Test system	Notes	Tested in PDT
Ganetespib [311, 312]	Inhibition of HSP90	Downregulation of MET, EGFR, and Akt protein levels	Inhibition of tumor growth; antiproliferative; induction of tumor regression; cell cycle arrest	*In vitro*: numerous cell lines, particularly NCI-H1975 *In vivo*: MKN45 xenografts in female nude Zrtl:CD1-Foxn1 mice; NCI-H1395 and MV4-11 xenografts in CB-17/Icr-prkdc^{SCID}/Crl mice	Is potent against drug-resistant NSCLC containing EGFR mutations	No
Geldanamycin [313, 314]	Inhibition of HSP90	Increased degradation of HIF-1α protein; inhibition of *VEGF* transcription	Antiproliferative	*In vitro*: PCA, PC-3, and LNCaP cells; panel of 60 human tumor cell lines	Derivative of geldanamycin (17-AAG)	No
GL331 [315, 316]	Inhibition of HIF-1α mRNA expression	Inhibition of HIF-1α transcriptional activity; inhibition of genes such as *CCND1* (cyclin D1)	Apoptosis; decreased cell viability	*In vitro*: NPC-TW01, NPC-TW04, KB, Hep3B, HCC36, SW620, B77, SC-M1, HeLa S3, and HTB-11	More potent homolog of VP-16	No
Glyceollin isomer 1, 2, and 3 (mixture type 1, 2, and 3) [317–319]	Inhibition of HIF-1α synthesis and decrease in HIF-1α stability; blocked binding of HSP90 with HIF-1α	Blockade of the PI3K/Akt/mTOR pathway and HSP90-binding activity; downregulation of HIF-1α target genes such as *VEGF*	Inhibition of tumor growth; anti-angiogenic; antiproliferative; antimigratory [319, 317]	*In vitro*: MKN1, SNU668, MDA-MB-231, HepG2, Hep3B, PC-3, and Lewis lung carcinoma cells *In vivo*: LLC xenografts in C57BL/6J mice [319, 317]	–	No

Hypericin [143, 176, 320–324]	Induction of HSP90 ubiquitination and subsequent degradation [321]	Enhanced proteasomal degradation of HIF-1α; concomitant downregulation of target genes such as *VEGF*; downregulation of cell cycle regulators such as cyclin A, cyclin B1, cyclin H, and $p27^{KIP1}$ [176, 321]	Antimetastatic; inhibition of tumor growth; anti-angiogenic; antiproliferative [320, 143]	*In vitro*: ARPE-19, U87-MG, SKBR-3, DA3, SQ2, B16-F10, SNU1, MCF-7, and RCC2($VHL^{-/-}$) cells *In vivo*: DA3 and SQ2 xenografts in BALB/c mice (9–10 weeks); SNU1 xenografts in athymic nude mice (6–8 weeks) [143, 176, 320–322, 324]	Hypericin is a natural PS	Yes [143, 322]
Idarubicin [163, 162]	Inhibition of HIF-1α DNA-binding activity	Inhibition of HIF-1α transcriptional activity and concomitant downregulation of HIF-1α target genes such as *VEGF* and *GLUT1*	Anti-angiogenic	*In vitro*: Hep3B-c1 and HEK 293 cells *Clinical*: patients with advanced cancer (majority non-Hodgkin lymphoma)	Anthracycline	No
Kamebakaurin [325, 326]	Inhibition of HIF-1α protein synthesis	Downregulation of HIF-1α and HIF-1α target genes such as *VEGF* and *EPO*	Antiproliferative; cell cycle arrest (G_1); apoptosis	*In vitro*: HCT116, KM12C, SNU638, K562, KBM5, KBM5-T315I, L929, NCM-460, and HeLa cells *In vivo*: female athymic HCTT116 xenografts in female Crj:BALB/c nu/nu mice (6 weeks)	–	No
KC7F2 [327]	Inhibition of mTOR complex	Downregulation of HIF-1α protein synthesis through suppression of phosphorylation of 4EBP1 and p70S6K;	Enhanced cytotoxicity under hypoxic conditions; antiproliferative	*In vitro*: LN229, LN229-HRE-AP, LNZ308, U251MG, MCF-7, PC-3, D54MG,	–	No

(continued)

Table 1
(continued)

Name	Mechanism	Pharmacological effect	Biological effect	Test system	Notes	Tested in PDT
		inhibition of HRE-mediated alkaline phosphatase; downregulation of HIF-1α target genes *CA9*, *MMP2*, *ENOL1*, and *EDN1*		HDMEV, HFF-1, and mouse neuronal cells		
KCN1 [328, 329]	Inhibition of HIF-1α/p300/CBP complex formation	Antagonism of hypoxia-inducible transcription by disruption of protein-protein interactions between HIF-1α and transcriptional co-activators p300/CBP; downregulation of HIF-1α target genes *VEGF*, *GLUT1*, and *CA9*	Inhibition of tumor growth (no effect in melanoma metastasis to the brain); antiproliferative; apoptosis, cell cycle arrest (G_1)	*In vitro*: numerous cell lines; including U251MG, D54MG, D645MG, LN443, HPAC, Panc-1, BxPC3, and MIA PaCa-2 cells *In vivo*: LN229HRE-luc/lacZ or CMV-luc xenografts in athymic nude mice; B16LS9 xenografts in C57BL/6 mice; Panc-1 or MIA PaCa-2 xenografts in female athymic nude mice (6 wk)	Has effect in NSCLC, melanoma, and leukemia cell lines	No
KF58333 [330, 331]	Inhibition of Hsp90	Downregulation of HIF-1α protein and VEGF mRNA and protein levels	Inhibition of tumor growth; anti-angiogenic; antiproliferative; cell cycle arrest (G_1)	*In vitro*: KPL-1 KPL-4, and K562 cells *In vivo*: KPL-1 and KPL-4 xenografts in female BALB/c nu/nu mice (9 weeks)	Radicicol derivative	No

KST012174 [332]	Inhibition of HIF-1α/p300/CBP complex formation	Antagonism of hypoxia-inducible transcription by disruption of protein-protein interactions between HIF-1α and transcriptional co-activators p300/CBP; downregulation of HIF-1α target genes such as *VEGF*	Decreased cell viability	*In vitro*: HeLa cells	–	No
Largazole [216, 253, 333, 334]	Inhibition of class I histone deacetylase	Complete inhibition of HIF-1α protein expression and downregulation of HIF-1α target genes such as *VEGFA*	Antiproliferative	*In vitro*: HCT116, HCT116$^{HIF\text{-}1\alpha-/-HIF\text{-}2\alpha-/-}$, and HCT116$^{WT\ KRAS}$ [216, 253]	More potent than caldoramide and dolastatin 10 for the tested cells	No
Liquiritigenin (LQ) [335–337]	Inhibition of mTOR pathway and blocking of the PKB/Akt signaling pathway	Dephosphorylation of mTOR and p70S6K; attenuation of the PKB/Akt signaling pathway; reduced HIF-1α protein and VEGF mRNA/protein expression	Anti-angiogenic; antiproliferative	*In vitro*: HUVEC and HeLa cells	–	No
Luteolin [153, 243]	Inhibition of HIF-1α by impairing its nuclear accumulation	Impairment of MAPK-dependent phosphorylation of HIF-1α; decreased HIF-1α nuclear accumulation; induced HIF-1α levels, but reduced VEGF;	Antiproliferative [243]	*In vitro*: HeLa and H157 cells [153, 243]	–	No

(continued)

Table 1
(continued)

Name	Mechanism	Pharmacological effect	Biological effect	Test system	Notes	Tested in PDT
		possibly inhibition of STAT3 function				
LW6 [263, 338]	Inhibition of HIF-1α protein stabilization	Downregulation of HIF-1α protein expression by increased HIF-1α proteasomal degradation; increased VHL expression	Inhibition of tumor growth; antiproliferative [338]	*In vitro*: HCT116, Caki-1, SK-HEP1, HUVEC, and PC-3 cells *In vivo*: HCT116 xenografts in female athymic nude Crj: BALB/c mice (6 weeks) [338]	–	No
LY294002 [177, 178, 339, 340]	Inhibition of PI3K	Downregulation of HIF-1α protein levels but not mRNA; inhibition of mTOR at higher doses; downregulation of EGFR, PI3K, and Akt protein levels; inhibition of PKB phosphorylation [177, 178]	Anti-angiogenic; decreased cell viability [178]	*In vitro*: PC-3, Eca-109, HepG2, CHO-IR, 3T3-L1, and DU145 cells, human neutrophils [177, 178, 339, 340] *Ex-vivo:* Rabbit aortic segments	–	Yes [178]
Magnolol [341–343]	Increased HIF-1α protein degradation through enhancement of prolyl hydroxylase activity; inhibition of the mTOR pathway	Antagonism of VEGFR2; attenuation of Akt/mTOR/p70S6K/4E-BP-1 kinase and downregulation of HIF-1α, VEGF, and CD31 protein levels	Inhibition of tumor growth; anti-angiogenic; anti-inflammatory; decreased cell viability; apoptosis [341, 343]	*In vitro*: HUVEC, MCF-7, and T24 cells *In vivo*: T24 xenografts in female athymic nude BALB/c mice (7 weeks) [341, 343]	Prevents platelet aggregation and thrombus formation [342]	No

Melittin (Forapin) [344–347]	Inhibition of the mTOR pathway; inhibition of EGF-induced HIF-1α expression [344]	Suppression of phosphorylation of mTOR, ERK, and p70S6K, leading to a decrease in HIF-1α and VEGF protein levels; blocking of EGF-induced DNA-binding activity of HIF-1α and secretion of VEGF [344]	Anti-angiogenic; antiproliferative; inhibition of tumor growth [344, 347]	*In vitro*: CaSki, HeLa, erythrocytes, and B16F10 cells *In vivo*: CaSki Matrigel plug assay in female C57BL/6N mice (5 weeks); MDA-MB-435 xenografts in athymic nude mice (6 weeks); B16F10 xenografts in C57BL/6 mice (4–6 weeks) [344, 347]	–	No
Menadione (vitamin K3) [257, 348]	Inhibition of HIF-1α/p300/CBP complex formation	Blockade of protein-protein interaction between the CTAD domain of HIF-1α and the CH1 region of p300/CBP; downregulation of HIF-1α target genes, specifically *VEGF*	Decreased cell viability	*In vitro*: HeLa cells	–	No
Methylseleninic acid (MSeA) [349–353]	Inhibition of mTOR; inhibition of DNA-binding activity of HIF-1α	Downregulation of HIF-1 protein levels; activation of Akt through increased phosphorylation or inhibition of the PI3K/Akt/FOXO pathway; induction of REDD1; dysregulation of mTOR; increased cysteine, glutathione, and methionine levels under hypoxic	Inhibition of tumor growth; antiproliferative; apoptosis; decreased cell viability; cell cycle arrest (G_1) [349–353]	*In vitro*: LNCaP, DU145, PC-3, PC-3M, MDA-MB-231, PAIII, A549, HCT116, MCF-7, OVCAR-3, NCI-H460, 3T3-L1, HEK293, U2OS, and MEFs ($REDD1^{-/-}$ and $REDD^{+/+}$) cells *In vivo*: male C57BL/6 mice TRAMP mice (8 weeks); PC-3M-Luc	Combination treatment with cisplatin or carboplatin synergistically improved the antiproliferative effect in A549, HCT116, MCF-7, and OVCAR-3 cells [353]	No

(continued)

Table 1
(continued)

Name	Mechanism	Pharmacological effect	Biological effect	Test system	Notes	Tested in PDT
		conditions; downregulation of HIF-1α target genes such as *VEGF* and *GLUT1* [349, 350, 353]		xenografts in male athymic nude mice (8 weeks); PAIII tumors in LW rats [349–353]		
Minocycline [187, 188, 354, 355]	Inhibition of mTOR pathway	Dephosphorylation of mTOR, p70S6K, RPS6, and 4E-BP1; reduction of HIF-1α and VEGF protein expression; downregulation of HIF-1α target genes such as *VEGF, GLUT1, BNIP3*, and *MMP-9* [187, 188, 355]	Anti-angiogenic; antiproliferative; decreased cell viability [187, 188]	*In vitro*: U87MG, DU145, S462, and human aortic smooth muscle cells *In vivo:* male CD-1 mice [187, 188, 355]	Minocycline causes a dark discoloration of the thyroid in animals (rats, minipigs, dogs, and monkeys). In rats, chronic treatment with minocycline results in goiter accompanied by elevated radioactive iodine uptake and evidence of thyroid tumorigenesis. Minocycline also produces thyroid hyperplasia in rats and dogs; combination with 5-ALA PDT resulted in a synergistic antiproliferative effect [188]	Yes [188]

MLN0128 (sapanisertib) [356–359]	Inhibition of mTOR pathway	Downregulation of TORC1 targets 4EBP1, p-S6K1, HIF-1α, and MTA1 and the TORC2 target c-MYC [356]	Inhibition of VEGF-induced lung metastasis; inhibition of tumor growth [356]	*In vitro*: panel of 20 bone and soft-tissue sarcoma cells *In vivo*: patient-derived metastatic renal cell carcinoma tissue slice xenografts in RAG2$^{-/-}\gamma C^{-/-}$ mice (6–8 weeks) *Clinical*: patients with relapsed or refractory multiple myeloma, non-Hodgkin lymphoma, or Waldenström macroglobulinemia [356, 357, 359]	–	No
Neriifolin [234, 360]	Unclear mechanism	Inhibition of HIF-1α protein expression	Inhibition of tumor growth	*In vitro*: Hep3B-c1 cells	Cardiac glycoside	No
Novobiocin [361, 362]	Inhibition of HIF-1α/p300/CBP complex formation	Blockade of protein-protein interaction between the CTAD domain of HIF-1α and the CH1 region of p300/CBP; downregulation HIF-1α target genes, specifically *CA9*, *Akt1*, and *mTOR*	Inhibition of colony formation; antiproliferative	*In vitro*: MCF-7 and A549 cells	Tested in antibacterial PDT for killing gram-negative bacteria	No
NVP-AUY922 (luminespib) [363–365]	Inhibition of HSP90 (competitive inhibitor of ATPase activity)	Misfolding and degradation of Akt, VEGFR, HIF-1α, HER2, and CDK4 [365, 364]	Antiproliferative; inhibition of chemomigration; tubular differentiation of human endothelial	*In vitro*: HUVEC, HDMEC, PC-3, PC-3LN3, MCF10A, PNT2, HB119, and mutant *KRAS*	–	No

(continued)

Table 1
(continued)

Name	Mechanism	Pharmacological effect	Biological effect	Test system	Notes	Tested in PDT
			cells; anti-angiogenic; cell cycle arrest (G_1/G_2) [365, 364]	HCT116 cells; gastric cancer cell line panel *In vivo*: WM266.4 xenografts in female athymic NCr mice [365, 364]		
NVP-LAQ824 (dacinostat) [309, 366, 367]	Inhibition of histone deacetylases 1 and 2	Downregulation of HIF-1α protein but not mRNA levels; inhibition of downstream VEGF protein expression	Inhibition of tumor growth; anti-angiogenic; antiproliferative; cell cycle arrest (G_2/M) [309, 366]	*In vitro*: UMRC2, C2VHL, H1299, HCT116, A549, DU145, PC-3, MDA435, normal dermal human fibroblast and normal human bronchial epithelial cells *Clinical*: patients with advanced solid tumors [309, 366, 367]	More potent than vorinostat (SAHA) and MS-275 against HCT116 cells [366]	No
Oligoamine α-helix mimetics [368]	Binding in the HIF-1α C-TAD helix 3-binding cleft	Inhibition of HIF-1α/p300 complex formation	–	*In silico*: docking and fluorescence anisotropy competition titration	–	No
Ouabain [282, 369–372]	Binding to eIF4E and disruption of eIF4E/eIF4G association; inhibitor of NA^+,K^+-ATPase [369, 370]	Inhibition of Cap-dependent translation; inhibition of HIF-1α protein synthesis [369, 370]	Anti-angiogenic; antiproliferative; apoptosis [370, 372]	*In vitro*: DU145, U2OS, AGS, OVCAR8, Y-1, PC-3, U937, HepG2, A549, SKOV3, SMMC-7721, 95D, and HeLa cells [369, 370, 372]	Cardiac glycoside	No

Parbendazole [216, 291]	Unclear mechanism but known tubulin destabilizer	Downregulation of HIF-1α mRNA but not protein expression; downregulation of HIF-1α target genes such as *VEGFA* [216]	Exacerbated cytotoxicity in cells that express functional HIF-1, HIF-2, and KRAS compared to cells where proteins were knocked out; decreased cell viability	*In vitro*: HCT116, HCT116$^{WT\ KRAS}$, and HCT116$^{HIF\text{-}1\alpha-/-HIF\text{-}2\alpha-/-}$ cells	–	No
Periplocymarin [234, 372, 373]	Unclear mechanism; inhibitor of NA^+, K^+-ATPase	Inhibition of HIF-1α protein expression	Inhibition of tumor growth; apoptosis; antiproliferative; cell cycle arrest (G_2/M) [372]	*In vitro*: Hep3B-c1, PC-3, and U937 cells [234, 372]	Cardiac glycoside	No
Peruvoside [216, 234, 266, 374]	Unclear mechanism	Complete inhibition of HIF-1α protein expression and downregulation of HIF-1α target genes such as *VEGFA* [216, 234]	Exacerbated cytotoxicity in cells that express functional HIF-1, HIF-2, and KRAS compared to cells where proteins were knocked out; antiproliferative; decreased cell viability, cell cycle arrest (G_0/G_1); apoptosis [216, 266]	*In vitro*: MCF-7, Hep3B-c1, MDA-MB-231, HCT116, HCT116$^{WT\ KRAS}$, HCT116$^{HIF\text{-}1\alpha-/-HIF\text{-}2\alpha-/-}$, and MDA-MB-468 cells [216, 234, 266]	Cardiac glycoside	No
Phenethyl isothiocyanate (PEITC) [375, 376]	Inhibition of HIF-1α accumulation	Decrease in HIF-1α protein levels; induction of HIF-1α target genes *CA9*, *GLUT1*, *BNIP3*, and *VEGFA*	Anti-angiogenic; antiproliferative; apoptosis	*In vitro*: MCF-7 cells	–	No
Pleurotin [377, 378]	Inhibition of thioredoxin	Decrease in HIF-1α protein levels; inhibition of HIF-1-	Inhibition of tumor growth; anti-angiogenic [377]	*In vitro*: MCF-7, HT-29, RCC4, and RCC4/VHL cells [377]	–	No

(continued)

Table 1
(continued)

Name	Mechanism	Pharmacological effect	Biological effect	Test system	Notes	Tested in PDT
		transactivating activity and VEGF production [377]				
Proscillaridin A [216, 234, 270, 281, 379]	Unclear mechanism	Complete inhibition of HIF-1α protein expression but increase in *HIF1* mRNA levels; downregulation of HIF-1α target genes [216, 234]	Exacerbated cytotoxicity in cells that express functional HIF-1, HIF-2, and KRAS compared to cells where proteins were knocked out; antiproliferative; antimigratory; decreased cell viability; inhibition of tumor growth; cell cycle arrest (G_2/M) [216, 270, 379]	*In vitro*: Hep3B, Hep3B-c1 HCT116, HCT116$^{WT\ KRAS}$, HCT116$^{HIF\text{-}1\alpha-/-HIF\text{-}2\alpha-/-}$, GBM6, GBM9, U87-MG, U251-MG, HT29, CC20, and PC-3 cells *In vivo*: GBM6 and U87-MG xenografts in athymic nude mice (6 weeks) [216, 234, 270, 379]	Cardiac glycoside	No
Purine scaffold compound 16 [380]	Inhibition of HSP90	Inhibition of HSP90, leading to degradation of HER2 and possibly other (oncogenic) proteins such as ER, AR, and BCR-ABL, RAF-1, p-Akt, CDK4, mutant p53, and FLT-3	Inhibition of tumor growth	*In vitro*: MCF-7 and BT474 cells *In vivo*: N87 xenografts in BALB/c and female nu/nu athymic mice (6–8 weeks)	–	No

Purine scaffold compound 20 [380]	Inhibition of HSP90	Inhibition of HSP90, leading to degradation of HER2 and possibly other (oncogenic) proteins such as ER, AR, and BCR-ABL, RAF-1, p-Akt, CDK4, mutant p53, and FLT-3	Inhibition of tumor growth	*In vitro*: MCF-7 and BT474 cells *In vivo*: N87 xenografts in BALB/c and female nu/nu athymic mice (6–8 weeks)	–	No
Purine scaffold PU-H71 [381–383]	Inhibition of HSP90	Caspase activation; PARP cleavage; Akt inactivation; induction of ER stress (increase in HSP90 paralogs GRP94, GRP78); upregulation of ATF4 and CHOP; activation of PERK/ATF4 and IRE1/XBP1 arms of unfolded protein response [381, 382]	Intrinsic apoptosis; necrosis; decreased cell viability; antiproliferative, cell cycle arrest (G_2/M); inhibition of tumor growth [381, 382]	*In vitro*: HeLa (with *BCL-2* gene, cytomegalovirus UL37 exon 1 gene coding for vMIA, or with pcDNA3.1 vector containing neomycin resistance gene), HCT116, HCT116 $Bax^{-/-}$, MDA-MB-468, MDA-MB-231, HCC-1806, Mel501, primary human fibroblasts, A549, and HepG2 cells *In vivo*: MDA-MB-468, MDA-MB-231, and HCC-1806 xenografts in female athymic nu/nu mice (6 weeks) *Clinical*: patients with progressed or recurrent solid tumors [381–383]	Complete response in MDA-MB-231 xenografts [382]	No

(continued)

Table 1
(continued)

Name	Mechanism	Pharmacological effect	Biological effect	Test system	Notes	Tested in PDT
PX-12 [377]	Inhibition of HIF-1α	Decrease in HIF-1α protein levels and inhibition of HIF-1α transactivating activity and VEGF production	Inhibition of tumor growth; anti-angiogenic; decreased cell viability	*In vitro*: MCF-7, HT-29, RCC4, and RCC4/VHL cells *In vivo*: MCF-7 xenografts in SCID mice	Unclear what causes the HIF-1α inhibition	No
PX-478 [384, 385]	Inhibition of HIF-1α	Reduction of HIF-1α levels and inhibition of HIF-1α-dependent downstream transcription	Tumor regression; stalled tumor growth	*In vitro*: PC-3, MCF-7, HT29, Panc-1, BxPC-3, $HCT116^{+/+}$ (WT p53), and $HCT166^{-/-}$ (deleted p53) cells *In vivo*: MCF-7, HT-29, PC-3, DU-145, OVCAR-3, A549, SHP-77, and Caki-1 xenografts in female SCID mice	GLUT1 but not VEGF was inhibited for over 24 h after a single i.p. dose of 120 mg/kg in mice with HT-29 xenografts [384]	No
Pyrazoles (VER-49009) [386]	Inhibition of HSP90	Induction of HSP27 and HSP72, resulting in depletion of C-RAF, B-RAF, survivin, and PRMT5; downregulation of Akt, p-Akt, and ERBB2 protein levels	Apoptosis; antiproliferative; G_1- and G_2/M-phase cell cycle arrest	*In vitro*: HUVEC, MCF10a, PNT2, SKMEL2, SKMEL 5, SKMEL 28, WM266.4, HT29, HT29oxaliR, CH1, BT20, BT-474, HCT116, CH1, MB-231, MB-468, ZR751, and BEneg	–	No

				cells *In vivo*: HCT116 and OVCAR-3 xenografts in female athymic NCr mice (6–8 weeks)		
Pyrazoles (VER-50589) [386]	Inhibition of HSP90	Induction of HSP27 and HSP72, resulting in depletion of C-RAF, B-RAF, survivin, and PRMT5; downregulation of p-Akt and ERBB2 protein levels	Apoptosis; antiproliferative, G_1- and G_2/M-phase cell cycle arrest	*In vitro*: HUVEC, MCF10a, PNT2, SKMEL 2, SKMEL 5, SKMEL 28, WM266.4, HT29, HT29oxaliR, CH1, BT20, BT-474, HCT116, CH1, MB-231, MB-468, ZR751, and BEneg cells *In vivo*: HCT116 and OVCAR-3 xenografts in female athymic NCr mice (6–8 weeks)	–	No
Pyridylpyrimidine scaffold P2630 [387]	Selective inhibitor of HIF-1α	Decrease in VEGF protein and mRNA expression (under hypoxic conditions)	Anti-angiogenic, inhibition of tumor growth; antiproliferative	*In vitro*: PC-3, HCT-116, U251, U251-pGL3, U251-HRE, OVCAR-3, DU-145, Panc-1, MRC-5, and WI-38 cells *In vivo*: PC-3 xenografts in SCID mice	–	No
Pyridylpyrimidine scaffold P3155 [388]	Decreased phosphorylation of HIF-1α, P13K, Akt, and 4E-BP1; inhibition of HIF-1α	Suppression of the PI3K/Akt pathway; decreased phosphorylation of Akt and 4E-BP1; downregulation of HIF-1α, VEGF, p-Akt protein levels	Anti-angiogenic; anti-migratory; inhibition of tumor growth	*In vitro*: PC-3, U251-pGL3, U251-HRE, HUVEC, and DU145 cells *In vivo*: PC-3 xenografts in SCID mice	–	No

(continued)

Table 1
(continued)

Name	Mechanism	Pharmacological effect	Biological effect	Test system	Notes	Tested in PDT
Quercetin [153, 243, 389, 390]	Impairment of MAPK-dependent phosphorylation of HIF-1α	Inhibition/induction of HIF-1α; decreased HIF-1α nuclear accumulation; downregulation of VEGF and p-Akt protein expression [153, 243]	Antiproliferative; decreased cell viability; cell cycle arrest (G_2/M) [243, 390, 389]	*In vitro*: HeLa, HEp-2, HL-60, and NCI-H157 cells [153, 243, 390, 389]	–	Yes [390]
Radicicol (monorden) [391, 392]	Inhibition of HSP90	Inhibition of hypoxia-induced expression of VEGF and inhibition of HRE binding by the HIF-1α/Arnt heterodimer	Anti-angiogenic	*In vitro*: Hep3B cells	–	No
Rapamycin (sirolimus) [189, 191–194, 393, 394]	Inhibition of mTOR by binding to the FKBP12 protein [194]	Inhibition of HIF-1α accumulation and HIF-1α-dependent downstream transcription; downregulation of BMI-1 protein and mRNA levels and decreased cyclin E1 and GLUT1 protein levels; attenuation of mTOR phosphorylation [192, 394]	Antiproliferative; G_1-phase cell cycle arrest; immunosuppressive; delayed tumor growth [189–193, 394]	*In vitro*: PC-3, Y79, SZ95, WiDr, and VCP patient myoblasts *In vivo*: WiDr xenografts in female BALB/c nu/nu mice (5–8 weeks); $VCP^{R155H/+}$ mouse cells [192–194, 393, 394]	Administration directly after $AlPcS_{2a}$-PDT resulted in a synergistic cytotoxic effect but administration before PDT resulted in an antagonistic effect in WiDr cells [193]	Yes [194, 193]

Resveratrol [195, 197, 243, 395–399]	Inhibition of HIF-1α protein accumulation without affecting HIF-1α mRNA levels	Inhibition of hypoxia-mediated activation of ERK1/2 and Akt, leading to a decrease in HIF-1α protein accumulation and *VEGF* transcriptional activation; upregulation of caspase-3, p53, p-ERK, and p-p38 protein levels (without PDT and in combination with PDT) [195, 243, 399]	Anti-angiogenic, antiproliferative; apoptosis; anti-invasive; decreased cell viability, increased survival, inhibition of tumor growth rate [195, 197, 243, 398, 399]	*In vitro*: SCC-9, HaCaT, A431, NCI-H157, RT-2, ECV304, MDA-MB-231, and HepG2 cells *In vivo*: MDA-MB-231 xenografts in female athymic nude mice (6–8 weeks); RT-2 xenografts in Fischer 344 rats [197, 395, 399]	Has been investigated in many in vivo studies on breast, colorectal, liver, pancreatic, and prostate cancer [395, 398]	Yes [197]
Rotenone [29, 400]	Inhibition of mitochondrial complex I	Downregulation of HIF-1α, VEGF, and Bcl-2 protein expression	Inhibition of tumor growth; decreased cell viability; apoptosis, cell cycle arrest (subG$_1$) [400]	*In vitro*: MCF-7, Hs29-4T, and NIH-3T3 cells	–	No
SCH66336 (lonafarnib) [401, 402]	Inhibition of HIF-1α interaction with HSP90	Downregulation of HIF-1α and VEGF protein expression	Anti-angiogenic; antiproliferative	*In vitro*: UMSCC38, HUVEC, and H1299 cells; chick aortic arch assay *In vivo*: UMSCC38 xenografts in female nude mice (6 weeks) *Clinical*: patients with advanced solid tumors	Farnesyl transferase derivative	No
Schiff bases (compound 13) [403]	Inhibition of Hsp90 ATPase activity	Inhibition of HSP90	Antiproliferative	*In vitro*: PC-3, Caco, and MDCK cells	–	No

(continued)

Table 1
(continued)

Name	Mechanism	Pharmacological effect	Biological effect	Test system	Notes	Tested in PDT
SH-1242 [404]	Inhibition of HSP90	HIF-1α destabilization through HSP90 inhibition, resulting in decreased *VEGFA*, *EDN1*, *EPO*, and *NOS2* expression	Anti-angiogenic; antiproliferative	*In vitro*: ARPE-19, HRMEC, and SNUOT-Rb1 cells and human brain astrocytes *In vivo*: retinas of OIR and C57BL/6 mice	–	No
SH-1280 [404]	Inhibition of HSP90	HIF-1α destabilization through HSP90 inhibition, resulting in decreased *VEGFA*, *EDN1*, *EPO*, and *NOS2* expression	Anti-angiogenic; antiproliferative	*In vitro*: ARPE-19, HRMEC, and SNUOT-Rb1 cells and human brain astrocytes *In vivo*: retinas of OIR and C57BL/6 mice	–	No
Silibinin [196, 198, 199, 405]	Dephosphorylation of mTOR, p70S6K, and 4E-BP1	Inhibition of HIF-1α accumulation and transcriptional activity; inhibition of mTOR pathway; reduction in VEGF release; decreased HIF-1α nuclear accumulation; downregulation of ERK1/2, Akt phosphorylation, cyclin D1, NOS, NOS3, COX-1, COX-2, HIF-1α, and VEGF protein expression [196, 199]	Inhibition of tumor growth; anti-angiogenic; hepatoprotective; decreased cell viability; apoptosis; antiproliferative [196, 198, 199]	*In vitro*: HeLa, T24, MB49, and Hep3B cells *In vivo*: HT29 xenografts in male BALB/c nu/nu mice [196, 198]	Combination treatment with 5-ALA-PDT has either a synergistic or an additive effect on cell death, depending on light dose and cell type, compared to individual treatments [198]	Yes [198]

SN38 [200–202, 406]	Inhibition of topoisomerase I	Downregulation of HIF-1α protein levels and VEGF protein and mRNA expression [200, 202]	Anti-angiogenic; antiproliferative (endothelial cell); inhibition of tumor growth [200, 202]	*In vitro*: U87-MG, HT-29, U251, U251-MG, CPAE, GL261, and TE-1 cells *In vivo*: HT-29 xenografts in female athymic BALB/c nu/nu mice (5–6 weeks) [200, 202]	Metabolite of irinotecan; in combination with CSBC-PDT, tumor growth was synergistically inhibited compared to individual therapies [202]	Yes [202]
Sodium butyrate [203–205, 407, 408]	Inhibition of histone deacetylases (most except classes 2, 3, 6, and 10)	Downregulation of HIF-1α protein levels and transcriptional activity of HIF-1α; cell-dependent up- and downregulation of caspase-3, caspase-9, Bcl-2, LHX1, and Bax mRNA expression [204, 205, 203, 408]	Anti-angiogenic; antiproliferative; decreased cell viability; apoptosis [203–205, 408]	*In vitro*: 293T, HeLa, B16F10, HT-29, HCT-116, U373-MG, and D54-MG and 293T (transfected with pSV40pro-EpoHRE-Luc, pBOS-hHIF-1α, and pBOS-hHIF-1β) cells *Clinical*: patients with acute leukemia [203–205, 407, 408]	Combination therapy with 5-ALA-PDT resulted in an additive cytotoxic effect compared to individual treatment [204, 205]	Yes [204, 205]
Sorafenib [206, 207, 209, 409–411]	Suppression of phosphorylation of mTOR, ERK, p70S6K, RP-S6, 4e-BP1, and elF4E	Inhibition of HIF-1α protein synthesis; decrease in HIF-1α and VEGF protein levels [206]	Inhibition of tumor growth; anti-angiogenic; antiproliferative [206, 207, 209]	*In vitro*: U373-MG, D54-MG, PLC/PRF/5, HepG2, Hep3B, HuH-7, HuH-7^{R}, and MCF-7 cells *In vivo*: PLC/PRF/5 xenografts in male nude mice (6–8 weeks); A2789 xenografts in chicken embryo chorioallantoic membrane model *Clinical*: patients with advanced refractory	Galectin-1 levels are associated with poor tumor control and response rates in patients with HCC [411]	Yes [207]

(continued)

Table 1
(continued)

Name	Mechanism	Pharmacological effect	Biological effect	Test system	Notes	Tested in PDT
				solid tumors (HCC) [206, 207, 209, 410, 411]		
Strophanthin-K [234, 412]	Unclear mechanism	Inhibition of HIF-1α protein expression	Inhibition of tumor growth	*In vitro*: Hep3B-c1 cells	Cardiac glycoside	No
Tanshinone-IIA [413–419]	Inhibition of phosphorylation of mTOR, p70S6K (Thr421/Ser424), RPS6 (Ser235/236 and Ser240/244), 4E-BP1 (Thr37/46)	Inhibition of HIF-1α protein synthesis; inhibition of MMP-2 activity; activation of caspase-3; increased BAX:BCL-xL ratio; epigenetic modification of Aurora A expression; downregulation of VEGF, GLUT1, and EPO protein expression [413, 416–419]	Anti-angiogenic, anti-migratory, anti-invasive; decreased cell viability; inhibition of colony formation; antiproliferative; pro-apoptotic; inhibition of tumor growth [413, 416–419]	*In vitro*: MDA-MB-231, MCF-7, SKBR3, MDA-MB-453, HMEC, and HUVEC cells *In vivo*: MDA-MB-231 xenografts in nude mice (5 weeks); human infiltrating ductal carcinoma xenografts in female nude mice (6 weeks); chicken embryo chorioallantoic membrane model (10 days) [413, 416–419]	–	No
TAT-cyclo-CLLFVY [420]	Binding to the PAS-B domain of HIF-1α	Inhibition of HIF-1α/HIF-1β dimerization; prevention of HIF-1α transcription activity; decrease in *VEGF*	No effect on cell proliferation over 72 h	*In vitro*: MCF-7 and U2OS cells	–	No

		mRNA and VEGF protein levels				
Temsirolimus [421]	Inhibition of mTOR	Decrease in HIF-1α expression; inhibition of mTOR and its downstream effectors	Antiproliferative; inhibition of tumor growth	*In vitro*: KOB9N, KOB12N, KOB9C, TE-1, TE-8, and TE-10 cells *In vivo*: TE-8 xenografts in male nude BALB/cA mice (6 weeks)	–	No
Topotecan [208, 209, 422–425]	Known topoisomerase inhibitor (unknown cause of HIF-1α inhibition)	Downregulation of VEGF and GLUT1 mRNA and protein levels and HIF-1α protein levels; downregulation of HIF-1α transcriptional activity [208, 422]	Antiproliferative; anti-angiogenic; inhibition of tumor growth; apoptosis [209, 422, 423, 425]	*In vitro*: HeyA8, SKOV3ip1, MCF-7, MCF-10A, U251, MCF-7/MR, MCF-7 Luc, and DU-145 Luc cells *In vivo*: U251-HRE and U251-mutHRE xenografts in female athymic nude NCr mice; HeyA8 and SKOV3ip1 xenografts in female athymic nude mice; MCF-7 Luc and DU-156 Luc xenografts in female athymic nu/nu mice (8–10 weeks) *Clinical*: patients with solid malignancies [208, 209, 422, 423, 425]	HIF-1α nuclear staining in tumor parenchymal cells of patients with metastatic malignancies did not show any HIF-1α [208]	Yes [209]
Trichostatin A [203, 211–213, 426]	Inhibition of histone deacetylases 1, 4, and 6	Downregulation of HIF-1α protein levels and	Antiproliferative; anti-migratory; anti-	*In vitro*: SCC-6, HT-29, HCT 116, mouse embryonic stem cells,	Combination treatment with hypericin-PDT upregulated *CDKN1A*	Yes [211]

(continued)

Table 1
(continued)

Name	Mechanism	Pharmacological effect	Biological effect	Test system	Notes	Tested in PDT
		transcriptional activity of HIF-1α [211–213]	angiogenic; apoptosis [211, 212]	HeLa, B16F10, and 293T (transfected with pSV40pro-EpoHRE-Luc, pBOS-hHIF-1α, and pBOS-hHIF-1β) cells [203, 211–213]	mRNA as well as its protein product $p21^{Cip1}$ and synergistically increased cell death and S-phase cell cycle arrest and reduced colony formation in HT-29 and HCT 116 cells [211]	
Valproic acid [203, 211, 213]	Inhibition of histone deacetylase 1	Downregulation of HIF-1α protein levels and transcriptional activity of HIF-1α [211, 213]	Antiproliferative; apoptosis [211]	*In vitro*: HT-29, HCT 116, HeLa, B16F10, and 293T (transfected with pSV40pro-EpoHRE-Luc, pBOS-hHIF-1α, pBOS-hHIF-1β), and mouse embryonic stem cells [203, 211, 213]	Reduces HIF-1α protein levels more potently than other HDACs, such as sodium butyrate and trichostatin A [213]; combination treatment with hypericin-PDT upregulated *CDKN1A* and its protein product $p21^{Cip1}$ and synergistically increased cell death and S-phase cell cycle arrest and reduced colony formation in HT-29	Yes [211]

					and HCT 116 cells [211]	
Verteporfin [214–217]	Unclear mechanism	Downregulation of HIF-1α mRNA expression, but no effect on protein levels; downregulation of HIF-1α target genes such as *VEGFA*; downregulation of survivin, c-Myc, and AXL protein levels [215–217]	Antiproliferative; anti-migratory; apoptosis; G_1-phase cell cycle arrest; anti-angiogenic; inhibition of tumor growth; pro-apoptotic; decreased cell viability [214–217]	*In vitro*: Y79, WERI, HUVEC, HCT116, HCT116$^{WT\ KRAS}$, HCT116$^{HIF\text{-}1\alpha-/-HIF\text{-}2\alpha-/-}$, HPDE6, PANC-1, SW1990, AsPC-1, BxPC-3, and Capan-1 cells *In vivo*: PANC-1 and SW1990 xenografts in male BALB/c nu/nu mice (6 weeks) [214–217]	Treatment where verteporfin itself was used as PS decreased BCL-xL expression and increased BAX/BCL-xL ratio compared to the dark toxicity group and induced near-complete cell death in pancreatic cancer cells [217]	Yes [217]
Vincristine [179, 185, 186]	Inhibition of HIF-1α pathway through disruption of the microtubule cytoskeleton	Downregulation of HIF-1α protein but not mRNA levels; inhibition of HIF-1α transcriptional activity; inhibition of VEGF [179]	Inhibition of tumor growth; anti-angiogenic; cell cycle arrest (G_1/G_2); decreased cell viability [185, 186]	*In vitro*: 1A9, LBR, MDA-MB-231, MCF-7, HS0578T, BT20, MDA-MB-468, LBR-V160, LBR-D160, and primary human mammary epithelial cells; panel of breast cancer cell lines [179, 185, 186]	5-ALA-PDT + vincristine was more cytotoxic than 5-ALA-PDT + doxorubicin in LBR cells; combination treatment with 5-ALA-PDT yielded an additive effect compared to the individual treatments in terms of mainly apoptosis [185, 186]	Yes [186]
Vorinostat (SAHA) [211, 218, 219]	Inhibition of histone deacetylases (specifically HDAC9) [218]	Inhibition of HIF-1α translation; downregulation of VEGF, CDK-2, and p53 protein expression (independently of	Anti-angiogenic; antiproliferative; apoptosis; G_1-phase cell cycle arrest (in cells with defective apoptotic signaling); increased S-phase cell	*In vitro*: HuH7, Hep3B, HCT 116, HT-29, Raji-4RH, RL-4RH, RL, and patient-derived diffuse large B-cell lymphoma cells [211, 218, 219]	Combination treatment with hypericin-PDT significantly upregulated p21^{cip1} transcript and protein levels and synergistically	Yes [211]

(continued)

Table 1
(continued)

Name	Mechanism	Pharmacological effect	Biological effect	Test system	Notes	Tested in PDT
		protein degradation) [218, 219]	cycle arrest in HT-29 cells; decreased cell viability; decreased colony formation [211, 218, 219]		increased cell death and disrupted cell cycle regulation and colony-forming capabilities compared to the singular therapies [211]	
Wogonin [427, 428]	Inhibition of HSP90; upregulation of PHD1, 2, 3 and VHL	Prevention of HSP90 binding to HIF-1α; decreased HIF-1α nuclear import; downregulation of the HSP90 client proteins EGFR, CDK4, and survivin; promotion of HIF-1α degradation by increasing prolyl hydroxylation and ubiquitination (upregulation of PHD1, 2, and 3 and VHL protein levels); inhibition of VEGF secretion and VEGF mRNA expression [427]	Anti-angiogenic; inhibition of tumor growth [427]	*In vitro*: MCF-7, MDA-MB-231, HepG2, HUVEC, and HCT116 cells; rat aortic ring assay *In vivo*: MCF-7 xenografts in female nude BALB/c mice (5–6 weeks) [427]	–	No
Wortmannin [177, 220, 429]	Inhibition of PI3K		Anti-angiogenic; antiproliferative	*In vitro*: A549, PC-3, DU145, U2-OS,	Combination therapy with 9-capronylo	Yes [220]

		Downregulation of HIF-1α protein levels but not mRNA [177]		ACHN, and L1210 cells [177, 220, 429]		xytetrakis-(methoxyethyl)-porphycene-PDT induced apoptotic and autophagic cell death in L1210 cells and only autophagic cell death in DU145 cells (BAX-deficient); preincubation prior to PDT increased morphological appearance of apoptosis and inhibited autophagy in both L1210 and DU145 cells [220]	
YC-1 [430–432]	Inhibition of HIF-1α DNA-binding activity and suppression of hypoxic accumulation of HIF-1α	Downregulation of HIF-1α expression and HIF-1α target genes such as *VEGF* and *EP*	Antiproliferative	*In vitro*: Hep3B, HEK293, and Caki-1 cells *In vivo*: Hep3B, NCI-H87, A549, HCT-116, Caki-1, SiHa, and SK-N-MC xenografts in male nude BALB/cAnNCrj mice	–		No

17-AAG (Tanespimycin)

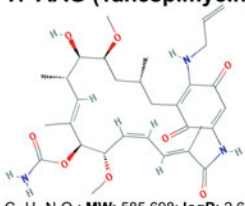

$C_{31}H_{43}N_3O_8$; **MW:** 585.698; **logP:** 2.6
t1/2: 1.1 - 6.6 hr
Fluorescence: NA; **λmax**: 242, 334, 532 nm
IC50: Proliferation in TGB lymphoma - 238 nM, Hsp90 - 5,64 nM; migration of HUVEC (FGF-2 induced) - 50 nM, (VEGF-induced) - 23 nM
LC50: NA
LD50: NA; **TDLO**: 125 mg/kg (ip) - mouse

17-DMAG (Alvespimycin)

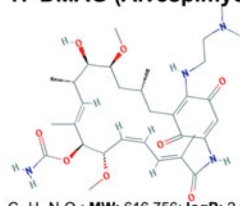

$C_{32}H_{48}N_4O_8$; **MW:** 616.756; **logP:** 2.0
t1/2: 9.9 - 54.1 hr
Fluorescence: NA; **λmax**: 220, 332, 529 nm
IC50: Proliferation in NCI human tumor cell line panel, mean - 63 nM
LC50: NA
LD50: NA

2ME2

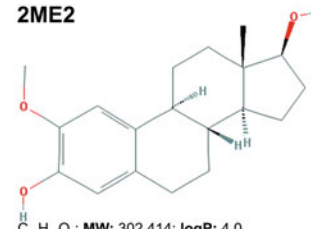

$C_{19}H_{26}O_3$; **MW:** 302.414; **logP:** 4.0
t1/2: 5.21 mg/kg (iv) 59 min - Sprague Dawley rats
Fluorescence: NA; **λmax**: 212, 254, 317 nm
IC50: HIF-1α (20 min normoxia) 20-25 μM - PC-3, 40-50 μM - DU-145; proliferation 82.5 μM (HT-29)
GI50: large cancer cell line panel ~2.46 μM
LC50: NA; **LD50**: NA; **TDLO**: 100 mg/kg/2D (oral) - mouse, 270 mg/kg/9 d (ip) - rat, 400 mg/kg/16 d (sc) - man

AC1-004

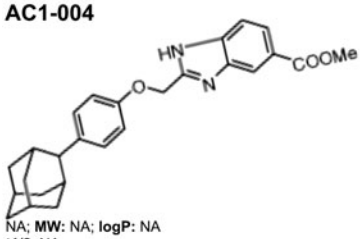

NA; **MW:** NA; **logP:** NA
t1/2: NA
Fluorescence: NA; **λmax**: NA
IC50: NA; **IC50**: Varying in cell lines 5.5 - 44.9 μM
LC50: NA
LD50: NA

Acetyldigoxin

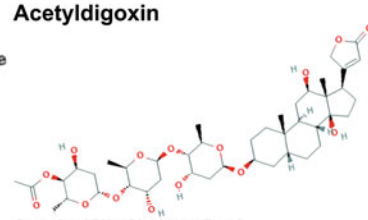

$C_{43}H_{66}O_{15}$; **MW:** 823.000; **logP:** 1.8
t1/2: 7.5 hr
Fluorescence: NA; **λmax**: NA
IC50: NA; **LC50**: NA
LD50: 0.422 mg/kg (oral) - dog, 2.4 mg/kg (oral) - Guinea pig; **TDLO50**: 0.372 mg/kg (oral) - child

Acriflavine

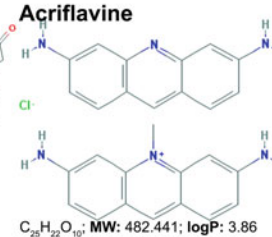

$C_{25}H_{22}O_{10}$; **MW:** 482.441; **logP:** 3.86
t1/2: < 5 (iv) - rat (blood)
Fluorescence: Ex 453 nm, Em 507 nm
λmax: 460 ± 4 nm (methanol)
IC50: HIF-1α dimerization ~1 μM, viability 23 μM (normoxia), 73 μM (hypoxia) - SK-Cha-1,
LC50: NA; **LD50**: NA

AJM290

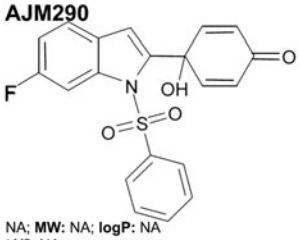

NA; **MW:** NA; **logP:** NA
t1/2: NA
Fluorescence: NA; **λmax**: NA
IC50: HIF-1α transactivation activity of phosphoglycerate kinase luciferase 0.44 μM; for VEGF 1.26 μM - MDA-MD-468
LC50: Cell viability 8.2 μM - MDA-MB-468
LD50: NA

Aminoflavone

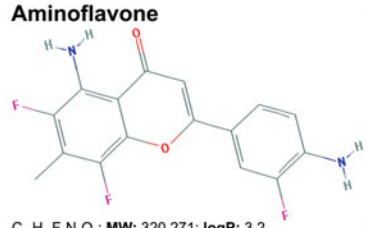

$C_{16}H_{11}F_3N_2O_2$; **MW:** 320.271; **logP:** 3.2
t1/2: NA
Fluorescence: NA; **λmax**: NA
IC50: NA
LC50: NA
LD50: NA

Amphotericin B

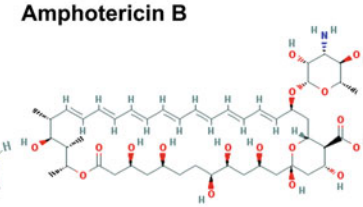

$C_{47}H_{73}NO_{17}$; **MW:** 924.091; **logP:** 0.0
t1/2: t1/2,α = 0.2 - 2 hr, t1/2,β = 10 - 17 hr, t1/2,γ = 71 hr
Fluorescence: NA; **λmax**: 227, 283, 346, 364, 383, 407 nm
IC50: NA; **LC50**: NA; **LD50**: >5 g/kg (oral, ip) - rat 280 mg/kg (oral) - mouse, 27740 μg/kg (ip) - mouse

Apicidin

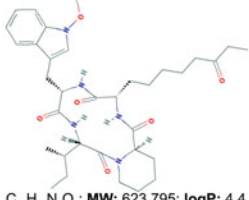

$C_{34}H_{49}N_5O_6$; **MW:** 623.795; **logP:** 4.4
t1/2: 0.5, 1.0, 2.0, and 4.0 mg/kg (iv) in male Sprague Dawley rats 0,8 - 1,1 hr
Fluorescence: NA; **λmax**: 221 nm
IC50: 15.8 nM - HDAC3, 665.1 nM - HDAC6
LC50: NA
LD50: NA

Apigenin

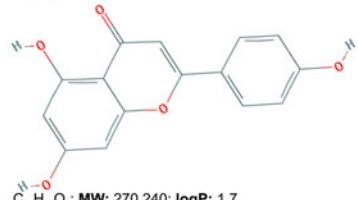

$C_{15}H_{10}O_5$; **MW:** 270.240; **logP:** 1.7
t1/2: 10 μCi/kg (oral) 91.8 ± 5.6 hr - rat
Fluorescence: Ex 260 nm, 325 nm Em 370, 375 nm, respectively (acetronitrile, methanol); **λmax**: 212, 269, 334 nm
IC50: 35 ± 4 μM - H157 (proliferation) >100 μM - H157 (viability, hypoxia/normoxia) 5.9 ± 0.1 μM - VEGF; **LC50**: NA
LD50: 14.5 mg/kg (oral) - rat 40.250 ppm 4 hr (inhale) - rat 5 mg/kg (dermal) - rabbit

Ascofuranone

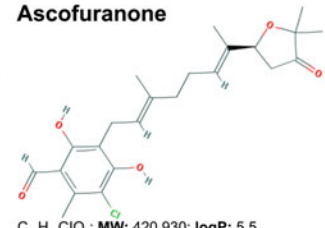

$C_{23}H_{29}ClO_5$; **MW:** 420.930; **logP:** 5.5
t1/2: NA
Fluorescence: NA; **λmax**: 250, 290, 350 nm (methanol)
IC50: NA; **LC50**: NA
LD50: >3700 mg/kg (oral), 2220 mg/kg (ip) - male mouse, >4000 mg/kg (oral), 2250 mg/kg (ip) - female mouse

Fig. 6 Molecular structure, chemical attributes, spectral properties, and pharmacodynamic properties of HIF-1α pathway inhibitors. LogP (octanol:water partition coefficient) values were retrieved from PubChem or were predicted with XLogP2 or XlogP3 software. The half maximum inhibitory concentration (IC_{50}, enzymes), half maximum lethal concentration (LC_{50}, in vitro), half maximum lethal dose (LD_{50}, in vivo), $t_{1/2}$ (circulation half-life), and spectral properties were obtained from the material safety data sheets (retrieved from the

opposite of additive/synergistic effects; it occurs when the combined effect of the treatments is less than would be expected for the sum of the individual treatments (e.g., 1 + 1 = 0.5) [141].

4.1 17-AAG (Tanespimycin)

17-AAG (tanespimycin) is a derivative of the antibiotic geldanamycin, which binds to the amino terminal ATP-binding pocket of 90 kDa heat-shock protein (Hsp90), thereby blocking its direct binding to HIF-1α. This prevents the conformational changes in the HIF-1α structure that are necessary for the heterodimerization with HIF-1β [7, 142].

Mice bearing mammary (BA) carcinoma xenografts that were treated with a combination of 17-AAG and Photofrin-PDT (quartz fiber microlens, 630 nm, 75 mW/cm^2, cumulative radiant exposure of 200 J/cm^2) responded with a strong decrease in Akt, p-Akt, survivin, and p-survivin protein expression compared to the single treatments. Photofrin-PDT-induced HIF-1α was reduced to baseline values, expression and proteolytic activity of MMP-2 and MMP-9 were inhibited, and VEGF expression was reduced when 17-AAG was added. The reduction and inhibition of these proteins translated to a statistically significant improvement in long-term tumoricidal response (90 days) when compared to the respective individual treatments (50% cure rate for PDT + 17-AAG versus 25% cure rate for PDT and 0% for 17-AAG). After PDT, 17-AAG was administered thrice per week for up to two weeks intraperitoneally at a dose of 75 mg/kg [7].

Similar to 17-AAG, 17-DMAG (alvespimycin) is a derivative of geldanamycin that is capable of blocking nucleotide binding of Hsp90, resulting in ubiquitination and proteasomal degradation of its client proteins [143]. Hypericin-PDT (21 nM) (*see* Subheading 4.12) in combination with 17-DMAG at IC_{10} (5 nM) resulted in synergistically increased cell death in human breast adenocarcinoma (SKBR-3) cells after 48 h compared to the monotherapies, which was corroborated through clonogenic assays (L18W/30

Fig. 6 (continued) Cayman Chemicals, Cymitquimica, and Spectrum Chemical websites), PubChem (https:/pubchem.ncbi.nlm.nih.gov/), Drugbank (https:/www.drugbank.ca/), Drugfuture (https:/www.drugfuture.com/), Druglead (http:/www.druglead.com/), LC Laboratories (http:/www.lclabs.com/), National Center for Advancing Translational Sciences (https:/ncats.nih.gov/), Merck-Millipore (http:/merckmillipore.com/), Pfizer (https:/www.safetydatasheets.pfizer.com/), Santa Cruz Biotechnology (https:/www.scbt.com/), Selleckchem (http:/www.selleckchem.com/), and the Toxicological Data Network (TOXNET, https:/toxnet.nlm.nih.gov/). The half maximum inhibitory concentration (IC_{50}, used for proliferation and enzymes) and half maximum growth inhibitory concentrations (GI_{50}) were obtained from the available literature. This also applies to LC_{50}, LD_{50}, and $t_{1/2}$ data that were missing from or inconsistent in the abovementioned databases. *Abbreviations: Em* emission, *Ex* excitation, *ip* intraperitoneal, *iv* intravenous, *LDLO* lowest dose causing death, *Max. TLD* maximum tolerated dose, *MW* molecular weight, *NA* information not available, *sc* subcutaneous, *TDLO* the lowest dose causing a toxic effect, λ_{max} the wavelength at which there is an absorption maximum (may be multiple absorption bands)

Ascorbic acid (vitamin C)

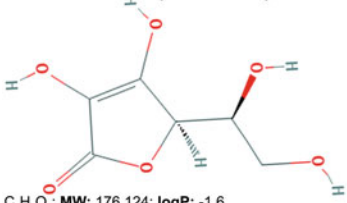

$C_6H_8O_6$; **MW:** 176.124; **logP:** -1.6
t1/2: 16 d (plasma, low dose)
Fluorescence: NA; **λmax**: 244 nm
IC50: NA; **LC50**: NA
LD50: 11.9 g/kg (oral), 5 g/kg (sc), 1 g/kg (iv) - rat
3367 mg/kg (oral), 50.5 g/kg (iv), 5 g/kg (sc)
2 g/kg (ip) - mouse

AW464

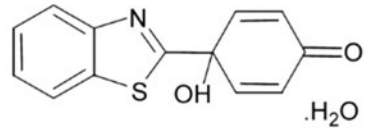

$C_{16}H_9NO_2S$; **MW:** 243.280; **logP:** 2.0
t1/2: NA
Fluorescence: NA; **λmax**: NA
IC50: 0.85 μM - HIF-1α transactivation activity of phosphoglycerate kinase luciferase
LC50: NA
LD50: NA

Baicalein

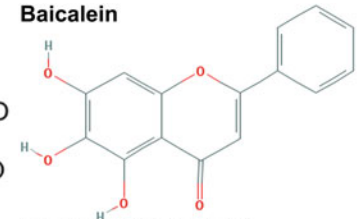

$C_{15}H_{10}O_5$; **MW:** 270.240; **logP:** 1.31
t1/2: NA
Fluorescence: NA; **λmax**: 276, 324 nm (ethanol)
IC50: 6.2 ± 1.3 μM - LNCaP,
21.3 ± 2.5 μM - CWR22Rv1, 15.2 ± 2 μM - C4-2
27.3 ± 3 μM - PC-3, 33.8 ± 3.5 μM - DU145
LC50: NA; **LD50**: NA;
TDLO: 24.6 μg/kg (sc) - mouse,
10 mg/kg (ip) - mouse, 30 mg/kg (ip) - rat

BAY 87-2243

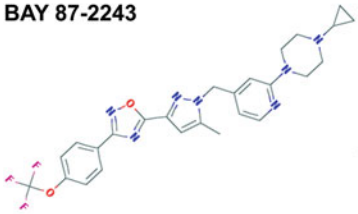

$C_{26}H_{26}F_3N_7O_2$; **MW:** 525.536; **logP:** 4.7
t1/2: NA
Fluorescence: NA; **λmax**: 250 nm
IC50: ~0.7 nM - VEGF HRE luciferase assay,
2.0 nM - CA-9 (HCT-116 lysate)
LC50: NA
LD50: NA

Berberine

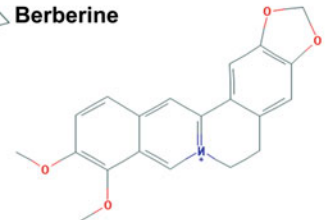

$C_{20}H_{18}NO_4^+$; **MW:** 336.367; **logP:** 3.6
t1/2: Berberin hydrochloride 25 mg/kg (22 mg/kg berberine) (oral) - rats, 573.21 ± 127.53 min (plasma)
Fluorescence: Ex 425 nm, Em 553 nm (cyclohexane)
Ex 429 nm, Em 534 nm (1-butanol)
λmax: 434 nm (DMSO), 433 nm (ethanol)
416 nm (PBS); **IC50**: ~7.5 μM - CL-1-5, SC-M1
LC50: NA; **LD50**: 37 mg/kg (ip) - mouse,
>29.6 g/kg (oral) - mouse, >15 g/kg (oral) - rat

Bortezomib

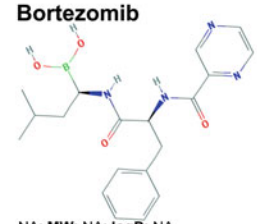

NA; **MW:** NA; **logP:** NA
t1/2: 1 mg/m² ~40 - 193 hr, 1.3 mg/m² ~76 - 108 hr
Fluorescence: Ex 265 nm, Em 420 nm
λmax: 270 nm
IC50: ~10 nM - ARH77, U266
>1 μM - Hep3B
LC50: NA; **LD50**: NA;
TDLO: 1.6 mg/kg/12 d (sc) - mouse,
5 mg/kg/14 d (ip) - mouse

Caldoramide

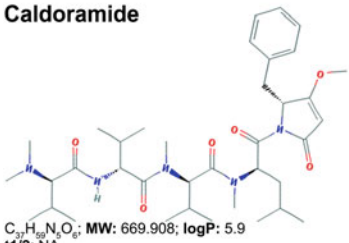

$C_{31}H_{56}N_4O_6$; **MW:** 669.908; **logP:** 5.9
t1/2: NA
Fluorescence: NA; **λmax**: NA
IC50: 3.9 μM - HCT116, 5.2 μM - HCT116$^{HIF\text{-}1\alpha-/-2\alpha-/-}$,
8.6 μM - HCT116$^{WT\ KRAS}$; **LC50**: NA
LD50: NA

Chaetocin

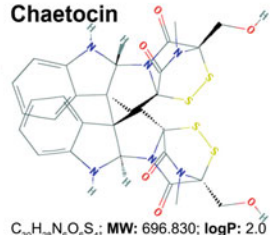

$C_{30}H_{28}N_6O_6S_4$; **MW:** 696.830; **logP:** 2.0
t1/2: NA; **Fluorescence**: NA; **λmax**: NA
IC50: 0.6 μM - SU(VAR)3-9, 0.8 μM - SUV39H1,
3.0 μM - G9a (mouse); **GI50**: 8 nM - aortic ring - rat
LC50: NA; **LD50**: 1200 mg/kg (oral) - mouse,
1700 μg/kg (ip) - mouse

Chetomin

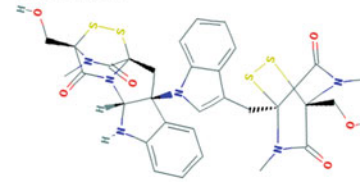

$C_{31}H_{30}N_8O_6S_4$; **MW:** 710.857; **logP:** 1.9
t1/2: 2 mg/kg (iv) 4 hr - mouse
Fluorescence: NA; **λmax**: NA
IC50: NA; **GI50**: 4.1 nM (2.29-6.89) - HMCL panel
20 nM - aortic ring - rat, 1.56 nM - MM (patient)
861,3 ± 29,7 nM - HeLa
LC50: NA; **LD50**: 75 mg/kg (oral) - rat

Cinnamic aldehyde

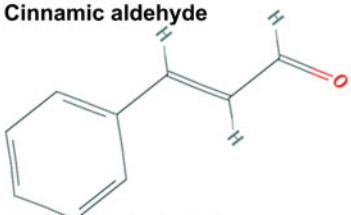

C_9H_8O; **MW:** 132.162; **logP:** 1.9
t1/2: 37°C in blood 4.3 min - human
room temperature plasma 24 hr - rat
oral administration 6.7 hr - rat
Fluorescence: NA; **λmax**: 291 nm (ethanol)
IC50: 9.76 ± 0.67 μM - HepG2; **LC50**: NA
LD50: 3400 mg/kg (oral), 1200 mg/kg (dermal) - rat
200 mg/kg (oral), 200 mg/kg (ip), 75 mg/kg (iv) -
mouse, 1600 mg/kg (oral) - Guinea pig
0.59 mg/kg (dermal) - rabbit

Colchicine

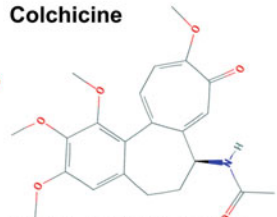

$C_{22}H_{25}NO_6$; **MW:** 399.443; **logP:** 4.1
t1/2: 9 - 10.5 hr - healthy humans
2 hr - patients with alcoholic cirrhosis
Fluorescence: NA; **λmax**: 351 nm (ethanol);
202, 243, 352 nm
IC50: 3 nM - microtubule poolymerization; **LC50**: NA
LD50: 0.25 mg/kg (iv) - cat, 5886 μg/kg (oral)
2 mg/kg (ip), 4.13 mg/kg (iv), 11.97 μg/kg (im)
1700 μg/kg (sc) - mouse, 26 mg/kg (oral)
1.6 mg/kg (iv), 1.4 mg/kg (ip) - rat

Compound 7

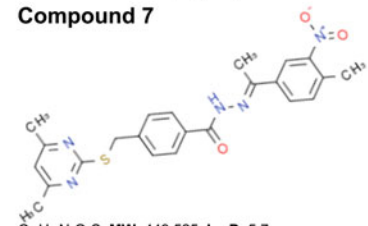

$C_{23}H_{23}N_5O_3S$; **MW:** 449.525; **logP:** 5.7
t1/2: NA
Fluorescence: NA; **λmax**: NA
IC50: 3.9 μM - malate dehydrogenase-2
LC50: NA
LD50: NA

Fig. 6 (continued)

Compound DJ12

NA

NA; **MW:** NA; **logP:** NA
t1/2: NA
Fluorescence: NA; **λmax**: NA
IC50: VEGF 50 μM 16 hr - MDA-MB-468
LC50: 191 μM 16 hr - MDA-MB-468 (normoxia), 19 μM 3 d - MDA-MB-468 (normoxia) 26 μM 3 d - MDA-MB-468 (hypoxia)
LD50: NA

Convallatoxin

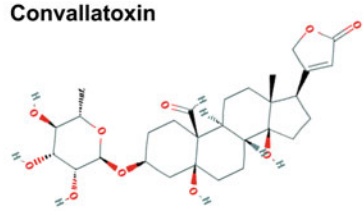

$C_{29}H_{42}O_{10}$; **MW:** 550.645; **logP:** -0.7
t1/2: 40 - 50 hr; **Fluorescence**: NA; **λmax**: NA
IC50: 0.02 - HIF-1
27.65 ± 8.5 nM (24 hr) - MCF-7,
5.32 ± 0.15 (72 hr) - MCF-7,
41.30 ± 6.33 nM (24 hr) - MDA-MB-468,
22.90 ± 1.10 nM (72 hr) - MDA-MB-468,
281.03 ± 36.01 nM (24 hr) - MDA-MB-231,
155.55 ± 28.49 nM (72 hr) - MDA-MB-231
LC50: NA; **LD50**: 6.3 mg/kg (iv) - mouse

Cucurbitacin B

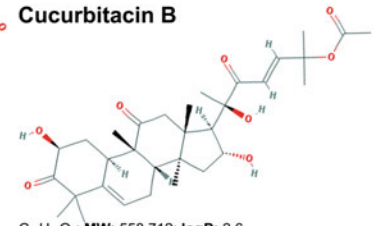

$C_{32}H_{48}O_8$; **MW:** 558.712; **logP:** 2.6
t1/2: Micellar formulation (iv) 0.75 hr
Fluorescence: NA; **λmax**: 228 nm (ethanol)
IC50: 70.14 nM - U87
LC50: 4.6 μg/mL - SKBR-3, 88.75 μg/mL - MCF-7
LD50: 14 mg/kg (oral) 1 mg/kg (sc, ip) - mouse

Cymarin

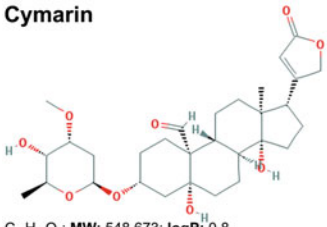

$C_{30}H_{44}O_9$; **MW:** 548.673; **logP:** 0.8
t1/2: 13 - 23 hr
Fluorescence: NA; **λmax**: NA
IC50: NA
LC50: NA
LD50: NA

Daunorubicin

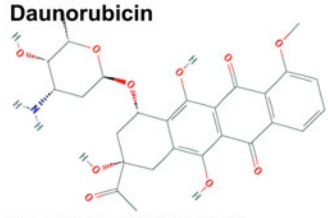

$C_{27}H_{29}NO_{10}$; **MW:** 527.526; **logP:** 1.8
t1/2: Oral administration ~18.5 hr (plasma)
Fluorescence: NA
λmax: 234, 252, 290, 480, 495, 532 nm
IC50: 0.4 μM - L3.6
LC50: 12.6, 3.2, 0.4 μM - H9c2 (6, 24, 48 hr)
10.2, 3.2, 0.4 μM - PC-3 (6, 24, 48 hr)
LD50: 20 mg/kg (iv) - mouse, 13 mg/kg (iv) - rat

Deoxysappanone B 7,3'-dimethyl ether acetate

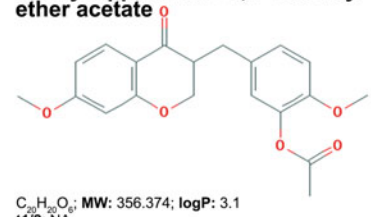

$C_{20}H_{20}O_6$; **MW:** 356.374; **logP:** 3.1
t1/2: NA
Fluorescence: NA; **λmax**: NA
IC50: 1.32 μM - NSC
Survival at 10 μM: 28.6% - SN143, 28.6% - SN175
39.5% - SN179, 36.24% - SN 186, 38.3% - G144
LC50: NA
LD50: NA

Digitoxin

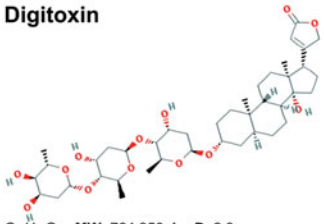

$C_{41}H_{64}O_{13}$; **MW:** 764.950; **logP:** 2.3
t1/2: 4 - 14 d - human, 4.1 days - guinea pig
Fluorescence: NA; **λmax**: 217 nm
IC50: 0.74 μM - HCT116, 0.41 μM - CC20,
3.2 ± 0.1 nM - TK10, 10.2 ± 0.3 nM - MCF-7,
33.5 ± 0.9 - UACC-62
LC50: NA; **LD50**: 4950 μg/kg (oral) - mouse,
3900 μg/kg (ip) - mouse, 22180 μg/kg (sc) - mouse,
23750 μg/kg (oral) - rat, 16430 μg/kg (sc) - rat
TDLO: 286 μg/kg - human

Digoxin

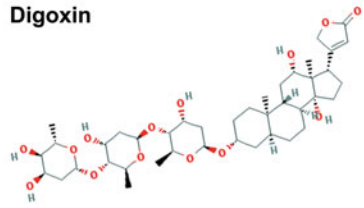

$C_{41}H_{64}O_{14}$; **MW:** 780.949; **logP:** 1.3
t1/2: 34 - 44 hr. Patients with renal failure >4.5 days
Fluorescence: NA; **λmax**: 220 nm (methanol)
IC50: 0.27 μM - HCT116, 1.40 μM - HT29
0.24 μM - CC20, 14.6 ± 2.2 nM - TK10,
24.1 ± 2.1 nM - MCF-7, 29.5 ± 4.8 - UACC-62
LC50: NA; **LD50**: 7.8 mg/kg (oral) - mouse,
3964 μg/kg (ip) - mouse, 28270 μg/kg (oral) - rat,
4 mg/kg (ip) - rat, 8900 ng/kg (sc) - rat
TDLO: 100 μg/kg - woman

Dihydrotanshinone I (DHTS)

$C_{18}H_{14}O_3$; **MW:** 278.307; **logP:** 3.2
t1/2: NA
Fluorescence: NA; **λmax**: 215, 241, 290 nm
IC50: SGC7901 cells, 9.14 μM - 24 hr
3.46 μM - 48 hr
MGC803 cells, 5.39 μM - 24 hr
4.32 μM - 48 hr
LC50: NA
LD50: NA; **TDLO**: 10 mg/kg (oral) - mouse

Diphenylene iodonium

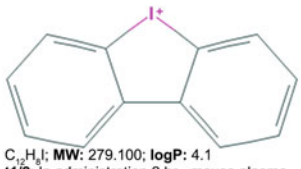

$C_{12}H_8I$; **MW:** 279.100; **logP:** 4.1
t1/2: Ip administration 2 hr - mouse plasma
Fluorescence: NA; **λmax**: NA
IC50: 1.4 μM - PI3K, 10 nM - Caco2, 100 nM - HT-29,
250 nM - LS-174T, >2500 nM - DU145
Colony formation (HT-29) 9.257 ± 3.920 nM - 2 hr,
799 ± 180 nM - 6 hr, 39 ± 23 nM - 10 d
LC50: NA; **LD50**: NA

Discodermolide

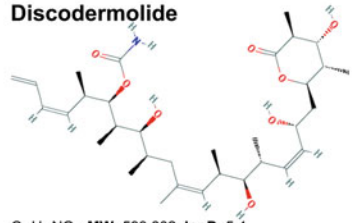

$C_{33}H_{53}NO_8$; **MW:** 593.802; **logP:** 5.4
t1/2: NA
Fluorescence: NA; **λmax**: NA
IC50: 7 nM - A549 (72 hr)
LC50: NA
LD50: NA

Docetaxel (taxotere)

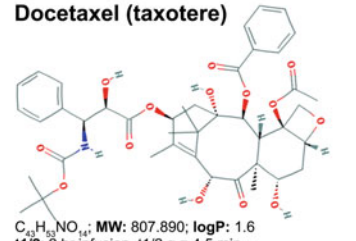

$C_{43}H_{53}NO_{14}$; **MW:** 807.890; **logP:** 1.6
t1/2: 2 hr infusion t1/2,α = 4.5 min
t1/2,β = 38.3 min, t1/2,γ = 12.2 hr. biphasic t1/2 =
7 min and 1.2 hr - mouse, 4 min and 6.6 hr - dogs
Fluorescence: NA; **λmax**: 230, 275, 283 nm
IC50: NA; **LC50**: NA; **LD50**: >2000 mg/kg (oral) - rat
overdose 150-200 mg/m^2 1 hr infusion
TDLO: 12.5 mg/kg (ip) - mouse,
15 mg/kg/11 d (ip, intermittent) - rat

Fig. 6 (continued)

Dolastatin 10

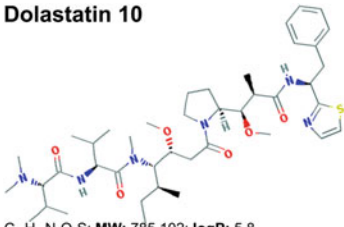

$C_{42}H_{68}N_6O_6S$; **MW:** 785.102; **logP:** 5.8
t1/2: 12.7 - 18.9 hr - human, 5.6 hr - mouse
Fluorescence: NA; **λmax**: NA
IC50: 1.2 μM - tubulin polymerization,
0.5 nM - L1210, 0.48 nM - HCT116
65 nM - HCT116$^{HIF\text{-}1\alpha-/-2\alpha-/-}$, 24 nM - HCT116$^{WT\ KRAS}$
LC50: NA; **LD50**: NA

Doxorubicin

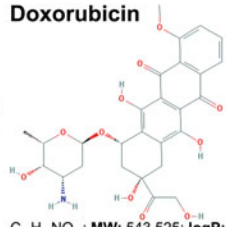

$C_{27}H_{29}NO_{11}$; **MW:** 543.525; **logP:** 1.3
t1/2: 20 - 48 hr; **Fluorescence**: NA
λmax: 233, 253, 290, 477, 495 nm (56 °C methanol)
IC50: 2.2 μM - L3.6
LC50: 5.1, 1.1, 0.2 μM - H9c2 (6, 24, 48 hr)
15.1, 0.9, 0.2 μM - PC-3 (6, 24, 48 hr)
LD50: 21.8 mg/kg (sc) - rat

Echinomycin

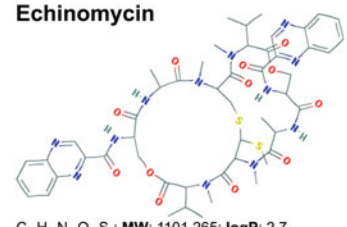

$C_{51}H_{64}N_{12}O_{12}S_2$; **MW**: 1101.265; **logP**: 2.7
t1/2: nucleotide dependent An-Tn < 3 min - 35 min
(TAA)4CG(TTA)4 ~ 35 min; **Fluorescence**: NA
λmax: 321 nm, 243 nm (methanol)
LC50: NA; **LD50**: 400 μg/kg (ip), 3800 μg/kg (sc),
629 μg/kg (iv) - mouse; **LDLO**: 89 μg/kg - dog

ENMD-1198

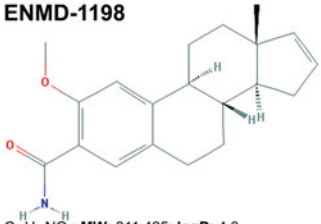

$C_{20}H_{25}NO_2$; **MW:** 311.425; **logP:** 4.3
t1/2: 15 mg/kg (oral) 31.7 hr - mouse
15.5 hr - dog
Fluorescence: NA; **λmax**: NA
IC50: 0.44 μM - HT-29; **GI50**: large cell panel
~0.1 μM;
LC50: NA
LD50: NA

ENMD-1200

NA

NA; **MW:** NA; **logP:** NA
t1/2: 15 mg/kg (oral) - 7.4 hr - mouse
15 mg/kg (oral) - 14 hr - dog
Fluorescence: NA; **λmax**: NA
IC50: 0.78 μM - HT-29
GI50: ~0.34 μM - large cell line panel
LC50: NA
LD50: NA

ENMD-1237

NA

NA; **MW:** NA; **logP:** NA
t1/2: 151 mg/kg (oral) - 11.2 hr - mouse
15 mg/kg (oral) - 7.9 hrs - dog
Fluorescence: NA; **λmax**: NA
IC50: 3.64 μM
GI50: ~2.22 μM - large cell line panel
LC50: NA
LD50: NA

Epirubicin

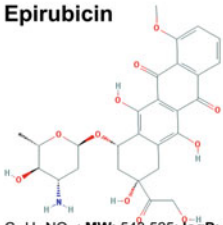

$C_{27}H_{29}NO_{11}$; **MW:** 543.525; **logP:** 1.3
t1/2: t1/2,α = 3.0 min,
t1/2,β = 2.5 hr, t1/2,γ = 33 hr
Fluorescence: Ex 482 nm, Em 570 nm in
phosphate buffer (0.1 mol/L pH = 7.4)
λmax: 234, 252, 289, 479 nm
IC50: NA
LC50: NA
LD50: 14.27 mg/kg (iv) - rat
16.07 mg/kg (iv) - mouse, 2 mg/kg (iv) - dog

Epothilone B

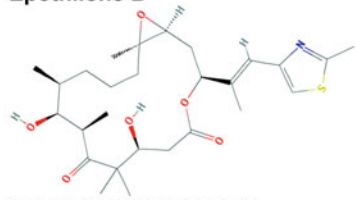

$C_{27}H_{41}INO_6S$; **MW:** 507.686; **logP:** 4.2
t1/2: 6.5 - 10.0 mg/m² (24 hr infusion), init rapid
decline then long terminal half-life 4 - 7 d
Fluorescence: NA; **λmax**: 212, 250 nm
IC50: 0.8 nM - HCT116
1-10 nM - RPMI 8826, U266, MM. 1S, LR5, MR20,
3-92 nM - KB3-1, KBV-1, HeLa (mitotic arrest),
Hs578T
LC50: NA; **LD50**: NA
TDLO: 2.4 mg/kg/4 d (ip) - mouse

Ethacrynic acid

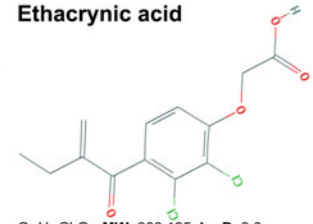

$C_{13}H_{12}Cl_2O_4$; **MW:** 303.135; **logP:** 3.8
t1/2: 12 - 160 min
Fluorescence: NA
λmax: Ethacrynate sodium 225 nm (water), 270 nm
IC50: ~131.1 ± 5.8 μM - HIF-1α binding with p300
GI50: 234.4 ± 6.5 μM - HeLa; **LC50**: NA
LD50: 1 g/kg (oral) - rat, 43 mg/kg (ip) - rat,
600 mg/kg (oral) - mouse, 160 mg/kg (ip) - mouse
189 mg/kg (sc) - mouse
TDLO: 4 mg/kg (oral) - woman, 3 mg/kg (oral) - man

ETPs (gliotoxin)

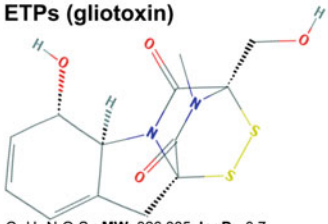

$C_{13}H_{14}N_2O_4S_2$; **MW:** 326.385; **logP:** -0.7
t1/2: NA; **Fluorescence**: NA; **λmax**: 202, 269 nm
IC50: 289 ± 328 μM - breast cancer cell line panel
GI50: 151 nM - aortic ring - rat
LC50: NA; **LD50**: 67 mg/kg (oral) - mouse,
32 mg/kg (ip) - mouse, 25 mg/kg (sc) - mouse

Everolimus

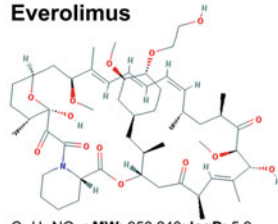

$C_{53}H_{83}NO_{14}$; **MW:** 958.240; **logP:** 5.9
t1/2: ~30 hr
Fluorescence: NA; **λmax**: 268, 277, 289 nm
IC50: 3227 nm - primary breast cancer stem cells
2054 nM - BT474 stem cells
LC50: NA; **LD50**: >2000 mg/kg (oral) - mouse, rat
TDLO: 25-150 mg/kg (oral) - Mouse,
18-21 mg/kg (oral) - rat

EZN-2208

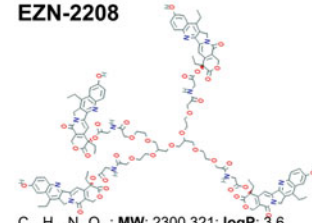

$C_{118}H_{122}N_{12}O_{34}$; **MW**: 2300.321; **logP**: 3.6
t1/2: 19.4 ± 3.4 hr
Fluorescence: NA; **λmax**: NA
Max. TLD: 10 mg/m² per 3 wk
LC50: NA **LD50**: NA
Note: PEGylated analog of SN38

Fig. 6 (continued)

EZN-2968

5'-TGGcaagcatccTGTa-3'

NA; **MW:** NA; **logP:** NA
t1/2: NA
Fluorescence: NA; **λmax**: NA
IC50: 1-5 nM - HIF-1α mRNA
82 ± 73 nM - DU145, >20 nM - A549
LC50: NA
LD50: NA

Fisetin

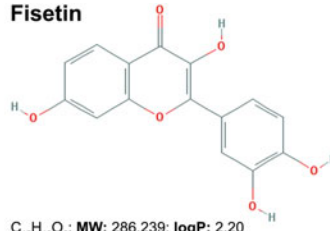

$C_{15}H_{10}O_6$; **MW:** 286.239; **logP:** 2.20
t1/2: NA; **Fluorescence**: Two-photon microscopy
Ex 780 nm, Em 550 nm (DMSO)
λmax: 252, 320, 360 nm (ethanol)
IC50: 26 ± 1 μM - H157 (proliferation)
21 ± 4 - H157 (viability, hypoxia),
28 ± 2 μM - H157 (viability, normoxia),
5.5 ± 0.7 μM - VEGF
LC50: NA; **LD50**: NA; **TDLO**: 10 mg/kg (oral) - mouse

FK228 (romidepsin)

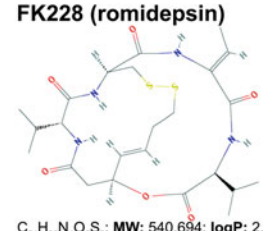

$C_{24}H_{36}N_4O_6S_2$; **MW:** 540.694; **logP:** 2.2
t1/2: ~3 hr
Fluorescence: NA; **λmax**: NA
IC50: 3 nM - HDAC1, 39 nM - HDAC2,
53 nM - HDAC3, 26 nM - HDAC8
LC50: NA
LD50: 6400 μg/kg (ip), 10 mg/kg (iv) - mouse
TDLO: 0.8 mg/kg/60 d (iv) intermittent - mouse
5.4 mg/kg/12 d (ip), 4.48 mg/kg/12 d (ip) - mouse

G0811

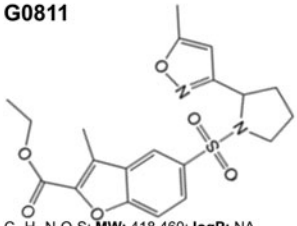

$C_{20}H_{22}N_2O_6S$; **MW:** 418.460; **logP:** NA
t1/2: NA
Fluorescence: NA; **λmax**: NA
IC50: NA
LC50: NA
LD50: NA

Ganetespib

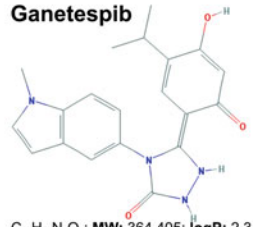

$C_{20}H_{20}N_2O_3$; **MW:** 364.405; **logP:** 2.3
t1/2: 125 mg/kg (iv) NCI-H1975 xenograft mice
3 hr (plasma), 5 - 6 hr - normal liver/lung
58 hr in tumor
Fluorescence: NA; **λmax**: 227, 276, 299 nm
IC50: 2-600 nM - 57 cell lines
LC50: NA; **LD50**: NA

Geldanamycin

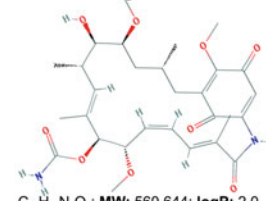

$C_{29}H_{40}N_2O_9$; **MW:** 560.644; **logP:** 2.0
t1/2: 77.7 min - mouse, 57.9 min - dog
Fluorescence: NA; **λmax**: 257, 306 nm
IC50: 60 ± 18 nM - PCA
GI50: mean 0.18 μM - 60 cell lines
LC50: mean 21 μM - 60 cell lines
LD50: 2500 mg/kg (oral) - rat, 1 mg/kg (ip) - mouse

GL331

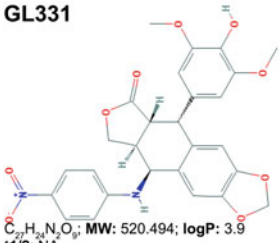

$C_{22}H_{24}N_2O_9$; **MW:** 520.494; **logP:** 3.9
t1/2: NA
Fluorescence: NA; **λmax**: NA
IC50: 0.5-2 μM - cell line panel
LC50: NA
LD50: NA

Glyceollin isomer 1, 2, 3 (mix)

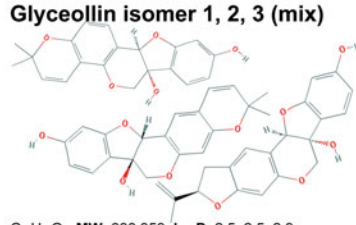

$C_{20}H_{18}O_4$; **MW:** 338.359; **logP:** 2.5, 2.5, 2.9
t1/2: NA
Fluorescence: NA
λmax: Glyceollin 1 (210, 230, 282 nm)
Glyceollin 2 (211, 228, 283, 307 nm)
Glyceollin 3 (211, 227, 289, 354 nm)
IC50: 6 μM - VEGR-2; **LC50**: NA; **LD50**: NA

Hypericin

$C_{30}H_{16}O_8$; **MW:** 504.450; **logP:** 6.9
t1/2: 0.05 mg/kg/d - 36.1 hr
0.10 mg/kg/d - 33.8 hr
Fluorescence: Ex 545, 593 nm,
Em 593, 640 nm (DMSO)
λmax: 514, 550, 593 nm (complete RPMI 1640)
217, 286, 328, 385, 476, 511, 548, 591 nm
IC50: NA; **LC50**: 5 μg/mL - MCF-7; **LD50**: NA
TDLO: 0.01 mg/kg/2 hr (oral) - mouse

Idarubicin

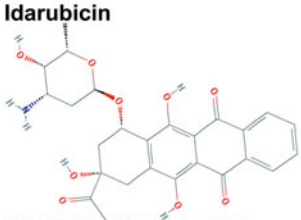

$C_{26}H_{27}NO_9$; **MW:** 497.500; **logP:** 1.9
t1/2: 22 hr
Fluorescence: Ex 570 nm, Em 545 nm in 31:69 v/v
(acetonitrile/ammonium formate buffer, pH = 4.0)
λmax: 252, 287, 482 nm; **IC50**: NA; **LC50**: NA
LD50: 5.43 mg/kg (oral), 2.93 mg/kg (sc)
3.08 mg/kg (iv) - rat, 13.98 mg/kg (oral)
4.69 mg/kg (sc), 4.1 mg/kg (iv) - mouse
LDLO50: 700 μg/kg (ip) - mouse

Kamebakaurin

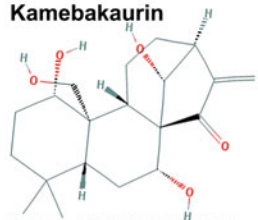

$C_{20}H_{30}O_5$; **MW:** 350.455; **logP:** 1.4
t1/2: NA
Fluorescence: NA; **λmax**: NA
IC50: 9.49 μM - K562, 24.3 μM - KBM5,
35.9 μM - KBM5-T315I, >30 μM - L929, NCM-460
LC50: NA
LD50: NA

KC7F2

$C_{16}H_{16}Cl_4N_2O_4S_4$; **MW:** 570.354; **logP:** 4.7
t1/2: NA
Fluorescence: NA; **λmax**: NA
IC50: Proliferation in cells 15 - 25 μM
LC50: NA
LD50: NA

Fig. 6 (continued)

KCN1

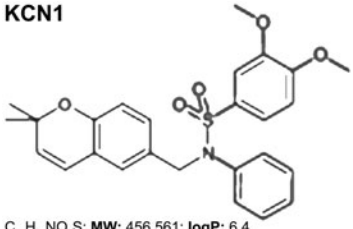

$C_{26}H_{27}NO_5S$; **MW:** 456.561; **logP:** 6.4
t1/2: Tissue-dependent 35 mg/kg (iv) 0.16 - 23.17 hr, 35 mg/kg (ip) 0.60 - 22.42 hr - mouse
Fluorescence: NA; **λmax**: NA
IC50: 593 ± 63 nM - HIF-1α transcriptional activity in LN229CMV-luc cells, 17.91 ± 0.12 μM - HPAC 99.99 ± 2.35 μM - Panc-1, 14.62 ± 0.10 μM - BxPC3 69.91 ± 2.12 μM - MIA PaCa-2
LC50: NA; **LD50**: NA

KF58333

$C_{24}H_{27}IN_2O_7$; **MW:** 490.937 NA; **logP:** 3.5
t1/2: NA
Fluorescence: NA; **λmax**: NA
IC50: 0.033 μM - K562
LC50: NA
LD50: NA

KST012174

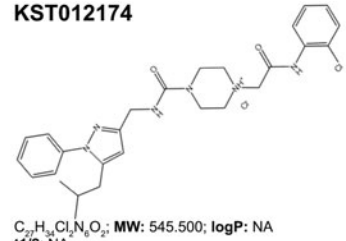

$C_{27}H_{34}Cl_2N_6O_2$; **MW:** 545.500; **logP:** NA
t1/2: NA
Fluorescence: NA; **λmax**: NA
IC50: ~107 μM - HIF-1α binding with p300
LC50: NA
LD50: NA

Largazole

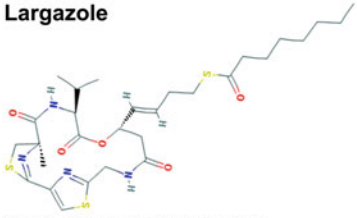

$C_{26}H_{42}N_4O_5S_3$; **MW:** 622.858; **logP:** 5.5
t1/2: 0.5 ± 0.07 hr - rats
Fluorescence: NA; **λmax**: NA
IC50: NA; **GI50**: 7.7 nM - MDA-MB-231 122 nM - NMuMG, 55 nM - U2OS, 480 nM - NIH-3T3 16 nM - IMR-32, 6.41 nM - HCT116, 18 nM - HCT116$^{HIF\text{-}1\alpha-/-2\alpha-/-}$, 3.7 nM - HCT116$^{WT\ KRAS}$
LC50: 94 nM - U2OS, >8 μM - NIH-3T3 22 nM - HT29, 22 nM - IMR-32; **LD50**: NA

Liquiritigenin (LQ)

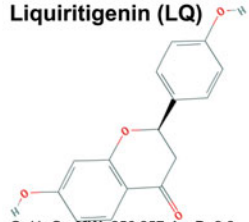

$C_{15}H_{12}O_4$; **MW:** 256.257; **logP:** 2.2
t1/2: 0.1 - 1.17 hr - different animals
Fluorescence: NA; **λmax**: 215, 232, 276, 311 nm
IC50: 49.3 μM - xanthine oxidase
LC50: NA
LD50: NA

Luteolin

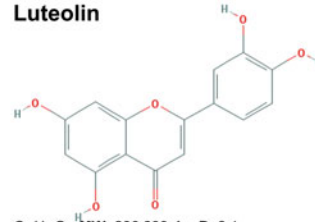

$C_{15}H_{10}O_6$; **MW:** 286.239; **logP:** 2.1
t1/2: NA
Fluorescence: NA; **λmax**: 255, 348 nm
IC50: 13 ± 2 μM - H157 (proliferation) 21 ± 3 μM - H157 (viability, hypoxia) 19 ± 5 μM - H157 (viability, normoxia) 5.5 ± 0.2 μM - VEGF; **LC50**: NA
LD50: 180 mg/kg (ip) - mouse,
TDLO50: 20 mg/kg (oral) - mouse, 140 mg/kg/2 wk (intermittent) - mouse

LW6

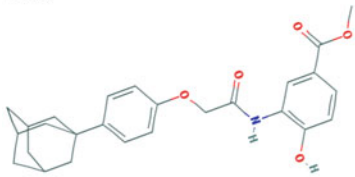

$C_{25}H_{25}NO_5$; **MW:** 435.520; **logP:** 5.7
t1/2: NA
Fluorescence: NA; **λmax**: NA
IC50: HRE luciferase assay 4.4 ± 1.1 μM - HCT116 6.3 ± 0.6 μM - HCT116 (MDH2)
LC50: NA
LD50: NA

LY294002

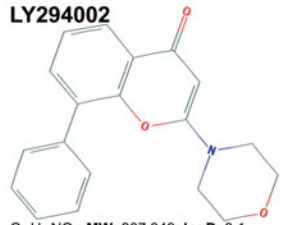

$C_{19}H_{17}NO_3$; **MW:** 307.349; **logP:** 3.1
t1/2: NA
Fluorescence: NA; **λmax**: 223, 302 nm
IC50: 0.5 μM - PI3Kα, 0.97 μM - PI3Kβ, 0.57 μM - PI3Kδ
LC50: NA
LD50: NA

Magnolol

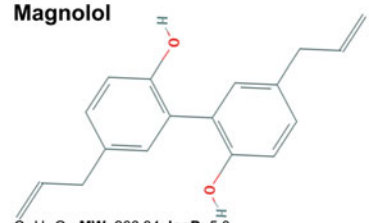

$C_{18}H_{18}O_2$; **MW:** 266.34; **logP:** 5.0
t1/2: 2 - 10 mg/kg (oral) ~15 min
Fluorescence: NA; **λmax**: 215, 292 nm
IC50: 26.6 μM - MCF-7
LC50: NA
LD50: 2200 mg/kg (oral) - mouse

Melittin (Forapin)

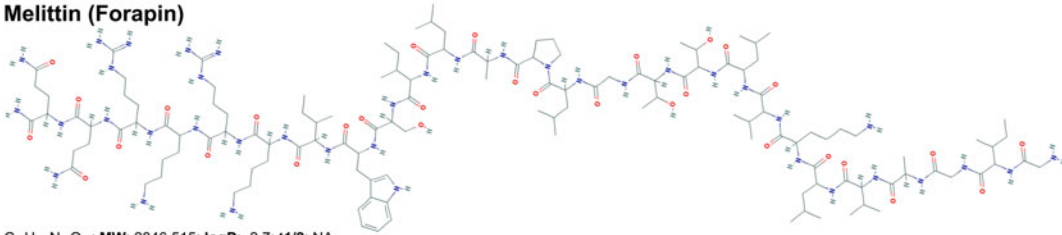

$C_{131}H_{229}N_{39}O_{31}$; **MW**: 2846.515; **logP**: -2.7; **t1/2**: NA
Fluorescence: Ex 295 nm, Em 354 nm, in 25 mM Tris-HCl (pH = 7.5, 0.2 mM EDTA, 3 mM DTT); **λmax**: 280 nm
IC50: 0.51 μM - red blood cells, 0.75 ± 0.19 μM - B16F10; **IC50**: NA
LD50: 5.0 or 7.4 mg/kg (ip) - mouse, 17.7 mg/kg (ip) - rat

Fig. 6 (continued)

Menadione (vitamin K3)

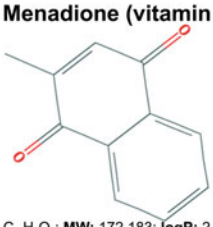

$C_{11}H_8O_2$; **MW:** 172.183; **logP:** 2.2
t1/2: Iv administration precursor menadiol 26.3 ± 2.97 min (plasma)
Fluorescence: NA; **λmax**: 246, 262 nm (in ALC) 251, 332 nm
IC50: HIF-1α binding with p300 ~9.2 ± 1.2 μM
LC50: NA; **LD50**: NA

Methylseleninic acid (MSeA)

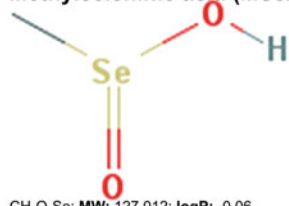

CH_4O_2Se; **MW:** 127.012; **logP:** -0.06
t1/2: 3 mg/kg (oral) 8 hr - nude mouse (serum)
Fluorescence: NA; **λmax**: NA
IC50: NA; **GI50**: <5 μM - PAIII (normoxia/hypoxia)
LC50: NA
LD50: NA

Minocycline

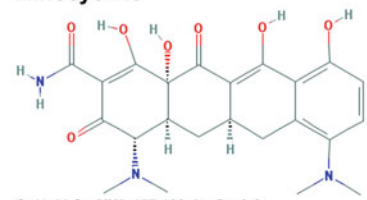

$C_{23}H_{27}N_3O_7$; **MW:** 457.483; **logP:** -0.6
t1/2: 11 - 22 hr
Fluorescence: Ex 458 nm, Em 521 nm
λmax: 263, 352 nm (0.1 N HCl)
342, 380 nm (0.1 N NaOH)
IC50: 10.7 μM - MMP-9; **LC50**: NA
LD50: 2380 mg/kg (oral) - rat
3600 mg/kg (oral) - mouse

MLN0128 (sapanisertib)

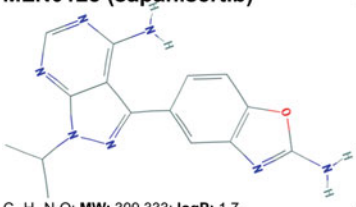

$C_{15}H_{18}N_2O$; **MW:** 309.333; **logP:** 1.7
t1/2: 2 - 12 mg (oral) in patients, 6 - 8 hr (plasma)
Fluorescence: NA; **λmax**: 205, 243, 292 nm
IC50: 1 nM - mTOR , 2-130 nM - proliferation in bone and tissue sarcomas
LC50: NA
LD50: NA

Nerifolin

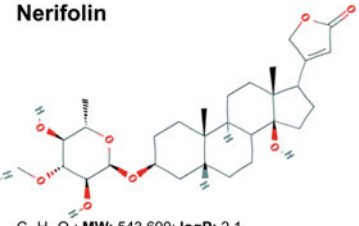

$C_{30}H_{46}O_8$; **MW:** 543.690; **logP:** 2.1
t1/2: NA
Fluorescence: NA; **λmax**: NA
IC50: 17 nM - MCF-7, 21 nM - T47D, 28 nM - SKOV3, 24 nM - CaOV3, Vero
LC50: NA
LD50: NA

Novobiocin

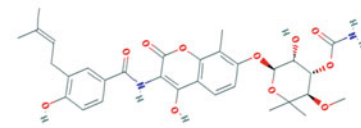

$C_{31}H_{36}N_2O_{11}$; **MW:** 612.632; **logP:** 3.3
t1/2: 500 mg (oral) 5.85 ± 1.20 hr
Fluorescence: NA; **λmax**: 307 nm (0.1 N NaOH), 324 nm (0.1 N methanolic HCl), 390 nm (phosphate buffer, pH = 7)
IC50: 700 μM - HSP90; **LC50**: NA
LD50: 3500 mg/kg (oral), 450 mg/kg (sc) - rat
262 mg/kg (ip) - mouse

NVP-AUY922 (luminespib)

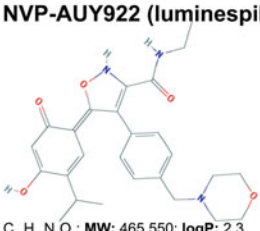

$C_{26}H_{31}N_3O_5$; **MW:** 465.550; **logP:** 2.3
t1/2: 14.7 - 15.5 hr - female mouse (WM266.4 human melanoma xenograft)
Fluorescence: NA; **λmax**: 310 nm
IC50: 2-40 nM - SNU-1,-5,-16,-216,-484, -601,-620,-638,-668,-719, NCI N87
LC50: NA; **LD50**: NA

NVP-LAQ824 (dacinostat)

$C_{22}H_{25}N_3O_3$; **MW:** 379.460; **logP:** 2.6
t1/2: 8 - 14 hr
Fluorescence: NA; **λmax**: 222, 281, 352 nm
IC50: 24, 48, and 72 hr in cells: 0.01 μM - HCT116 0.05, 0.03, 0.03 μM - A549
>3.75, 0.13, 0.04 μM - NDHF
LC50: 24, 48, and 72 hr in cells: 0.64, 0.04, 0.04 μM - HCT116, >3.75, 0.20, 0.16 μM - A549, >3.75, >3.75, 0.61 μM - NDHF; **LD50**: NA

Oligoamine α-helix mimetics

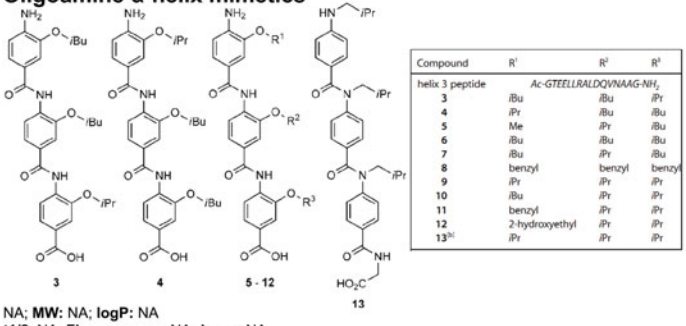

Compound	R^1	R^2	R^3
helix 3 peptide	*Ac-GTEELLRALDQVNAAG-NH_2*		
3	*i*Bu	*i*Bu	*i*Pr
4	*i*Pr	*i*Bu	*i*Bu
5	Me	*i*Pr	*i*Bu
6	*i*Bu	*i*Bu	*i*Bu
7	*i*Bu	*i*Pr	*i*Bu
8	benzyl	benzyl	benzyl
9	*i*Pr	*i*Pr	*i*Pr
10	*i*Bu	*i*Pr	*i*Pr
11	benzyl	*i*Pr	*i*Pr
12	2-hydroxyethyl	*i*Pr	*i*Pr
13[b]	*i*Pr	*i*Pr	*i*Pr

NA; **MW:** NA; **logP:** NA
t1/2: NA; **Fluorescence**: NA; **λmax**: NA
IC50: Varying per compound 9 ± 0.9 - 416 ± 64 μM; **LC50**: NA; **LD50**: NA

Ouabain

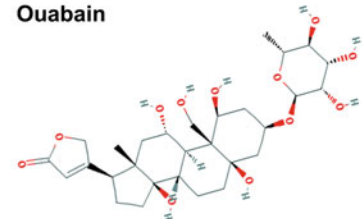

$C_{29}H_{44}O_{12}$; **MW:** 584.659; **logP:** -1.7
t1/2: 11 hr - Guinea pig
Fluorescence: NA; **λmax**: 220 nm
IC50: 63.4 ± 2.9 - human kidney NA+,K+-ATPase
LC50: NA; **GI50**: NA 210 ± 18 - nM - PC-3, 94 ± 11 nM - U937; **LD50**: 14 mg/kg (iv) - rat
11 mg/kg (ip), 2.2 mg/kg (iv) - mouse

Fig. 6 (continued)

Parbendazole

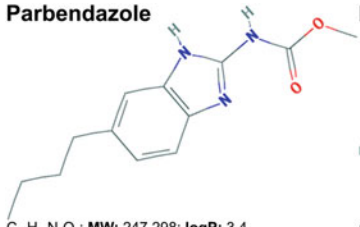

$C_{13}H_{17}N_3O_2$; **MW:** 247.298; **logP:** 3.4
t1/2: 5 mg/kg (iv) 720.0 ± 21.27 min - goat
Fluorescence: NA
λmax: 208, 244, 285, 291 nm (methanol)
IC50: NA; **LC50:** NA; **EC50;** 8.79 nM - tubulin destabilization; **LD50:** >40 mg/kg (oral) - rat
>1.7 mg/kg (oral) - mouse

Periplocymarin

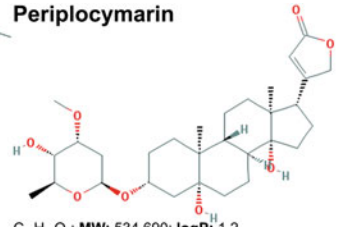

$C_{30}H_{46}O_8$; **MW:** 534.690; **logP:** 1.2
t1/2: 5 mg/kg (oral) 1.36 ± 0.29 hr - rat
10 mg/kg (oral) 1.17 ± 0.26 hr - rat
20 mg/kg (oral) 1.28 ± 0.37 hr - rat
Fluorescence: NA; **λmax:** NA
IC50: NA **GI50:** 180 ± 10 nM - PC-3
83 ± 9 nM - U937
LC50: NA
LD50: NA

Peruvoside

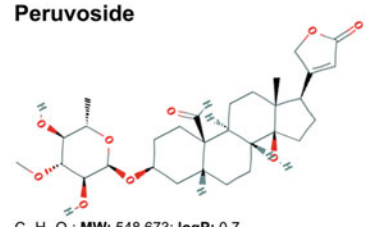

$C_{30}H_{44}O_9$; **MW:** 548.673; **logP:** 0.7
t1/2: 40 - 70 hr; **Fluorescence:** NA; **λmax:** NA
IC50: 27.65 ± 8.5 nM (24 hr) - MCF-7
5.32 ± 0.15 (72 hr) - MCF-7,
79.87 ± 2.19 (24 hr) - MDA-MB-468,
44.66 ± 5.17 (72 hr) - MDA-MB-468,
565.08 ± 56.47 (24 hr) - MDA-MB-231,
308.05 ± 56.39 (72 hr) - MDA-MB-231
LC50: NA; **LD50:** NA

Phenethyl isothiocyanate

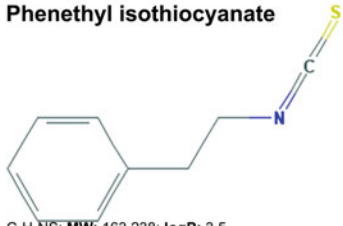

C_9H_9NS; **MW:** 163.238; **logP:** 3.5
t1/2: 50 μmol/kg (oral) 21.7 hr
Fluorescence: NA; **λmax:** NA
IC50: 10.8 ± 1.7 μM - MCF7 (growth)
3 μM - MCF7 (decrease in HIF reporter - hypoxia)
LC50: NA
LD50: 700 mg/kg (oral) - mouse

Pleurotin

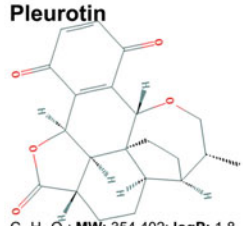

$C_{21}H_{22}O_5$; **MW:** 354.402; **logP:** 1.8
t1/2: NA
Fluorescence: NA; **λmax:** 250 nm
IC50: 0.9 ± 1.0 μM - MCF-7
0.9 ± 1.2 μM - HT-29
LC50: NA
LD50: NA

Proscillaridin A

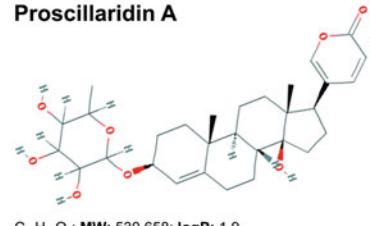

$C_{30}H_{42}O_8$; **MW:** 530.658; **logP:** 1.9
t1/2: 23 - 49 hr
Fluorescence: NA; **λmax:** 297 nm (methanol)
IC50: 0.06 μM - HCT116, 4 ± 6 nM - GMB6,
3 ± 5 nM - GMB9, 2 ± 4 nM - U87-MG
3 ± 5 nM - U251-MG, 0.55 μM - HT29, 9.6 μM - CC20
LC50: NA; **LD50:** 56 mg/kg (oral) - rat,
>1 g/kg (sc) - rat, 30.5 mg/kg (oral) - mouse

Purine scaffold compound 16

NA

NA; **MW:** NA; **logP:** NA
t1/2: 9 hr (oral) - BALB/c mice (serum)
Fluorescence: NA; **λmax:** NA
IC50: Proliferation in HER-2 expressing cell lines
0.15 μM - MCF-7, 0.05 μM - BT474
LC50: NA
LD50: NA

Purine scaffold compound 20

NA

NA; **MW:** NA; **logP:** NA
t1/2: 0.8 hr (oral) - BALB/c mice (serum)
Fluorescence: NA; **λmax:** NA
IC50: Proliferation in HER-2 expressing cell lines
0.10 μM - MCF-7, 0.10 μM - BT474
LC50: NA
LD50: NA

PU-H71

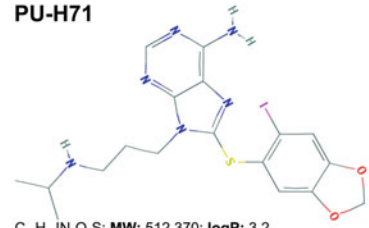

$C_{18}H_{21}IN_6O_2S$; **MW:** 512.370; **logP:** 3.2
t1/2: Iv administration cancer patients ~8.4 ± 3.6 hr
Fluorescence: NA; **λmax:** NA
IC50: 51 ± 7 nM - MDA-MB-468
140 ± 5 nM - MDA-MB-231, 87 ± 3 nM - HCC-1806
LC50: NA
LD50: NA

PX-12

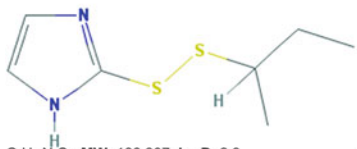

$C_7H_{12}N_2S_2$; **MW:** 188.307; **logP:** 2.3
t1/2: NA
Fluorescence: NA; **λmax:** 235 nm
IC50: 1.9 ± 0.8 μM - MCF-7
2.9 ± 0.0 μM - HT29
LC50: NA
LD50: NA

PX-478

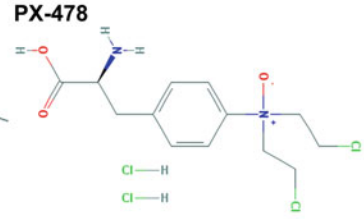

$C_{11}H_{20}Cl_2N_2O_3$; **MW:** 394.114; **logP:** NA
t1/2: 150 mg/kg (iv, ip, oral gavage) ~47 min
- male C57BL/6 mice
Fluorescence: NA; **λmax:** 209, 253, 301 nm
IC50: 2.5 ± 1.2 μM - PC-3 (normoxia)
3.2 ± 1.2 μM - Panc-1 (normoxia)
3.9 ± 2.0 μM - PC-3 (hypoxia)
10.1 ± 1.9 μM - Panc-1 (hypoxia)
LC50: NA; **LD50:** NA; **TDLO:** 120 mg/kg (ip) - mouse
125 mg/kg/5 d (oral) - mouse

Pyrazoles (VER-49009)

$C_{19}H_{18}ClN_3O_4$; **MW:** 387.820; **logP:** 2.5
t1/2: 20 mg/kg (iv) ~0.2 - 0.3 hr - athymic mouse
Fluorescence: NA; **λmax:** NA
IC50: 47 ± 9 nM - human HSP90β;
GI50: Mean 685 ± 119 nM - human
cancer cell line panel
LC50: NA
LD50: NA

Fig. 6 (continued)

Pyrazoles (VER-50589)

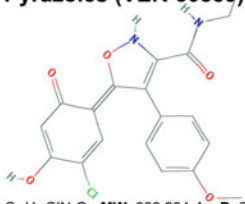

$C_{19}H_{17}ClN_2O_5$; **MW:** 388.804; **logP:** 2.5
t1/2: 20 mg/kg (iv) ~0.2 - 0.3 hr - athymic mice
Fluorescence: NA; **λmax**: NA
IC50: 21 ± 4 nM human HSP90β
GI50: Mean ~75 ± 15 nM - human cancer cell line panel; **LC50**: NA
LD50: NA

Pyridylpyrimidine scaffold P2630

NA

NA; **MW:** NA; **logP:** NA
t1/2: NA
Fluorescence: NA; **λmax**: NA
IC50: 1 μM - PC-3, 0.8 μM - HCT-116, 1.5 μM - U251, 3.5 μM - OVCAR-3, 1.2 μM - DU-145, 2.0 μM - Panc-1 >10 μM - MRC-5, 6.5 μM - WI-38
LC50: NA; **LD50**: NA

Pyridylpyrimidine scaffold P3155

NA

NA; **MW:** NA; **logP:** NA
t1/2: NA
Fluorescence: NA; **λmax**: NA
IC50: 1.4 μM - U251-HRE reporter gene assay (hypoxia), >10 μM - U251-pGL3 (normoxia) reporter gene assay; **LC50**: NA; **LD50**: NA

Quercetin

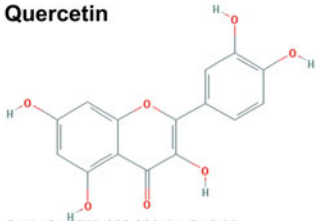

$C_{15}H_{10}O_7$; **MW:** 302.238; **logP:** 2.26
t1/2: NA
Fluorescence: Ex ~380, 440 nm, Em 540 nm intracellular Jurkat cells (RPMI 1640 medium); spectral properties change when bound to different proteins; **λmax**: 256, 367 nm
IC50: 7.7 μM - HL-60, 30.9 μM - PKC, 20.1 μM - TPK, 8.5 ± 1.9 μM - VEGF,
48 ± 8 μM - H157 (viability, hypoxia),
45 ± 6 μM - H157 (viability, normoxia),
33 ± 3 μM - H157 (proliferation)
LC50: NA; **LD50**: 161 mg/kg (oral) - rat,
159 mg/kg (oral) - mouse, 3000 mg/kg (ip) - mouse,
97 mg/kg (sc) - mouse, 18 mg/kg (iv) - mouse

Radicicol (Monorden)

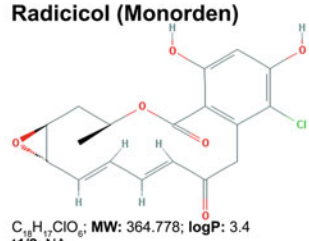

$C_{18}H_{17}ClO_6$; **MW:** 364.778; **logP:** 3.4
t1/2: NA
Fluorescence: NA; **λmax**: 264, 272 nm (ethanol)
IC50: <1 μM - Hsp90
LC50: NA
LD50: 300 mg/kg (oral), 175 mg/kg (iv)
10 mg/kg (sc) - mouse

Rapamycin

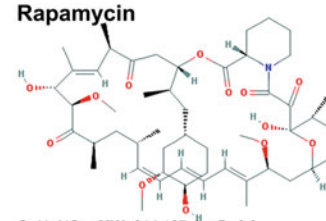

$C_{51}H_{79}NO_{13}$; **MW:** 914.187; **logP:** 6.0
t1/2: 3 mg/kg (ip) in $VCP^{R155H/+}$ mice ~58 - 63 hr
Fluorescence: NA
λmax: 267, 277, 288 nm (95% ethanol)
IC50: 0.122 ± 0.026 μmol/L - mTOR in Y79 cells
LC50: NA
LD50: >2500 mg/kg (oral) - mouse,
18220 μg/kg (ip) - rat, 597 mg/kg (ip) - mouse,
TDLO50: 4.2 mg/kg/8 wk (intermittent) - human

Resveratrol

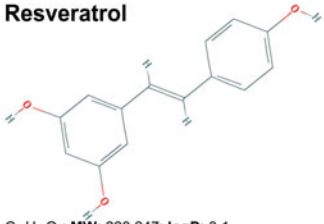

$C_{14}H_{12}O_3$; **MW:** 228.247; **logP:** 3.1
t1/2: Trans-resveratrol 1.48 hr (agylcone form)
1.58 hr (glucuronide form)
Fluorescence: Ex 310 nm (constant in following solvents) Em 380 nm (DMSO), 385-415 nm (water) 378 nm (95% ethanol), 376 nm (isopropanol), 370 nm (ethyl acetate); **λmax**: 218, 307, 321 nm
IC50: Proliferation of ECV304 cells 6 hr - 240.1 μM 24 hr - 70 μM, 48 hr - 54.4 μM,
25 ± 3 μM - VEGF,
104 ± 3 μM - H157 (viability, hypoxia),
100 ± 2 μM - H157 (viability, normoxia),
57 ± 6 μM - H157 (proliferation)
LC50: NA; **LD50**: **TDLO50**: 650 mg/kg (oral) - human

Rotenone

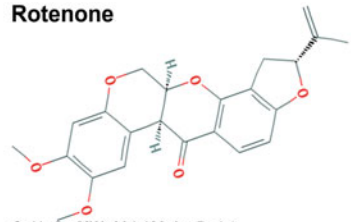

$C_{23}H_{22}O_6$; **MW:** 394.423; **logP:** 4.1
t1/2: NA; **Fluorescence**: NA
λmax: 237, 240, 331 nm (ethanol),
236, 294 nm
IC50: 28.8 nM - NADH/DB oxidoreductase,
5.1 nM - NADH oxidase; **LC50**: NA
LD50: 300 mg/kg (oral) - human,
>940 mg/kg (skin) - rat, 1600 μg/kg (ip) - rat,
200 μg/kg (iv) - rat, 2800 μg/kg (oral) - mouse,
>1 g/kg (skin) - rat, 20 mg/kg (sc) - rabbit
LDLO: 143 mg/kg (oral) - human,
1500 mg/kg (oral) - rabbit
Lethal dose: 0.3 - 0.5 g/kg - human

SCH66336 (lonafarnib)

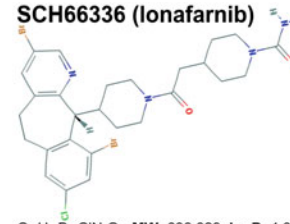

$C_{27}H_{32}Br_2ClN_4O_2$; **MW:** 638.829; **logP:** 4.8
t1/2: Patients with solid tumors 300 - 400 mg
5 - 9 hr
Fluorescence: NA; **λmax**: 278 nm
IC50: NA; **LC50**: NA
LD50: NA

Schiff bases (compound 13)

NA

NA; **MW:** NA; **logP:** 3.49
t1/2: NA
Fluorescence: NA; **λmax**: NA
IC50: 0.15 μM - PC-3
LC50: NA
LD50: NA

SH-1242

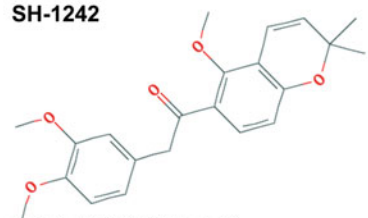

$C_{22}H_{24}O_5$; **MW:** 368.429; **logP:** 4.0
t1/2: NA
Fluorescence: NA; **λmax**: NA
IC50: NA
LC50: NA
LD50: NA

SH-1280

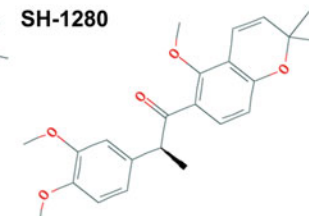

$C_{23}H_{26}O_5$; **MW:** 482.456; **logP:** 4.6
t1/2: NA
Fluorescence: NA; **λmax**: NA
IC50: NA
LC50: NA
LD50: NA

Fig. 6 (continued)

Silibinin

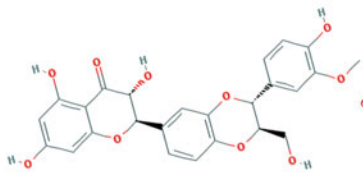

$C_{25}H_{22}O_{10}$; **MW:** 482.441; **logP:** 2.4
t1/2: 50 mg/kg (oral) 57 - 124 min - SENCAR mice
Fluorescence: NA; **λmax**: 229, 288 nm
IC50: HIF-1α ~150 μM - HeLa, Hep3B (hypoxia)
LC50: NA
LD50: NA
TDLO: 400 mg/kg/2 d (oral, intermittent) - rat, 100 mg/kg (ip) - mouse

SN38

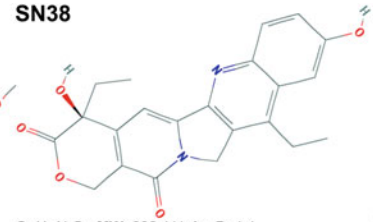

$C_{22}H_{20}N_2O_5$; **MW:** 392.411; **logP:** 1.4
t1/2: 6 - 30 hr
Fluorescence: NA
λmax: 224, 267, 331, 368, 383 nm
IC50: 0.3 nM - TE-1, 37.7 μM - GL261 8.8 nM - HT-28
LC50: NA
LD50: NA

Sodium butyrate

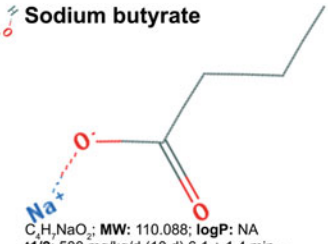

$C_4H_7NaO_2$; **MW:** 110.088; **logP:** NA
t1/2: 500 mg/kg/d (10 d) 6.1 ± 1.4 min - patients with leukemia
Fluorescence: NA; **λmax**: NA
IC50: 65, 18.2, 9.2 mM - HT-29 (24, 48, 72 hr) 35.5, 9.6, 10.0 mM - HCT-116 (24, 48, 72 hr)
LC50: 5 mg/L 24 hr - bluegill sunfish, 1.950 mg/L 24 hr - water flea; **LD50**: NA

Sorafenib

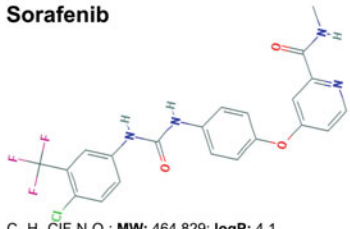

$C_{21}H_{16}ClF_3N_4O_3$; **MW:** 464.829; **logP:** 4.1
t1/2: 600 mg (oral) Japanese patients 24 - 30 hr (plasma)
Fluorescence: NA; **λmax**: 204, 266 nm
IC50: ~4.13 μM - HUH-7 ~8.75 μM - HUH-7^R
LC50: NA
LD50: >2000 mg/kg (oral) - rat
TDLO: 2.84 mg/kg/21 d (oral, intermittent) - human

Strophanthin-K

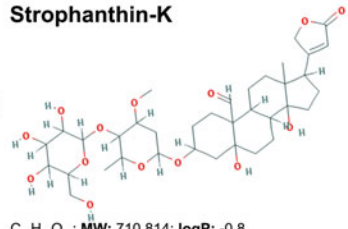

$C_{36}H_{54}O_{14}$; **MW:** 710.814; **logP:** -0.8
t1/2: 0.5 mg (iv, urinary excretion) 98.9 ± 8.4 hr 4.7 mg (oral, urinary excretion) 22.1 ± 2.6 hr
Fluorescence: NA; **λmax**: NA
IC50: NA; **LC50**: NA
LD50: 2.8 mg/kg (iv), 12 mg/kg (ip), 41 μg/kg (ic) - mouse, 20 mg/kg (iv) - rat

Tanshinone-IIA

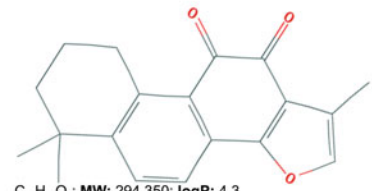

$C_{19}H_{18}O_3$; **MW:** 294.350; **logP:** 4.3
t1/2: Oral administration 237.37 ± 23.03 min - rat
Fluorescence: Ex 328 nm, Em 470 nm (methanol)
λmax: 250, 263, 265 nm (water, ethanol, cyclohexane)
IC50: 65, 18.6, 9.2 mM - HT-29 for 24, 48, and 72 hr, respectively
LC50: 10 μM - LNCaP, 8-15 μM - different prostate cancer cell lines
LD50: NA; **TDLO50**: 50 mg/kg (oral) - mouse, 10 mg/kg (ip) - mouse, 420 mg/kg/wk (oral, intermittent) - rat

TAT-cyclo-CLLFVY

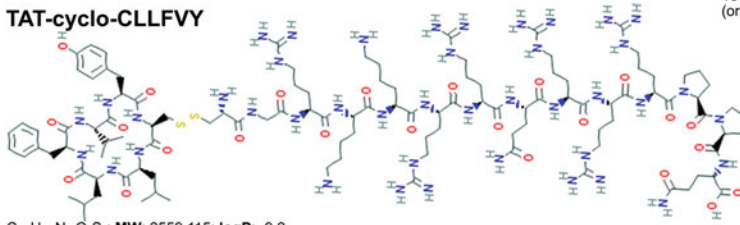

$C_{111}H_{169}N_{42}O_{24}S_4$; **MW**: 2559.115; **logP**: -9.2
t1/2: NA; **Fluorescence**: NA; **λmax**: NA
IC50: HIF-1α dimerization in ELISA ~1.3 μM
LC50: NA; **LD50**: NA

Temsirolimus

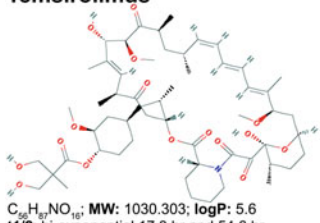

$C_{56}H_{87}NO_{16}$; **MW:** 1030.303; **logP:** 5.6
t1/2: bi-exponential 17.3 hr and 54.6 hr
Fluorescence: NA; **λmax**: 268, 277, 289 nm
IC50: 0.08 nM - A549
LC50: NA
LD50: >50 mg/kg (iv) - mouse, >50 mg/kg (iv) - rat
TDLO: 75 mg/kg/3 wk (ip, intermittent) - mouse

Topotecan

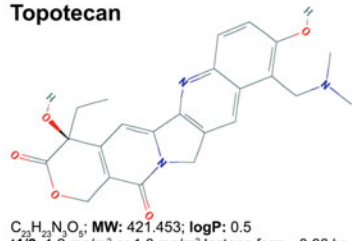

$C_{23}H_{23}N_3O_5$; **MW:** 421.453; **logP:** 0.5
t1/2: 1.2 mg/m^2 or 1.6 mg/m^2 lactone form - 3.86 hr and 3.26 hr, carboxylate form - 3.55 hr and 2.34 hr
Fluorescence: One-photon Ex <400 nm, Em 530 nm two-photon Ex 730, 820 nm, Em 525 nm
λmax: 224, 267, 318, 333, 384 nm
IC50: 13 nM - topoisomerase I (MCF-7 Luc), 13 nM - topoisomerase I (DU-145 Luc); **LC50**: NA
LD50: 74.85 mg/m^2 (iv) - mouse
TDLO: 5.4 mg/kg/3 d (ip, intermittent) - mouse, 40 mg/kg/21 d (oral, intermittent) - mouse

Trichostatin A

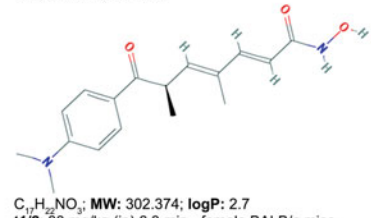

$C_{17}H_{22}NO_3$; **MW:** 302.374; **logP:** 2.7
t1/2: 80 mg/kg (ip) 6.3 min - female BALB/c mice (plasma)
Fluorescence: NA; **λmax**: 265, 340 nm
IC50: HDAC1, 4, 6, 6 nM, 38 nM and 8.6 nM, cell proliferation ~124.4 nM (26.4 - 308.1 nM) - MCF-7, T47D, ZR-75-1, BT-474, MDA-MB-231, MDA-MB-453, Cal 51, SK-BR-3
LC50: NA; **LD50**: 14500 mg/kg (oral) - rat, **TDLO50**: 1800 mg/kg (dermal) - woman, 17.5 mg/kg/5 wk (sc, intermittent) - mouse, 7 mg/kg/7 d (ip, intermittent) - mouse

Fig. 6 (continued)

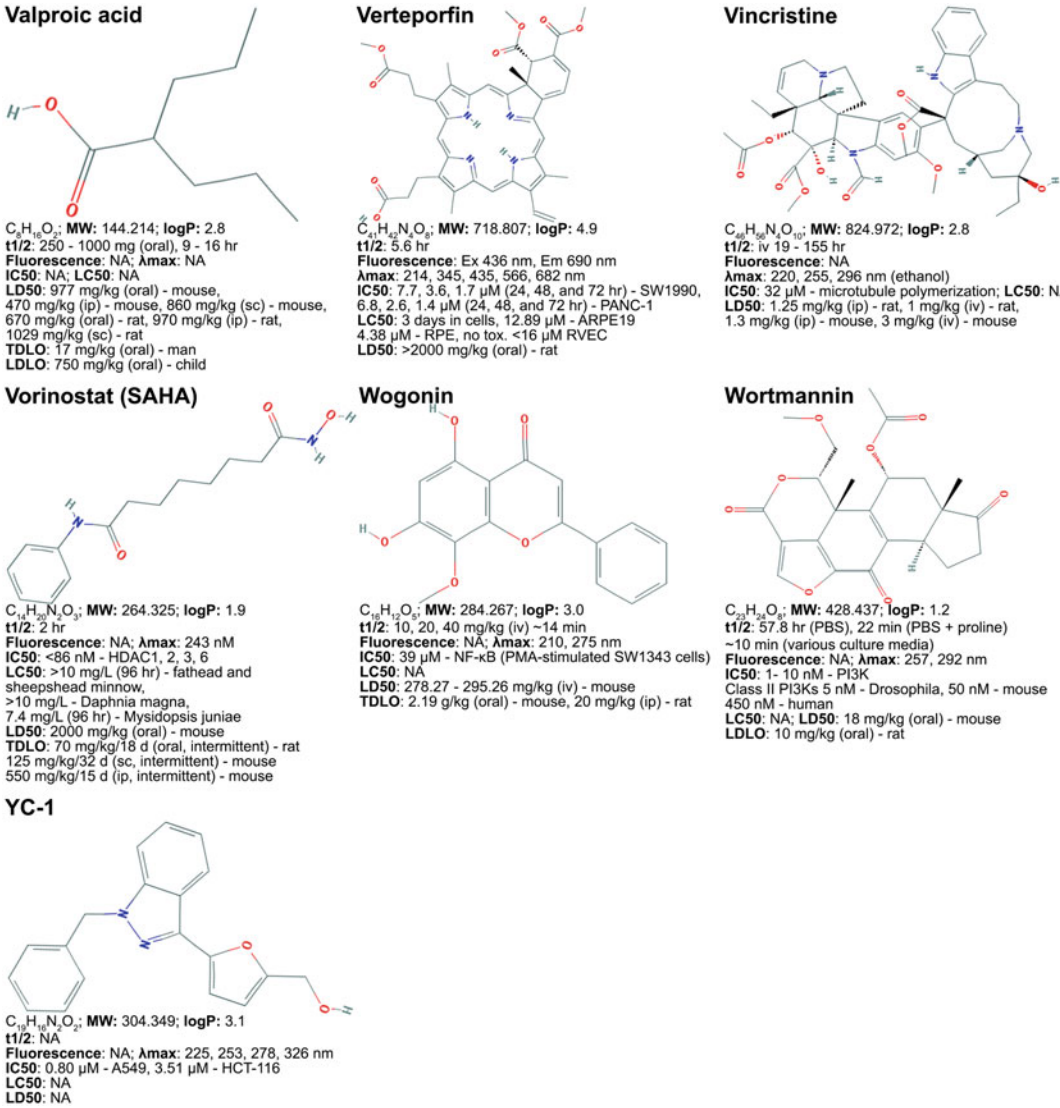

Fig. 6 (continued)

lamps, 530–620 nm, illumination time of 16 min 40 s, irradiance of 4.4 mW/cm^2, cumulative radiant exposure of 4.4 J/cm^2). Akt and p-ERK1/2 protein levels were completely depleted and survivin protein levels had decreased after 48 h [143].

4.2 Acriflavine

Acriflavine is an antiseptic dye extracted from coal tar that deters dimerization of the HIF-1α and HIF-1β subunits in the nucleus, thereby blocking transcription of HIF-1 target genes. Docking studies evinced that acriflavine binds to the dimerization domain of HIF-1α. The translocation of acriflavine to the nucleus was

confirmed by confocal microscopy in human epidermoid carcinoma (A431) cells [8].

Pretreatment of cells with acriflavine (3 μM) enhanced ZnPC-PDT efficacy in Sk-ChA-1 and A431 cells. The therapy-enhancing effect of acriflavine was particularly notable in A431 cells that had been subjected to PDT and cultured under hypoxic conditions compared to PDT-treated A431 cells cultured under normoxic conditions after PDT [8, 9]. Further experimental results are detailed in Subheading 3.

4.3 Amphotericin B

Amphotericin B is an antimicrobial agent [144] that inhibits the transcriptional activity of HIF-1α through repression of its CAD domain by enhancing the binding of FIH-1 to the Asn803 site. However, the expression level and localization of the HIF-1 subunits in cells remain unaltered [23].

Amphotericin B has been applied in combination with the PS merocyanine 540 (MC540) in both preclinical models and phase I/II clinical trials for the extracorporeal purging of autologous stem cell grafts. The compound potentiates photokilling of MC540-sensitized L1210 murine leukemia (CCL 219) cells, wild-type small cell lung cancer (H69) cells, human and murine normal colony forming unit-granulocyte/macrophage progenitors (hCFU-GM and mCFU-GM), and cisplatin-resistant small cell lung cancer (H69/CDDP) cells [145].

4.4 Ascorbic Acid (Vitamin C)

Ascorbic acid, which is commonly found in citrus fruits and taken as an oral food supplement, decreases intratumoral levels of HIF-1α protein and its transcriptional target proteins CA-IX, GLUT1, and VEGF. Ascorbic acid was given to mice bearing B16-F10 melanoma and LL/2 Lewis lung carcinoma xenografts via drinking water before and after subcutaneous inoculation with cancer cells. Intratumoral ascorbic acid concentration was inversely correlated to levels of HIF-1 and its transcriptional targets [146].

Verteporfin-mediated PDT (30 W daylight fluorescent bulbs and UV light-removing surface, illumination time of 10–20 min, irradiance of 2.2 mW/cm^2, cumulative radiant exposure of 1.32–2.62 J/cm^2) in combination with ascorbic acid resulted in decreased survival of human leukemia (HL-60) cells but protected human histiocytic lymphoma (U973) cells. Ascorbic acid is a hydrophilic antioxidant that can react with $^1O_2$ and produce hydrogen peroxide, which could be further neutralized/dismutated through peroxide-removing systems such as glutathione and catalase. Its antioxidant properties may therefore ameliorate the extent of photoinduced hyperoxidative stress. Addition of 4-aminobenzoic acid hydrazide, a known inhibitor of myeloperoxidase activity, to HL-60 cell cultures decreased cell survival post-PDT. Contrastingly, 4-aminobenzoic acid hydrazide had no effect on U937 cells in terms of PDT outcome, altogether

indicating that ascorbic acid can be either advantageous, ineffectual, or disadvantageous in conjunction with PDT [147].

4.5 Baicalein

Baicalein is a flavonoid that is isolated from *Scutellaria baicalensis* and is commonly used in Chinese medicine for the treatment of chronic hepatitis. Baicalein inhibits the lipoxygenase (LOX) pathway and attenuates cell growth in LOX-12-overexpressing human pancreatic cancer (HPAF, MIA PaCa-2, Capan-2, Panc-1) cells [148–152]. The tumor-inhibiting and apoptosis-inducing properties of baicalein were confirmed in female nude BALB/c mice bearing human pancreatic cancer (HPAC and AsPC-1) xenografts that received oral baicalein doses of 250 mg/kg per day [149]. In addition, baicalein was shown to stabilize HIF-1α in the cytoplasm and prevent the nuclear accumulation and transcriptional activity of HIF-1α in human cervix carcinoma (HeLa) cells [153].

Pretreatment of human colon cancer (HT-29) cells with baicalein prior to hypericin-PDT (L18W/30 lamps, 530–620 nm, irradiance of 4.4 mW/cm^2, cumulative radiant exposure of 4.4 J/cm^2) resulted in a synergistic decrease in cell viability and increase in the population of S phase-arrested cells compared to the singular treatments [154].

4.6 Berberine

Berberine is a phytochemical alkaloid with potent anti-inflammatory and antimicrobial properties. A study on berberine (10 mg/kg i.p.) in C57BL/6 mice bearing B16F-10 melanoma xenografts demonstrated significant inhibition of tumor-directed capillary formation as a result of decreased VEGF, IL-1β, IL-6, TNF-α, and granulocyte-macrophage colony-stimulating factor (GM-CSF). Under hypoxic conditions, addition of berberine to B16F-10 melanoma cells drastically curtailed mRNA expression of HIF-1 and VEGF [155].

Berberine has been used as a PS in cultured human glioblastoma (U87-MG) cells. When associated with low-density lipoprotein (LDL), berberine exhibited increased photo-oxidation as evidenced by elevated levels of malondialdehyde, a secondary metabolite of lipid peroxidation reactions. Additionally, PDT reduced the viability of LDL receptor-overexpressing U87-MG cells in a light dose-dependent manner (xenon lamp, 410 ± 10 nm, radiant exposure of 10–100 J/cm^2, irradiance of 65 ± 0.5 mW/cm^2, illumination time of 2.5–23 min) [156]. The phytochemical can therefore be concurrently employed as a light-activatable drug and HIF-1 pathway inhibitor. In cultured human breast cancer (MCF-7) cells, berberine reversed hypoxia-induced chemoresistance to doxorubicin, another HIF-1α inhibitor (*see* Subheading 4.10) [157].

4.7 Bortezomib

Bortezomib is a proteasome inhibitor that binds and inhibits the catalytic center of the 26S proteasome, indirectly repressing HIF-1α protein expression and nuclear accumulation by blocking the PI3K/Akt/TOR and MAPK pathways [158–160]. Reduction in HIF-1α protein expression by bortezomib was demonstrated in cultured prostate cancer (LNCap and PC-3) cells under both normoxic and hypoxic conditions. The lowering of HIF-1α levels coincided with the dephosphorylation of p-Akt, p-p70S6K, and p-S6RP, which inactivated an essential pathway that leads to HIF-1α protein expression [160].

The efficacy of verteporfin-PDT on mouse endothelial (SVEC4–10) cells and human prostate cancer (PC-3) cells was enhanced when PDT (diode laser, 690 nm, irradiance of 5 mW/cm^2 for 100 s, cumulative radiant exposure of 0.5 J/cm^2) was combined with bortezomib, as reflected by more profound accumulation of ubiquitinated proteins within 10 h after treatment compared to the PDT group alone. Furthermore, bortezomib (2 mg/kg i.p.) + verteporfin-PDT strongly reduced tumor volume in athymic nude NCR mice bearing PC-3 tumor xenografts compared to animals that had been treated by verteporfin-PDT in the absence of bortezomib (diode laser, 690 nm, irradiance of 50 mW/cm^2 for 600 s, cumulative radiant exposure of 30 J/cm^2) [161].

4.8 Daunorubicin

Daunorubicin is an anthracycline antineoplastic antibiotic that blocks the binding of HIF-1 to DNA and prevents HIF-1 transcriptional activity [162, 163].

Combination therapy consisting of the PS IR-768 in mPEG-b-PLGA micelles co-encapsulating daunorubicin and PDT synergistically enhanced anticancer activity in human melanoma (A375) cells compared to the singular treatments (LED light, 630 nm, illumination time of 5 min, cumulative radiant exposure of 8 J/cm^2) [164]. Treatment of human hepatocarcinoma (SMMC-7721) cells with ZnO nanorods that were loaded with daunorubicin with subsequent illumination resulted in enhanced anticancer activity compared to the individual treatments (germicidal UV lamp, illumination time of 3 min, irradiance of 0.1 mW/cm^2) [165]. Similar results were obtained in another study where human cervical carcinoma (HeLa) cells were treated with ZnO/PVP nanorods that were loaded with daunorubicin (150 W medium-pressure mercury vapor lamp and tungsten-halogen lamp with 10 cm potassium iodide and 1 cm pyridine filter, 300–700 nm) [166].

4.9 Diphenylene Iodonium (DPI)

Diphenylene iodonium (DPI) is an iodonium-class flavoprotein dehydrogenase inhibitor that blocks the activity of NADPH oxidases (NOX). DPI has been studied as an anticancer agent in NADPH oxidase (NOX)-overexpressing cancers, including breast cancer [167], colorectal liver metastases [168], and enteral cancers [168] that rely on NOX for growth and survival. Growth of NOX1-

overexpressing human colon cancer (Caco2, HT-29, LS-174T) cells was retarded at 0.01, 0.1, and 0.25 μM DPI IC_{50} concentrations, respectively, which coincided with decreased steady-state ROS production and reduced NOX1 transcript levels and antioxidant enzymes. This in turn resulted in G_1/S-phase cell cycle arrest, reduced proliferative signaling at the level of the transcriptome, and apoptosis in some of the cell lines. Additionally, DPI decreased the expression of cyclin A, D1, and E in vitro [168]. The relation between NOX and HIF-1 was explored in human ovarian (OVCAR-3 and A2789) cells and immortalized ovarian surface epithelial (IOSE-397 and IOSE-386) cells, where elevated levels of ROS were required for the induction of angiogenesis and tumor growth. Consequently, inhibition of COX4 with DPI resulted in reduced ROS production and concomitant reduction in HIF-1 and VEGF protein expression [169]. The tumor growth inhibitory properties of DPI were confirmed in athymic nude mice bearing HT-29 and LS-174T xenografts, where tumor volume was decreased by ~40% by DPI compared to the vehicle control group [168].

Treatment of human cervical carcinoma (HeLa) cells with Mitotracker Red-PDT (as a mitochondria-targeted PS) in conjunction with DPI resulted in complete abolition of ROS production (Axiovert 200 M microscope as light source, 545/25 nm bandpass, irradiance of 30 mW/cm^2, cumulative radiant exposure 23.4 J/cm^2 or 34.8 J/cm^2, illumination time of 1–1.5 min) [170]. HIF-1 signaling was not investigated. In light of the above, it is imperative that DPI should be administered after PDT inasmuch as it acts as an antioxidant [170, 171] that could otherwise counteract the efficacy of PDT.

4.10 Doxorubicin

Doxorubicin is an anthracycline antineoplastic antibiotic that inhibits the transcription of HIF-1 target genes by blocking HIF-1 binding to DNA [163]. HIF-1 is capable of causing doxorubicin chemoresistance in breast cancer cells through its transcriptional upregulation of P-glycoprotein, which could be countered by HIF-1α siRNA [172]. Addition of berberine also reverses hypoxia-induced chemoresistance to doxorubicin (*see* Subheading 4.5) [157].

PDT with hematoporphyrin-modified doxorubicin-loaded nanoparticles had an additive effect on anticancer efficacy in HepG2 tumor-bearing male nude BALB/c mice when compared to the modified nanoparticles without PDT and free hematoporphyrin-mediated PDT (630 nm, irradiance of 400 mW/cm^2, illumination time of 250 or 500 s, cumulative radiant exposure of 100 or 200 J/cm^2). This was reflected by a decrease in tumor volume over a period of 4 weeks. Double treatment with the combinatorial modality only slightly increased the

anticancer efficacy compared to a single treatment (7-day interval between treatments) [173]. HIF-1 signaling was not investigated.

4.11 Epirubicin

Epirubicin is an anthracycline antineoplastic antibiotic that deters HIF-1-DNA association and transcription of HIF-1 target genes [163].

Lippert et al. used epirubicin as a PS and found that cell viability was substantially diminished in ten different head and neck squamous cell carcinoma cell lines following PDT (500 nm argon laser, cumulative radiant exposure of 5 J/cm^2) compared to non-illuminated controls (i.e., epirubicin dark toxicity) [174]. HIF-1 signaling was not investigated.

4.12 Hypericin

Hypericin is an anthraquinone derivative and photodynamically active plant pigment that is naturally found in St. John's wort and harnesses antidepressant, antiviral, immunostimulating, and antineoplastic activity [175]. Hypericin amplifies ubiquitination of Hsp90, abrogating its functionality, and displaces its client proteins mutant p53, CDK4, RAF-1, and PLK. This indirectly leads to increased degradation of HIF-1α [176, 321].

PDT with hypericin as PS of human breast adenocarcinoma (SKBR-3) cells profoundly decreased metabolic activity at hypericin concentrations of >21 nM (L18W/30 lamps, 530–620 nm, irradiance of 4.4 mW/cm^2, 16 min 40 s exposure time, cumulative radiant exposure of 4.4 J/cm^2). Single treatment with 17-DMAG (*see* Subheading 4.1) at an IC_{10} concentration of 5 nM did not significantly influence survival and/or proliferation of SKBR-3 cells at 24 h. However, after 48 h approximately 20% of the cells had died. Single treatment with 21 nM of hypericin did not significantly influence survival and/or proliferation of SKBR-3 cells after 24 and 48 hours. However, hypericin-PDT (21 nM) in combination with 17-DMAG at IC_{10} resulted in an increased synergistic antineoplastic effect in SKBR-3 cells at 48 h. Additionally, Akt and p-ERK1/2 were totally depleted and survivin levels were decreased [143].

4.13 LY294002

LY294002 is a potent PI3K-specific inhibitor. Inhibition of PI3K results in inhibition of HIF-1α. The PI3K-HIF-1α interconnectedness was demonstrated in vitro where PTEN, a negative regulator of PI3K, was studied in the PTEN wild-type cell lines ACHN (human metastatic renal adenocarcinoma), DU145 (human prostate cancer), and U2-OS (human osteosarcoma) and in the PTEN-negative cell line PC-3 (human prostate cancer). Cells that lacked PTEN had higher HIF-1α protein levels when insulin or EGF was added to the medium to stimulate the activation of PI3K. Insulin and EGF are known inducers of VEGF through activation of the PI3K pathway, resulting in downstream upregulation of HIF-1, that in turn transcriptionally regulates VEGF (*see* Subheading 2.2). HIF-1α mRNA levels remained unchanged in PTEN-lacking

cells. Addition of LY294002 resulted in a dose-dependent reduction in HIF-1α protein levels, regardless of the presence of functional PTEN. These data indicate that HIF-1α upregulation as a result of loss-of-function mutations in PTEN (no negative regulation of PI3K) can possibly be remediated with LY294002 [177].

5-ALA-PDT of human esophageal squamous carcinoma (Eca-109) cells in combination with LY294002 resulted in a synergistic reduction in cell growth and migration ability and significantly downregulated protein expression of PI3K and Akt compared to the singular treatments [178]. Downregulation of Akt reverberates the role of LY294002 as a direct PI3K inhibitor and indirect inhibitor of HIF-1α. In the PI3K pathway, Akt is activated by PI3K which in turn activates mTOR, an upstream regulator of HIF-1α [35, 37]. However, HIF-1 signaling was not directly investigated.

4.14 Microtubule-Targeting Drugs

A mechanistic link was found in human ovarian cancer (1A9) cells between various microtubule-targeting agents that mediate cytoskeleton disruption and a reduction in HIF-1α protein levels without affecting HIF-1α mRNA. The disrupting agents included 2-methoxyestradiol, docetaxel, vincristine, epothilone B, and discodermolide [179]. The exact molecular mechanisms that effectuate the lowering of HIF-1α protein levels by these agents are currently elusive.

4.14.1 2-Methoxyestradiol (2ME2)

2-Methoxyestradiol (2ME2) is a tubulin polymerization inhibitor that binds to the colchicine domain of tubulin, leading to G_2/M cell cycle arrest and apoptosis. Furthermore, 2ME2 inhibits superoxide dismutase, an antioxidant enzyme that dismutates $O_2^{\bullet -}$ into the less noxious hydrogen peroxide.

PDT with the PS redaporfin in conjunction with 2ME2 resulted in synergistically increased human lung adenocarcinoma (A549) cell death compared to the sum of the singular treatments, an effect that was not observed in mouse colon adenocarcinoma (CT26) cells (LED light, 740 nm (max), irradiance of 410 μW/cm^2, cumulative radiant exposure of 50 mJ/cm^2 — A549 cells and 80 mJ/cm^2 — CT26 cells) [180]. In another study, pre-incubation of cells with 2ME2 before Photofrin-PDT (He-Ne ion laser, 630 nm, cumulative radiant exposure 0–12 J/cm^2) produced a synergistic cytotoxic effect in 3 murine (C-26, LLC, and MDC) and 5 human cell lines (T47-D, PANC-1, HPAF-II, HPAC, and T24). Furthermore, the combination of 2ME2 with Photofrin-PDT in C26 tumor-bearing BALB/c mice and LLC-bearing B6D2F$_1$ mice significantly potentiated the antitumor effects, resulting in retardation of tumor growth and prolongation of survival time (He-Ne ion laser, 630 nm, irradiance of 80 mW/cm^2, cumulative radiant exposure of 150 J/cm^2). Sixty percent of the

C26 tumor-bearing mice was completely cured by the combination treatment (no tumor after 150 days of observation) [181].

More potent antiproliferative and anti-angiogenic effects have been achieved with ENMD-1198 and ENMD-1200, which are synthetic analogs of 2ME2. Additionally, ENMD-1198 and ENMD-1200 inhibited HIF-1α more potently than 2ME2 at lower concentrations (0.5 μM) under hypoxic conditions but achieved a similar degree of HIF-1α inhibition at higher equimolar dosages (5 μM). However, these synthetic analogs of 2ME2 have not yet been tested in combination with PDT [182].

4.14.2 Docetaxel

Docetaxel (Taxotere) is a tubulin depolymerization inhibitor, resulting in stabilization of the microtubules and excessive polymerization that causes G_2/M cell cycle arrest and apoptosis [183].

Combination treatment of docetaxel and the PS IR820 loaded into m-Lyp-1 micelles (Lyp-1 is a tumor-targeting peptide) with subsequent illumination resulted in an additive cytotoxic effect in mouse breast cancer (4T1) cells (808 nm laser, irradiance of 2.5 W/cm^2, 5-min illumination). The in vitro results were echoed in BALB/c mice bearing 4T1 xenografts, with increased PDT efficacy attained with the combination treatment as opposed to micellar IR820-PDT alone (808 nm laser, 2.5 W/cm^2, 10-min illumination) or PDT with free IR820 [184]. HIF-1 signaling was not investigated.

4.14.3 Vincristine

Vincristine is a microtubule-targeting agent that is used as a cytostatic drug. Vincristine induces G_1- and G_2-phase cell cycle arrest by binding to the vinca domain of tubulin and preventing polymerization of the microtubules (even when mitotic checkpoint proteins are present), suggesting the manifestation of a microtubule integrity failure that prevents the cell's entry into M-phase [185].

Treatment of mouse leukemia (LBR) cells with vincristine and 5-ALA-PDT yielded an additive effect compared to the single vincristine and 5-ALA-PDT treatments (fluorescent lamps, 400–700 nm (600 nm max), illumination time 0–20 min). This was characterized by strongly reduced cell viability, especially at an illumination time of 20 min. The induction of necrosis was very low compared to apoptosis, suggesting that apoptosis constituted the major mode of cell death. Vincristine + 5-ALA-PDT of LBR cells was more cytotoxic than 5-ALA-PDT in conjunction with doxorubicin (*see* Subheading 4.10) [186]. HIF-1 signaling was not investigated.

4.15 Minocycline

Minocycline is a second-generation tetracycline antibiotic used in the treatment of infectious diseases. Minocycline inhibits HIF-1α protein expression and suppresses its transcriptional activity, as in part evidenced by a reduction in VEGF expression to baseline

values in cultured human glioma (U87MG) and prostate cancer (DU145) cells under hypoxic conditions [187].

Combination treatment encompassing minocycline (50 μg/mL) and 5-ALA PDT in malignant peripheral nerve sheath tumor (S462) cells resulted in a synergistic effect on cell viability in a light dose-dependent manner compared to the individual treatments (diode laser, 635 nm, irradiance of 30 mW/cm^2, cumulative radiant exposure of 0–12 J/cm^2) [188]. HIF-1 signaling was not investigated.

4.16 Rapamycin

Rapamycin (sirolimus) is an antifungal metabolite produced by *Streptomyces hygroscopicus* that possesses immunosuppressive and antiproliferative properties in mammalian cells. Rapamycin binds to the cytoplasmic receptor FKBP12, forming a complex that in turn binds and inhibits mTOR. mTOR is a master regulator of cell growth and metabolism upstream of HIF-1α (*see* Subheading 2.1.4) [189–191]. Rapamycin induced growth inhibition in human retinoblastoma (Y79) cells through downregulation of polycomb group RING finger protein 4 (BMI-1) that in turn decreased cyclin E1 levels, accounting for rapamycin-mediated G_1-phase cell cycle arrest [192].

The addition of rapamycin to human colon adenocarcinoma (WiDr) cells directly after low-power $AlPcS_{2a}$-PDT resulted in a synergistic cytotoxic effect (Philips Fluotone 18 W/950 light source, 620 nm long pass, irradiance of 1.5 W/cm^2). Rapamycin (10 nM) attenuated Ser^{2448} phosphorylation of mTOR by roughly 25% after 4 h of incubation, with the attenuating effect plateauing within 24 h without compromising cell viability during 72-h sustained incubation. However, the priming of WiDr cells with rapamycin both before and after PDT resulted in an antagonistic effect with respect to cell death compared to the sum of singular treatments [193]. These data suggest that rapamycin dosing regimens should be optimized before using this compound as an adjuvant in PDT. Combination therapy of 5-ALA-PDT and rapamycin had an additive effect on the growth of human sebaceous gland (SZ95) cells compared to the individual treatments (LED light, 635 nm, irradiance of 115 mW/cm^2, cumulative radiant exposure of 10 J/cm^2) [194]. HIF-1 signaling was not directly investigated.

4.17 Resveratrol

Resveratrol is a natural polyphenolic antioxidant primarily found in grape skin. Resveratrol significantly inhibits HIF-1α protein accumulation under normoxic and hypoxic conditions without affecting HIF-1α mRNA levels, as was shown in human tongue squamous cell carcinoma (SCC-9) and hepatocellular carcinoma (HepG2) cells. Specifically, resveratrol inhibits hypoxia-mediated activation of ERK1/2 and Akt, which leads to a decrease in

HIF-1α protein accumulation and VEGF transcription. The phytochemical also reduces basal HIF-1α levels but does not affect HIF-1α mRNA levels, even under hypoxic conditions [195]. Resveratrol significantly inhibited both basal level and hypoxia-induced HIF-1α protein accumulation in A431 cells but did not affect HIF-1α mRNA levels [195].

Combination treatment of 5-ALA-PDT and resveratrol resulted in enhanced antiproliferative and pro-apoptotic effects in human epidermoid carcinoma (A431) cells. Resveratrol also upregulated caspase-3, p53, p-ERK, and p-p38 protein levels as single treatment and in combination with 5-ALA PDT [197].

4.18 Silibinin

Silibinin is a natural polyphenolic flavonoid sourced from milk thistle seeds that has been used for its hepatoprotective effects [198]. Silibinin inhibits HIF-1α accumulation and HIF-1 transcriptional activity without affecting prolyl hydroxylase-driven HIF-1α degradation or HIF-1α mRNA levels, as evinced in cultured human cervical carcinoma (HeLa) and hepatoma (Hep3B) cells. Instead, silibinin decreased the rate of HIF-1α protein synthesis. Silibinin's inhibition of HIF-1α concurs with a reduction in hypoxia-induced VEGF release [199]. Silibinin treatment of human colorectal carcinoma (HT29) xenografts in male athymic nude BALB/c mice inhibited tumor growth that accounted for decrease in tumor volume (~48%), tumor weight (~42%), and proliferation index (~40%). Microvessel density was reduced by ~36%. These effects were associated with downregulation of ERK1/2, p-Akt, cyclin D1, NOS, NOS3, cyclooxygenase 1 (COX-1), COX-2, HIF-1α, and VEGF protein expression [196].

Combination treatment of bladder cancer (T24 and MB49) cells with 5-ALA-PDT and silibinin had a synergistic or additive effect on cell viability, depending on the light dose and cell type, compared to the individual treatments [198]. HIF-1 signaling was not investigated.

4.19 SN38

SN38 is an active metabolite of the cytostatic agent irinotecan that has dual angiosuppressive properties in terms of inhibition of endothelial proliferation and tube formation as well as inhibition of the angiogenic signaling cascade, at least in glioma cells (human: U87-MG and U251-MG; mouse: GL261). These properties are in part instilled through blockade of topoisomerase I, culminating in the deterrence of HIF-1α accumulation and transcriptional activity. Accordingly, SN38 also downmodulates VEGF expression under normoxic and hypoxic conditions [200, 201].

Treatment of human colon cancer (HT-29) xenografts in female athymic nude BALB/c mice with polymeric micelle-encapsulated chlorin-PDT in conjunction with SN38 synergistically inhibited tumor growth compared to the single therapies (diode laser, 652 nm, irradiance of 100 mW/cm^2, cumulative

radiant exposure of 30 or 90 J/cm^2 for single and multiple treatments, respectively) [202]. HIF-1 signaling was not investigated.

4.20 Sodium Butyrate

Sodium butyrate is a histone deacetylase inhibitor. Histone deacetylases 1 and 3 enhance HIF-1α stability and HIF-1α transactivation functions under hypoxic conditions. Both histone deacetylases bind directly to the oxygen-dependent degradation domain of HIF-1α. Consequently, their inhibition by sodium butyrate results in decreased HIF-1α protein levels and transcriptional activity, as was shown in cultured human cervical carcinoma (HeLa), mouse melanoma (B16F10), and human embryonic kidney (293T) cells [203]. Sodium butyrate induced caspase-3, caspase-9, BCL-2, BAX, and BAK-1 expression in human glioblastoma astrocytoma (U373-MG) cells but not in human malignant glioma (D54-MG) cells, where BAX and BCL-2 were repressed [204].

Combination therapy of 5-ALA-PDT (argon laser, 488 nm, cumulative radiant exposure of 80 J/cm^2, illumination time of 435 s) with sodium butyrate (80 μg/mL) resulted in a synergistic effect on cell death compared to the individual treatments in U-373-MG and D54-MG cells, especially when sodium butyrate was administered 24 h before 5-ALA-PDT [204, 205]. HIF-1 signaling was not investigated.

4.21 Sorafenib

Sorafenib inhibits HIF-1α protein synthesis by suppressing the phosphorylation of mTOR, ERK, p70S6K, RP-S6, 4E-BP1, and eIF4E, as was evidenced in the human hepatocellular carcinoma cell lines PLC/PRF/5, HepG2, and Hep3B. Sorafenib further decreases tumor vascularization and stalls the growth of PLC/PRF/5 tumor xenografts in mice [206].

Combination therapy comprising sorafenib (85 μg/kg) and verteporfin-PDT (420 ± 20 nm, irradiance of 35 mW/cm^2, cumulative radiant exposure of 5 J/cm^2) synergistically reduced tumor growth in a chicken embryo chorioallantoic membrane (CAM) model hosting human ovarian carcinoma (A2789) xenografts compared to the individual treatments. Additionally, the combination therapy significantly decreased microvessel density but increased the fraction of larger vessels with an open lumen [207]. HIF-1 signaling was not investigated.

4.22 Topotecan

Topotecan is a synthetic analog of the phytochemical camptothecin and mainly acts as a topoisomerase inhibitor. The compound also inhibits HIF-1, although the exact mechanism is elusive. HIF-1α nuclear staining in tumor parenchymal cells was absent in patients with metastatic malignancies that had received topotecan (1.2 mg/m^2/day) [208]. Administration of topotecan in cancer patients also leads to decreased tumor blood flow and permeability [208].

When cultured human breast cancer (MCF-7) cells were incubated with topotecan as a PS, the compound accumulated

exclusively in extracellular vesicles owing to a multidrug resistance response mediated by efflux transporters of the ATP-binding cassette superfamily, including ABCG2, ABCB1, and ABCC1. Photosensitization and PDT (470 ± 27 nm, illumination time 10 min) of extracellular vesicles loaded with topotecan resulted in destruction of the extracellular vesicles and subsequent reconstitution of topotecan in tumor cells, which consequently underwent cell lysis [209]. HIF-1 signaling was not investigated.

4.23 Trichostatin A

Trichostatin A is a histone deacetylase inhibitor that reduces HIF-1α protein accumulation and curtails downstream VEGF transcript and protein levels, which was demonstrated in head and neck squamous carcinoma (UM-SCC-6) cells [210].

Treatment of human colon cancer (HT-29 and HCT 116) cells with hypericin-PDT (L18W/30 lamps, 530–620 nm maximum emission, irradiance of 3.15 mW/cm^2, cumulative radiant exposure of 3.15 J/cm^2) and trichostatin A resulted in a synergistic effect in HT-29 cells with respect to cell death, reduced colony formation, and perturbed cell cycle regulation compared to the respective singular therapies. Additionally, the combination therapy more significantly upregulated *CDKN1A* mRNA as well as its protein product (p21^{CIP1}). P21^{CIP1} inhibits cyclin-dependent kinases that play a direct role in the G_1-S transition of the cell cycle, and p21^{CIP1} overexpression can cause S-phase arrest, which was confirmed to be the case for this combination therapy. The HCT 116 cells were less resistant to hypericin-PDT than HT-29 cells, resulting in a slight additive effect for the combination therapy compared to the individual therapies, although the tumor-killing capacity for both cell lines was comparable [211, 212]. HIF-1 signaling was not directly investigated.

4.24 Valproic Acid

Valproic acid is a class I histone deacetylase inhibitor that reduces HIF-1α protein levels more potently than trichostatin A (*see* Subheading 4.23) and sodium butyrate (*see* Subheading 4.20), at least in cultured mouse embryonic stem cells [213].

Treatment of human colon cancer (HT-29 and HCT 116) cells with hypericin-PDT (L18W/30 lamps, 530–620 nm maximum emission, irradiance of 3.15 mW/cm^2, cumulative radiant exposure of 3.15 J/cm^2) and valproic acid resulted in a synergistic effect in HT-29 cells in terms of cell death and perturbed cell cycle regulation compared to the respective singular therapies. As with trichostatin A (*see* Subheading 4.23), the combination therapy more significantly upregulated p21^{CIP1} transcript and protein levels. A slight additive effect for the combination therapy compared to the individual therapies was observed in HCT 116 [211]. HIF-1 signaling was not directly investigated.

4.25 Verteporfin

Verteporfin, a benzoporphyrin derivative, is a PS that is widely employed in a clinical PDT setting to treat neovascularization caused by age-related macular degeneration. Verteporfin inhibits angiogenesis and the growth and migration of human retinoblastoma (Y79 and WERI) cells in a dose-dependent manner by disrupting YAP-TEAD-associated downstream proto-oncogenes [214, 215].

Multidimensional screening for KRAS and HIF pathways in human colorectal cancer cell lines (HCT116, HCT116$^{HIF\text{-}1\alpha-/-\ HIF\text{-}2\alpha-/-}$, HCT116$^{WT\ KRAS}$) revealed that verteporfin caused downregulation of HIF-1 target genes without affecting HIF-1α and HIF-1β protein levels. The mechanism underlying the transcriptional dysregulation is currently unknown [216]. Verteporfin-PDT (diode laser, 690 nm, irradiance of 100 mW/cm^2, cell type-specific cumulative radiant exposure of 4–20 J/cm^2) killed pancreatic cancer cells (AsPC-1, BxPC-3, PANC-1, Capan-1, Capan-2) that are resistant to gemcitabine, a drug often incorporated into palliative chemotherapeutic regimens. Near-complete cell death was observed at a verteporfin dose of 6 μM per J/cm^2. Verteporfin-PDT significantly decreased Bcl-XL expression and increased the BAX/BCL-xL ratio toward a pro-apoptotic balance at sublethal doses (0.06–0.12 μM per J/cm^2) compared to the dark toxicity group (verteporfin, 250 nM) [217]. HIF-1 signaling was not directly investigated in the latter study.

4.26 Vorinostat (SAHA)

Vorinostat is a histone deacetylase inhibitor that acts on class I and class II histone deacetylases and consequently lowers cytosolic HIF-1α levels and transcription of HIF-1 target genes, as was shown in human hepatoma (HuH7 and Hep3B) cells [218]. Vorinostat induced apoptosis in rituximab-sensitive human B-cell lymphoma (BL and GCB DLBCL) cells and G_1-phase cell cycle arrest in rituximab-resistant B-cell lymphoma (Raji-4RH and RL-4RH) cells. The rituximab-resistant cells were associated with reduced BAX and BAK protein expression, indicating that cells with an impaired apoptosis signaling machinery may get arrested in the G_1 phase of the cell cycle instead of undergoing apoptotic cell death [219].

Treatment of human colon cancer (HT-29 and HCT 116) cells with hypericin-PDT (L18W/30 lamps, 530–620 nm maximum emission, irradiance of 3.15 mW/cm^2, cumulative radiant exposure of 3.15 J/cm^2) and vorinostat resulted in a synergistic effect in HT-29 cells with respect to cell death and disrupted cell cycle regulation compared to the respective singular therapies. The colony-forming capability was reduced in an additive manner compared to the singular therapies. Additionally, the combination therapy more significantly upregulated p21^{CIP1} transcript and protein levels [211]. HIF-1 signaling was not investigated.

4.27 Wortmannin

Wortmannin is a potent specific PI3K inhibitor, the mechanisms of which have been described in the context of HIF-1 in Subheading 4.13. As was reported for LY294002, wortmannin mediates a dose-dependent reduction in HIF-1α protein levels in PTEN wild-type human renal cell adenocarcinoma (ACHN), human prostate carcinoma (DU145), and human osteosarcoma (U2-OS) cells as well as PTEN-negative human prostate cancer (PC-3) cells, i.e., regardless of whether cells contain a functional PTEN [177].

PDT (600 W quartz-halogen lamp, 600–650 nm band-pass) with 9-capronyloxytetrakis-(methoxyethyl)-porphycene induced apoptotic and autophagic cell death in mouse lymphocytic leukemia (L1210) cells and only autophagic cell death in BAX-deficient human prostate cancer (DU145) cells. Pre-incubation of cells with wortmannin prior to PDT increased morphological appearance of apoptosis and inhibited autophagy in both cell lines 24 h after PDT [220]. HIF-1 signaling was not investigated.

References

1. Plaetzer K, Krammer B, Berlanda J, Berr F, Kiesslich T (2009) Photophysics and photochemistry of photodynamic therapy: fundamental aspects. Lasers Med Sci 24(2):259–268. https://doi.org/10.1007/s10103-008-0539-1
2. Agostinis P, Berg K, Cengel KA, Foster TH, Girotti AW, Gollnick SO, Hahn SM, Hamblin MR, Juzeniene A, Kessel D, Korbelik M, Moan J, Mroz P, Nowis D, Piette J, Wilson BC, Golab J (2011) Photodynamic therapy of cancer: an update. CA Cancer J Clin 61(4):250–281. https://doi.org/10.3322/caac.20114
3. Castano AP, Mroz P, Hamblin MR (2006) Photodynamic therapy and anti-tumour immunity. Nat Rev Cancer 6(7):535–545. https://doi.org/10.1038/nrc1894
4. Falk-Mahapatra R, Gollnick SO (2020) Photodynamic Therapy and Immunity: An Update. Photochem Photobiol, 96: 550–559. https://doi.org/10.1111/php.13253
5. Broekgaarden M, Weijer R, van Gulik TM, Hamblin MR, Heger M (2015) Tumor cell survival pathways activated by photodynamic therapy: a molecular basis for pharmacological inhibition strategies. Cancer Metastasis Rev 34(4):643–690. https://doi.org/10.1007/s10555-015-9588-7
6. Weijer R, Broekgaarden M, van Golen RF, Bulle E, Nieuwenhuis E, Jongejan A, Moerland PD, van Kampen AHC, van Gulik TM, Heger M (2015) Low-power photodynamic therapy induces survival signaling in perihilar cholangiocarcinoma cells. BMC Cancer 15(1):1014. https://doi.org/10.1186/s12885-015-1994-2
7. Ferrario A, Gomer CJ (2010) Targeting the 90 kDa heat shock protein improves photodynamic therapy. Cancer Lett 289(2):188–194. https://doi.org/10.1016/j.canlet.2009.08.015
8. Broekgaarden M, Weijer R, Krekorian M, van den Ijssel B, Kos M, Alles LK, van Wijk AC, Bikadi Z, Hazai E, van Gulik TM, Heger M (2016) Inhibition of hypoxia-inducible factor 1 with acriflavine sensitizes hypoxic tumor cells to photodynamic therapy with zinc phthalocyanine-encapsulating cationic liposomes. Nano Res 9(6):1639–1662. https://doi.org/10.1007/s12274-016-1059-0
9. Weijer R, Broekgaarden M, Krekorian M, Alles LK, van Wijk AC, Mackaaij C, Verheij J, van der Wal AC, van Gulik TM, Storm G, Heger M (2016) Inhibition of hypoxia inducible factor 1 and topoisomerase with acriflavine sensitizes perihilar cholangiocarcinomas to photodynamic therapy. Oncotarget 7(3):3341–3356. https://doi.org/10.18632/oncotarget.6490
10. Semenza GL (2007) Evaluation of HIF-1 inhibitors as anticancer agents. Drug Discov Today 12(19):853–859. https://doi.org/10.1016/j.drudis.2007.08.006

11. Benita Y, Kikuchi H, Smith AD, Zhang MQ, Chung DC, Xavier RJ (2009) An integrative genomics approach identifies hypoxia inducible Factor-1 (HIF-1)-target genes that form the core response to hypoxia. Nucleic Acids Res 37(14):4587–4602. https://doi.org/10.1093/nar/gkp425
12. Schodel J, Oikonomopoulos S, Ragoussis J, Pugh CW, Ratcliffe PJ, Mole DR (2011) High-resolution genome-wide mapping of HIF-binding sites by ChIP-seq. Blood 117(23):e207–e217. https://doi.org/10.1182/blood-2010-10-314427
13. Semenza GL (2012) Hypoxia-inducible factors: mediators of cancer progression and targets for cancer therapy. Trends Pharmacol Sci 33(4):207–214. https://doi.org/10.1016/j.tips.2012.01.005
14. Kallio PJ, Pongratz I, Gradin K, McGuire J, Poellinger L (1997) Activation of hypoxia-inducible factor 1α: posttranscriptional regulation and conformational change by recruitment of the Arnt transcription factor. Proc Natl Acad Sci U S A 94(11):5667–5672. https://doi.org/10.1073/pnas.94.11.5667
15. Ke Q, Costa M (2006) Hypoxia-inducible Factor-1 (HIF-1). Mol Pharmacol 70(5):1469–1480. https://doi.org/10.1124/mol.106.027029
16. Buckley DL, Van Molle I, Gareiss PC, Tae HS, Michel J, Noblin DJ, Jorgensen WL, Ciulli A, Crews CM (2012) Targeting the von Hippel–Lindau E3 ubiquitin ligase using small molecules to disrupt the VHL/HIF-1α interaction. J Am Chem Soc 134(10):4465–4468. https://doi.org/10.1021/ja209924v
17. Weidemann A, Johnson RS (2008) Biology of HIF-1α. Cell Death Differ 15:621. https://doi.org/10.1038/cdd.2008.12
18. Yasumoto K-i, Kowata Y, Yoshida A, Torii S, Sogawa K (2009) Role of the intracellular localization of HIF-prolyl hydroxylases. Biochim Biophys Acta 1793(5):792–797. https://doi.org/10.1016/j.bbamcr.2009.01.014
19. Krek W (2000) VHL takes HIF's breath away. Nat Cell Biol 2:E121. https://doi.org/10.1038/35017129
20. Lando D, Peet DJ, Whelan DA, Gorman JJ, Whitelaw ML (2002) Asparagine hydroxylation of the HIF transactivation domain: a hypoxic switch. Science 295(5556):858–861. https://doi.org/10.1126/science.1068592
21. Lau KW, Tian YM, Raval RR, Ratcliffe PJ, Pugh CW (2007) Target gene selectivity of hypoxia-inducible factor-α in renal cancer cells is conveyed by post-DNA-binding mechanisms. Br J Cancer 96:1284. https://doi.org/10.1038/sj.bjc.6603675. https://www.nature.com/articles/6603675#supplementary-information
22. Rey S, Semenza GL (2010) Hypoxia-inducible factor-1-dependent mechanisms of vascularization and vascular remodelling. Cardiovasc Res 86(2):236–242. https://doi.org/10.1093/cvr/cvq045
23. Yeo E-J, Ryu J-H, Cho Y-S, Chun Y-S, Huang LE, Kim M-S, Park J-W (2006) Amphotericin B blunts erythropoietin response to hypoxia by reinforcing FIH-mediated repression of HIF-1. Blood 107(3):916–923. https://doi.org/10.1182/blood-2005-06-2564
24. Elkins JM, Hewitson KS, McNeill LA, Seibel JF, Schlemminger I, Pugh CW, Ratcliffe PJ, Schofield CJ (2003) Structure of factor-inhibiting hypoxia-inducible factor (HIF) reveals mechanism of oxidative modification of HIF-1 alpha. J Biol Chem 278(3):1802–1806. https://doi.org/10.1074/jbc.C200644200
25. Lu H, Dalgard CL, Mohyeldin A, McFate T, Tait AS, Verma A (2005) Reversible inactivation of HIF-1 prolyl hydroxylases allows cell metabolism to control basal HIF-1. J Biol Chem 280(51):41928–41939. https://doi.org/10.1074/jbc.M508718200
26. Schofield CJ, Ratcliffe PJ (2004) Oxygen sensing by HIF hydroxylases. Nat Rev Mol Cell Biol 5:343. https://doi.org/10.1038/nrm1366. https://www.nature.com/articles/nrm1366#supplementary-information
27. Patten DA, Lafleur VN, Robitaille GA, Chan DA, Giaccia AJ, Richard DE, Gutkind JS (2010) Hypoxia-inducible Factor-1 activation in nonhypoxic conditions: the essential role of mitochondrial-derived reactive oxygen species. Mol Biol Cell 21(18):3247–3257. https://doi.org/10.1091/mbc.e10-01-0025
28. Bleier L, Dröse S (2013) Superoxide generation by complex III: from mechanistic rationales to functional consequences. Biochim Biophys Acta 1827(11):1320–1331. https://doi.org/10.1016/j.bbabio.2012.12.002
29. Calvani M, Comito G, Giannoni E, Chiarugi P (2012) Time-dependent stabilization of hypoxia inducible factor-1α by different intracellular sources of reactive oxygen species. PLoS One 7(10):e38388. https://doi.org/10.1371/journal.pone.0038388
30. Juhasz A, Markel S, Gaur S, Liu H, Lu J, Jiang G, Wu X, Antony S, Wu Y, Melillo G,

Meitzler JL, Haines DC, Butcher D, Roy K, Doroshow JH (2017) NADPH oxidase 1 supports proliferation of colon cancer cells by modulating reactive oxygen species-dependent signal transduction. J Biol Chem 292(19):7866–7887. https://doi.org/10.1074/jbc.M116.768283

31. Taylor CT, Cummins EP (2009) The role of NF-κB in hypoxia-induced gene expression. Ann N Y Acad Sci 1177(1):178–184. https://doi.org/10.1111/j.1749-6632.2009.05024.x
32. Beinke S, Ley SC (2004) Functions of NF-κB1 and NF-κB2 in immune cell biology. Biochem J 382(2):393–409. https://doi.org/10.1042/bj20040544
33. Jiang Y, Zhu Y, Wang X, Gong J, Hu C, Guo B, Zhu B, Li Y (2015) Temporal regulation of HIF-1 and NF-kappaB in hypoxic hepatocarcinoma cells. Oncotarget 6(11):9409–9419. https://doi.org/10.18632/oncotarget.3352
34. Figueroa YG, Chan AK, Ibrahim R, Tang Y, Burow ME, Alam J, Scandurro AB, Beckman BS (2002) NF-kappaB plays a key role in hypoxia-inducible factor-1-regulated erythropoietin gene expression. Exp Hematol 30(12):1419–1427
35. Hirota K, Semenza GL (2006) Regulation of angiogenesis by hypoxia-inducible factor 1. Crit Rev Oncol Hematol 59(1):15–26. https://doi.org/10.1016/j.critrevonc.2005.12.003
36. Land SC, Tee AR (2007) Hypoxia-inducible factor 1alpha is regulated by the mammalian target of rapamycin (mTOR) via an mTOR signaling motif. J Biol Chem 282(28):20534–20543. https://doi.org/10.1074/jbc.M611782200
37. Hopkins BD, Hodakoski C, Barrows D, Mense SM, Parsons RE (2014) PTEN function: the long and the short of it. Trends Biochem Sci 39(4):183–190. https://doi.org/10.1016/j.tibs.2014.02.006
38. Stott FJ, Bates S, James MC, McConnell BB, Starborg M, Brookes S, Palmero I, Ryan K, Hara E, Vousden KH, Peters G (1998) The alternative product from the human CDKN2A locus, p14(ARF), participates in a regulatory feedback loop with p53 and MDM2. EMBO J 17(17):5001–5014. https://doi.org/10.1093/emboj/17.17.5001
39. Weber JD, Jeffers JR, Rehg JE, Randle DH, Lozano G, Roussel MF, Sherr CJ, Zambetti GP (2000) p53-independent functions of the p19(ARF) tumor suppressor. Genes Dev 14(18):2358–2365
40. Brown VL, Harwood CA, Crook T, Cronin JG, Kelsell DP, Proby CM (2004) p16INK4a and p14ARF tumor suppressor genes are commonly inactivated in cutaneous squamous cell carcinoma. J Investig Dermatol 122(5):1284–1292. https://doi.org/10.1111/j.0022-202X.2004.22501.x
41. Fatyol K, Szalay AA (2001) The p14ARF tumor suppressor protein facilitates nucleolar sequestration of hypoxia-inducible factor-1alpha (HIF-1alpha) and inhibits HIF-1-mediated transcription. J Biol Chem 276(30):28421–28429. https://doi.org/10.1074/jbc.M102847200
42. Karni R, Dor Y, Keshet E, Meyuhas O, Levitzki A (2002) Activated pp60c-Src leads to elevated hypoxia-inducible factor (HIF)-1alpha expression under normoxia. J Biol Chem 277(45):42919–42925. https://doi.org/10.1074/jbc.M206141200
43. Lee H-Y, Lee T, Lee N, Yang EG, Lee C, Lee J, Moon E-Y, Ha J, Park H (2011) Src activates HIF-1α not through direct phosphorylation of HIF-1α-specific prolyl-4 hydroxylase 2 but through activation of the NADPH oxidase/Rac pathway. Carcinogenesis 32(5):703–712. https://doi.org/10.1093/carcin/bgr034
44. Brown JM (2014) Vasculogenesis: a crucial player in the resistance of solid tumours to radiotherapy. Br J Radiol 87(1035):20130686. https://doi.org/10.1259/bjr.20130686
45. Kelly BD, Hackett SF, Hirota K, Oshima Y, Cai Z, Berg-Dixon S, Rowan A, Yan Z, Campochiaro PA, Semenza GL (2003) Cell type-specific regulation of angiogenic growth factor gene expression and induction of angiogenesis in nonischemic tissue by a constitutively active form of hypoxia-inducible factor 1. Circ Res 93(11):1074–1081. https://doi.org/10.1161/01.res.0000102937.50486.1b
46. Li N, Li Y, Li Z, Huang C, Yang Y, Lang M, Cao J, Jiang W, Xu Y, Dong J, Ren H (2016) Hypoxia inducible factor 1 (HIF-1) recruits macrophage to activate pancreatic stellate cells in pancreatic ductal adenocarcinoma. Int J Mol Sci 17(6):799. https://doi.org/10.3390/ijms17060799
47. McMurtry S (2013) Angiogenesis, arteriogenesis, and mitochondrial dysfunction. https://doi.org/10.1007/978-1-4614-5930-9_15
48. Yu JL, Rak JW (2003) Host microenvironment in breast cancer development inflammatory and immune cells in tumour angiogenesis

and arteriogenesis. Breast Cancer Res 5(2):83. https://doi.org/10.1186/bcr573

49. Urry LA, Cain ML, Wasserman SA, Minorsky PV, Reece JB (2017) Campbell biology
50. Vander Heiden MG, Cantley LC, Thompson CB (2009) Understanding the Warburg effect: the metabolic requirements of cell proliferation. Science 324(5930):1029–1033. https://doi.org/10.1126/science.1160809
51. Iyer NV, Kotch LE, Agani F, Leung SW, Laughner E, Wenger RH, Gassmann M, Gearhart JD, Lawler AM, Yu AY, Semenza GL (1998) Cellular and developmental control of O2 homeostasis by hypoxia-inducible factor 1 alpha. Genes Dev 12(2):149–162
52. Osada-Oka M, Hashiba Y, Akiba S, Imaoka S, Sato T (2010) Glucose is necessary for stabilization of hypoxia-inducible factor-1α under hypoxia: contribution of the pentose phosphate pathway to this stabilization. FEBS Lett 584(14):3073–3079. https://doi.org/10.1016/j.febslet.2010.05.046
53. Mathupala SP, Rempel A, Pedersen PL (2001) Glucose catabolism in cancer cells: identification and characterization of a marked activation response of the type II hexokinase gene to hypoxic conditions. J Biol Chem 276(46):43407–43412. https://doi.org/10.1074/jbc.M108181200
54. Minchenko O, Opentanova I, Caro J (2003) Hypoxic regulation of the 6-phosphofructo-2-kinase/fructose-2,6-bisphosphatase gene family (PFKFB-1–4) expression in vivo. FEBS Lett 554(3):264–270. https://doi.org/10.1016/S0014-5793(03)01179-7
55. Maltepe E, Schmidt JV, Baunoch D, Bradfield CA, Simon MC (1997) Abnormal angiogenesis and responses to glucose and oxygen deprivation in mice lacking the protein ARNT. Nature 386:403. https://doi.org/10.1038/386403a0
56. Semenza GL, Roth PH, Fang HM, Wang GL (1994) Transcriptional regulation of genes encoding glycolytic enzymes by hypoxia-inducible factor 1. J Biol Chem 269(38):23757–23763
57. Hu C-J, Wang L-Y, Chodosh LA, Keith B, Simon MC (2003) Differential roles of hypoxia-inducible factor 1α (HIF-1α) and HIF-2α in hypoxic gene regulation. Mol Cell Biol 23(24):9361–9374. https://doi.org/10.1128/mcb.23.24.9361-9374.2003
58. Denko NC (2008) Hypoxia, HIF1 and glucose metabolism in the solid tumour. Nat Rev Cancer 8:705. https://doi.org/10.1038/nrc2468
59. Ullah MS, Davies AJ, Halestrap AP (2006) The plasma membrane lactate transporter MCT4, but not MCT1, is up-regulated by hypoxia through a HIF-1alpha-dependent mechanism. J Biol Chem 281(14):9030–9037. https://doi.org/10.1074/jbc.M511397200
60. Tannock IF, Rotin D (1989) Acid pH in tumors and its potential for therapeutic exploitation. Cancer Res 49(16):4373–4384
61. Fukuda R, Zhang H, Kim JW, Shimoda L, Dang CV, Semenza GL (2007) HIF-1 regulates cytochrome oxidase subunits to optimize efficiency of respiration in hypoxic cells. Cell 129(1):111–122. https://doi.org/10.1016/j.cell.2007.01.047
62. Sutphin PD, Giaccia AJ, Chan DA (2007) Energy regulation: HIF MXIes it up with the C-MYC powerhouse. Dev Cell 12(6):845–846. https://doi.org/10.1016/j.devcel.2007.05.006
63. Corn PG, Ricci MS, Scata KA, Arsham AM, Simon MC, Dicker DT, El-Deiry WS (2005) Mxi1 is induced by hypoxia in a HIF-1–dependent manner and protects cells from c-Myc-induced apoptosis. Cancer Biol Ther 4(11):1285–1294. https://doi.org/10.4161/cbt.4.11.2299
64. Lee TC, Ziff EB (1999) Mxi1 is a repressor of the c-Myc promoter and reverses activation by USF. J Biol Chem 274(2):595–606
65. Zhang H, Gao P, Fukuda R, Kumar G, Krishnamachary B, Zeller KI, Dang Chi V, Semenza GL (2007) HIF-1 inhibits mitochondrial biogenesis and cellular respiration in VHL-deficient renal cell carcinoma by repression of C-MYC activity. Cancer Cell 11(5):407–420. https://doi.org/10.1016/j.ccr.2007.04.001
66. LaGory EL, Wu C, Taniguchi Cullen M, Cornelia Ding C-K, Chi J-T, von Eyben R, Scott David A, Richardson Adam D, Giaccia Amato J (2015) Suppression of PGC-1α is critical for reprogramming oxidative metabolism in renal cell carcinoma. Cell Rep 12(1):116–127. https://doi.org/10.1016/j.celrep.2015.06.006
67. Sweeney C, Murphy M, Kubelka M, Ravnik SE, Hawkins CF, Wolgemuth DJ, Carrington M (1996) A distinct cyclin a is expressed in germ cells in the mouse. Development 122(1):53–64
68. Nguyen TB, Manova K, Capodieci P, Lindon C, Bottega S, Wang XY, Refik-Rogers J, Pines J, Wolgemuth DJ, Koff A (2002) Characterization and expression of mammalian cyclin b3, a prepachytene meiotic

cyclin. J Biol Chem 277(44):41960–41969. https://doi.org/10.1074/jbc.M203951200

69. Bretones G, Delgado MD, León J (2015) Myc and cell cycle control. Biochim Biophys Acta 1849(5):506–516. https://doi.org/10.1016/j.bbagrm.2014.03.013
70. Florenes VA, Faye RS, Maelandsmo GM, Nesland JM, Holm R (2000) Levels of cyclin D1 and D3 in malignant melanoma: deregulated cyclin D3 expression is associated with poor clinical outcome in superficial melanoma. Clin Cancer Res 6(9):3614–3620
71. Hubbi ME, Semenza GL (2015) Regulation of cell proliferation by hypoxia-inducible factors. Am J Physiol Cell Physiol 309(12): C775–C782. https://doi.org/10.1152/ajpcell.00279.2015
72. Montagnoli A, Moll J, Colotta F (2010) Targeting cell division cycle 7 kinase: a new approach for cancer therapy. Clin Cancer Res 16(18):4503–4508. https://doi.org/10.1158/1078-0432.ccr-10-0185
73. Pucci B, Kasten M, Giordano A (2000) Cell cycle and apoptosis. Neoplasia (New York, NY) 2(4):291–299. https://doi.org/10.1038/sj.neo.7900101
74. Masai H, Taniyama C, Ogino K, Matsui E, Kakusho N, Matsumoto S, Kim JM, Ishii A, Tanaka T, Kobayashi T, Tamai K, Ohtani K, Arai K (2006) Phosphorylation of MCM4 by Cdc7 kinase facilitates its interaction with Cdc45 on the chromatin. J Biol Chem 281(51):39249–39261. https://doi.org/10.1074/jbc.M608935200
75. Hamilton E, Infante JR (2016) Targeting CDK4/6 in patients with cancer. Cancer Treat Rev 45:129–138. https://doi.org/10.1016/j.ctrv.2016.03.002
76. Joaquin M, Gubern A, Posas F (2012) A novel G1 checkpoint mediated by the p57 CDK inhibitor and p38 SAPK promotes cell survival upon stress. Cell Cycle 11(18):3339–3340. https://doi.org/10.4161/cc.21840
77. Goda N, Ryan HE, Khadivi B, McNulty W, Rickert RC, Johnson RS (2003) Hypoxia-inducible factor 1α is essential for cell cycle arrest during hypoxia. Mol Cell Biol 23(1):359–369. https://doi.org/10.1128/mcb.23.1.359-369.2003
78. Iida T, Mine S, Fujimoto H, Suzuki K, Minami Y, Tanaka Y (2002) Hypoxia-inducible factor-1α induces cell cycle arrest of endothelial cells. Genes Cells 7(2):143–149. https://doi.org/10.1046/j.1356-9597.2001.00512.x
79. Carmeliet P, Dor Y, Herbert J-M, Fukumura D, Brusselmans K, Dewerchin M, Neeman M, Bono F, Abramovitch R, Maxwell P, Koch CJ, Ratcliffe P, Moons L, Jain RK, Collen D, Keshet E (1998) Role of HIF-1α in hypoxia-mediated apoptosis, cell proliferation and tumour angiogenesis. Nature 394:485. https://doi.org/10.1038/28867. https://www.nature.com/articles/28867#supplementary-information
80. Obacz J, Pastorekova S, Vojtesek B, Hrstka R (2013) Cross-talk between HIF and p53 as mediators of molecular responses to physiological and genotoxic stresses. Mol Cancer 12(1):93. https://doi.org/10.1186/1476-4598-12-93
81. Ortmann B, Druker J, Rocha S (2014) Cell cycle progression in response to oxygen levels. Cell Mol Life Sci 71(18):3569–3582. https://doi.org/10.1007/s00018-014-1645-9
82. Miller M, Shirole N, Tian R, Pal D, Sordella R (2016) The evolution of TP53 mutations: from loss-of-function to separation-of-function mutants. J Cancer Biol Res 4(4):1091
83. Hubbi ME, Kshitiz GDM, Rey S, Wong CC, Luo W, Kim D-H, Dang CV, Levchenko A, Semenza GL (2013) A nontranscriptional role for HIF-1α as a direct inhibitor of DNA replication. Sci Signal 6(262):ra10–ra10. https://doi.org/10.1126/scisignal.2003417
84. Moser Sandra C, Bensaddek D, Ortmann B, Maure J-F, Mudie S, Blow JJ, Lamond Angus I, Swedlow Jason R, Rocha S (2013) PHD1 links cell-cycle progression to oxygen sensing through hydroxylation of the Centrosomal protein Cep192. Dev Cell 26(4):381–392. https://doi.org/10.1016/j.devcel.2013.06.014
85. Ortmann B, Bensaddek D, Carvalhal S, Moser SC, Mudie S, Griffis ER, Swedlow JR, Lamond AI, Rocha S (2016) CDK-dependent phosphorylation of PHD1 on serine 130 alters its substrate preference in cells. J Cell Sci 129(1):191–205. https://doi.org/10.1242/jcs.179911
86. Greijer AE, van der Wall E (2004) The role of hypoxia inducible factor 1 (HIF-1) in hypoxia induced apoptosis. J Clin Pathol 57(10):1009–1014. https://doi.org/10.1136/jcp.2003.015032
87. van de Schepop HA, de Jong JS, van Diest PJ, Baak JP (1996) Counting of apoptotic cells: a methodological study in invasive breast cancer. Clin Mol Pathol 49(4):M214–M217
88. Elmore S (2007) Apoptosis: a review of programmed cell death. Toxicol Pathol

35(4):495–516. https://doi.org/10.1080/01926230701320337

89. Ichim G, Tait SWG (2016) A fate worse than death: apoptosis as an oncogenic process. Nat Rev Cancer 16:539. https://doi.org/10.1038/nrc.2016.58
90. Thorburn A (2007) Tumor necrosis factor-related apoptosis-inducing ligand (TRAIL) pathway signaling. J Thorac Oncol 2(6):461–465. https://doi.org/10.1097/JTO.0b013e31805fea64
91. Happo L, Strasser A, Cory S (2012) BH3-only proteins in apoptosis at a glance. J Cell Sci 125(Pt 5):1081–1087. https://doi.org/10.1242/jcs.090514
92. Findley HW, Gu L, Yeager AM, Zhou M (1997) Expression and regulation of Bcl-2, Bcl-xl, and Bax correlate with p53 status and sensitivity to apoptosis in childhood acute lymphoblastic leukemia. Blood 89(8):2986–2993
93. Yu J, Wang Z, Kinzler KW, Vogelstein B, Zhang L (2003) PUMA mediates the apoptotic response to p53 in colorectal cancer cells. Proc Natl Acad Sci U S A 100(4):1931–1936. https://doi.org/10.1073/pnas.2627984100
94. Yuan Z, Cao K, Lin C, Li L, Liu HY, Zhao XY, Liu L, Deng HX, Li J, Nie CL, Wei YQ (2011) The p53 upregulated modulator of apoptosis (PUMA) chemosensitizes intrinsically resistant ovarian cancer cells to cisplatin by lowering the threshold set by Bcl-x(L) and Mcl-1. Mol Med (Cambridge, Mass) 17(11–12):1262–1274. https://doi.org/10.2119/molmed.2011.00176
95. Sasabe E, Tatemoto Y, Li D, Yamamoto T, Osaki T (2005) Mechanism of HIF-1-α-dependent suppression of hypoxia-induced apoptosis in squamous cell carcinoma cells. Cancer Sci 96(7):394–402. https://doi.org/10.1111/j.1349-7006.2005.00065.x
96. An WG, Kanekal M, Simon MC, Maltepe E, Blagosklonny MV, Neckers LM (1998) Stabilization of wild-type p53 by hypoxia-inducible factor 1alpha. Nature 392(6674):405–408. https://doi.org/10.1038/32925
97. Hansson LO, Friedler A, Freund S, Rudiger S, Fersht AR (2002) Two sequence motifs from HIF-1alpha bind to the DNA-binding site of p53. Proc Natl Acad Sci U S A 99(16):10305–10309. https://doi.org/10.1073/pnas.122347199
98. Parandavar E, Yazdanparast R (2017) Differential impact of various reactive oxygen species (ROS) on HIF-1alpha/p53 direct interaction in SK-N-MC neuroblastoma cells. Cell Biosci 7:52. https://doi.org/10.1186/s13578-017-0180-4
99. Burton TR, Gibson SB (2009) The role of Bcl-2 family member BNIP3 in cell death and disease: NIPping at the heels of cell death. Cell Death Differ 16:515. https://doi.org/10.1038/cdd.2008.185
100. Kubli Dieter A, Ycaza John E, Gustafsson Åsa B (2007) Bnip3 mediates mitochondrial dysfunction and cell death through Bax and Bak. Biochem J 405(3):407–415. https://doi.org/10.1042/bj20070319
101. Sowter HM, Ratcliffe PJ, Watson P, Greenberg AH, Harris AL (2001) HIF-1-dependent regulation of hypoxic induction of the cell death factors BNIP3 and NIX in human tumors. Cancer Res 61(18):6669–6673
102. Liu KE, Frazier WA (2015) Phosphorylation of the BNIP3 C-terminus inhibits mitochondrial damage and cell death without blocking autophagy. PLoS One 10(6):e0129667. https://doi.org/10.1371/journal.pone.0129667
103. Kothari S, Cizeau J, McMillan-Ward E, Israels SJ, Bailes M, Ens K, Kirshenbaum LA, Gibson SB (2003) BNIP3 plays a role in hypoxic cell death in human epithelial cells that is inhibited by growth factors EGF and IGF. Oncogene 22:4734. https://doi.org/10.1038/sj.onc.1206666
104. Liu X-H, Yu EZ, Li Y-Y, Kagan E (2006) HIF-1α has an anti-apoptotic effect in human airway epithelium that is mediated via Mcl-1 gene expression. J Cell Biochem 97(4):755–765. https://doi.org/10.1002/jcb.20683
105. Sendoel A, Hengartner MO (2014) Apoptotic Cell Death Under Hypoxia. Phys Ther 29(3):168–176. https://doi.org/10.1152/physiol.00016.2013
106. Piret JP, Minet E, Cosse JP, Ninane N, Debacq C, Raes M, Michiels C (2005) Hypoxia-inducible factor-1-dependent overexpression of myeloid cell factor-1 protects hypoxic cells against tert-butyl hydroperoxide-induced apoptosis. J Biol Chem 280(10):9336–9344. https://doi.org/10.1074/jbc.M411858200
107. Kilic M, Kasperczyk H, Fulda S, Debatin KM (2006) Role of hypoxia inducible factor-1 alpha in modulation of apoptosis resistance. Oncogene 26:2027. https://doi.org/10.1038/sj.onc.1210008. https://www.nature.com/articles/1210008#supplementary-information
108. Bao B, Azmi AS, Ali S, Ahmad A, Li Y, Banerjee S, Kong D, Sarkar FH (2012) The

biological kinship of hypoxia with CSC and EMT and their relationship with deregulated expression of miRNAs and tumor aggressiveness. Biochim Biophys Acta 1826(2):272–296. https://doi.org/10.1016/j.bbcan.2012.04.008

109. Heerboth S, Housman G, Leary M, Longacre M, Byler S, Lapinska K, Willbanks A, Sarkar S (2015) EMT and tumor metastasis. Clin Transl Med 4(1):6. https://doi.org/10.1186/s40169-015-0048-3
110. Kalluri R, Neilson EG (2003) Epithelial-mesenchymal transition and its implications for fibrosis. J Clin Invest 112(12):1776–1784. https://doi.org/10.1172/JCI20530
111. Kalluri R, Weinberg RA (2009) The basics of epithelial-mesenchymal transition. J Clin Invest 119(6):1420–1428. https://doi.org/10.1172/JCI39104
112. Valastyan S, Weinberg Robert A (2011) Tumor metastasis: molecular insights and evolving paradigms. Cell 147(2):275–292. https://doi.org/10.1016/j.cell.2011.09.024
113. Liu Y, Cao X (2016) Characteristics and significance of the pre-metastatic niche. Cancer Cell 30(5):668–681. https://doi.org/10.1016/j.ccell.2016.09.011
114. Cao H, Xu E, Liu H, Wan L, Lai M (2015) Epithelial–mesenchymal transition in colorectal cancer metastasis: a system review. Pathol Res Pract 211(8):557–569. https://doi.org/10.1016/j.prp.2015.05.010
115. Bielenberg DR, Zetter BR (2015) The contribution of angiogenesis to the process of metastasis. Cancer J 21(4):267–273. https://doi.org/10.1097/ppo.0000000000000138
116. Cavallaro U, Christofori G (2004) Cell adhesion and signalling by cadherins and Ig-CAMs in cancer. Nat Rev Cancer 4:118. https://doi.org/10.1038/nrc1276
117. Krishnamachary B, Zagzag D, Nagasawa H, Rainey K, Okuyama H, Baek JH, Semenza GL (2006) Hypoxia-inducible factor-1-dependent repression of E-cadherin in von Hippel-Lindau tumor suppressor-null renal cell carcinoma mediated by TCF3, ZFHX1A, and ZFHX1B. Cancer Res 66(5):2725–2731. https://doi.org/10.1158/0008-5472.can-05-3719
118. Eckert Mark A, Lwin Thinzar M, Chang Andrew T, Kim J, Danis E, Ohno-Machado L, Yang J (2011) Twist1-induced invadopodia formation promotes tumor metastasis. Cancer Cell 19(3):372–386. https://doi.org/10.1016/j.ccr.2011.01.036
119. Zhu Q-Q, Ma C, Wang Q, Song Y, Lv T (2016) The role of TWIST1 in epithelial-mesenchymal transition and cancers. Tumor Biol 37(1):185–197. https://doi.org/10.1007/s13277-015-4450-7
120. Linder S (2007) The matrix corroded: podosomes and invadopodia in extracellular matrix degradation. Trends Cell Biol 17(3):107–117. https://doi.org/10.1016/j.tcb.2007.01.002
121. Sun T, Zhao N, Zhao XL, Gu Q, Zhang SW, Che N, Wang XH, Du J, Liu YX, Sun BC (2010) Expression and functional significance of Twist1 in hepatocellular carcinoma: its role in vasculogenic mimicry. Hepatology 51(2):545–556. https://doi.org/10.1002/hep.23311
122. Chaturvedi P, Gilkes DM, Takano N, Semenza GL (2014) Hypoxia-inducible factor-dependent signaling between triple-negative breast cancer cells and mesenchymal stem cells promotes macrophage recruitment. Proc Natl Acad Sci 111(20):E2120–E2129. https://doi.org/10.1073/pnas.1406655111
123. Poggi A, Musso A, Dapino I, Zocchi MR (2014) Mechanisms of tumor escape from immune system: role of mesenchymal stromal cells. Immunol Lett 159(1):55–72. https://doi.org/10.1016/j.imlet.2014.03.001
124. Noy R, Pollard Jeffrey W (2014) Tumor-Associated Macrophages: From Mechanisms to Therapy. Immunity 41(1):49–61. https://doi.org/10.1016/j.immuni.2014.06.010
125. Qiang L, Wu T, Zhang HW, Lu N, Hu R, Wang YJ, Zhao L, Chen FH, Wang XT, You QD, Guo QL (2011) HIF-1α is critical for hypoxia-mediated maintenance of glioblastoma stem cells by activating Notch signaling pathway. Cell Death Differ 19:284. https://doi.org/10.1038/cdd.2011.95. https://www.nature.com/articles/cdd201195#supplementary-information
126. Shao S, Zhao X, Zhang X, Luo M, Zuo X, Huang S, Wang Y, Gu S, Zhao X (2015) Notch1 signaling regulates the epithelial–mesenchymal transition and invasion of breast cancer in a Slug-dependent manner. Mol Cancer 14(1):28. https://doi.org/10.1186/s12943-015-0295-3
127. Gupta R, Chetty C, Bhoopathi P, Lakka S, Mohanam S, Rao JS, Dinh DE (2011) Down-regulation of uPA/uPAR inhibits intermittent hypoxia-induced epithelial-mesenchymal transition (EMT) in DAOY and D283

medulloblastoma cells. Int J Oncol 38(3):733–744. https://doi.org/10.3892/ijo.2010.883

128. Tian B, Chen X, Zhang H, Li X, Wang J, Han W, Zhang LY, Fu L, Li Y, Nie C, Zhao Y, Tan X, Wang H, Guan XY, Hong A (2017) Urokinase plasminogen activator secreted by cancer-associated fibroblasts induces tumor progression via PI3K/AKT and ERK signaling in esophageal squamous cell carcinoma. Oncotarget 8(26):42300–42313. https://doi.org/10.18632/oncotarget.15857
129. Erler JT, Bennewith KL, Nicolau M, Dornhöfer N, Kong C, Le QT CJTA, Jeffrey SS, Giaccia AJ (2006) Lysyl oxidase is essential for hypoxia-induced metastasis. Nature 440:1222. https://doi.org/10.1038/nature04695. https://www.nature.com/articles/nature04695#supplementary-information
130. Smith-Mungo LI, Kagan HM (1998) Lysyl oxidase: Properties, regulation and multiple functions in biology. Matrix Biol 16(7):387–398. https://doi.org/10.1016/S0945-053X(98)90012-9
131. Baker A-M, Bird D, Welti JC, Gourlaouen M, Lang G, Murray GI, Reynolds AR, Cox TR, Erler JT (2013) Lysyl oxidase plays a critical role in endothelial cell stimulation to drive tumor angiogenesis. Cancer Res 73(2):583–594. https://doi.org/10.1158/0008-5472.can-12-2447
132. Semenza GL (2009) Defining the role of hypoxia-inducible factor 1 in cancer biology and therapeutics. Oncogene 29:625. https://doi.org/10.1038/onc.2009.441
133. Weijer R, Broekgaarden M, Kos M, van Vught R, Rauws EAJ, Breukink E, van Gulik TM, Storm G, Heger M (2015) Enhancing photodynamic therapy of refractory solid cancers: Combining second-generation photosensitizers with multi-targeted liposomal delivery. J Photochem Photobiol C Photchem Rev 23:103–131. https://doi.org/10.1016/j.jphotochemrev.2015.05.002
134. Weijer R, Clavier S, Zaal EA, Pijls MM, van Kooten RT, Vermaas K, Leen R, Jongejan A, Moerland PD, van Kampen AH, van Kuilenburg AB, Berkers CR, Lemeer S, Heger M (2017) Multi-OMIC profiling of survival and metabolic signaling networks in cells subjected to photodynamic therapy. Cell Mol Life Sci 74(6):1133–1151. https://doi.org/10.1007/s00018-016-2401-0
135. Reiss M, Brash DE, Muñoz-Antonia T, Simon JA, Ziegler A, Vellucci VF, Zhou ZL (1992) Status of the p53 tumor suppressor gene in human squamous carcinoma cell lines. Oncol Res 4(8–9):349–357
136. Muller PA, Vousden KH (2014) Mutant p53 in cancer: new functions and therapeutic opportunities. Cancer Cell 25(3):304–317. https://doi.org/10.1016/j.ccr.2014.01.021
137. Lamberti MJ, Pansa MF, Vera RE, Fernández-Zapico ME, Rumie Vittar NB, Rivarola VA (2017) Transcriptional activation of HIF-1 by a ROS-ERK axis underlies the resistance to photodynamic therapy. PLoS One 12(5):e0177801. https://doi.org/10.1371/journal.pone.0177801
138. Ferrario A, von Tiehl KF, Rucker N, Schwarz MA, Gill PS, Gomer CJ (2000) Antiangiogenic treatment enhances photodynamic therapy responsiveness in a mouse mammary carcinoma. Cancer Res 60(15):4066–4069
139. Zhan Q, Yue W, Hu S (2011) Effect of photodynamic therapy and endostatin on human glioma xenografts in nude mice. Photodiagnosis Photodyn Ther 8(4):314–320. https://doi.org/10.1016/j.pdpdt.2011.04.002
140. Koukourakis MI, Giatromanolaki A, Skarlatos J, Corti L, Blandamura S, Piazza M, Gatter KC, Harris AL (2001) Hypoxia inducible factor (HIF-1a and HIF-2a) expression in early esophageal cancer and response to photodynamic therapy and radiotherapy. Cancer Res 61(5):1830–1832
141. Roell KR, Reif DM, Motsinger-Reif AA (2017) An introduction to terminology and methodology of chemical synergy—perspectives from across disciplines. Front Pharmacol 8:158. https://doi.org/10.3389/fphar.2017.00158
142. Isaacs JS, Jung YJ, Mimnaugh EG, Martinez A, Cuttitta F, Neckers LM (2002) Hsp90 regulates a von Hippel Lindau-independent hypoxia-inducible factor-1 alpha-degradative pathway. J Biol Chem 277(33):29936–29944. https://doi.org/10.1074/jbc.M204733200
143. Solár P, Chytilová M, Solárová Z, Mojžiš J, Ferenc P, Fedoročko P (2011) Photodynamic Therapy with hypericin improved by targeting HSP90 associated proteins. Pharmaceuticals 4(11):1488
144. Al-Saigh R, Siopi M, Siafakas N, Velegraki A, Zerva L, Meletiadis J (2013) Single-dose pharmacodynamics of amphotericin B against Aspergillus species in an in vitro pharmacokinetic/pharmacodynamic model. Antimicrob Agents Chemother 57(8):3713–3718. https://doi.org/10.1128/aac.02484-12
145. Tsujino I, Miyagi K, Sampson RW, Sieber F (2006) Potentiation of the antitumor effect of

merocyanine 540-mediated photodynamic therapy by amifostine and amphotericin B. Photochem Photobiol 82(2):458–465. https://doi.org/10.1562/2005-09-02-ra-672

146. Campbell EJ, Vissers MCM, Bozonet S, Dyer A, Robinson BA, Dachs GU (2015) Restoring physiological levels of ascorbate slows tumor growth and moderates HIF-1 pathway activity in Gulo−/− mice. Cancer Med 4(2):303–314. https://doi.org/10.1002/cam4.349
147. Kramarenko GG, Wilke WW, Dayal D, Buettner GR, Schafer FQ (2006) Ascorbate enhances the toxicity of the photodynamic action of Verteporfin in HL-60 cells. Free Radic Biol Med 40(9):1615–1627. https://doi.org/10.1016/j.freeradbiomed.2005.12.027
148. Donald G, Hertzer K, Eibl G (2012) Baicalein--an intriguing therapeutic phytochemical in pancreatic cancer. Curr Drug Targets 13(14):1772–1776. https://doi.org/10.2174/138945012804545470
149. Tong WG, Ding XZ, Witt RC, Adrian TE (2002) Lipoxygenase inhibitors attenuate growth of human pancreatic cancer xenografts and induce apoptosis through the mitochondrial pathway. Mol Cancer Ther 1(11):929–935
150. Ding X-Z, Tong W-G, Adrian TE (2001) 12-lipoxygenase metabolite 12(S)-HETE stimulates human pancreatic cancer cell proliferation via protein tyrosine phosphorylation and ERK activation. Int J Cancer 94(5):630–636. https://doi.org/10.1002/ijc.1527
151. Ding X-Z, Kuszynski CA, El-Metwally TH, Adrian TE (1999) Lipoxygenase inhibition induced apoptosis, morphological changes, and carbonic anhydrase expression in human pancreatic cancer cells. Biochem Biophys Res Commun 266(2):392–399. https://doi.org/10.1006/bbrc.1999.1824
152. Ding X-Z, Iversen P, Cluck MW, Knezetic JA, Adrian TE (1999) Lipoxygenase Inhibitors Abolish Proliferation of Human Pancreatic Cancer Cells. Biochem Biophys Res Commun 261(1):218–223. https://doi.org/10.1006/bbrc.1999.1012
153. Triantafyllou A, Mylonis I, Simos G, Bonanou S, Tsakalof A (2008) Flavonoids induce HIF-1α but impair its nuclear accumulation and activity. Free Radic Biol Med 44(4):657–670. https://doi.org/10.1016/j.freeradbiomed.2007.10.050
154. Kleban J, Mikes J, Szilardiova B, Koval J, Sackova V, Solar P, Horvath V, Hofmanova J, Kozubik A, Fedorocko P (2007) Modulation of hypericin photodynamic therapy by pretreatment with 12 various inhibitors of arachidonic acid metabolism in colon adenocarcinoma HT-29 cells. Photochem Photobiol 83(5):1174–1185. https://doi.org/10.1111/j.1751-1097.2007.00127.x
155. Hamsa TP, Kuttan G (2012) Antiangiogenic activity of berberine is mediated through the downregulation of hypoxia-inducible factor-1, VEGF, and proinflammatory mediators. Drug Chem Toxicol 35(1):57–70. https://doi.org/10.3109/01480545.2011.589437
156. Luiza Andreazza N, Vevert-Bizet C, Bourg-Heckly G, Sureau F, Jose Salvador M, Bonneau S (2016) Berberine as a photosensitizing agent for antitumoral photodynamic therapy: insights into its association to low density lipoproteins. Int J Pharm 510(1):240–249. https://doi.org/10.1016/j.ijpharm.2016.06.009
157. Pan Y, Shao D, Zhao Y, Zhang F, Zheng X, Tan Y, He K, Li J, Chen L (2017) Berberine Reverses hypoxia-induced chemoresistance in breast cancer through the inhibition of AMPK- HIF-1α. Int J Biol Sci 13(6):794–803. https://doi.org/10.7150/ijbs.18969
158. Bonvini P, Zorzi E, Basso G, Rosolen A (2007) Bortezomib-mediated 26S proteasome inhibition causes cell-cycle arrest and induces apoptosis in CD-30+ anaplastic large cell lymphoma. Leukemia 21(4):838–842. https://doi.org/10.1038/sj.leu.2404528
159. Shin DH, Chun YS, Lee DS, Huang LE, Park JW (2008) Bortezomib inhibits tumor adaptation to hypoxia by stimulating the FIH-mediated repression of hypoxia-inducible factor-1. Blood 111(6):3131–3136. https://doi.org/10.1182/blood-2007-11-120576
160. Befani CD, Vlachostergios PJ, Hatzidaki E, Patrikidou A, Bonanou S, Simos G, Papandreou CN, Liakos P (2012) Bortezomib represses HIF-1α protein expression and nuclear accumulation by inhibiting both PI3K/Akt/TOR and MAPK pathways in prostate cancer cells. J Mol Med 90(1):45–54. https://doi.org/10.1007/s00109-011-0805-8
161. Li Z, Agharkar P, Chen B (2013) Therapeutic enhancement of vascular-targeted photodynamic therapy by inhibiting proteasomal function. Cancer Lett 339(1):128–134. https://doi.org/10.1016/j.canlet.2013.07.012

162. Gillies HC, Herriott D, Liang R, Ohashi K, Rogers HJ, Harper PG (1987) Pharmacokinetics of idarubicin (4-demethoxydaunorubicin; IMI-30; NSC 256439) following intravenous and oral administration in patients with advanced cancer. Br J Clin Pharmacol 23(3):303–310
163. Lee K, Qian DZ, Rey S, Wei H, Liu JO, Semenza GL (2009) Anthracycline chemotherapy inhibits HIF-1 transcriptional activity and tumor-induced mobilization of circulating angiogenic cells. Proc Natl Acad Sci 106(7):2353–2358. https://doi.org/10.1073/pnas.0812801106
164. Tokarska K, Lamch Ł, Piechota B, Żukowski K, Chudy M, Wilk KA, Brzózka Z (2020) Co-delivery of IR-768 and daunorubicin using mPEG-b-PLGA micelles for synergistic enhancement of combination therapy of melanoma. J Photochem Photobiol B Biol 211:111981. https://doi.org/10.1016/j.jphotobiol.2020.111981
165. Zhang H, Chen B, Jiang H, Wang C, Wang H, Wang X (2011) A strategy for ZnO nanorod mediated multi-mode cancer treatment. Biomaterials 32(7):1906–1914. https://doi.org/10.1016/j.biomaterials.2010.11.027
166. Hariharan R, Senthilkumar S, Suganthi A, Rajarajan M (2013) Synthesis and characterization of daunorubicin modified ZnO/PVP nanorods and its photodynamic action. J Photochem Photobiol A Chem 252:107–115. https://doi.org/10.1016/j.jphotochem.2012.11.017
167. Graham KA, Kulawiec M, Owens KM, Li X, Desouki MM, Chandra D, Singh KK (2010) NADPH oxidase 4 is an oncoprotein localized to mitochondria. Cancer Biol Ther 10(3):223–231. https://doi.org/10.4161/cbt.10.3.12207
168. Doroshow JH, Gaur S, Markel S, Lu J, van Balgooy J, Synold TW, Xi B, Wu X, Juhasz A (2013) Effects of iodonium-class flavin dehydrogenase inhibitors on growth, reactive oxygen production, cell cycle progression, NADPH oxidase 1 levels, and gene expression in human colon cancer cells and xenografts. Free Radic Biol Med 57:162–175. https://doi.org/10.1016/j.freeradbiomed.2013.01.002
169. Xia C, Meng Q, Liu LZ, Rojanasakul Y, Wang XR, Jiang BH (2007) Reactive oxygen species regulate angiogenesis and tumor growth through vascular endothelial growth factor. Cancer Res 67(22):10823–10830. https://doi.org/10.1158/0008-5472.can-07-0783
170. Chernyak BV, Izyumov DS, Lyamzaev KG, Pashkovskaya AA, Pletjushkina OY, Antonenko YN, Sakharov DV, Wirtz KW, Skulachev VP (2006) Production of reactive oxygen species in mitochondria of HeLa cells under oxidative stress. Biochim Biophys Acta 1757(5–6):525–534. https://doi.org/10.1016/j.bbabio.2006.02.019
171. Rubio N, Rajadurai A, Held KD, Prise KM, Liber HL, Redmond RW (2009) Real-time imaging of novel spatial and temporal responses to photodynamic stress. Free Radic Biol Med 47(3):283–290. https://doi.org/10.1016/j.freeradbiomed.2009.04.024
172. Doublier S, Belisario DC, Polimeni M, Annaratone L, Riganti C, Allia E, Ghigo D, Bosia A, Sapino A (2012) HIF-1 activation induces doxorubicin resistance in MCF7 3-D spheroids via P-glycoprotein expression: a potential model of the chemo-resistance of invasive micropapillary carcinoma of the breast. BMC Cancer 12:4. https://doi.org/10.1186/1471-2407-12-4
173. Chang J-E, Yoon I-S, Sun P-L, Yi E, Jheon S, Shim C-K (2014) Anticancer efficacy of photodynamic therapy with hematoporphyrin-modified, doxorubicin-loaded nanoparticles in liver cancer. J Photochem Photobiol B Biol 140:49–56. https://doi.org/10.1016/j.jphotobiol.2014.07.005
174. Lippert BM, Teymoortash A, Külkens C, Folz BJ, Werner JA (2004) Photodynamic effects of anthracyclin derivatives on squamous cell carcinoma cell lines of the head and neck. Lasers Surg Med 34(5):391–397. https://doi.org/10.1002/lsm.20040
175. Jendželovská Z, Jendželovský R, Kuchárová B, Fedoročko P (2016) Hypericin in the light and in the dark: two sides of the same coin. Front Plant Sci 7:560. https://doi.org/10.3389/fpls.2016.00560
176. Barliya T, Mandel M, Livnat T, Weinberger D, Lavie G (2011) Degradation of HIF-1alpha under hypoxia combined with induction of Hsp90 polyubiquitination in cancer cells by hypericin: a unique cancer therapy. PLoS One 6(9):e22849. https://doi.org/10.1371/journal.pone.0022849
177. Jiang BH, Jiang G, Zheng JZ, Lu Z, Hunter T, Vogt PK (2001) Phosphatidylinositol 3-kinase signaling controls levels of hypoxia-inducible factor 1. Cell Growth Differ 12(7):363–369
178. Zhang X, Cai L, He J, Li X, Li L, Chen X, Lan P (2017) Influence and mechanism of 5-aminolevulinic acid-photodynamic therapy on the metastasis of esophageal carcinoma. Photodiagnosis Photodyn Ther 20:78–85.

https://doi.org/10.1016/j.pdpdt.2017.08.004

179. Escuin D, Kline ER, Giannakakou P (2005) Both microtubule-stabilizing and microtubule-destabilizing drugs inhibit hypoxia-inducible factor-1alpha accumulation and activity by disrupting microtubule function. Cancer Res 65(19):9021–9028. https://doi.org/10.1158/0008-5472.can-04-4095
180. Soares HT, Campos JRS, Gomes-da-Silva LC, Schaberle FA, Dabrowski JM, Arnaut LG (2016) Pro-oxidant and antioxidant effects in photodynamic therapy: cells recognise that not all exogenous ROS are alike. Chem Bio Chem 17(9):836–842. https://doi.org/10.1002/cbic.201500573
181. Golab J, Nowis D, Skrzycki M, Czeczot H, Baranczyk-Kuzma A, Wilczynski GM, Makowski M, Mroz P, Kozar K, Kaminski R, Jalili A, Kopec M, Grzela T, Jakobisiak M (2003) Antitumor effects of photodynamic therapy are potentiated by 2-methoxyestradiol. A superoxide dismutase inhibitor. J Biol Chem 278(1):407–414. https://doi.org/10.1074/jbc.M209125200
182. LaVallee TM, Burke PA, Swartz GM, Hamel E, Agoston GE, Shah J, Suwandi L, Hanson AD, Fogler WE, Sidor CF, Treston AM (2008) Significant antitumor activity in vivo following treatment with the microtubule agent ENMD-1198. Mol Cancer Ther 7(6):1472–1482. https://doi.org/10.1158/1535-7163.mct-08-0107
183. Clarke SJ, Rivory LP (1999) Clinical pharmacokinetics of docetaxel. Clin Pharmacokinet 36(2):99–114. https://doi.org/10.2165/00003088-199936020-00002
184. Li W, Peng J, Tan L, Wu J, Shi K, Qu Y, Wei X, Qian Z (2016) Mild photothermal therapy/photodynamic therapy/chemotherapy of breast cancer by Lyp-1 modified Docetaxel/IR820 Co-loaded micelles. Biomaterials 106:119–133. https://doi.org/10.1016/j.biomaterials.2016.08.016
185. Blajeski AL, Phan VA, Kottke TJ, Kaufmann SH (2002) G(1) and G(2) cell-cycle arrest following microtubule depolymerization in human breast cancer cells. J Clin Invest 110(1):91–99. https://doi.org/10.1172/jci13275
186. Diez B, Ernst G, Teijo MJ, Batlle A, Hajos S, Fukuda H (2012) Combined chemotherapy and ALA-based photodynamic therapy in leukemic murine cells. Leuk Res 36(9):1179–1184. https://doi.org/10.1016/j.leukres.2012.04.027
187. Jung HJ, Seo I, Jha BK, Suh SI, Suh MH, Baek WK (2014) Minocycline inhibits angiogenesis in vitro through the translational suppression of HIF-1alpha. Arch Biochem Biophys 545:74–82. https://doi.org/10.1016/j.abb.2013.12.023
188. Lee M-J, Hung S-H, Huang M-C, Tsai T, Chen C-T (2017) Doxycycline potentiates antitumor effect of 5-aminolevulinic acid-mediated photodynamic therapy in malignant peripheral nerve sheath tumor cells. PLoS One 12(5):e0178493. https://doi.org/10.1371/journal.pone.0178493
189. Li J, Kim SG, Blenis J (2014) Rapamycin: one drug, many effects. Cell Metab 19(3):373–379. https://doi.org/10.1016/j.cmet.2014.01.001
190. Masoud GN, Li W (2015) HIF-1α pathway: role, regulation and intervention for cancer therapy. Acta Pharmac Sin B 5(5):378–389. https://doi.org/10.1016/j.apsb.2015.05.007
191. Chan S (2004) Targeting the mammalian target of rapamycin (mTOR): a new approach to treating cancer. Br J Cancer 91(8):1420–1424. https://doi.org/10.1038/sj.bjc.6602162
192. Wang YD, Su YJ, Li JY, Yao XC, Liang GJ (2015) Rapamycin, a mTOR inhibitor, induced growth inhibition in retinoblastoma Y79 cell via down-regulation of Bmi-1. Int J Clin Exp Pathol 8(5):5182–5188
193. Weyergang A, Berg K, Kaalhus O, Peng Q, Selbo PK (2009) Photodynamic therapy targets the mTOR signaling network in vitro and in vivo. Mol Pharm 6(1):255–264. https://doi.org/10.1021/mp800156e
194. Tuo J, Wang Q, Zouboulis CC, Liu Y, Ma Y, Ma L, Ying J, Zhang C, Xiang L (2017) ALA-PDT suppressing the cell growth and reducing the lipogenesis in human SZ95 sebocytes by mTOR signaling pathway in vitro. Photodiagnosis Photodyn Ther 18:295–301. https://doi.org/10.1016/j.pdpdt.2017.03.006
195. Zhang Q, Tang X, Lu QY, Zhang ZF, Brown J, Le AD (2005) Resveratrol inhibits hypoxia-induced accumulation of hypoxia-inducible factor-1alpha and VEGF expression in human tongue squamous cell carcinoma and hepatoma cells. Mol Cancer Ther 4(10):1465–1474. https://doi.org/10.1158/1535-7163.mct-05-0198
196. Singh RP, Gu M, Agarwal R (2008) Silibinin inhibits colorectal cancer growth by inhibiting tumor cell proliferation and angiogenesis. Cancer Res 68(6):2043–2050. https://doi.org/10.1158/0008-5472.can-07-6247

197. Zhang X, Liu X, Kang S, Liu C, Hao Y (2018) Resveratrol enhances the effects of ALA-PDT on skin squamous cells A431 through p38/MAPK signaling pathway. Cancer Biomark 21(4):797–803. https://doi.org/10.3233/cbm-170495

198. Gandara L, Sandes E, Di Venosa G, Prack Mc Cormick B, Rodriguez L, Mamone L, Batlle A, Eijan AM, Casas A (2014) The natural flavonoid silybin improves the response to photodynamic therapy of bladder cancer cells. J Photochem Photobiol B Biol 133:55–64. https://doi.org/10.1016/j.jphotobiol.2014.03.006

199. García-Maceira P, Mateo J (2008) Silibinin inhibits hypoxia-inducible factor-1α and mTOR/p70S6K/4E-BP1 signalling pathway in human cervical and hepatoma cancer cells: implications for anticancer therapy. Oncogene 28:313. https://doi.org/10.1038/onc.2008.398. https://www.nature.com/articles/onc2008398#supplementary-information

200. Kamiyama H, Takano S, Tsuboi K, Matsumura A (2005) Anti-angiogenic effects of SN38 (active metabolite of irinotecan): inhibition of hypoxia-inducible factor 1 alpha (HIF-1α)/vascular endothelial growth factor (VEGF) expression of glioma and growth of endothelial cells. J Cancer Res Clin Oncol 131(4):205–213. https://doi.org/10.1007/s00432-004-0642-z

201. Rapisarda A, Uranchimeg B, Sordet O, Pommier Y, Shoemaker RH, Melillo G (2004) Topoisomerase I-mediated inhibition of hypoxia-inducible factor 1. Cancer Res 64(4):1475. https://doi.org/10.1158/0008-5472.CAN-03-3139

202. Peng CL, Lai PS, Lin FH, Yueh-Hsiu Wu S, Shieh MJ (2009) Dual chemotherapy and photodynamic therapy in an HT-29 human colon cancer xenograft model using SN-38-loaded chlorin-core star block copolymer micelles. Biomaterials 30(21):3614–3625. https://doi.org/10.1016/j.biomaterials.2009.03.048

203. Kim SH, Jeong JW, Park JA, Lee JW, Seo JH, Jung BK, Bae MK, Kim KW (2007) Regulation of the HIF-1alpha stability by histone deacetylases. Oncol Rep 17(3):647–651

204. Bueno-Carrazco J, Castro-Leyva V, García-Gomez F, Solís-Paredes M, Ramon-Gallegos-E, Cruz-Orea A, Eguía-Aguilar P, Arenas-Huertero F (2012) Sodium butyrate increases the effect of the photodynamic therapy: a mechanism that involves modulation of gene expression and differentiation in astrocytoma cells. Childs Nerv Syst 28(10):1723–1730. https://doi.org/10.1007/s00381-012-1828-3

205. Flores-Ancona RM, Garcia-Gomez FY, Jimenez-Betanzos AM, Solis-Paredes M, Castro-Leyva V, Cruz-Orea A, Arenas-Huertero F, Ramon-Gallegos E (2009) Effects of sodium butyrate on cell death induced by photodynamic therapy in U373-MG and D54-MG astrocytoma cell lines. Photochem Photobiol 85(5):1182–1188. https://doi.org/10.1111/j.1751-1097.2009.00561.x

206. L-p L, Ho RLK, Chen GG, Lai PBS (2012) Sorafenib inhibits hypoxia-inducible factor-1α synthesis: implications for antiangiogenic activity in hepatocellular carcinoma. Clin Cancer Res 18(20):5662–5671. https://doi.org/10.1158/1078-0432.ccr-12-0552

207. Weiss A, van Beijnum JR, Bonvin D, Jichlinski P, Dyson PJ, Griffioen AW, Nowak-Sliwinska P (2014) Low-dose angiostatic tyrosine kinase inhibitors improve photodynamic therapy for cancer: lack of vascular normalization. J Cell Mol Med 18(3):480–491. https://doi.org/10.1111/jcmm.12199

208. Kummar S, Raffeld M, Juwara L, Horneffer Y, Strassberger A, Allen D, Steinberg SM, Rapisarda A, Spencer SD, Figg WD, Chen X, Turkbey IB, Choyke P, Murgo AJ, Doroshow JH, Melillo G (2011) Multihistology, target-driven pilot trial of oral topotecan as an inhibitor of hypoxia-inducible factor-1alpha in advanced solid tumors. Clin Cancer Res 17(15):5123–5131. https://doi.org/10.1158/1078-0432.ccr-11-0682

209. Goler-Baron V, Assaraf YG (2012) Overcoming multidrug resistance via photodestruction of ABCG2-rich extracellular vesicles sequestering photosensitive chemotherapeutics. PLoS One 7(4):e35487. https://doi.org/10.1371/journal.pone.0035487

210. Knuth J, Sharma SJ, Würdemann N, Holler C, Garvalov BK, Acker T, Wittekindt C, Wagner S, Klussmann JP (2017) Hypoxia-inducible factor-1α activation in HPV-positive head and neck squamous cell carcinoma cell lines. Oncotarget 8(52):89681–89691. https://doi.org/10.18632/oncotarget.20813

211. Halaburkova A, Jendzelovsky R, Koval J, Herceg Z, Fedorocko P, Ghantous A (2017) Histone deacetylase inhibitors potentiate photodynamic therapy in colon cancer cells marked by chromatin-mediated epigenetic regulation of CDKN1A. Clin Epigenetics 9:62. https://doi.org/10.1186/s13148-017-0359-x

212. Kang FW, Que L, Wu M, Wang ZL, Sun J (2012) Effects of trichostatin A on HIF-1α and VEGF expression in human tongue squamous cell carcinoma cells in vitro. Oncol Rep 28(1):193–199. https://doi.org/10.3892/or.2012.1784
213. Lee HJ, Kim KW (2012) Suppression of HIF-1α by valproic acid sustains self-renewal of mouse embryonic stem cells under hypoxia in vitro. Biomol Therap 20(3):280–285. https://doi.org/10.4062/biomolther.2012.20.3.280
214. Wei H, Wang F, Wang Y, Li T, Xiu P, Zhong J, Sun X, Li J (2017) Verteporfin suppresses cell survival, angiogenesis and vasculogenic mimicry of pancreatic ductal adenocarcinoma via disrupting the YAP-TEAD complex. Cancer Sci 108(3):478–487. https://doi.org/10.1111/cas.13138
215. Brodowska K, Al-Moujahed A, Marmalidou A, Meyer Zu Horste M, Cichy J, Miller JW, Gragoudas E, Vavvas DG (2014) The clinically used photosensitizer verteporfin (VP) inhibits YAP-TEAD and human retinoblastoma cell growth in vitro without light activation. Exp Eye Res 124:67–73. https://doi.org/10.1016/j.exer.2014.04.011
216. Bousquet MS, Ma JJ, Ratnayake R, Havre PA, Yao J, Dang NH, Paul VJ, Carney TJ, Dang LH, Luesch H (2016) Multidimensional screening platform for simultaneously targeting oncogenic kras and hypoxia-inducible factors pathways in colorectal cancer. ACS Chem Biol 11(5):1322–1331. https://doi.org/10.1021/acschembio.5b00860
217. Celli JP, Solban N, Liang A, Pereira SP, Hasan T (2011) Verteporfin-based photodynamic therapy overcomes gemcitabine insensitivity in a panel of pancreatic cancer cell lines. Lasers Surg Med 43(7):565–574. https://doi.org/10.1002/lsm.21093
218. Hutt DM, Roth DM, Vignaud H, Cullin C, Bouchecareilh M (2014) The histone deacetylase inhibitor, vorinostat, represses hypoxia inducible factor 1 alpha expression through translational inhibition. PLoS One 9(8):e106224. https://doi.org/10.1371/journal.pone.0106224
219. Xue K, Gu JJ, Zhang Q, Mavis C, Hernandez-Ilizaliturri FJ, Czuczman MS, Guo Y (2016) Vorinostat, a histone deacetylase (HDAC) inhibitor, promotes cell cycle arrest and re-sensitizes rituximab- and chemo-resistant lymphoma cells to chemotherapy agents. J Cancer Res Clin Oncol 142(2):379–387. https://doi.org/10.1007/s00432-015-2026-y
220. Kessel D, Vicente MG, Reiners JJ Jr (2006) Initiation of apoptosis and autophagy by photodynamic therapy. Lasers Surg Med 38(5):482–488. https://doi.org/10.1002/lsm.20334
221. Ibrahim NO, Hahn T, Franke C, Stiehl DP, Wirthner R, Wenger RH, Katschinski DM (2005) Induction of the hypoxia-inducible factor system by low levels of heat shock protein 90 inhibitors. Cancer Res 65(23):11094–11100. https://doi.org/10.1158/0008-5472.can-05-1877
222. Lang W, Caldwell GW, Li J, Leo GC, Jones WJ, Masucci JA (2007) Biotransformation of geldanamycin and 17-allylamino-17-demethoxygeldanamycin by human liver microsomes: reductive versus oxidative metabolism and implications. Drug Metab Dispos 35(1):21–29. https://doi.org/10.1124/dmd.106.009639
223. Newman B, Liu Y, Lee HF, Sun D, Wang Y (2012) HSP90 inhibitor 17-AAG selectively eradicates lymphoma stem cells. Cancer Res 72(17):4551–4561. https://doi.org/10.1158/0008-5472.can-11-3600
224. Vaishampayan UN, Burger AM, Sausville EA, Heilbrun LK, Li J, Horiba MN, Egorin MJ, Ivy P, Pacey S, Lorusso PM (2010) Safety, efficacy, pharmacokinetics, and pharmacodynamics of the combination of sorafenib and tanespimycin. Clin Cancer Res 16(14):3795–3804. https://doi.org/10.1158/1078-0432.ccr-10-0503
225. Kaur G, Belotti D, Burger AM, Fisher-Nielson K, Borsotti P, Riccardi E, Thillainathan J, Hollingshead M, Sausville EA, Giavazzi R (2004) Antiangiogenic properties of 17-(dimethylaminoethylamino)-17-demethoxygeldanamycin: an orally bioavailable heat shock protein 90 modulator. Clin Cancer Res 10(14):4813–4821. https://doi.org/10.1158/1078-0432.ccr-03-0795
226. Joshi SS, Jiang S, Unni E, Goding SR, Fan T, Antony PA, Hornyak TJ (2018) 17-AAG inhibits vemurafenib-associated MAP kinase activation and is synergistic with cellular immunotherapy in a murine melanoma model. PLoS One 13(2):e0191264. https://doi.org/10.1371/journal.pone.0191264
227. Smith V, Sausville EA, Camalier RF, Fiebig HH, Burger AM (2005) Comparison of 17-dimethylaminoethylamino-17-demethoxy-geldanamycin (17DMAG) and 17-allylamino-17-demethoxygeldanamycin (17AAG) in vitro: effects on Hsp90 and client proteins in melanoma models. Cancer Chemother Pharmacol 56(2):126–137. https://doi.org/10.1007/s00280-004-0947-2

228. Pacey S, Wilson RH, Walton M, Eatock MM, Hardcastle A, Zetterlund A, Arkenau HT, Moreno-Farre J, Banerji U, Roels B, Peachey H, Aherne W, de Bono JS, Raynaud F, Workman P, Judson I (2011) A phase I study of the heat shock protein 90 inhibitor alvespimycin (17-DMAG) given intravenously to patients with advanced solid tumors. Clin Cancer Res 17(6):1561–1570. https://doi.org/10.1158/1078-0432.ccr-10-1927

229. Mabjeesh NJ, Escuin D, LaVallee TM, Pribluda VS, Swartz GM, Johnson MS, Willard MT, Zhong H, Simons JW, Giannakakou P (2003) 2ME2 inhibits tumor growth and angiogenesis by disrupting microtubules and dysregulating HIF. Cancer Cell 3(4):363–375. https://doi.org/10.1016/S1535-6108(03)00077-1

230. Dahut WL, Lakhani NJ, Gulley JL, Arlen PM, Kohn EC, Kotz H, McNally D, Parr A, Parr A, Nguyen D, Yang SX, Steinberg SM, Venitz J, Sparreboom A, Figg IIW (2006) Phase I clinical trial of oral 2-methoxyestradiol, an antiangiogenic and apoptotic agent, in patients with solid tumors. Cancer Biol Ther 5(1):22–27. https://doi.org/10.4161/cbt.5.1.2349

231. Kambhampati S, Rajewski RA, Tanol M, Haque I, Das A, Banerjee S, Jha S, Burns D, Borrego-Diaz E, Van Veldhuizen P, Banerjee SK (2013) A second generation 2-methoxyestradiol prodrug is effective against Barrett's adenocarcinoma in a mouse xenograft model. Mol Cancer Ther 12(3):255–263. https://doi.org/10.1158/1535-7163.mct-12-0777

232. Won MS, Im N, Park S, Boovanahalli SK, Jin Y, Jin X, Chung KS, Kang M, Lee K, Park SK, Kim HM, Kwon BM, Lee JJ, Lee K (2009) A novel benzimidazole analogue inhibits the hypoxia-inducible factor (HIF)-1 pathway. Biochem Biophys Res Commun 385(1):16–21. https://doi.org/10.1016/j.bbrc.2009.05.022

233. Rietbrock N, Abshagen U, Bergmann KV, Kewitz H (1972) Pharmacokinetics of digoxin and its 4‴-acetyl-and methylderivates in the rat. Naunyn Schmiedebergs Arch Pharmacol 274(2):171–181. https://doi.org/10.1007/bf00501851

234. Zhang H, Qian DZ, Tan YS, Lee K, Gao P, Ren YR, Rey S, Hammers H, Chang D, Pili R, Dang CV, Liu JO, Semenza GL (2008) Digoxin and other cardiac glycosides inhibit HIF-1α synthesis and block tumor growth. Proc Natl Acad Sci U S A 105(50):19579–19586. https://doi.org/10.1073/pnas.0809763105

235. Lee K, Zhang H, Qian DZ, Rey S, Liu JO, Semenza GL (2009) Acriflavine inhibits HIF-1 dimerization, tumor growth, and vascularization. Proc Natl Acad Sci U S A 106(42):17910–17915. https://doi.org/10.1073/pnas.0909353106

236. Dana S, Prusty D, Dhayal D, Gupta MK, Dar A, Sen S, Mukhopadhyay P, Adak T, Dhar SK (2014) Potent antimalarial activity of acriflavine in vitro and in vivo. ACS Chem Biol 9(10):2366–2373. https://doi.org/10.1021/cb500476q

237. Jones DT, Pugh CW, Wigfield S, Stevens MF, Harris AL (2006) Novel thioredoxin inhibitors paradoxically increase hypoxia-inducible factor-alpha expression but decrease functional transcriptional activity, DNA binding, and degradation. Clin Cancer Res 12(18):5384–5394. https://doi.org/10.1158/1078-0432.ccr-05-2380

238. Terzuoli E, Puppo M, Rapisarda A, Uranchimeg B, Cao L, Burger AM, Ziche M, Melillo G (2010) Aminoflavone, a Ligand of the Aryl Hydrocarbon Receptor, Inhibits HIF-1α Expression in an AhR-Independent Fashion. Cancer Res 70(17):6837–6848. https://doi.org/10.1158/0008-5472.can-10-1075

239. Loaiza-Pérez AI, Kenney S, Boswell J, Hollingshead M, Alley MC, Hose C, Ciolino HP, Yeh GC, Trepel JB, Vistica DT, Sausville EA (2004) Aryl hydrocarbon receptor activation of an antitumor aminoflavone: basis of selective toxicity for MCF-7 breast tumor cells. Mol Cancer Ther 3(6):715–725

240. Osada M, Imaoka S, Funae Y (2004) Apigenin suppresses the expression of VEGF, an important factor for angiogenesis, in endothelial cells via degradation of HIF-1α protein. FEBS Letters 575(1–3):59–63. https://doi.org/10.1016/j.febslet.2004.08.036

241. Gradolatto A, Basly J-P, Berges R, Teyssier C, Chagnon M-C, Siess M-H, Canivenc-Lavier M-C (2005) Pharmacokinetics and metabolism of apigenin in female and male rats after a single oral administration. Drug Metab Dispos 33(1):49–54. https://doi.org/10.1124/dmd.104.000893

242. Park H-R, Daun Y, Keun Park J, Bark K-M (2013) Spectroscopic properties of flavonoids in various aqueous-organic solvent mixtures. Bull Korean Chem Soc 34. https://doi.org/10.5012/bkcs.2013.34.1.211

243. Ansó E, Zuazo A, Irigoyen M, Urdaci MC, Rouzaut A, Martínez-Irujo JJ (2010) Flavonoids inhibit hypoxia-induced vascular

endothelial growth factor expression by a HIF-1 independent mechanism. Biochem Pharmacol 79(11):1600–1609. https://doi.org/10.1016/j.bcp.2010.02.004

244. Jeong YJ, Cho HJ, Magae J, Lee IK, Park KG, Chang YC (2013) Ascofuranone suppresses EGF-induced HIF-1alpha protein synthesis by inhibition of the Akt/mTOR/p70S6K pathway in MDA-MB-231 breast cancer cells. Toxicol Appl Pharmacol 273(3):542–550. https://doi.org/10.1016/j.taap.2013.09.027
245. Sawada M, Hosokawa T, Okutomi T, Ando K (1973) Hypolipidemic property of ascofuranone. J Antibiot 26(11):681–686
246. Sasaki H, Hosokawa T, Sawada M, Ando K (1973) Isolation and structure of ascofuranone and ascofranol, antibiotics with hypolipidemic activity. J Antibiot 26(11):676–680. https://doi.org/10.7164/antibiotics.26.676
247. Xu D, Chen Q, Liu Y, Wen X (2017) Baicalein suppresses the androgen receptor (AR)-mediated prostate cancer progression via inhibiting the AR N-C dimerization and AR-coactivators interaction. Oncotarget 8:105561–105573. https://doi.org/10.18632/oncotarget.22319
248. Ellinghaus P, Heisler I, Unterschemmann K, Haerter M, Beck H, Greschat S, Ehrmann A, Summer H, Flamme I, Oehme F, Thierauch K, Michels M, Hess-Stumpp H, Ziegelbauer K (2013) BAY 87–2243, a highly potent and selective inhibitor of hypoxia-induced gene activation has antitumor activities by inhibition of mitochondrial complex I. Cancer Med 2(5):611–624. https://doi.org/10.1002/cam4.112
249. Lin S, Tsai SC, Lee CC, Wang BW, Liou JY, Shyu KG (2004) Berberine inhibits HIF-1alpha expression via enhanced proteolysis. Mol Pharmacol 66(3):612–619
250. Gong Z, Chen Y, Zhang R, Yang Q, Wang Y, Guo Y, Zhou B, Weng X, Liu X, Li Y, Zhu X, Dong Y (2015) Pharmacokinetic difference of berberine between normal and chronic visceral hypersensitivity irritable bowel syndrome rats and its mechanism. Arch Pharm Res 38(10):1888–1896. https://doi.org/10.1007/s12272-015-0568-9
251. Vicas L, Teusdea A, Vicas S, Marian E, Tunde J, Muresan M, Gligor F (2015) Assessment of antioxidant capacity of some extracts for further use in therapy. Farmacia 63:267–274
252. Walker SE, Charbonneau LF, Law S (2014) Stability of bortezomib 2.5 mg/mL in vials and syringes stored at 4 degrees C and room temperature (23 degrees C). Can J Hosp Pharm 67(2):102–107
253. Gunasekera SP, Imperial L, Garst C, Ratnayake R, Dang LH, Paul VJ, Luesch H (2016) Caldoramide, a modified pentapeptide from the marine cyanobacterium caldora penicillata. J Nat Prod 79(7):1867–1871. https://doi.org/10.1021/acs.jnatprod.6b00203
254. Reece KM, Richardson ED, Cook KM, Campbell TJ, Pisle ST, Holly AJ, Venzon DJ, Liewehr DJ, Chau CH, Price DK, Figg WD (2014) Epidithiodiketopiperazines (ETPs) exhibit in vitro antiangiogenic and in vivo antitumor activity by disrupting the HIF-1alpha/p300 complex in a preclinical model of prostate cancer. Mol Cancer 13:91. https://doi.org/10.1186/1476-4598-13-91
255. Frye SV, Heightman T, Jin J (2010) Chapter 20 - Targeting methyl lysine. In: Macor JE (ed) Annual reports in medicinal chemistry, vol 45. Academic Press, London, pp 329–343. https://doi.org/10.1016/S0065-7743(10)45020-4
256. Kung AL, Zabludoff SD, France DS, Freedman SJ, Tanner EA, Vieira A, Cornell-Kennon S, Lee J, Wang B, Wang J, Memmert K, Naegeli H-U, Petersen F, Eck MJ, Bair KW, Wood AW, Livingston DM (2004) Small molecule blockade of transcriptional coactivation of the hypoxia-inducible factor pathway. Cancer Cell 6(1):33–43. https://doi.org/10.1016/j.ccr.2004.06.009
257. Na Y-R, Han K-C, Park H, Yang EG (2013) Menadione and ethacrynic acid inhibit the hypoxia-inducible factor (HIF) pathway by disrupting HIF-1α interaction with p300. Biochem Biophys Res Commun 434(4):879–884. https://doi.org/10.1016/j.bbrc.2013.04.044
258. Viziteu E, Grandmougin C, Goldschmidt H, Seckinger A, Hose D, Klein B, Moreaux J (2016) Chetomin, targeting HIF-1α/p300 complex, exhibits antitumour activity in multiple myeloma. Br J Cancer 114(5):519–523. https://doi.org/10.1038/bjc.2016.20
259. Bae W-Y, Choi J-S, Kim J-E, Jeong J-W (2015) Cinnamic aldehyde suppresses hypoxia-induced angiogenesis via inhibition of hypoxia-inducible factor-1α expression during tumor progression. Biochem Pharmacol 98(1):41–50. https://doi.org/10.1016/j.bcp.2015.08.095
260. Hong S-H, Ismail IA, Kang S-M, Han DC, Kwon B-M (2016) Cinnamaldehydes in cancer chemotherapy. Phytother Res

30(5):754–767. https://doi.org/10.1002/ptr.5592

261. Ng L-T, Wu S-J (2011) Antiproliferative activity of cinnamomum cassia constituents and effects of pifithrin-alpha on their apoptotic signaling pathways in Hep G2 cells. Evid Based Complement Alternat Med 2011: 492148. https://doi.org/10.1093/ecam/nep220
262. Ban HS, Xu X, Jang K, Kim I, Kim B-K, Lee K, Won M (2016) A novel malate dehydrogenase 2 inhibitor suppresses hypoxia-inducible factor-1 by regulating mitochondrial respiration. PLoS One 11(9): e0162568. https://doi.org/10.1371/journal.pone.0162568
263. Naik R, Won M, Ban HS, Bhattarai D, Xu X, Eo Y, Hong YS, Singh S, Choi Y, Ahn HC, Lee K (2014) Synthesis and structure-activity relationship study of chemical probes as hypoxia induced factor-1alpha/malate dehydrogenase 2 inhibitors. J Med Chem 57(22):9522–9538. https://doi.org/10.1021/jm501241g
264. Jones DT, Harris AL (2006) Identification of novel small-molecule inhibitors of hypoxia-inducible factor-1 transactivation and DNA binding. Mol Cancer Ther 5(9):2193–2202. https://doi.org/10.1158/1535-7163.mct-05-0443
265. Klausmeyer P, Zhou Q, Scudiero DA, Uranchimeg B, Melillo G, Cardellina JH, Shoemaker RH, Chang CJ, McCloud TG (2009) Cytotoxic and HIF-1alpha inhibitory compounds from Crossosoma bigelovii. J Nat Prod 72(5):805–812. https://doi.org/10.1021/np8006342
266. Kaushik V, Azad N, Yakisich JS, Iyer AK (2017) Antitumor effects of naturally occurring cardiac glycosides convallatoxin and peruvoside on human ER+ and triple-negative breast cancers. Cell Death Dis 3:17009. https://doi.org/10.1038/cddiscovery.2017.9
267. Ma J, Zi Jiang Y, Shi H, Mi C, Li J, Xing Nan J, Wu X, Joon Lee J, Jin X (2014) Cucurbitacin B inhibits the translational expression of hypoxia-inducible factor-1α. Eur J Pharmacol 723:46–54. https://doi.org/10.1016/j.ejphar.2013.12.005
268. Molavi O, Shayeganpour A, Somayaji V, Hamdy S, Brocks DR, Lavasanifar A, Kwon GS, Samuel J (2006) Development of a sensitive and specific liquid chromatography/mass spectrometry method for the quantification of cucurbitacin I (JSI-124) in rat plasma. J Pharm Pharmac Sci 9(2):158–164
269. Nishida R, Yokoyama M, Fukami H (1992) Sequestration of cucurbitacin analogs by New and Old World chrysomelid leaf beetles in the tribe Luperini. Chemoecology 3(1):19–24. https://doi.org/10.1007/bf01261452
270. Schulz V, Hänsel R, Blumenthal M, Tyler VE (2004) Rational phytotherapy : a reference guide for physicians and pharmacists
271. Dakeng S, Duangmano S, Jiratchariyakul W, U-Pratya Y, Bögler O, Patmasiriwat P (2012) Inhibition of Wnt signaling by cucurbitacin B in breast cancer cells: Reduction of Wnt-associated proteins and reduced translocation of galectin-3-mediated β-catenin to the nucleus. J Cell Biochem 113(1):49–60. https://doi.org/10.1002/jcb.23326
272. Touihri-Barakati I, Kallech-Ziri O, Ayadi W, Kovacic H, Hanchi B, Hosni K, Luis J (2017) Cucurbitacin B purified from Ecballium elaterium (L.) A. Rich from Tunisia inhibits α5β1 integrin-mediated adhesion, migration, proliferation of human glioblastoma cell line and angiogenesis. Eur J Pharmacol 797: 153–161. https://doi.org/10.1016/j.ejphar.2017.01.006
273. Didiot M-C, Hewett J, Varin T, Freuler F, Selinger D, Nick H, Reinhardt J, Buckler A, Myer V, Schuffenhauer A, Guy CT, Parker CN (2013) Identification of cardiac glycoside molecules as inhibitors of c-Myc IRES-mediated translation. J Biomol Screen 18(4):407–419. https://doi.org/10.1177/1087057112466698
274. Gervasoni JE Jr, Hindenburg AA, Vezeridis MP, Schulze S, Wanebo HJ, Mehta S (2004) An effective in vitro antitumor response against human pancreatic carcinoma with paclitaxel and daunorubicin by induction of both necrosis and apoptosis. Anticancer Res 24(5a):2617–2626
275. Bains OS, Szeitz A, Lubieniecka JM, Cragg GE, Grigliatti TA, Riggs KW, Reid RE (2013) A correlation between cytotoxicity and reductase-mediated metabolism in cell lines treated with doxorubicin and daunorubicin. J Pharmac Exp Therap 347(2):375. https://doi.org/10.1124/jpet.113.206805
276. Hothi P, Martins TJ, Chen L, Deleyrolle L, Yoon JG, Reynolds B, Foltz G (2012) High-throughput chemical screens identify disulfiram as an inhibitor of human glioblastoma stem cells. Oncotarget 3(10):1124–1136. https://doi.org/10.18632/oncotarget.707
277. López-Lázaro M, Pastor N, Azrak SS, Ayuso MJ, Austin CA, Cortés F (2005) Digitoxin inhibits the growth of cancer cell lines at concentrations commonly found in cardiac

patients. J Nat Prod 68(11):1642–1645. https://doi.org/10.1021/np050226l

278. Lin J, Carducci MA (2009) HIF-1α inhibition as a novel mechanism of cardiac glycosides in cancer therapeutics. Expert Opin Investig Drugs 18(2):241–243. https://doi.org/10.1517/13543780802683081
279. Ouyang X, Han S-N, Zhang J-Y, Dioletis E, Nemeth BT, Pacher P, Feng D, Bataller R, Cabezas J, Stärkel P, Caballeria J, Pongratz RL, Cai S-Y, Schnabl B, Hoque R, Chen Y, Yang WH, Garcia-Martinez I, Wang FS, Gao B, Torok NJ, Kibbey RG, Mehal WZ (2018) Digoxin suppresses pyruvate kinase M2-promoted HIF-1α; transactivation in steatohepatitis. Cell Metab 27(2):339–350. e333. https://doi.org/10.1016/j.cmet.2018.01.007
280. Wei D, Peng JJ, Gao H, Li H, Li D, Tan Y, Zhang T (2013) Digoxin downregulates NDRG1 and VEGF through the inhibition of HIF-1alpha under hypoxic conditions in human lung adenocarcinoma A549 cells. Int J Mol Sci 14(4):7273–7285. https://doi.org/10.3390/ijms14047273
281. Felth J, Rickardson L, Rosén J, Wickström M, Fryknäs M, Lindskog M, Bohlin L, Gullbo J (2009) Cytotoxic effects of cardiac glycosides in colon cancer cells, alone and in combination with standard chemotherapeutic drugs. J Nat Prod 72(11):1969–1974. https://doi.org/10.1021/np900210m
282. Touza NA, Pôças ES, Quintas LE, Cunha-Filho G, Santos ML, Noël F (2011) Inhibitory effect of combinations of digoxin and endogenous cardiotonic steroids on Na+/K+-ATPase activity in human kidney membrane preparation. Life Sci 88(1–2):39–42. https://doi.org/10.1016/j.lfs.2010.10.027
283. Li J, Mi C, Ma J, Wang KS, Lee JJ, Jin X (2015) Dihydrotanshinone I inhibits the translational expression of hypoxia-inducible factor-1α. Chem Biol Interact 240:48–58. https://doi.org/10.1016/j.cbi.2015.08.006
284. Cheng R, Chen J, Wang Y, Ge Y, Huang Z, Zhang G (2016) Dihydrotanshinone induces apoptosis of SGC7901 and MGC803 cells via activation of JNK and p38 signalling pathways. Pharm Biol 54(12):3019–3025. https://doi.org/10.1080/13880209.2016.1199045
285. Sun J, Yang M, Han J, Wang B, Ma X, Xu M, Liu P, Guo D (2007) Profiling the metabolic difference of seven tanshinones using high-performance liquid chromatography/multi-stage mass spectrometry with data-dependent acquisition. Rapid Commun Mass Spectrom 21(14):2211–2226. https://doi.org/10.1002/rcm.3080
286. Lu J, Risbood P, Kane CT Jr, Hossain MT, Anderson L, Hill K, Monks A, Wu Y, Antony S, Juhasz A, Liu H, Jiang G, Harris E, Roy K, Meitzler JL, Konaté M, Doroshow JH (2017) Characterization of potent and selective iodonium-class inhibitors of NADPH oxidases. Biochem Pharmacol 143:25–38. https://doi.org/10.1016/j.bcp.2017.07.007
287. Honore S, Kamath K, Braguer D, Wilson L, Briand C, Jordan MA (2003) Suppression of microtubule dynamics by discodermolide by a novel mechanism is associated with mitotic arrest and inhibition of tumor cell proliferation. Mol Cancer Ther 2(12):1303–1311
288. Gajula PK, Asthana J, Panda D, Chakraborty TK (2013) A synthetic dolastatin 10 analogue suppresses microtubule dynamics, inhibits cell proliferation, and induces apoptotic cell death. J Med Chem 56(6):2235–2245. https://doi.org/10.1021/jm3009629
289. Bai R, Petit GR, Hamel E (1990) Dolastatin 10, a powerful cytostatic peptide derived from a marine animal: Inhibition of tubulin polymerization mediated through the vinca alkaloid binding domain. Biochem Pharmacol 39(12):1941–1949. https://doi.org/10.1016/0006-2952(90)90613-P
290. Tomaszewski JE, Smith AC, Covey JM, Donohue SJ, Rhie JK, Schweikart KM (2002) Chapter 17 - Relevance of preclinical pharmacology and toxicology to phase i trial extrapolation techniques: relevance of animal toxicology. In: Baguley BC, Kerr DJ (eds) Anticancer drug development. Academic Press, San Diego, CA, pp 301–328. https://doi.org/10.1016/B978-012072651-6/50018-8
291. Al-Hadiya BMH (2010) Chapter 5 - Parbendazole. In: Brittain HG (ed) Profiles of drug substances, excipients and related methodology, vol 35. Academic Press, New York, pp 263–284. https://doi.org/10.1016/S1871-5125(10)35005-9
292. Kong D, Park EJ, Stephen AG, Calvani M, Cardellina JH, Monks A, Fisher RJ, Shoemaker RH, Melillo G (2005) Echinomycin, a small-molecule inhibitor of hypoxia-inducible factor-1 DNA-binding activity. Cancer Res 65(19):9047–9055. https://doi.org/10.1158/0008-5472.can-05-1235
293. Yonekura S, Itoh MAI, Okuhashi Y, Takahashi Y, Ono AYA, Nara N, Tohda S (2013) Effects of the HIF1 inhibitor, echinomycin, on growth and NOTCH signalling in leukaemia cells. Anticancer Res 33(8):3099

294. Hajian R, Ekhlasi E, Daneshvar R (2012) Spectroscopic and Electrochemical Studies on the Interaction of Epirubicin with Fish Sperm DNA. E-J Chem 9(3):1587–1598. https://doi.org/10.1155/2012/738678
295. Bollag DM, McQueney PA, Zhu J, Hensens O, Koupal L, Liesch J, Goetz M, Lazarides E, Woods CM (1995) Epothilones, a new class of microtubule-stabilizing agents with a taxol-like mechanism of action. Cancer Res 55(11):2325–2333
296. Lin B, Catley L, LeBlanc R, Mitsiades C, Burger R, Tai Y-T, Podar K, Wartmann M, Chauhan D, Griffin JD, Anderson KC (2005) Patupilone (epothilone B) inhibits growth and survival of multiple myeloma cells in vitro and in vivo. Blood 105(1):350–357. https://doi.org/10.1182/blood-2004-06-2499
297. Melichar B, Casado E, Bridgewater J, Bennouna J, Campone M, Vitek P, Delord JP, Cerman J Jr, Salazar R, Dvorak J, Sguotti C, Urban P, Viraswami-Appanna K, Tan E, Tabernero J (2011) Clinical activity of patupilone in patients with pretreated advanced/metastatic colon cancer: results of a phase I dose escalation trial. Br J Cancer 105(11):1646–1653. https://doi.org/10.1038/bjc.2011.438
298. Regueiro-Ren A, Borzilleri RM, Zheng X, Kim S-H, Johnson JA, Fairchild CR, Lee FYF, Long BH, Vite GD (2001) Synthesis and biological activity of novel epothilone aziridines. Org Lett 3(17):2693–2696. https://doi.org/10.1021/ol016273w
299. Molnar J, Somberg JC (2009) The clinical pharmacology of ethacrynic acid. Am J Ther 16(1):86–92. https://doi.org/10.1097/MJT.0b013e318195e460
300. Vigushin DM, Mirsaidi N, Brooke G, Sun C, Pace P, Inman L, Moody CJ, Coombes RC (2004) Gliotoxin is a dual inhibitor of farnesyltransferase and geranylgeranyltransferase I with antitumor activity against breast cancer in vivo. Med Oncol 21(1):21–30. https://doi.org/10.1385/MO:21:1:21
301. Miyazawa M, Yasuda M, Fujita M, Kajiwara H, Hirabayashi K, Takekoshi S, Hirasawa T, Murakami M, Ogane N, Kiguchi K, Ishiwata I, Mikami M, Osamura RY (2009) Therapeutic strategy targeting the mTOR-HIF-1alpha-VEGF pathway in ovarian clear cell adenocarcinoma. Pathol Int 59(1):19–27. https://doi.org/10.1111/j.1440-1827.2008.02320.x
302. Zhu Y, Zhang X, Liu Y, Zhang S, Liu J, Ma Y, Zhang J (2012) Antitumor effect of the mTOR inhibitor everolimus in combination with trastuzumab on human breast cancer stem cells in vitro and in vivo. Tumor Biol 33(5):1349–1362. https://doi.org/10.1007/s13277-012-0383-6
303. Sapra P, Kraft P, Pastorino F, Ribatti D, Dumble M, Mehlig M, Wang M, Ponzoni M, Greenberger LM, Horak ID (2011) Potent and sustained inhibition of HIF-1alpha and downstream genes by a polyethyleneglycol-SN38 conjugate, EZN-2208, results in anti-angiogenic effects. Angiogenesis 14(3):245–253. https://doi.org/10.1007/s10456-011-9209-1
304. Kurzrock R, Goel S, Wheler J, Hong D, Fu S, Rezai K, Morgan-Linnell SK, Urien S, Mani S, Chaudhary I, Ghalib MH, Buchbinder A, Lokiec F, Mulcahy M (2012) Safety, pharmacokinetics, and activity of EZN-2208, a novel conjugate of polyethylene glycol and SN38, in patients with advanced malignancies. Cancer 118(24):6144–6151. https://doi.org/10.1002/cncr.27647
305. Greenberger LM, Horak ID, Filpula D, Sapra P, Westergaard M, Frydenlund HF, Albæk C, Schrøder H, Ørum H (2008) A RNA antagonist of hypoxia-inducible factor-1α, EZN-2968, inhibits tumor cell growth. Mol Cancer Ther 7(11):3598–3608. https://doi.org/10.1158/1535-7163.mct-08-0510
306. Krasieva TB, Ehren J, O'Sullivan T, Tromberg BJ, Maher P (2015) Cell and brain tissue imaging of the flavonoid fisetin using label-free two-photon microscopy. Neurochem Int 89:243–248. https://doi.org/10.1016/j.neuint.2015.08.003
307. Bhat TA, Nambiar D, Pal A, Agarwal R, Singh RP (2011) Fisetin inhibits various attributes of angiogenesis in vitro and in vivo —implications for angioprevention. Carcinogenesis 33(2):385–393. https://doi.org/10.1093/carcin/bgr282
308. Mie Lee Y, Kim S-H, Kim H-S, Jin Son M, Nakajima H, Jeong Kwon H, Kim K-W (2003) Inhibition of hypoxia-induced angiogenesis by FK228, a specific histone deacetylase inhibitor, via suppression of HIF-1α activity. Biochem Biophys Res Commun 300(1):241–246. https://doi.org/10.1016/S0006-291X(02)02787-0
309. Qian DZ, Kachhap SK, Collis SJ, Verheul HM, Carducci MA, Atadja P, Pili R (2006) Class II histone deacetylases are associated with VHL-independent regulation of hypoxia-inducible factor 1 alpha. Cancer Res 66(17):8814–8821. https://doi.org/10.1158/0008-5472.can-05-4598

310. Kim KH, Jung HJ, Kwon HJ (2013) A new anti-angiogenic small molecule, G0811, inhibits angiogenesis via targeting hypoxia inducible factor (HIF)-1α signal transduction. Biochem Biophys Res Commun 441(2):399–404. https://doi.org/10.1016/j.bbrc.2013.10.075
311. Ying W, Du Z, Sun L, Foley KP, Proia DA, Blackman RK, Zhou D, Inoue T, Tatsuta N, Sang J, Ye S, Acquaviva J, Ogawa LS, Wada Y, Barsoum J, Koya K (2012) Ganetespib, a unique triazolone-containing Hsp90 inhibitor, exhibits potent antitumor activity and a superior safety profile for cancer therapy. Mol Cancer Ther 11(2):475–484. https://doi.org/10.1158/1535-7163.mct-11-0755
312. Shimamura T, Perera SA, Foley KP, Sang J, Rodig SJ, Inoue T, Chen L, Li D, Carretero J, Li YC, Sinha P, Carey CD, Borgman CL, Jimenez JP, Meyerson M, Ying W, Barsoum J, Wong KK, Shapiro GI (2012) Ganetespib (STA-9090), a nongeldanamycin HSP90 inhibitor, has potent antitumor activity in in vitro and in vivo models of non-small cell lung cancer. Clin Cancer Res 18(18):4973–4985. https://doi.org/10.1158/1078-0432.ccr-11-2967
313. Mabjeesh NJ, Post DE, Willard MT, Kaur B, Van Meir EG, Simons JW, Zhong H (2002) Geldanamycin induces degradation of hypoxia-inducible factor 1alpha protein via the proteosome pathway in prostate cancer cells. Cancer Res 62(9):2478–2482
314. Supko JG, Hickman RL, Grever MR, Malspeis L (1995) Preclinical pharmacologic evaluation of geldanamycin as an antitumor agent. Cancer Chemother Pharmacol 36(4):305–315. https://doi.org/10.1007/bf00689048
315. Nagle DG, Zhou YD (2006) Natural product-based inhibitors of hypoxia-inducible factor-1 (HIF-1). Curr Drug Targets 7(3):355–369
316. Huang T-S, Lee C-C, Chao Y, Shu C-H, Chen L-T, Chen L-L, Chen M-H, Yuan C-C, Whang-Peng J (1999) A novel podophyllotoxin-derived compound GL331 is more potent than its congener VP-16 in killing refractory cancer cells. Pharm Res 16(7):997–1002. https://doi.org/10.1023/A:1018971313256
317. Lee S-H, Jee J-G, Bae J-S, Liu K-H, Lee YM (2015) A group of novel HIF-1α inhibitors, glyceollins, blocks HIF-1α synthesis and decreases its stability via inhibition of the PI3K/AKT/mTOR pathway and hsp90 binding. J Cell Physiol 230(4):853–862. https://doi.org/10.1002/jcp.24813
318. Simons R, Vincken J-P, Bohin MC, Kuijpers TFM, Verbruggen MA, Gruppen H (2011) Identification of prenylated pterocarpans and other isoflavonoids in Rhizopus spp. elicited soya bean seedlings by electrospray ionisation mass spectrometry. Rapid Commun Mass Spectrom 25(1):55–65. https://doi.org/10.1002/rcm.4826
319. Lee SH, Lee J, Jung MH, Lee YM (2013) Glyceollins, a novel class of soy phytoalexins, inhibit angiogenesis by blocking the VEGF and bFGF signaling pathways. Mol Nutr Food Res 57(2):225–234. https://doi.org/10.1002/mnfr.201200489
320. Blank M, Lavie G, Mandel M, Hazan S, Orenstein A, Meruelo D, Keisari Y (2004) Antimetastatic activity of the photodynamic agent hypericin in the dark. Int J Cancer 111(4):596–603. https://doi.org/10.1002/ijc.20285
321. Blank M, Mandel M, Keisari Y, Meruelo D, Lavie G (2003) Enhanced ubiquitinylation of heat shock protein 90 as a potential mechanism for mitotic cell death in cancer cells induced with hypericin. Cancer Res 63(23):8241–8247
322. Head CS, Luu Q, Sercarz J, Saxton R (2006) Photodynamic therapy and tumor imaging of hypericin-treated squamous cell carcinoma. World J Surg Oncol 4(1):87. https://doi.org/10.1186/1477-7819-4-87
323. Jacobson JM, Feinman L, Liebes L, Ostrow N, Koslowski V, Tobia A, Cabana BE, Lee D-H, Spritzler J, Prince AM (2001) Pharmacokinetics, safety, and antiviral effects of hypericin, a derivative of St. John's Wort plant, in patients with chronic hepatitis C virus infection. Antimicrob Agents Chemother 45(2):517–524. https://doi.org/10.1128/aac.45.2.517-524.2001
324. Mirmalek SA, Azizi MA, Jangholi E, Yadollah-Damavandi S, Javidi MA, Parsa Y, Parsa T, Salimi-Tabatabaee SA, Ghasemzadeh Kolagar H, Alizadeh-Navaei R (2016) Cytotoxic and apoptogenic effect of hypericin, the bioactive component of Hypericum perforatum on the MCF-7 human breast cancer cell line. Cancer Cell Int 16(1):3. https://doi.org/10.1186/s12935-016-0279-4
325. Wang KS, Ma J, Mi C, Li J, Lee JJ, Jin X (2016) Kamebakaurin inhibits the expression of hypoxia-inducible factor-1alpha and its target genes to confer antitumor activity. Oncol Rep 35(4):2045–2052. https://doi.org/10.3892/or.2016.4576
326. Xia Y, Feng M, Wang E, Chen L, Wang J, Hou R, Zhao Y (2019) An ent-Kaurane diterpenoid isolated from rabdosia excisa

suppresses Bcr-Abl protein expression in vitro and in vivo and induces apoptosis of CML cells. Chem Biodivers 16(10):e1900443. https://doi.org/10.1002/cbdv.201900443

327. Narita T, Yin S, Gelin CF, Moreno CS, Yepes M, Nicolaou KC, Van Meir EG (2009) Identification of a novel small molecule HIF-1alpha translation inhibitor. Clin Cancer Res 15(19):6128–6136. https://doi.org/10.1158/1078-0432.ccr-08-3180
328. Yin S, Kaluz S, Devi NS, Jabbar AA, de Noronha RG, Mun J, Zhang Z, Boreddy PR, Wang W, Wang Z, Abbruscato T, Chen Z, Olson JJ, Zhang R, Goodman MM, Nicolaou KC, Van Meir EG (2012) Arylsulfonamide KCN1 inhibits in vivo glioma growth and interferes with HIF signaling by disrupting HIF-1α interaction with cofactors p300/CBP. Clin Cancer Res 18(24):6623–6633. https://doi.org/10.1158/1078-0432.ccr-12-0861
329. Wang W, Ao L, Rayburn ER, Xu H, Zhang X, Zhang X, Nag SA, Wu X, Wang MH, Wang H, Van Meir EG, Zhang R (2012) KCN1, a novel synthetic sulfonamide anticancer agent: in vitro and in vivo anti-pancreatic cancer activities and preclinical pharmacology. PLoS One 7(9):e44883. https://doi.org/10.1371/journal.pone.0044883
330. Kurebayashi J, Otsuki T, Kurosumi M, Soga S, Akinaga S, Sonoo H (2001) A radicicol derivative, KF58333, inhibits expression of hypoxia-inducible factor-1α and vascular endothelial growth factor, angiogenesis and growth of human breast cancer xenografts. Jpn J Cancer Res 92(12):1342–1351. https://doi.org/10.1111/j.1349-7006.2001.tb02159.x
331. Shiotsu Y, Neckers LM, Wortman I, An WG, Schulte TW, Soga S, Murakata C, Tamaoki T, Akinaga S (2000) Novel oxime derivatives of radicicol induce erythroid differentiation associated with preferential G(1) phase accumulation against chronic myelogenous leukemia cells through destabilization of Bcr-Abl with Hsp90 complex. Blood 96(6):2284–2291
332. Kwon HS, Kim D-R, Yang EG, Park YK, Ahn H-C, Min S-J, Ahn D-R (2012) Inhibition of VEGF transcription through blockade of the hypoxia inducible factor-1α–p300 interaction by a small molecule. Bioorg Med Chem Lett 22(16):5249–5252. https://doi.org/10.1016/j.bmcl.2012.06.054
333. Brahmachari G (2013) Chemistry and pharmacology of naturally occurring bioactive compounds. CRC Press, Boca Raton, FL
334. Yu M, Salvador LA, Sy SK, Tang Y, Singh RS, Chen QY, Liu Y, Hong J, Derendorf H, Luesch H (2014) Largazole pharmacokinetics in rats by LC-MS/MS. Mar Drugs 12(3):1623–1640. https://doi.org/10.3390/md12031623
335. Xie SR, Wang Y, Liu CW, Luo K, Cai YQ (2012) Liquiritigenin inhibits serum-induced HIF-1alpha and VEGF expression via the AKT/mTOR-p70S6K signalling pathway in HeLa cells. Phytother Res 26(8):1133–1141. https://doi.org/10.1002/ptr.3696
336. Spencer JPE, Crozier RA (2016) Flavonoids and related compounds : bioavailability and function
337. Kong LD, Zhang Y, Pan X, Tan RX, CHK C (2000) Inhibition of xanthine oxidase by liquiritigenin and isoliquiritigenin isolated from Sinofranchetia chinensis. Cell Mol Life Sci 57(3):500–505. https://doi.org/10.1007/PL00000710
338. Lee K, Kang JE, Park S-K, Jin Y, Chung K-S, Kim H-M, Lee K, Kang MR, Lee MK, Song KB, Yang E-G, Lee J-J, Won M (2010) LW6, a novel HIF-1 inhibitor, promotes proteasomal degradation of HIF-1α via upregulation of VHL in a colon cancer cell line. Biochem Pharmacol 80(7):982–989. https://doi.org/10.1016/j.bcp.2010.06.018
339. Vlahos CJ, Matter WF, Hui KY, Brown RF (1994) A specific inhibitor of phosphatidylinositol 3-kinase, 2-(4-morpholinyl)-8-phenyl-4H-1-benzopyran-4-one (LY294002). J Biol Chem 269(7):5241–5248
340. Chaussade C, Rewcastle GW, Kendall JD, Denny WA, Cho K, Grønning LM, Chong ML, Anagnostou SH, Jackson SP, Daniele N, Shepherd PR (2007) Evidence for functional redundancy of class IA PI3K isoforms in insulin signalling. Biochem J 404(3):449–458. https://doi.org/10.1042/bj20070003
341. Chen MC, Lee CF, Huang WH, Chou TC (2013) Magnolol suppresses hypoxia-induced angiogenesis via inhibition of HIF-1alpha/VEGF signaling pathway in human bladder cancer cells. Biochem Pharmacol 85(9):1278–1287. https://doi.org/10.1016/j.bcp.2013.02.009
342. Ho JH-C, Hong C-Y (2012) Cardiovascular protection of magnolol: cell-type specificity and dose-related effects. J Biomed Sci 19(1):70. https://doi.org/10.1186/1423-0127-19-70
343. He X, Zhang P, Saqib M, Wang S, Hou X (2017) Screening active anti-breast cancer compounds from Cortex Magnolia Officinalis

by MCF-7 cell membrane chromatography coupled with UHPLC-ESI-MS/MS. Anal Methods 9(33):4828–4836. https://doi.org/10.1039/C7AY01213F

344. Shin J-M, Jeong Y-J, Cho H-J, Park K-K, Chung I-K, Lee I-K, Kwak J-Y, Chang H-W, Kim C-H, Moon S-K, Kim W-J, Choi Y-H, Chang Y-C (2013) Melittin suppresses HIF-1α/VEGF expression through inhibition of ERK and mTOR/p70S6K pathway in human cervical carcinoma cells. PLoS One 8(7):e69380. https://doi.org/10.1371/journal.pone.0069380
345. Gribenko AV, Guzmán-Casado M, Lopez MM, Makhatadze GI (2002) Conformational and thermodynamic properties of peptide binding to the human S100P protein. Prot Sci 11(6):1367–1375. https://doi.org/10.1110/ps.0202202
346. Ridgway Z, Picciano AL, Gosavi PM, Moroz YS, Angevine CE, Chavis AE, Reiner JE, Korendovych IV, Caputo GA (2015) Functional characterization of a melittin analog containing a non-natural tryptophan analog. Biopolymers 104(4):384–394. https://doi.org/10.1002/bip.22624
347. Soman NR, Baldwin SL, Hu G, Marsh JN, Lanza GM, Heuser JE, Arbeit JM, Wickline SA, Schlesinger PH (2009) Molecularly targeted nanocarriers deliver the cytolytic peptide melittin specifically to tumor cells in mice, reducing tumor growth. J Clin Invest 119(9):2830–2842. https://doi.org/10.1172/jci38842
348. Hu OY, Wu CY, Chan WK, Wu FY (1995) Determination of anticancer drug vitamin K3 in plasma by high-performance liquid chromatography. J Chromatogr B Biomed Sci Appl 666(2):299–305. https://doi.org/10.1016/0378-4347(94)00572-M
349. Wang L, Bonorden MJ, Li GX, Lee HJ, Hu H, Zhang Y, Liao JD, Cleary MP, Lu J (2009) Methyl-selenium compounds inhibit prostate carcinogenesis in the transgenic adenocarcinoma of mouse prostate model with survival benefit. Cancer Prev Res (Phila) 2(5):484–495. https://doi.org/10.1158/1940-6207.capr-08-0173
350. Sinha I, Allen JE, Pinto JT, Sinha R (2014) Methylseleninic acid elevates REDD1 and inhibits prostate cancer cell growth despite AKT activation and mTOR dysregulation in hypoxia. Cancer Med 3(2):252–264. https://doi.org/10.1002/cam4.198
351. Guo X, Yin S, Dong Y, Fan L, Ye M, Lu J, Hu H (2012) Enhanced apoptotic effects by the combination of curcumin and methylseleninic acid: potential role of mcl-1 and fak. Mol Carcinog 52(11):879–889. https://doi.org/10.1002/mc.21933
352. Sinha I, Null K, Wolter W, Suckow MA, King T, Pinto JT, Sinha R (2012) Methylseleninic acid downregulates hypoxia-inducible factor-1alpha in invasive prostate cancer. Int J Cancer 130(6):1430–1439. https://doi.org/10.1002/ijc.26141
353. Tarrado-Castellarnau M, Cortés R, Zanuy M, Tarragó-Celada J, Polat IH, Hill R, Fan TWM, Link W, Cascante M (2015) Methylseleninic acid promotes antitumour effects via nuclear FOXO3a translocation through Akt inhibition. Pharmacol Res 102:218–234. https://doi.org/10.1016/j.phrs.2015.09.009
354. Pautke C, Vogt S, Kreutzer K, Haczek C, Wexel G, Kolk A, Imhoff AB, Zitzelsberger H, Milz S, Tischer T (2010) Characterization of eight different tetracyclines: advances in fluorescence bone labeling. J Anat 217(1):76–82. https://doi.org/10.1111/j.1469-7580.2010.01237.x
355. Modheji M, Olapour S, Khodayar M, Jalili A, Yaghooti H (2016) Minocycline is more potent than tetracycline and doxycycline in inhibiting MMP-9 in vitro. Jundishapur J Nat Pharmac Prod. https://doi.org/10.17795/jjnpp-27377
356. Ingels A, Zhao H, Thong AE, Saar M, Valta MP, Nolley R, Santos J, Peehl DM (2014) Preclinical trial of a new dual mTOR inhibitor, MLN0128, using renal cell carcinoma tumor grafts. Int J Cancer 134(10):2322–2329. https://doi.org/10.1002/ijc.28579
357. Ghobrial IM, Siegel DS, Vij R, Berdeja JG, Richardson PG, Neuwirth R, Patel CG, Zohren F, Wolf JL (2016) TAK-228 (formerly MLN0128), an investigational oral dual TORC1/2 inhibitor: a phase I dose escalation study in patients with relapsed or refractory multiple myeloma, non-Hodgkin lymphoma, or Waldenström's macroglobulinemia. Am J Hematol 91(4):400–405. https://doi.org/10.1002/ajh.24300
358. Liu Q, Thoreen C, Wang J, Sabatini D, Gray NS (2009) mTOR mediated anti-cancer drug discovery. Drug Discov Today Therap Strat 6(2):47–55. https://doi.org/10.1016/j.ddstr.2009.12.001
359. Slotkin EK, Patwardhan PP, Vasudeva SD, de Stanchina E, Tap WD, Schwartz GK (2014) MLN0128, an ATP-competitive mTOR kinase inhibitor with potent in vitro and in vivo antitumor activity, as potential therapy for bone and soft-tissue sarcoma. Mol Cancer

Ther 14(2):395–406. https://doi.org/10.1158/1535-7163.mct-14-0711

360. Siti MM, Yunos N, Jauri MH, Alias M, Krishnasamy G, Osman A, Norhayati I, Sahira L, Suryani S (2011) Potential anticancer compound from Cerbera odollam. J Trop For Sci 23:89–96
361. Wu D, Zhang R, Zhao R, Chen G, Cai Y, Jin J (2013) A novel function of novobiocin: disrupting the interaction of HIF 1α and p300/CBP through direct binding to the HIF1α C-terminal activation domain. PLoS One 8(5):e62014. https://doi.org/10.1371/journal.pone.0062014
362. Drusano GL, Townsend RJ, Walsh TJ, Forrest A, Antal EJ, Standiford HC (1986) Steady-state serum pharmacokinetics of novobiocin and rifampin alone and in combination. Antimicrob Agents Chemother 30(1):42–45
363. Bendell JC, Jones SF, Hart L, Pant S, Moyhuddin A, Lane CM, Earwood C, Murphy P, Patton J, Penley WC, Thompson D, Infante JR (2015) A phase I study of the Hsp90 inhibitor AUY922 plus capecitabine for the treatment of patients with advanced solid tumors. Cancer Invest 33(10):477–482. https://doi.org/10.3109/07357907.2015.1069834
364. Eccles SA, Massey A, Raynaud FI, Sharp SY, Box G, Valenti M, Patterson L, de Haven BA, Gowan S, Boxall F, Aherne W, Rowlands M, Hayes A, Martins V, Urban F, Boxall K, Prodromou C, Pearl L, James K, Matthews TP, Cheung KM, Kalusa A, Jones K, McDonald E, Barril X, Brough PA, Cansfield JE, Dymock B, Drysdale MJ, Finch H, Howes R, Hubbard RE, Surgenor A, Webb P, Wood M, Wright L, Workman P (2008) NVP-AUY922: a novel heat shock protein 90 inhibitor active against xenograft tumor growth, angiogenesis, and metastasis. Cancer Res 68(8):2850–2860. https://doi.org/10.1158/0008-5472.can-07-5256
365. Lee KH, Lee JH, Han SW, Im SA, Kim TY, Oh DY, Bang YJ (2011) Antitumor activity of NVP-AUY922, a novel heat shock protein 90 inhibitor, in human gastric cancer cells is mediated through proteasomal degradation of client proteins. Cancer Sci 102(7):1388–1395. https://doi.org/10.1111/j.1349-7006.2011.01944.x
366. Atadja P, Gao L, Kwon P, Trogani N, Walker H, Hsu M, Yeleswarapu L, Chandramouli N, Perez L, Versace R, Wu A, Sambucetti L, Lassota P, Cohen D, Bair K, Wood A, Remiszewski S (2004) Selective growth inhibition of tumor cells by a novel histone deacetylase inhibitor, NVP-LAQ824. Cancer Res 64(2):689–695. https://doi.org/10.1158/0008-5472.can-03-2043
367. de Bono JS, Kristeleit R, Tolcher A, Fong P, Pacey S, Karavasilis V, Mita M, Shaw H, Workman P, Kaye S, Rowinsky EK, Aherne W, Atadja P, Scott JW, Patnaik A (2008) Phase I pharmacokinetic and pharmacodynamic study of LAQ824, a hydroxamate histone deacetylase inhibitor with a heat shock protein-90 inhibitory profile, in patients with advanced solid tumors. Clin Cancer Res 14(20):6663–6673. https://doi.org/10.1158/1078-0432.ccr-08-0376
368. Burslem GM, Kyle HF, Breeze AL, Edwards TA, Nelson A, Warriner SL, Wilson AJ (2014) Small-molecule proteomimetic inhibitors of the hif-1α–p300 protein–protein interaction. Chem Bio Chem 15(8):1083–1087. https://doi.org/10.1002/cbic.201400009
369. Qazzaz HMAM, El-Masri MA, Valdes JR (2000) Secretion of a lactone-hydrogenated ouabain-like effector of sodium, potassium-adenosine triphosphatase activity by adrenal cells. Endocrinology 141(9):3200–3209. https://doi.org/10.1210/endo.141.9.7664
370. Cao J, He L, Lin G, Hu C, Dong R, Zhang J, Zhu H, Hu Y, Wagner CR, He Q, Yang B (2014) Cap-dependent translation initiation factor, eIF4E, is the target for Ouabain-mediated inhibition of HIF-1alpha. Biochem Pharmacol 89(1):20–30. https://doi.org/10.1016/j.bcp.2013.12.002
371. Proppe D (1975) Pharmacokinetics of tritiated ouabain, digoxin and digitoxin in guinea-pigs. Clin Exp Pharmacol Physiol 2(6):489–502. https://doi.org/10.1111/j.1440-1681.1975.tb01854.x
372. Bloise E, Braca A, De Tommasi N, Belisario MA (2009) Pro-apoptotic and cytostatic activity of naturally occurring cardenolides. Cancer Chemother Pharmacol 64(4):793–802. https://doi.org/10.1007/s00280-009-0929-5
373. Yan K, Wang X, Jia Y, Chu Y, Guan X, Ma X, Li W, Pan G, Zhou S, Sun H, Liu C (2016) Quantitative determination of periplocymarin in rat plasma and tissue by LC-MS/MS: application to pharmacokinetic and tissue distribution study. Biomed Chromatogr 30(8):1195–1201. https://doi.org/10.1002/bmc.3667
374. Frölich JC, Falkner FC, Watson JT, Scheler F (1972) Metabolism of peruvoside in man. Eur J Clin Pharmacol 5(2):65–71. https://doi.org/10.1007/bf00561747
375. Ji Y, Kuo Y, Morris ME (2005) Pharmacokinetics of dietary phenethyl isothiocyanate in

rats. Pharm Res 22(10):1658–1666. https://doi.org/10.1007/s11095-005-7097-z

376. Wang X-H, Cavell BE, Syed Alwi SS, Packham G (2009) Inhibition of hypoxia inducible factor by phenethyl isothiocyanate. Biochem Pharmacol 78(3):261–272. https://doi.org/10.1016/j.bcp.2009.04.010
377. Welsh SJ, Williams RR, Birmingham A, Newman DJ, Kirkpatrick DL, Powis G (2003) The thioredoxin redox inhibitors 1-methylpropyl 2-imidazolyl disulfide and pleurotin inhibit hypoxia-induced factor 1alpha and vascular endothelial growth factor formation. Mol Cancer Ther 2(3):235–243
378. Al-Temimay IA, AL-Jibouri MH, Hassan AA, Mohammad FI (2015) The optimum conditions for pleurotin production by Pleurotus spp. local isolates. Iraqi J Sci 56(3C):2542–2552
379. Denicolaï E, Baeza-Kallee N, Tchoghandjian A, Carré M, Colin C, Jiglaire CJ, Mercurio S, Beclin C, Figarella-Branger D (2014) Proscillaridin A is cytotoxic for glioblastoma cell lines and controls tumor xenograft growth in vivo. Oncotarget 5(21):10934–10948. https://doi.org/10.18632/oncotarget.2541
380. Kasibhatla SR, Hong K, Biamonte MA, Busch DJ, Karjian PL, Sensintaffar JL, Kamal A, Lough RE, Brekken J, Lundgren K, Grecko R, Timony GA, Ran Y, Mansfield R, Fritz LC, Ulm E, Burrows FJ, Boehm MF (2007) Rationally designed high-affinity 2-amino-6-halopurine heat shock protein 90 inhibitors that exhibit potent antitumor activity. J Med Chem 50(12):2767–2778. https://doi.org/10.1021/jm050752+
381. Gallerne C, Prola A, Lemaire C (2013) Hsp90 inhibition by PU-H71 induces apoptosis through endoplasmic reticulum stress and mitochondrial pathway in cancer cells and overcomes the resistance conferred by Bcl-2. Biochim Biophys Acta 1833(6):1356–1366. https://doi.org/10.1016/j.bbamcr.2013.02.014
382. Caldas-Lopes E, Cerchietti L, Ahn JH, Clement CC, Robles AI, Rodina A, Moulick K, Taldone T, Gozman A, Guo Y, Wu N, de Stanchina E, White J, Gross SS, Ma Y, Varticovski L, Melnick A, Chiosis G (2009) Hsp90 inhibitor PU-H71, a multimodal inhibitor of malignancy, induces complete responses in triple-negative breast cancer models. Proc Natl Acad Sci U S A 106(20):8368–8373. https://doi.org/10.1073/pnas.0903392106
383. Speranza G, Anderson L, Chen AP, Do K, Eugeni M, Weil M, Rubinstein L, Majerova E, Collins J, Horneffer Y, Juwara L, Zlott J, Bishop R, Conley BA, Streicher H, Tomaszewski J, Doroshow JH, Kummar S (2018) First-in-human study of the epichaperome inhibitor PU-H71: clinical results and metabolic profile. Invest New Drugs 36(2):230–239. https://doi.org/10.1007/s10637-017-0495-3
384. Welsh S, Williams R, Kirkpatrick L, Paine-Murrieta G, Powis G (2004) Antitumor activity and pharmacodynamic properties of PX-478, an inhibitor of hypoxia-inducible factor-1alpha. Mol Cancer Ther 3(3):233–244
385. Koh MY, Spivak-Kroizman T, Venturini S, Welsh S, Williams RR, Kirkpatrick DL, Powis G (2008) Molecular mechanisms for the activity of PX-478, an antitumor inhibitor of the hypoxia-inducible factor-1alpha. Mol Cancer Ther 7(1):90–100. https://doi.org/10.1158/1535-7163.mct-07-0463
386. Sharp SY, Prodromou C, Boxall K, Powers MV, Holmes JL, Box G, Matthews TP, Cheung K-MJ, Kalusa A, James K, Hayes A, Hardcastle A, Dymock B, Brough PA, Barril X, Cansfield JE, Wright L, Surgenor A, Foloppe N, Hubbard RE, Aherne W, Pearl L, Jones K, McDonald E, Raynaud F, Eccles S, Drysdale M, Workman P (2007) Inhibition of the heat shock protein 90 molecular chaperone in vitro and in vivo by novel, synthetic, potent resorcinylic pyrazole/isoxazole amide analogues. Mol Cancer Ther 6(4):1198–1211. https://doi.org/10.1158/1535-7163.mct-07-0149
387. Yewalkar N, Deore V, Padgaonkar A, Manohar S, Sahu B, Kumar P, Jalota-Badhwar A, Joshi KS, Sharma S, Kumar S (2010) Development of novel inhibitors targeting HIF-1α towards anticancer drug discovery. Bioorg Med Chem Lett 20(22):6426–6429. https://doi.org/10.1016/j.bmcl.2010.09.083
388. Manohar SM, Padgaonkar AA, Jalota-Badhwar A, Sonawane V, Rathos MJ, Kumar S, Joshi KS (2011) A novel inhibitor of hypoxia-inducible factor-1α P3155 also modulates PI3K pathway and inhibits growth of prostate cancer cells. BMC Cancer 11:338–338. https://doi.org/10.1186/1471-2407-11-338
389. T-b K, Liang N-c (1997) Studies on the inhibitory effects of quercetin on the growth of HL-60 leukemia cells. Biochem Pharmacol 54(9):1013–1018. https://doi.org/10.1016/S0006-2952(97)00260-8
390. de Paula RR, Tini IR, Soares CP, da Silva NS (2014) Effect of photodynamic therapy

supplemented with quercetin in HEp-2 cells. Cell Biol Int 38(6):716–722. https://doi.org/10.1002/cbin.10251

391. Hur E, Kim H-H, Choi SM, Kim JH, Yim S, Kwon HJ, Choi Y, Kim DK, Lee M-O, Park H (2002) Reduction of hypoxia-induced transcription through the repression of hypoxia-inducible factor-1α/Aryl hydrocarbon receptor nuclear translocator DNA binding by the 90-kDa heat-shock protein inhibitor radicicol. Mol Pharmacol 62(5):975–982. https://doi.org/10.1124/mol.62.5.975
392. Roe SM, Prodromou C, O'Brien R, Ladbury JE, Piper PW, Pearl LH (1999) Structural basis for inhibition of the Hsp90 molecular chaperone by the antitumor antibiotics radicicol and geldanamycin. J Med Chem 42(2):260–266. https://doi.org/10.1021/jm980403y
393. Hudson CC, Liu M, Chiang GG, Otterness DM, Loomis DC, Kaper F, Giaccia AJ, Abraham RT (2002) Regulation of hypoxia-inducible factor 1α expression and function by the mammalian target of rapamycin. Mol Cell Biol 22(20):7004–7014. https://doi.org/10.1128/MCB.22.20.7004-7014.2002
394. Nalbandian A, Llewellyn KJ, Nguyen C, Yazdi PG, Kimonis VE (2015) Rapamycin and chloroquine: the in vitro and in vivo effects of autophagy-modifying drugs show promising results in valosin containing protein multisystem proteinopathy. PLoS One 10(4):e0122888. https://doi.org/10.1371/journal.pone.0122888
395. Carter LG, D'Orazio JA, Pearson KJ (2014) Resveratrol and cancer: focus on in vivo evidence. Endocr Relat Cancer 21(3):R209–R225. https://doi.org/10.1530/ERC-13-0171
396. Kim SH, Adhikari BB, Cruz S, Schramm MP, Vinson JA, Narayanaswami V (2015) Targeted intracellular delivery of resveratrol to glioblastoma cells using apolipoprotein E-containing reconstituted HDL as a nanovehicle. PLoS One 10(8):e0135130. https://doi.org/10.1371/journal.pone.0135130
397. Perrone D, Fuggetta MP, Ardito F, Cottarelli A, De Filippis A, Ravagnan G, De Maria S, Lo Muzio L (2017) Resveratrol (3,5,4′-trihydroxystilbene) and its properties in oral diseases. Exp Ther Med 14(1):3–9. https://doi.org/10.3892/etm.2017.4472
398. Tseng S-H, Lin S-M, Chen J-C, Su Y-H, Huang H-Y, Chen C-K, Lin P-Y, Chen Y (2004) Resveratrol suppresses the angiogenesis and tumor growth of gliomas in rats. Clin Cancer Res 10(6):2190–2202. https://doi.org/10.1158/1078-0432.ccr-03-0105
399. Garvin S, Ollinger K, Dabrosin C (2006) Resveratrol induces apoptosis and inhibits angiogenesis in human breast cancer xenografts in vivo. Cancer Lett 231(1):113–122. https://doi.org/10.1016/j.canlet.2005.01.031
400. Deng Y-T, Huang H-C, Lin J-K (2010) Rotenone induces apoptosis in MCF-7 human breast cancer cell-mediated ROS through JNK and p38 signaling. Mol Carcinog 49(2):141–151. https://doi.org/10.1002/mc.20583
401. Han J-Y, Oh SH, Morgillo F, Myers JN, Kim E, Hong WK, Lee H-Y (2005) Hypoxia-inducible factor 1α and antiangiogenic activity of farnesyltransferase inhibitor SCH66336 in human aerodigestive tract cancer. JNCI 97(17):1272–1286. https://doi.org/10.1093/jnci/dji251
402. Awada A, Eskens FALM, Piccart M, Cutler DL, van der Gaast A, Bleiberg H, Wanders J, Faber MN, Statkevich P, Fumoleau P, Verweij J (2002) Phase I and pharmacological study of the oral farnesyltransferase inhibitor SCH 66336 given once daily to patients with advanced solid tumours. Eur J Cancer 38(17):2272–2278. https://doi.org/10.1016/S0959-8049(02)00379-9
403. Dutta Gupta S, Revathi B, Mazaira GI, Galigniana MD, Subrahmanyam CVS, Gowrishankar NL, Raghavendra NM (2015) 2,4-dihydroxy benzaldehyde derived Schiff bases as small molecule Hsp90 inhibitors: Rational identification of a new anticancer lead. Bioorg Chem 59:97–105. https://doi.org/10.1016/j.bioorg.2015.02.003
404. Jo DH, An H, Chang D-J, Baek Y-Y, Cho CS, Jun HO, Park S-J, Kim JH, Lee H-Y, Kim K-W, Lee J, Park H-J, Kim Y-M, Suh Y-G, Kim JH (2014) Hypoxia-mediated retinal neovascularization and vascular leakage in diabetic retina is suppressed by HIF-1α destabilization by SH-1242 and SH-1280, novel hsp90 inhibitors. J Mol Med 92(10):1083–1092. https://doi.org/10.1007/s00109-014-1168-8
405. Zhao J, Agarwal R (1999) Tissue distribution of silibinin, the major active constituent of silymarin, in mice and its association with enhancement of phase II enzymes: implications in cancer chemoprevention. Carcinogenesis 20(11):2101–2108. https://doi.org/10.1093/carcin/20.11.2101
406. Chabot GG (1997) Clinical Pharmacokinetics of Irinotecan. Clin Pharmacokinet

33(4):245–259. https://doi.org/10.2165/00003088-199733040-00001

407. Miller AA, Kurschel E, Osieka R, Schmidt CG (1987) Clinical pharmacology of sodium butyrate in patients with acute leukemia. Eur J Cancer Clin Oncol 23(9):1283–1287. https://doi.org/10.1016/0277-5379(87)90109-X
408. Ghiaghi M, Forouzesh F, Rahimi H (2019) Effect of sodium butyrate on LHX1 mRNA expression as a transcription factor of HDAC8 in human colorectal cancer cell lines. Avicenna J Med Biotechnol 11(4):317–324
409. Lathia C, Lettieri J, Cihon F, Gallentine M, Radtke M, Sundaresan P (2006) Lack of effect of ketoconazole-mediated CYP3A inhibition on sorafenib clinical pharmacokinetics. Cancer Chemother Pharmacol 57(5):685–692. https://doi.org/10.1007/s00280-005-0068-6
410. Minami H, Kawada K, Ebi H, Kitagawa K, Kim YI, Araki K, Mukai H, Tahara M, Nakajima H, Nakajima K (2008) Phase I and pharmacokinetic study of sorafenib, an oral multikinase inhibitor, in Japanese patients with advanced refractory solid tumors. Cancer Sci 99(7):1492–1498. https://doi.org/10.1111/j.1349-7006.2008.00837.x
411. Yeh CC, Hsu CH, Shao YY, Ho WC, Tsai MH, Feng WC, Chow LP (2015) Integrated stable isotope labeling by amino acids in cell culture (SILAC) and isobaric tags for relative and absolute quantitation (iTRAQ) quantitative proteomic analysis identifies galectin-1 as a potential biomarker for predicting sorafenib resistance in liver cancer. Mol Cell Proteom 14(6):1527–1545. https://doi.org/10.1074/mcp.M114.046417
412. Strobach H, Wirth KE, Rojsathaporn K (1986) Absorption, metabolism and elimination of strophanthus glycosides in man. Naunyn Schmiedebergs Arch Pharmacol 334(4):496–500. https://doi.org/10.1007/bf00569392
413. Li G, Shan C, Liu L, Zhou T, Zhou J, Hu X, Chen Y, Cui H, Gao N (2015) Tanshinone IIA inhibits HIF-1α and VEGF expression in breast cancer cells via mTOR/p70S6K/RPS6/4E-BP1 signaling pathway. PLoS One 10(2):e0117440. https://doi.org/10.1371/journal.pone.0117440
414. Li JF, Wei YX, Xu ZC, Dong C, Shuang SM (2004) Studies on the spectroscopic behavior of cryptotanshinone, tanshinone IIA, and tanshinone I. Spectrochim Acta A Mol Biomol Spectrosc 60(4):751–756. https://doi.org/10.1016/s1386-1425(03)00286-5
415. Wang Y, Yan J, Li S, Cai X, Wang W, Luo K, Huang D, Gao J (2014) Pharmacokinetics and tissue distribution study of tanshinone IIA after oral administration of Bushen Huoxue Qubi granules to rats with blood stasis syndrome. Pharmaco Magaz 10(39):285–291. https://doi.org/10.4103/0973-1296.137369
416. Tsai M-Y, Yang R-C, Wu H-T, Pang J-HS, Huang S-T (2011) Anti-angiogenic effect of Tanshinone IIA involves inhibition of matrix invasion and modification of MMP-2/TIMP-2 secretion in vascular endothelial cells. Cancer Lett 310(2):198–206. https://doi.org/10.1016/j.canlet.2011.06.031
417. Wang X, Wei Y, Yuan S, Liu G, Lu Y, Zhang J, Wang W (2005) Potential anticancer activity of tanshinone IIA against human breast cancer. Int J Cancer 116(5):799–807. https://doi.org/10.1002/ijc.20880
418. Su C-C, Lin Y-H (2008) Tanshinone IIA inhibits human breast cancer cells through increased Bax to Bcl-xL ratios. Int J Mol Med 22(3):357–361. https://doi.org/10.3892/ijmm_00000030
419. Gong Y, Li Y, Abdolmaleky HM, Li L, Zhou JR (2012) Tanshinones inhibit the growth of breast cancer cells through epigenetic modification of Aurora A expression and function. PLoS One 7(4):e33656. https://doi.org/10.1371/journal.pone.0033656
420. Miranda E, Nordgren IK, Male AL, Lawrence CE, Hoakwie F, Cuda F, Court W, Fox KR, Townsend PA, Packham GK, Eccles SA, Tavassoli A (2013) A cyclic peptide inhibitor of HIF-1 heterodimerization that inhibits hypoxia signaling in cancer cells. J Am Chem Soc 135(28):10418–10425. https://doi.org/10.1021/ja402993u
421. Nishikawa T, Takaoka M, Ohara T, Tomono Y, Hao H, Bao X, Fukazawa T, Wang Z, Sakurama K, Fujiwara Y, Motoki T, Shirakawa Y, Yamatsuji T, Tanaka N, Fujiwara T, Naomoto Y (2013) Antiproliferative effect of a novel mTOR inhibitor temsirolimus contributes to the prolonged survival of orthotopic esophageal cancer-bearing mice. Cancer Biol Ther 14(3):230–236. https://doi.org/10.4161/cbt.23294
422. Merritt WM, Danes CG, Shahzad MMK, Lin YG, Kamat AA, Han LY, Spannuth WA, Nick AM, Mangala LS, Stone RL, Kim HS, Gershenson DM, Jaffe RB, Coleman RL, Chandra J, Sood AK (2009) Anti-angiogenic properties of metronomic topotecan in ovarian carcinoma. Cancer Biol Ther 8(16):1596–1603. https://doi.org/10.4161/cbt.8.16.9004

423. Rapisarda A, Zalek J, Hollingshead M, Braunschweig T, Uranchimeg B, Bonomi CA, Borgel SD, Carter JP, Hewitt SM, Shoemaker RH, Melillo G (2004) Schedule-dependent inhibition of hypoxia-inducible factor-1α protein accumulation, angiogenesis, and tumor growth by topotecan in U251-HRE glioblastoma xenografts. Cancer Res 64(19):6845–6848. https://doi.org/10.1158/0008-5472.can-04-2116

424. Burke TG, Malak H, Gryczynski I, Mi Z, Lakowicz JR (1996) Fluorescence detection of the anticancer drug topotecan in plasma and whole blood by two-photon excitation. Anal Biochem 242(2):266–270. https://doi.org/10.1006/abio.1996.0463

425. Caceres G, Zankina R, Zhu X, Jiao JA, Wong H, Aller A, Andreotti P (2003) Determination of chemotherapeutic activity in vivo by luminescent imaging of luciferase-transfected human tumors. Anticancer Drugs 14(7):569–574. https://doi.org/10.1097/00001813-200308000-00010

426. Sanderson L, Taylor GW, Aboagye EO, Alao JP, Latigo JR, Coombes RC, Vigushin DM (2004) Plasma pharmacokinetics and metabolism of the histone deacetylase inhibitor trichostatin a after intraperitoneal administration to mice. Drug Metab Dispos 32(10):1132–1138. https://doi.org/10.1124/dmd.104.000638

427. Song X, Yao J, Wang F, Zhou M, Zhou Y, Wang H, Wei L, Zhao L, Li Z, Lu N, Guo Q (2013) Wogonin inhibits tumor angiogenesis via degradation of HIF-1alpha protein. Toxicol Appl Pharmacol 271(2):144–155. https://doi.org/10.1016/j.taap.2013.04.031

428. Talbi A, Zhao D, Liu Q, Li J, Fan A, Yang W, Han X, Chen X (2014) Pharmacokinetics, tissue distribution, excretion and plasma protein binding studies of wogonin in rats. Molecules (Basel, Switzerland) 19(5):5538–5549. https://doi.org/10.3390/molecules19055538

429. Yuan H, Barnes KR, Weissleder R, Cantley L, Josephson L (2007) Covalent reactions of wortmannin under physiological conditions. Chem Biol 14(3):321–328. https://doi.org/10.1016/j.chembiol.2007.02.007

430. Yeo EJ, Ryu JH, Chun YS, Cho YS, Jang IJ, Cho H, Kim J, Kim MS, Park JW (2006) YC-1 induces S cell cycle arrest and apoptosis by activating checkpoint kinases. Cancer Res 66(12):6345–6352. https://doi.org/10.1158/0008-5472.can-05-4460

431. Yeo E-J, Chun Y-S, Cho Y-S, Kim J, Lee J-C, Kim M-S, Park J-W (2003) YC-1: a potential anticancer drug targeting hypoxia-inducible factor 1. JNCI 95(7):516–525. https://doi.org/10.1093/jnci/95.7.516

432. Xu Z, Zhao J, Gou S, Xu G (2017) Novel hypoxia-targeting Pt(IV) prodrugs. Chem Commun 53(26):3749–3752. https://doi.org/10.1039/C7CC01320E